UNIVERSITY OF SOUTHAMPTON

Improvements in the conduct and interpretation of ship seakeeping trials

Michael Charles Johnson

Thesis offered for the degree of
Doctor of Philosophy

School of Engineering Sciences – Ship Science

Faculty of Engineering and Applied Science

March 2004

UNIVERSITY OF SOUTHAMPTON

ABSTRACT

FACULTY OF ENGINEERING AND APPLIED SCIENCE
SCHOOL OF ENGINEERING SCIENCES – SHIP SCIENCE

Doctor of Philosophy

IMPROVEMENTS IN THE CONDUCT AND INTERPRETATION OF SHIP SEAKEEPING TRIALS

by Michael Charles Johnson

Although the complex nature of sea waves is often cited by authors as a reason for poor results, the published papers show little in the way of explanation of these complexities when treating full-scale trials data. In this thesis it is argued that measurement of the directional wave spectrum is essential for any seakeeping trial. Ways are demonstrated in which the wave complexity, particularly wave directionality, may be dealt with.

The consequences of assuming the seaway is long crested are explored with the aim of establishing guidelines for a generally applicable minimum wave height and maximum wave spreading for ship trials. The guidelines derived show that this assumption is unrealistic for a 5% uncertainty in the ship response.

Accepting that sea waves on a trial are likely to be multidirectional in nature, a case is made for a specific 'star' type ship evolution for trials so that the ship samples waves from all directions. The beneficial effects of this evolution are illustrated with trials results for five different ships of various types.

The direct validation of ship motion codes against trials data is not considered per se, however some guidance is given on using the sensitivity of ship motion codes to uncertainty in the exact ship condition during the trials. An efficient technique to include these error bands is proposed.

Validation of ship motion codes usually includes a great deal of simplification of the characteristics of the seaway, both in its directional nature and its spectral form. This thesis demonstrates that meaningful transfer function results can be achieved where the trials have been made with the ship in a strongly directional seaway. The theory of Fryer (1991) is used to calculate the transfer functions of a frigate ship operating in a clearly bimodal seaway.

Where sea trials currently take place, seakeeping performance assessment is rather a subjective process. Application of these methods shown here would assist in the process of demonstrating the seakeeping ability of new designs with sea trials, and hence allowing seakeeping to take a more accountable place in the procurement and acceptance cycle.

Furthermore two approaches are made to the 'reverse calculation' of the characteristics of the seaway based upon the ship motions, as if it were a moving wave buoy. In the first, a matrix solution at discrete frequencies of a set of simultaneous equations involving the transfer functions and ship motion results proved unsuccessful. It is suggested that making independent calculations at each frequency step is a fundamental source of difficulty with this method. A further complication arises as it is shown that derivation of wave slope encounter spectra from wave height encounter spectra requires knowledge of the stationary frequency, and is thus subject to the 'following seas' problem.

The second approach used multiple linear regression to derive simple formulae for the ship relative heading and significant wave height to an accuracy of the order 10% based purely on the RMS ship motions. This could find application in a shipboard guidance system.

Dedicated to my grandfather Charles Ronald Parsons, an engineer. He died before I was born. I would have liked to share some of the wonder with him.

Frontispiece: RV Triton conducts seakeeping trials in rough weather

CONTENTS

List of Tables

List of Figures

Acknowledgements

David Fryer recruited me to the Admiralty Research Establishment at Haslar and first aroused my interest in this research area. I was very pleased to assist David with some elements of his PhD thesis, and I have to thank him for giving me both initial guidance in direction and some building blocks to work with.

I was privileged also to work under Dr. Adrian Lloyd at Haslar (then as Defence Research Agency). Adrian was not directly involved with this thesis, but do I feel it is appropriate to make an acknowledgement. His book remains the benchmark text in seakeeping, and is a constant source of reference. I am sure this thesis has required only a fraction of the effort to write the book, publish it, and personally publish a revised edition. My thanks for this endeavour will be echoed by a generation of students and professionals alike.

This thesis was written almost entirely part time, but I must acknowledge my full time employer's support (as DRA, DERA and latterly QinetiQ at Haslar) with tuition fees, resources and of course the means to gather the data reported in this work. The trials data was gathered entirely with Ministry of Defence funding. My gratitude goes to the trials teams who were involved in collecting the data presented here, in particular Paul Crossland who has been friend, colleague and sounding board throughout.

Thanks to Kirsten for motivation in pulling it all together. It would have taken even longer without her.

Biggest thanks to my tutor Professor Philip Wilson. Philip has shown remarkable patience with me both in terms of time and effort, whilst I insisted on indulging myself in the odd blind alley. Our meetings were never a chore, always critical in a constructive way, and I always felt positively charged afterwards. Thank you Philip. I've learned a lot about myself as well as the subject matter. I hope it has been worthwhile for you too.

Haslar, December 2003

Nomenclature

Terminology

BST	British Summer Time
FFT	Fast Fourier Transform
GMT	Greenwich Mean Time
GPS	Global Positioning System
ITTC	International Towing Tank Conference
JONSWAP	Joint North Sea Wave Project
NATO	North Atlantic Treaty Organisation
RAO	Response Amplitude Operator
SS	Sea State

Roman notation

Symbol	*Description*	*unit*
a_i	Fourier expansion coefficient	
A	Area under a wave spectrum	
c	Wave phase velocity (celerity)	m/s
C_{ij}	Cross spectrum (or Auto spectrum C_{ii})	
d	Water depth	m
f	Wave frequency	Hz
f_e	Wave encounter frequency	Hz
f_m	Wave modal frequency	Hz
$H_{1/3}$	Significant Wave Height	m
g	Acceleration due to gravity	m/s^2
$G(\chi)$	Spreading function	
k	wave number	m^{-1}
m0,m2,m4	Statistical moments	$unit^2$,$unit/s^2$,$unit^2/s^4$
$\underline{M}$	Ship motion spectrum matrix	
M_e	Ship motion encounter spectral ordinate	$unit^2/Hz$

Q_{ij}	Quad-spectrum	
R	RMS motion	
R_i	RAO of motion type i	dimensionless
R_e	Encounter transfer function ordinate	
$\underline{R^2}$	Squared transfer function matrix	
s	Spreading parameter	
S	Wave elevation spectrum [S(f),S(f,χ) or S(ω) etc.]	m^2/Hz for S(f)
$\underline{S}$	Wave encounter spectrum matrix	
S_e	Wave encounter spectrum ordinate	m^2/Hz
T	Transformation	
$\underline{T}$	Transformation matrix	
T_m	Wave Modal Period	s
u	Ship Speed	m/s
v	Wind speed	m/s
W	Normalising factor for directional wave energy	
x	Longitudinal distance forward of CG	m
X	Surge	m
y	Lateral distance starboard of CG	m
Y	Sway	m
z	Vertical distance below CG	m
Z	Heave	m

Greek notation

Symbol	*Description*	*unit*
α	Instantaneous wave slope	rad
α_0	Wave slope amplitude	rad
α_{0e}	Encounter wave slope amplitude	rad
α_{n0e}	Encounter wave slope amplitude spectral ordinate	rad
χ	Compass heading	deg
θ	Pitch angle	rad
λ	Wavelength	m

ϕ	Roll angle	rad
γ	Peakiness factor (JONSWAP spectrum)	
ψ	Yaw angle	rad
Ψ_r	Relative Heading (180°=head seas)	deg
σ	Spectral width factor, standard deviation	
ω	Wave frequency	rad/s
ω_e	Wave encounter frequency	rad/s

1. INTRODUCTION

1.1 Opening remarks

The aim of this thesis is to arm the ship scientist with methods to assess the behaviour of displacement ships in the seaway. The major theme running through the thesis is that ship behaviour is complex principally because in real seas (as opposed to model test tanks or computer simulations) the wave field that the ship responds to is itself usually a complex mixture of waves of different frequencies and from several directions.

This work is illustrated with reference to wave and ship motion data acquired during the author's career, for Royal Navy warships and research vessels, including the world's first trimaran warship demonstrator. A foundation in ship science or naval architecture is assumed; in case of difficulty the reader is referred to the standard text in this area by Lloyd (1989) for enlightenment.

As far as possible this work is self-contained, and each chapter itself describes and deals with a particular problem. A general premise is that the majority of the ship motion data presented has actually been measured in trials – the data is neither the result of model tests nor computed by any particular theory. When comparison of trials data has been made with theory a single ship motion code has been used, but this is for illustration only and any other code might have been used instead. The work does not aim to validate the particular code used, though the results might assist this process.

1.2 Background

The ship designer has always faced a difficult task in building ships that perform well but will meet the often contradictory demands of good stability, resistance, seakeeping, manoeuvring and so on. As well as constructing a vessel that meets these demands, ships are usually built without the luxury of a full-scale prototype and must essentially be 'right first time'. Whilst most aspects of the performance of the ship can be measured

clearly with calm water trials, seakeeping trials have remained the most difficult to report and interpret in an objective and scientific way.

Model tests always have a fundamental degree of uncertainty because of the assumption that Froude scaling gives the correct balance of forces on the model, but also because of other non-geometrical factors. For example, typical towing tank tests constrain the model in surge – clearly the heave and pitch motions are modified, as variance in the forward speed of the ship is not modelled. The motions of free manoeuvring models rely heavily on the propulsion and autopilot characteristics – it is difficult to get reliable figures for in-service ships let alone ships still 'on the drawing board'. Tests at higher speeds in beam and quartering seas are also notoriously difficult because test basins have a finite width in which the model may only encounter a small number of waves during the test. Furthermore, using model roll results may be fundamentally flawed as roll damping is principally a viscous effect (forces due to water as a fluid) whereas the Froude scaling rationale correctly models gravitational forces (i.e. the waves).

Ship motion theories are almost invariably validated against the results of model tests rather than full-scale trials, yet ship motion prediction is often regarded as a reasonably mature science. Most ship motion codes do not give good predictions compared with model tests in quartering and following seas, particularly for roll motions. It may be that there is a strong link with the inherent difficulties in conducting model tests noted above. This author contends that every effort should still be made to quantify the seakeeping of ships at full-scale.

1.3 Scope of Thesis

Figure 1.1 illustrates aspects of full-scale ship behaviour in waves addressed in this thesis. The major difficulty in making seakeeping trials is that many variables affect the behaviour of the ship in a naturally occurring seaway, some of which may also be difficult to measure. This thesis suggests that the intellectual effort made in developing ship motion theories is not matched by the effort in validating them. In the literature in general, this shows as a lack of sophistication when attempting to validate theory with

full-scale results, both in the practical use of such computational models and the conduct and interpretation of full-scale trials. This thesis goes on to demonstrate how some of the uncertainties can be accounted for.

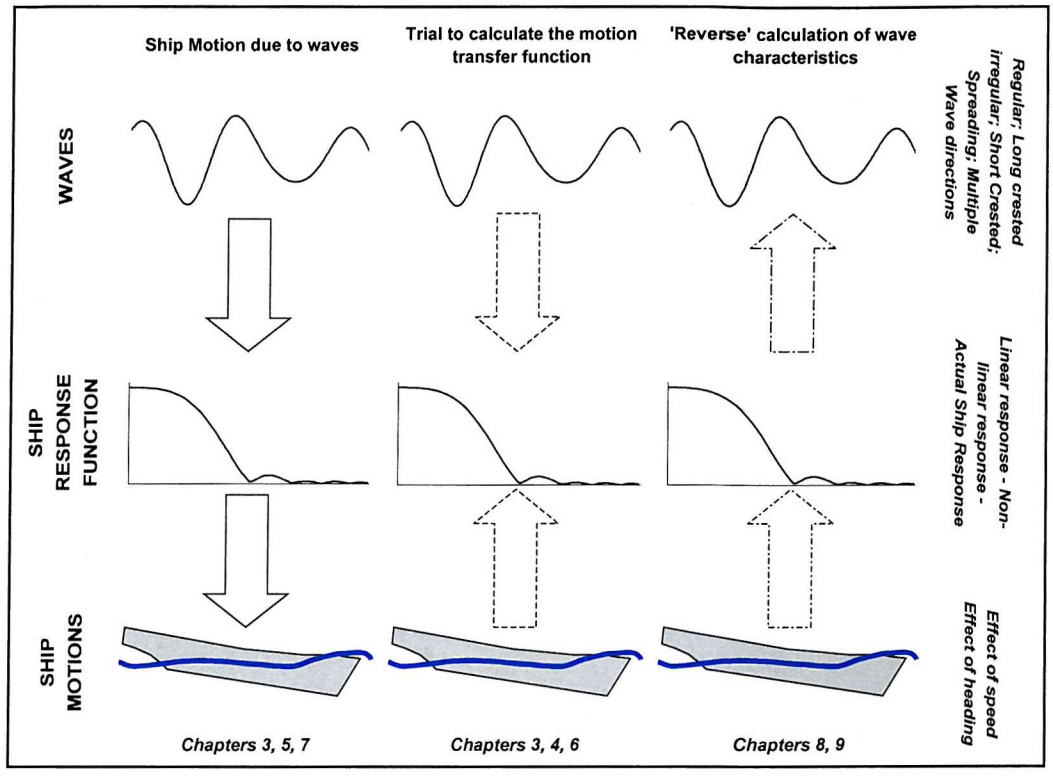

Figure 1.1 Ship behaviour in waves – summary diagram

Assessment methods are commonly based on a linear theory of ship motions - sea state, ship motion, and transfer function are all interrelated as shown in Figure 1.1. On the left-hand side of Figure 1.1, seakeeping software typically employs computation of the transfer functions from hydrodynamic principles, and application of a known sea description to yield the ship motions. Ship trials usually involve a direct measurement of the sea state and the ship motions, important in their own right, from which the transfer functions may be calculated.

Perhaps the major uncertainty to deal with for trials in naturally occurring seaways as opposed to most model test tanks, is that the ship may encounter waves from several directions simultaneously. The wave content of the seaway has a particularly important effect on the ship motions, in addition to the essentially fixed properties of the ship such as hull shape and mass distribution. The nature of sea waves is extremely complex and

has been the subject of a leap in understanding over the past fifty years or so with parallel development of measuring devices, and of several alternative theoretical models. Measuring ocean waves, and in particular their direction of travel, is itself a difficult task due to the harsh environment and the effect of tides and water depth. These techniques will be reviewed in Chapter 2.

The literature review in Chapter 2 will also show that although the complex nature of sea waves is often mentioned by authors and cited as a reason for disagreement between full scale and theoretical or model results, there is little in the way of treatment of full-scale or predicted data to properly explain the discrepancies. Though some papers do show quantitative approaches, these are not routinely used by the naval architect. This thesis will demonstrate some ways in which this complexity may be dealt with. One way is how the sea trials themselves are conducted, and a case is made for a specific ship evolution in Chapter 3. The beneficial effects of this evolution can be seen in Chapter 5 where trials results for several ship types are presented.

Analysis of ship trials to deduce the transfer functions, and computer ship motion calculations, usually involve some simplification of the directionality of the seaway. The consequences of such simplifications are considered in Chapter 4. It is often assumed that there is some minimum seaway to generate significant motions, but a criterion or even a rule of thumb has never been documented in procedures or the literature. This chapter aims to deduce guidelines for the sea conditions where the simplifications hold.

Ship sea trials are considered further as they usually present a unique set of uncertainties from which firm conclusions are required. Uncertainty arises in important characteristics defining the exact condition of the ship, for example its displacement and the location of the centre of gravity. These are naturally difficult to measure for such irregularly shaped and massive objects. Consideration is given in Chapter 6 to the sensitivity of computations to such uncertainties.

Ship motions are also heavily dependent on the waves which are encountered. The wave heights, period, direction, water depth and speed of encounter all affect the behaviour of the ship. Computational methods usually involve some simplification of the actual wave

spectra that occur in the ocean, for example smooth wave spectral models of fully developed wave systems, and the effects of such simplifications are considered. In Chapter 7, an advanced technique for calculation of transfer functions in arbitrary rather than simplified sea states is demonstrated.

The 'reverse calculation' on the right hand side of Figure 1.1 is made in Chapter 8 to calculate basic characteristics of the seaway based upon the ship motions, as if it were effectively a moving wave buoy. Separately, Chapter 9 continues this theme, applying the techniques developed for Chapter 7 to calculate the seaway characteristics in fuller detail. The characteristics of the ship motions in natural seas play a crucial part in the possibility of success for this research.

1.4 Summary of objectives

Without strong guidelines on the conduct of seakeeping trials, this has inevitably become a grey area, so much so that seakeeping trials have not featured as part of the acceptance process for recent Royal Navy vessels, for example. Chapters 3 to 7 are ultimately aimed at making demonstration of the seakeeping ability of new designs with sea trials less of a subjective process, and helping seakeeping performance take a more accountable place in the procurement and acceptance cycle. Chapters 8 and 9 aim to extrapolate the detailed knowledge gained from trials to provide advice during routine operations. These aims may be summarised by the following objectives for the thesis:

- Establish a rationale for seakeeping trials that has provision for the effects of short crested and multimodal natural seas.
- Show how uncertainty in the properties of the ship and the wave environment may be reflected in ship motion models.
- Demonstrate the effect of short crested and bimodal wave spectra on ship motions.
- Demonstrate the calculation of Response Amplitude Operators from sea trials.
- Demonstrate the calculation of wave characteristics based on the motions of the ship in natural seas.

2. LITERATURE REVIEW

2.1 Describing Natural Seas

A major theme of this thesis is that the behaviour of ships at sea is complex compared with the behaviour of ship models in a ship tank or basin. It is suggested that this is largely a consequence of the complexity of the natural seaway itself. In order to appreciate the meaning of a 'natural' sea, and hence the interpretation of wave data from trials, it will be useful to highlight relevant points from the field of oceanography, having roots stretching over the last 150 or so years.

The subject area is large, covering areas such as non-linearity, extreme wave statistics, shallow water effects and mechanisms of generation. Kinsman (1965) gives an excellent introduction, and Cartwright (1974) gives a review of the major topics up to 1974, whilst Komen et al. (1996) collect more up to date accounts from distinguished authors. Tucker (1991) gives the salient points treated from the point of view of the scientist or engineer. Seakeeping texts such as Lloyd (1998) give even more simplified treatments, limited to deep water, for example, and ignoring the effects of tide and current.

Sea waves are composed of a large range of frequencies, from very low frequencies of the large 'waves' which are the solar and lunar tides, down to tiny capillary waves of frequencies 10Hz or greater. Of principal interest to the maritime community are gravity waves of frequencies of the order of 0.1Hz.

The gravity waves present at a point in the ocean may be composed from two sources. 'Swell' waves of frequency <0.05Hz and wave lengths of many tens of metres may be present which can have originated in storms thousands of miles away. They can travel vast distances across the oceans as these low frequencies are not subject to large dissipative processes.

The second contribution, due to the locally present wind, is usually of more concern to the seaman in rough weather. No theory of the mechanism of generation of waves by the

wind has been universally adopted, but it is clear that development of waves requires some distance of undisturbed water surface ('fetch') and some time period with the wind blowing consistently. There is an equilibrium where energy lost is equal to the energy supplied by the wind, for constant wind speed and fetch, and in this case the sea state is said to be 'fully developed'. Energy is lost by the breaking of steep waves, from viscous effects, and indirectly by the non-linear transfer of energy between frequencies.

The simplest representation of waves is the regular wave, characterised by period or frequency and amplitude or height. Waves propagate in a single direction, so they may be known as 'long crested' regular waves. In deep water (or equivalently for low wave heights), the wave profile is approximately sinusoidal and the wave group velocity is dependent on the period. In general, however, wave crests tend to be sharper than troughs and the group velocity is dependent on depth as well as period.

The next stage in complexity is to consider a linear superposition of many regular waves. If the waves all travel in the same direction, they will still be long crested, but with a large number of waves the profile will be random. It is convenient to consider natural seas in this way. Given a randomly varying wave surface (which it can be shown has a virtually Gaussian distribution of amplitude), it is of principal interest to deduce the relative number of waves present at each wave frequency - equivalently, the form of the energy spectrum. Statistical analysis of the wave surface was pioneered by Longuet-Higgins (1956).

2.1.1 Wave spectra

Environmental conditions at the sea surface are constantly changing, but consideration of the wave energy spectrum typically shows relatively smooth distributions which are narrow banded - most energy is concentrated in a small band of frequencies. Furthermore, spectra may stay relatively constant over time periods of the order of hours and over areas of hundreds of square miles.

This is particularly useful to the ship designer attempting to make sense of the apparently confused sea surface, and much effort has been devoted to developing simple formulae

which describe the form of the wind generated, long crested wave energy spectrum in terms of observable parameters. Useful formulae have been adopted which can be applied in different conditions of fetch; unified theories have not been fully successful so far.

Phillips (1958) derived a simple spectral form S [m^2/Hz] given only the mean wind speed v [m/s]:

$$S(f)=\begin{cases}\dfrac{0.005g^2}{(2\pi f)^5} for f > \dfrac{2\pi g}{v} \\ 0 for f < \dfrac{2\pi g}{v}\end{cases} \qquad \ldots(2.1)$$

This formulation assumes no energy below the peak frequency, which is clearly an over simplification.

The fifth order hyperbolic 'tail' in frequency is in fair agreement with observations, though there is good evidence that f^4 is a better description in the central peak 'energy containing' area of the spectrum e.g. Donelan (1985). Arguments for the tail shape are based on energy conservation principles, but are difficult to prove or disprove empirically for the small, high frequency waves well beyond the spectral peak.

One of the most successful attempts to provide a unidirectional spectrum was the Pierson-Moskowitz (1964) spectrum which is still widely used:

$$S(f)=\frac{0.00810g^2}{(2\pi f)^5} exp\left(-0.74\left(\frac{g}{2\pi f v}\right)^4\right) \qquad \ldots(2.2)$$

$$v^2=\sqrt{\frac{0.74}{0.0081}}\frac{gH_{1/3}}{2} \qquad \ldots(2.3)$$

$$H_{1/3}=\frac{0.1962^2}{f_m{}^2} \qquad \ldots(2.4)$$

Here the wind speed v [m/s] is defined as the mean speed at 19.5m above the mean surface level. Particularly useful here are the relationships between v, $H_{1/3}$ and f_m which can be interchanged depending on which is available.

The modal frequency f_m is the most common wave frequency (the spectral peak frequency of an ideal spectrum). $H_{1/3}$ is the significant wave height which is defined as the mean amplitude of the one third highest waves present. More practically, Cartwright and Longuet-Higgins (1956) showed that for narrow banded spectra $H_{1/3}$ can be related directly to the total energy in the wave system:

$$H_{1/3} = 4\sqrt{m_0} \qquad \ldots(2.5)$$

m_0 is the zeroth moment of the wave energy spectrum, and is obtained by integration of the spectrum.

$H_{1/3}$ is approximately the wave height that is reported by human observers, who tend to ignore the contribution of high frequency (smaller) waves.

The Bretschneider (1959) spectrum, also adopted by the ITTC and known as the 'ITTC two parameter spectrum', gives the form of the fully developed open ocean spectrum S(f) as a function of wave frequency f given significant wave height $H_{1/3}$ and modal frequency f_m of the waves:

$$S(f) = 0.313 H_{1/3}{}^2 \frac{f_m{}^4}{f^5} \exp\left(-\frac{5}{4}\frac{f_m{}^4}{f^4}\right) \qquad \ldots(2.6)$$

Another example is the Joint North Sea Wave Project (JONSWAP) spectrum, the result of an extensive multinational effort to measure wave development in the German Bight [Hasselmann et al. (1973), Ewing (1974)]. In this case, fetch is much less than in the open ocean, and the spectral peak is sharper (Figure 2.1). The formulation may be expressed as:

$$S(f) = 0.206\, H_{1/3}{}^2 \frac{f_m{}^4}{f^5} \exp\left(-\frac{5}{4}\frac{f_m{}^4}{f^4}\right) \gamma^{\exp\left(-\frac{(f-f_m)^2}{2\sigma^2 f_m{}^2}\right)}$$

$$\sigma = \begin{cases} \sigma_a & for\ f < f_m \\ \sigma_b & for\ f > f_m \end{cases} \qquad \ldots(2.7)$$

$$typical\ values\ \gamma = 3.3, \sigma_a = 0.07, \sigma_b = 0.09$$

This spectrum is very similar to the Bretschneider spectrum except for a numerical factor and the factor gamma. This is a shape factor serving to make the JONSWAP spectra more highly peaked than the equivalent Bretschneider spectra for similar $H_{1/3}$ and f_m. Though formulated specifically for the North Sea, this spectrum can be widely applied in any sea area with limited fetch. Both the Bretschneider and JONSWAP spectra retain the f^5 tail.

Amongst other well known spectral formations are the Darbyshire (1952) spectrum, with wind speed as the only parameter, and the Neumann spectrum (1953), also with wind speed the only parameter.

2.1.2 Wave spectra with spreading

These are all unidirectional spectra, describing long crested random seas in deep water. The next stage of complexity is to introduce 'spreading' of wave energy over different directions which leads to 'short crested' seas.

Though wind generated long crested seas are a useful modelling tool, they hardly ever occur naturally, if at all. The wind does not blow in a constant direction, though there may be a definite main direction, and this leads to a spread of wave energy over a few tens of degrees about a central direction (which is usually the wind direction). Figure 2.2 gives an example of a spread spectrum.

The approach to representing the spread spectral energy distribution $S(f,\chi)$ [m^2/Hz/deg] adopted by most sources is to multiply the unidirectional spectrum S(f) [m^2/Hz] by a spreading function $G(\chi)$ [deg^{-1}] and a normalising factor $W(\chi)$:

$$S(f,\chi) = W(\chi)\,G(\chi)\,S(f)$$
$$\int W(\chi)\,G(\chi)\,d\chi = 1 \qquad \ldots(2.8)$$

The normalisation is to ensure that the total energy contained in the spread spectrum is equal to the energy contained in the parent unidirectional spectrum. χ is the wave direction relative to the primary wave direction.

Several forms of the spreading function $G(\chi)$ have been proposed [see Goda (1998)] with the aim of producing the best agreement with measured data.

The formulation:

$$G(\chi) = \begin{cases} \frac{2}{\pi}\cos^2\chi & for\ |\chi| \le 90^o \\ 0 & for\ |\chi| > 90^o \end{cases} \qquad \ldots(2.9)$$

is most widely used in the ship design community and known as the 'cosine squared' spreading function, originally used by Pierson, Neumann and James in the 1950s. The directional spectrum in Figure 2.2 is a Bretschneider spectrum with cosine squared spreading.

More advanced spreading functions are allowed to vary with frequency as well as with offset from the primary direction.

Half cosine type spreading functions are present in the literature:

$$G(\chi) = \frac{2^{2s-1}}{\pi}\frac{\gamma^2(s+1)}{\gamma(2s+1)}\cos^{2s}\frac{\chi}{2} \qquad \ldots(2.10)$$

where s is a spreading parameter and γ is a function. The main advantage of this spreading function is that wave components are not constrained to ±90°, but are allowed

to exist over a full ±180° - which is necessary for some wave data sets measured in the field. s may be set with some frequency dependence such as:

$$s = \begin{cases} s_{max}(f/f_m)^{2.5} & f \le f_m \\ s_{max}(f/f_m)^{-5} & f > f_m \end{cases} \qquad \ldots(2.11)$$

$$s_{max} = 10 \text{ for wind waves}$$

Donelan et al. (1985) used a hyperbolic secant squared for analysis of wave data from the Great Lakes:

$$G(\chi) = \frac{1}{2}\beta \operatorname{sech}^2(\beta\chi) \qquad \ldots(2.12)$$

The spreading parameter β is also dependent on frequency as well as wave direction.

Another spreading function with frequency dependence is the 'wrapped-normal' spreading function:

$$G(\chi) = \frac{1}{2\pi} + \frac{1}{\pi}\sum_{n=1}^{N} \exp\left(-\frac{(n\sigma)^2}{2}\right)\cos n\chi \qquad \ldots(2.13)$$

$$\sigma^2 = \int (\chi - \bar{\chi})^2 G(\chi) d\chi$$

σ is the standard deviation of the directional spreading function. The second equation defining σ^2 must still satisfy the normalisation condition, which occurs for ±180° about the primary direction. Equation 2.13 actually contains the definition of angular spreading, an indicator of practical use in analysis of waves measured in the field and usually requiring involved calculation to deduce. This formulation gives the spreading by a simple statistical analysis.

2.1.3 Multimodal spectra

The spreading functions in 2.1.2 are applied to unidirectional spectra to give short crested properties. They are unimodal spectra, and the final step in representing the general situation in the seaway is to integrate one or more secondary spectra together with the primary wind driven wave spectrum. The swell waves may arrive from completely different directions to the wind wave direction and each other. Figure 2.3 gives an example from the English Channel where swell and wind waves are nearly 90° apart. Beal (1991) reports on the results of an extensive survey of wave spectra 'LEWEX' off the Atlantic coast of Canada, and contains many examples of well spread, multimodal spectra.

Recent research e.g. Young et al. (1995) indicates that the spreading of purely wind driven spectra is a minimum at the peak frequency, but is naturally bimodal at high frequencies beyond $f=1.7f_m$. This is unlikely to be of great interest to the naval architect, however, as there is little energy present in the wave spectrum at these frequencies.

Development of parameterised spectral formulae to deal with the generalised multimodal situation has so far been made through the approach of summation of individual parameterised components. Ochi & Hubble (1976) showed how meaningful results could be obtained by summing two 3-parameter long crested wave spectra, giving a possible tetramodal directional spectrum. Juszko & Graham (1993) extended this model to 10 parameters including spreading components. They fitted the model to a data base of 4300 ocean wave spectra gathered over 3 years, obtaining 'good' fits for 92% of them.

This section concludes with the suggestion that the development of parameterised spectra for long and short crested unimodal random seas is a mature science. The extension to bimodal seas and greater is still undergoing an evolutionary process.

2.2 Ocean wave measurement techniques

This section will deal with the practical instrumental techniques for measuring ocean waves *in situ*. The simplest measurement involves obtaining purely the wave elevation time history at a single point, which gives frequency and periodic information, but does not give any evidence of the directions from which the waves arrive. Directional wave information is of interest for this thesis and more sophisticated instruments and techniques will be reviewed.

Panicker (1974) gives a good review of the available techniques which he classified as 'Direct Measurement' by array and by a buoy, and 'Remote Sensing' by optical, photgrammetric, optical analogue and electromagnetic wave backscatter techniques. The 'direct measurement' type involve measurement of the wave elevation and slope at essentially a single location, with integration over a period of time to obtain the wave directional statistics. The 'Remote Sensing' type measurements typically involve measurement of the wave elevation profile over a large area at a single instant in time, with integration over the area covered to deduce the directional statistics. Mention of the established 'Shipbourne Wave Recorder' is omitted by Panicker (1974) as the measurements are not directional; this is discussed further in section 2.2.4.

The techniques reviewed in Panicker (1974) have remained in essence largely unchanged, though naturally some have been more popular than others because of such factors as cost, ease of use, reliability and accuracy. A few new techniques may be added. In particular, satellite technology has had a major impact, and altimetry by radar from orbiting satellites has become a practicality. Also the GPS (Global Positioning Satellite) system has been used within wave buoys for motion measurement.

2.2.1 Arrays

A wave measuring array consists of an arrangement of at least 3 devices that each measure purely wave elevation. It can be used to deduce directional spectra because there are phase differences in the wave elevation measured at the points compared with each other.

The most common devices used for arrays are wave staffs and bottom mounted pressure transducers. Wave staffs consist of pilings mounted vertically from the sea bed. This limits the depth which they may be used at to a few metres, so they may be used in shallow coastal waters only. The actual wave height measurement is achieved using long parallel wires mounted along the length of the staff. An electrical potential is set up between the two wires from the top. The resistance or capacitance properties of the system vary according to the height of water on the staff. This is essentially the same instrument used in model test basins.

Bottom mounted pressure transducers have the advantage that they may be used in deeper water, several tens of metres. Pressure can be measured *in lieu* of wave elevation as it is linearly dependent on the height of the water column above a transducer.

The array is either in a line or in some sort of polygonal pattern in order to allow calculation of the directional wave spectrum. The line array has some ambiguity of wave direction, and so polygonal arrays are more popular. Barber (1954) was the first to obtain wave direction from a wave staff array.

A fixed spacing between detectors tends to optimise detection of wavelengths of double the spacing, and so arrays tend to be constructed with a range of spacings. Irregular spacing is also used as analysis is by Fourier methods, where in effect simultaneous equations constructed of the Fourier coefficients of the spectra recorded at each location are solved. Irregular spacing ensures that the simultaneous equations are linearly independent.

Arrays consisting of equilateral triangles, pentagons and stars with a range of numbers of recorders are reported in the literature since the 1950s. As the directional accuracy of the array is related to the number of recorders present, the number of staffs or transducers employed has tended to increase. For example, Fernandes et al. (2000) used a 15 pressure transducer array consisting of two crossed lines that was used in a coastal location with 8m water depth, one line approximately 140m in total and the other 300m. The smallest transducer separation was around 5m and the largest around 100m. Their

use to deduce directional spectra relies on the arrangement of a group of at least three staffs such that there are phase differences in the elevation measured at the different staffs compared with each other. The angular resolution is less than 3 degrees, and the highest frequency measurable around 0.3 Hz.

2.2.2 Optical techniques

In 1949 Barber (1949) showed that directional information could be derived from photographs of the sea surface, but he was unable to obtain wave height information; this step was made by Stilwell & Pilon (1974), who demonstrated wave parameter derivation with pictures taken with a 35mm camera from a tower 19m above sea level. When the negative is illuminated with monochromatic collimated (laser) light, a lens acts as a physical Fourier transforming device with a definite transfer function. The light intensity in the image produced is proportional to the wave spectral energy density.

The technique is sensitive and requires low wave slope amplitude, even illumination of the wave surface and low haze. Also wave whitecaps occurring with winds greater than around 12m/s interfere with the process. Despite advantages of accuracy and physical robustness, and the efficiency of film as a data storage medium, this method has not become popular as results cannot be supplied 'live' nor logged directly by computer.

A further optical technique was used by the Stereo Wave Observation Project of the mid 1950s, which actually gave the first calculation of a wave directional spectrum measured in the field. Kinsman (1965) gives a good summary. Simultaneous photograph pairs were taken of the sea surface, one photo from each of two aircraft, covering an area about 900 x 600m. Stereo photos give the image depth. Careful synchronisation of the aircraft altitude and heading was necessary, and synchronisation of the shutter trips by radio link. In addition, a ship towing a marker buoy at a known distance from the ship was required to give the pictures a scale. Laborious processing of the images was required, and only two of one hundred photograph pairs were deemed suitable. The technique is subject to ambiguity in the direction in which the waves are travelling - it is impossible to tell whether the front or back face of the waves is illuminated, which means it is unsuitable for many ocean situations where swell is superimposed on a local wind generated sea.

Though the project was successful, the amount of resources required meant that there were few further attempts to use the technique.

2.2.3 Buoys

Wave buoy systems measuring point wave height have been used for many years for wave height measurement. A buoy typically consists of a spherical body around 1m in diameter, moored in the sea and containing a vertical accelerometer. Accelerometer signals are either radioed to ship or shore, or acquired via umbilical cable. The signal is double integrated to obtain a displacement time history.

Enhancement of the wave measuring buoy to obtain directional characteristics was first performed by Longuet-Higgins et al. (1961). They used a disc shaped buoy of about 1.5m diameter which had roll and pitch gyros installed, as well as an accelerometer, gimballed so that it measured vertical acceleration to a first approximation. These are generically called "PRH" (Pitch, Roll, Heave) buoys. A sensitive barometer was also installed, though not used for the directional wave analysis. The buoy was tested in a ship tank to measure its frequency response, and RAOs and phases were derived which can be used to correct the measured time histories or motion spectra.

Longuet-Higgins et al. (1961) defined the following Auto- or Cross- (C_{ij}) and Quad- (Q_{ij}) spectra of the heave, roll and pitch time histories:

$$C_{11} = \int_0^{2\pi} F(\omega,\chi)d\chi \qquad \ldots(2.14)$$

$$C_{22} = \int_0^{2\pi} k^2 \cos^2\chi F(\omega,\chi)d\chi \qquad \ldots(2.15)$$

$$C_{33} = \int_0^{2\pi} k^2 \sin^2\chi F(\omega,\chi)d\chi \qquad \ldots(2.16)$$

$$C_{23} = \int_0^{2\pi} k^2 \cos\chi \sin\chi F(\omega,\chi)d\chi \qquad \ldots(2.17)$$

$$Q_{12} = \int_0^{2\pi} k\cos\chi\, F(\omega,\chi)d\chi \qquad \ldots(2.18)$$

$$Q_{13} = \int_0^{2\pi} k\sin\chi\, F(\omega,\chi)d\chi \qquad \ldots(2.19)$$

where $F(\omega,\chi)$ represents the directional spectrum, ω is frequency, χ is azimuth angle, and k is the wave number. The right hand sides of these equations may be related to Fourier Coefficients:

$$a_n + ib_n = \frac{1}{\pi}\int_0^{2\pi} e^{ni\phi} F(\omega,\chi)d\chi \qquad \ldots(2.20)$$

and it can be seen that:

$$a_0 = \frac{1}{\pi}C_{11} \qquad \ldots(2.21)$$

$$a_1 = \frac{1}{\pi k}Q_{12}, \quad b_1 = \frac{1}{\pi k}Q_{13} \qquad \ldots(2.22),(2.23)$$

$$a_2 = \frac{1}{\pi k^2}(C_{22} - C_{33}), \quad b_2 = \frac{2}{\pi k^2}C_{23} \qquad \ldots(2.24),(2.25)$$

which form the first five terms of the Fourier expansion of $F(\omega,\chi)$:

$$F(\omega,\chi) = \frac{1}{2}a_0 + (a_1\cos\chi + b_1\sin\chi) + (a_2\cos 2\chi + b_2\sin 2\chi) + \ldots. \qquad \ldots(2.26)$$

Hence the directional spectrum may be calculated from the motions of the buoy - assuming that the higher order Fourier terms are negligible.

Longuet-Higgins et al. (1961) actually calculated the directional wave spectrum with a weighting function to prevent negative values that would appear with the direct expression; the energy spectrum is essentially positive. The weighting function was used at the expense of reducing the angular resolution of the technique to 135 degrees from 72 degrees; the PRH buoy is not a sensitive device for measuring the directionality of bimodal spectra. In addition the authors derived expressions for the average direction of

the wave spectrum, and the spreading of the wave spectrum in terms of the Fourier coefficients, and also a peakiness factor. Much work was done in subsequent years on understanding the physical meaning of such parameters, and several alternative expressions have been developed.

Improvement of the directional resolution of buoys may be obtained by extending this technique to include higher harmonics in the Fourier expansion. In practice, this means measuring more derivatives of the wave surface to generate more Cross-spectral terms. Cartwright first extended the buoy technique using a 'cloverleaf' buoy with three lobes, which measured vertical acceleration, roll and pitch, and also the three components of wave surface curvature. Mitsuyasu (1975, 1980) in particular championed this buoy which could be used to find the directional spectrum up to the fourth harmonic of the Fourier expansion. However, high sampling rates are required to capture the high frequency wave slope time histories, requiring more power than the conventional PRH buoys, and the cloverleaf buoy has not become commercially successful.

The quality of PRH buoy data is largely dependent on ensuring that the acceleration is truly measured vertically and not aligned with the wave slope, which has resulted in much refinement of methods of mounting the accelerometer within the buoy and damping its motion appropriately. Onboard compasses are used to measure azimuthal angle - Longuet-Higgins et al. arranged for their buoy to align with the wind direction for their relatively short acquisition times.

With relatively low cost, robustness, easy deployment and reliability, the wave measuring buoy has become the most common device for measuring directional waves. Buoys of the order of 1m diameter have become popular for marine engineering applications; in Europe the Datawell Wavec and Waverider buoys have become particularly well known, and in the US the Endeco Wavetrack buoy.

In 1995 Seatex launched the Smart800 buoy which replaces the gyros and accelerometers of other buoys by a DGPS (Differential Global Positioning Satellite) system. Triangulation between the orbiting satellites and a known fixed location on land

gives the buoy motion displacements, and Fourier techniques similar to those for other buoys can then be applied to deduce the directional spectrum.

Alternatives to PRH buoys developed over the years have used the same Fourier analysis methodology of Longuet-Higgins et al., but different measured parameters. For example, two components of wave orbital velocity may be used, measured with current meters, or the buoy may be designed to follow and measure the wave slope.

The US NOAA operate a large fleet of moored buoys around the coastal United States through their National Data Buoy Center (NDBC). These buoys measure a variety of environmental properties, and a handful of them make directional wave measurements. The buoys are somewhat larger that those described already, between 1.5m and 12m in diameter, as they may be required to operate untouched for several years. The historical wave data are available freely over the internet, representing perhaps the most extensive repository of directional wave information in the world.

PRH buoys are still the subject of much development and improvement and there are some contentious issues - see Earle et al. (2000) for example. These include the signal processing techniques used to integrate the vertical acceleration, and derive the Cross- and Quad- spectra, the use of (cheaper) accelerometers which may not maintain a vertical attitude very well, the effects of currents, the influence of moorings, and the application of the buoy RAOs and phases.

2.2.4 Backscatter techniques

Radar altimeter measurement of the ocean surface from satellites has become a well established technique for measuring wave heights since the first demonstration on Skylab in the mid 1970s. The US GEOSAT was later launched as a dedicated remote sensing satellite. In Europe, the ERS-1 satellite has provided many years of data, and the ERS-2 satellite currently transmits on a regular basis. The other current satellite with an altimeter is the joint US/France satellite named Topex/Poseidon.

The altimeter emits a radar pulse directed at the ocean surface, and the reflected signal measured back at the satellite is analysed. Bragg scattering is the principal type of interaction of the radar wave with the ocean waves. Calm water gives a strong, sharp return pulse, whereas for a highly wavy surface the return signal is smeared. The degree of smearing is linearly related to the significant wave height to high accuracy, and so a calibration is possible.

The basic system is accurate to the greater of 0.5m or 10% of $H_{1/3}$ [Carter et al. (1995)]; this represents a large uncertainty for lower sea states in particular. In practice, altimeter measurements are further calibrated against data from wave buoys, which reduces the error to the order of 0.2m.

Satellite altimeters by their natural global coverage are excellent devices for compiling global wave statistics. However, they provide no information on wave direction, and typically the satellite only passes over the same point of the ocean once every several days, so there are major drawbacks for use on ship trials.

This is illustrated in Beal (1991), pp128-133, where GEOSAT altimeter results were calculated for the extensive 1987 Canadian LEWEX trials. The satellite tracks passed closely to the ship only twice during the seven day trials, and the sampling of the wind environment was also too sparse to form the basis of predictive wave models.

Another airborne wave measurement method which has had success from satellite platforms is the Synthetic Aperture Radar or SAR. Whereas the altimeter is a low resolution real aperture radar, SAR uses the distance travelled between pulse emission and reception, for a large number of signals, to effectively increase the aperture and hence the resolution of the images obtained. In fact one early demonstration of SAR was made from a van travelling on straight island runways alongside the sea [Teague et al. (1973)] before airborne and then spaceborne measurement became possible. Satellite measurement became available with the launch of SEASAT in 1978 and ERS-1 in 1991. The effect of wind is significant and processing of SAR images to produce directional wave spectra is difficult [Hasselmann & Alpers (1981)] with effects such as 'velocity bunching' to deal with, and interpretation of results which appear to depend on wave

slope rather than wave height, but where the detailed interaction of the radar waves with the water surface is not fully understood. Whilst the resolution and coverage provided by the satellite flight path are extremely attractive, the intellectual and computational effort required means that SAR measurements are not routine.

Electromagnetic (EM) wave backscatter may also be employed from ground (or sea) level. For example, Hisaki (1996) reports analysis of the backscatter spectra received at a radio observatory at a range of some 16km, using High Frequency radar. Since wave crests facing the source reflect the EM radiation more strongly than those facing at other angles, and much more strongly than troughs, with appropriate frequency analysis of the received signal it is possible to calculated the directional wave field. Inevitably there are some sources of error, such as the shadowing effect where a large wave crest may hide crests behind it, and currents may introduce an error due to Doppler shift. More importantly, and in common with other techniques, there remains a 180 degree ambiguity in the predicted spectrum - it is impossible to calculate whether a strong backscatter has been received from the back face of a receding wave or the front face of an approaching wave.

2.2.5 Ship mounted systems

Radar backscatter has been employed from ship mounted systems, for example the Canadian Macradar system and the Dutch SHIRA system. Indeed, in recent years, systems have become commercially available, notably the Norwegian Wavex system marketed by MIROS. This makes use of standard ship radar heads that typically scan an area of some 1.5 miles radius around the ship. The image displayed on the radar monitor is captured by a PC for analysis by the Wavex software. The radar head is located as high as practically possible on the ship, to minimise shadowing effects by the ship superstructure. Remaining areas of 'shadow' may be discounted from the analysis; these depend on the exact siting of the radar head on they ship but one may wish to account for reflections from a funnel for example. Figure 2.4 shows a typical Wavex display screen: the radar image captured, the directional spectrum (which always displays 180 degree ambiguity) and wave parameters such as significant height and period deduced from the spectrum.

Another ship borne wave sensor is the American "TSK" bow mounted radar, manufactured by TSKA Inc. TSK is mounted on the ship's stem head and consists of a downward facing Doppler microwave unit together with a gimballed accelerometer sensitive to vertical motions. The radar measures the relative velocity between stem head and wave from the time of back scatter, and the signal is integrated to obtain the relative motion displacement. The accelerometer signal is double integrated to give bow displacement above its mean level. Subtraction of this displacement plus the freeboard at the stem head from the relative motion should give the wave amplitude beneath the bow. The wave amplitude may be acquired as a time history and appropriate statistical and spectral analysis performed to give the overall wave parameters. The TSK is effectively a moving wave probe attached to the ship, and does not give directional information about the waves.

Dipper (1997) describes wave measurements during sea trials of the first of class SWATH ship USNS VICTORIOUS T-AGOS 19. The ship was equipped with a range of accelerometers, gyros, and strain gauges for motion measurement; waves were measured with a TSK system and occasionally with Endeco wave buoys. The TSK system gave good agreement with the buoy data, however it is noted that all the reported wave data was acquired at near zero speed in head seas.

In the 1950s, Tucker (1952, 1956) developed a shipbourne wave recorder (SBWR) which measured relative wave height using pressure transducers mounted below the ship waterline, and accelerometers to measure the vertical displacement. Two pressure transducers were used, port and starboard, and the average pressure time history used (which removed some errors due to the presence of the hull). In a similar way as for the TSK, the accelerometer signals were double integrated and combined with the relative height measurement to give an approximation of the true wave time history. The system was installed around half a dozen ships with some success, though calibration against waverider buoy data was necessary, for example Aken & Bouws (1981). Once again, it was necessary for the ship to be stationary in order to take measurements - as much to avoid the problem of calculating the stationary wave spectrum from the encounter spectrum as for the physical effect of forward speed on the pressures recorded. Wave

height and period are typically calculated from combining the SBWR accelerometer (low frequency) and pressure sensor (higher frequency) recordings, but again these are omnidirectional measures.

The SBWR has been most useful for ships permanently on station, and for example has provided many years of wave data at the Channel Light Vessel. Tucker (1991) pp68-73 reviewed the successes and limitations of 35 years use of the SBWR.

2.2.6 Summary

Of all the techniques for ocean wave measurement reviewed here, the waverider buoy remains the optimum for ship trials. The buoy combines accuracy, ease of operation, reliability, portability and reasonable operating costs.

Ship mounted radar systems are catching up fast. They offer the attraction of being able to start a seakeeping trial anytime, anywhere, without the need to deploy and recover a buoy. However, they are still relatively expensive to install, and though directional wave measurement is good, wave height reporting is considered less reliable.

Satellite altimetry may one day offer a viable alternative. Wave height reporting is good, but reliable and detailed directional information is currently not routine to calculate. With only two satellites available, coverage is not extensive. A proposed network of micro-satellites would enable wave measurement at any point of the earth with a repeat period of four hours, just sufficient for seakeeping trials. However, for the next twenty years or so wave measuring buoys will remain the system of choice for seakeeping trials.

2.3 Seakeeping and ship motion trials

This section is concerned with the reporting of full-scale trials in the literature. The papers are reviewed particularly from the perspective of how the issue of the seaway is dealt with. Attention is thus paid to how the wave environment is reported, especially its directionality.

The first papers giving quantitative analysis of seakeeping appeared in the 1950s. Early papers concentrated mainly on the ship motion measurements obtained, and in the absence of reliable and practical wave measuring devices, wave 'measurement' was limited to observation. For example, Williams (1952) reports trials where the seaway was estimated to comprise swell only, and reported wave height and length judged against the size of the ship and the 'mean period of encounter'; the ship motions reported are almost exclusively roll and pitch due to the lack of reliable technology to measure the other degrees of freedom.

Aertssen (1966, 1972) are further examples where ship RAOs have been calculated from the results of ship trials with estimated waves or waves measured by omnidirectional SBWR. The authors were certainly aware of the possible effects of directionality, and indeed care is taken to distinguish observations in swell from those in wind waves (and swell).

Canham et al. (1962) report on seakeeping trials of an Ocean Weather Ship and is an example of excellently conducted trials and analysis. Wave height was measured with the SBWR installed on the weather ship together with two early Longuet-Higgins wave buoys. Ship motions were measured with stabilised accelerometers and gyros. An 'octagon' type trajectory was steamed, with leg time adjusted according to relative heading to the waves.

The trials of Andrew & Lloyd (1977) compared the behaviour of two frigates proceeding side by side in severe head seas of significant height around 7m. An omnidirectional waverider and a directional buoy were deployed, but results were only obtained for the waverider, and only observation of the sea state direction was made: "it was the opinion of personnel on both ships that the waves were strongly unidirectional." Lateral plane motions are not reported to support this, though vertical plane motions show good correlation with strip theory. Goodrich, one of the co-authors of Canham (1962) raises the point in discussion that those trials were conducted in apparently long crested seas, but subsequent wave buoy analysis indicated multi-directional waves.

Hope (1995) reports trials of an Australian offshore patrol boat where the author demonstrates a clear appreciation of the effects of directional waves on the trials results. A waverider buoy was used to give omnidirectional energy spectra, with wave directions deduced from aerial photographs. An example omnidirectional wave spectrum is given that is broken down into a (long crested) wind sea component and seven swell components, and the conversion to encounter spectrum for one run is given. There is discussion of the ship motion energy spectra compared with this encounter spectrum (though the link between angular motions and wave *slope* amplitude spectrum is not made). The possibility of calculation of RAOs is suggested, but this step is not made, and instead the author cites Wachnik & Zarnick (1965) who give RAOs calculated from model basin experiments.

Sandison et al. (1994) report sea trials of a SWATH type ship. A programme of seakeeping trials including runs in 'octagons' are described in general terms. A pair (forward and aft) of omnidirectional TSK radar were used to measure wave amplitude; the low vessel roll is likely to give good performance. Deep consideration of wave directionality and spreading does not appear to have taken place, and omnidirectional TSK wave spectra presented do show some evidence of separate energy peaks. Though care was taken to achieve typical run times of an hour, results at complementary headings (e.g. 30°, 330°) are not presented. The trials results presented show further evidence of spreading, with significant pitch in beam seas and roll in head seas, for example. The global statistical results of the seakeeping runs are extrapolated to make statements about the ship operability rather than to make a more informed approach to operability via extraction of RAOs.

Reed et al. (1997) give results from seakeeping tests of an unusual ship, an 'A-frame' SWATH. An octagonal trajectory is mooted though there is no illustration and it is not clear if a full set of reciprocal headings were tested (i.e. 180° to 360° as well as 0°-180°). Wave height was measured with the omnidirectional TSK only, commendably at zero speed to negate encounter frequency analysis, but occasionally in beam seas for the same reason; in this candidate's experience ship roll seriously affects TSK wave height accuracy. A long period of time was available for these trials and the methodology was to wait for occasions when a stationary spectrum comprising only long crested waves

was present. Calculation of RAOs appears to be relatively successful except for roll. Much of the discrepancy between RAOs calculated from the trials and computer and model basin tests is attributed to short crestedness, but without directional wave measurement this is not certain.

Hirayama et al. (1997) present advanced analysis of the results of sea trials on a Japanese training vessel. An octagon course is used, which clearly employs separate results from headings around the compass at 45 degree intervals. However only 5 minutes were allowed for runs on each leg. Wave measurement appears limited to analysis of a single radar sea clutter image, which is presented in very fine frequency bands that are difficult to interpret, and a microwave relative wave height sensor.

Data extracted from the winter campaign of a research vessel are reported by Tedeschi (1999). Dedicated seakeeping trials did not take place, but analysis was performed for two speeds when the ship was close to head seas for two days when ERS1 SAR data was available. The satellite provided significant wave height and principal wave direction for comparison with observed (and calculated) values.

The following papers are not concerned with trials but are worthy of mention in this section. Hirayama (1992) and Takezawa & Hirayama (1992) describe experiments with a model underway in a ship tank using directional waves; the target spectrum was Bretschneider form with cosine squared spreading. The directional wave spectrum was calculated from wave height and slope time histories measured with a novel laser based wave height and slope probe. Transformation to encounter wave spectrum is demonstrated for head and following sea cases, and heave and roll frequency responses of the model also presented. Comparison is made with strip theory predictions based on the measured wave spectra, and there is a brief consideration of the effect of the spreading angle on the measured and calculated responses of the ship and also a moored semi-submersible platform model.

Of even greater interest in these papers is the estimation of directional transfer functions based on the motions of the model in the directional waves. The calculations require

estimation of the stationary directional wave spectrum (one of the idealised spectral formulations with spreading function), but potentially may be applied to ship trial results.

The RAO is formulated from

$$M(\omega_e) = \int_{-\pi}^{\pi} S(\omega_e, \chi) |R(\omega_e, \chi)|^2 \, d\chi \qquad \ldots(2.27)$$

where M is the RMS (linear) motion, S the directional wave spectrum, and R the motion RAO. For angular motions a similar expression applies but with the wave *slope* spectrum. The RAO is approximated by a Fourier series

$$|R(\omega_e, \chi)|^2 \approx \sum_{k=0}^{N} a_k(\omega_e) \cos k\chi \qquad \ldots(2.28)$$

and Hirayama describes how a matrix representation of these quantities can be used to solve for the RAO, at each discrete spectral frequency, using a minimisation function. A factor is also introduced to force the solution towards known boundary values e.g. 1.0 for low frequency heave RAO.

The transfer functions were averaged over the results obtained from eight different wave fields (a matrix of four spectra and two spreading functions). The papers give calculated heave and pitch transfer functions calculated for model tests of a SR108 ship in the ship tank, and compare with strip theory predictions. Fairly good qualitative and quantitative agreement is obtained, though heave resonance is much larger than predicted and smooth pitch functions at low frequencies near beam seas are not convincingly reproduced. Results are limited to seas forward of the beam (from head sea tests in the ship tank).

Fryer et al. (1994) describe the testing of a large SWATH model in a sea loch. A wind wave model relating wave heights from an omnidirectional waverider buoy and wind measurements was calibrated prior to the trial, and was used to estimate the stationary directional wave field at the time of the trials. Tests were made at a wide range of headings to the waves. The unimodal but asymmetrical spectrum was transformed into encounter wave spectra for all headings. A method for calculation of transfer functions using a matrix solution of linear simultaneous equations is then described (expanded upon in Chapter 5 of this thesis) that is demonstrated for heave motions of the SWATH

model. Problems of transforming from encounter frequency to actual frequency are noted but ignored in the analysis so that aliasing of the transfer function is present.

To summarise this section, there has been little standardisation in the conduct and interpretation of seakeeping trials, and furthermore there are relatively few trials reported in the literature. Where ship trajectory is reported, an 'octagon' type seems most common. Wave measurement is not usually detailed, sometimes relying on observation only, and often limited to omnidirectional measurement only. Only two papers were found which considered the effect of the wave directionality in some detail – Hirayama (1992) [but for model tests] and Fryer et. al. (1994), which this thesis builds upon. Clearly there is scope for work in this area to pioneer the presentation of trials results in a consistent and rational way, reflecting the properties of natural seas.

2.4 Deducing wave environment from ship motions

The idea of deducing the wave environment from the ship motions, as if it were a waverider buoy, is not new. The Tucker (1956) shipbourne wave recorder already described stirred discussion - however the ship remains stationary. The analysis becomes much more difficult when the ship is underway at any speed because the waves are Doppler shifted depending on the angle of encounter. For water waves the problem becomes more difficult because the wave speed is dependent on water depth, and further complicated because of the 'following seas problem' - for seas abaft the beam, waves *encountered* by the ship at a particular frequency may possibly have originated from source waves with up to three different frequencies.

The theory is well known and given in Lloyd (1989) for example. The wave phase velocity is dependent on depth and wavelength:

$$c = \sqrt{\left[\frac{g\lambda}{2\pi}\tanh\left(\frac{2\pi d}{\lambda}\right)\right]} \qquad \ldots(2.29)$$

and the encounter frequency is

$$\omega_e = \frac{2\pi}{\lambda}(c - U\cos\psi_r) \qquad \ldots(2.30)$$

The equation for phase velocity is not easy to solve, though it may be shown that it tends to more easily manipulated functions in shallow ($d<0.03\lambda$) and deep ($d>0.5\lambda$) water. In deep water the phase velocity tends to

$$c = \sqrt{\frac{g\lambda}{2\pi}} \qquad \ldots(2.31)$$

and encounter and actual wave frequency are related by

$$\omega_e = \omega - \frac{\omega^2 U}{g} cos\psi_r \qquad \ldots(2.32)$$

and so

$$\omega = \frac{g}{2U cos\psi_r}\left[1 \pm \sqrt{\left(1 - \frac{4\omega_e}{g} U cos\psi_r\right)}\right] \qquad \ldots(2.33)$$

Seas forward of the beam give a negative cosine term and hence a one to one relationship between actual and encounter frequency. Seas abaft the beam give a positive cosine term and there are three possible encounter frequencies that may satisfy the relationship.

Figure 2.5 gives some examples. In quartering seas, for instance, waves encountered at 0.05 Hz may originate from one or more of source waves of approximately 0.08 Hz, 0.135 Hz or 0.256 Hz.

Figure 2.6 shows the effect of relative heading for a ship travelling in a long crested Bretschneider spectrum. In beam seas, the spectrum is unchanged. Figure 2.7 extends this type of calculation to show encounter spectra expected from a hindcast directional wave spectrum.

When attempting to use the moving ship as the wave buoy, it is the transformation from the encounter wave spectrum to the stationary spectrum that proves particularly difficult, because of the triple frequency ambiguity of the following seas problem.

A time domain solution is proposed by Webster & Dillingham (1981), which is illustrated for a model with known RAOs in bimodal seas generated in a basin. However, the encounter frequency problem was avoided as the ship is assumed to be stationary.

Iseki & Ohtsu (1994) report trials using a 46m training ship at 13 knots. Only roll and pitch angles were recorded, and the sampling time was only 5 minutes for a small number of straight line runs. Omnidirectional wave height was recorded by a downward facing radar system similar to the TSK system described earlier. The author describes a minimisation method of separating the wave energy into 'relative power' contributions to roll and pitch. Transfer functions calculated using a strip theory are introduced and Bayes error minimisation method is used to solve for directional wave spectra. Three examples (from different ship headings) are given, which agree with the general wave direction from the ship, but are not consistent with each other. There was no alternative wave measurement with which to compare these results.

Iseki (1996) also presents a technique for estimation of stationary wave spectra from measured encounter wave time histories, using Bayes techniques. Assumptions such as spectral smoothness and near zero slope at zero and high frequencies are included in the minimisation, as well as full treatment of triple encounter frequencies in the following seas problem. The technique is demonstrated for following seas tests made on a ship tank carriage at various speeds, and there is successful comparison with the spectra obtained from stationary wave probes. However, extension of the technique for use with spread or multimodal seas is not discussed.

Hua & Palmquist (1995) report on the determination of omnidirectional wave spectra from the motions of a car transportation ship. Calculations from both the linear theory and from a difference minimisation method are given; these result in a wave spectrum calculated for each of the degrees of freedom considered. Though motion data was available for sixteen occasions over a year's operation of the ship, a single example is given where the wave spectra are calculated; the spectra from each source are consistent, and agree with the visually estimated sea state. The authors confess that the example is near ideal, relating to the ship in head seas which were very long crested. The possible

effects of non-linearity (of roll motion), wave spreading and bimodality are discussed, but "following, low and mixed seas are less reliably estimated".

The trials described earlier by Hirayama et al. (1997) were also used for directional wave spectrum measurement by a Maximum Likelihood Method. This is not described in great detail but again appears to produce a wave spectrum derived from each ship motion considered at the particular speed and ship heading. Pitch, roll and vertical acceleration, were measured, and relative motion was recorded at three locations. Results are calculated for a single hour of data, and compared with an attempted analysis of a radar image for direction and frequency. There is some inconsistency between the average directional wave spectra calculated from different ship headings, though the general directions and wave period in general agrees with the radar analysis. The authors conclude that buoy measurements must be made to verify the prediction quality.

Maximadji (1997) presents a method of estimating the wave modal period based on analysis of only the actual ship pitch motion, ship speed and relative heading to the waves. The study is based upon responses to a two parameter spectrum of long crested waves and is based on the notion that the mean recorded pitch period should occur between the natural pitch period of the ship and the modal (encounter) wave period. The technique seems rather unwieldy and was not validated with model or trial data; the effect of spreading or bimodality was not considered.

Tedeschi (1999) presents an estimation of significant wave height and modal period based on the heave and pitch motions of a 119m research vessel. The expected ship motions are calculated using a strip theory program for a set of design points at unit wave height covering a small range of ship relative headings and modal periods for the ship speed in question. The waves are assumed long crested. The results are dimensionalised by the RMS motions measured on the ship, to give significant wave heights, and the sea state is selected from the range in question as the one giving the lowest height. Though somewhat arbitrary, and with differences between the height from heave motion and pitch motion sources averaged out, the technique did show some success for a single example when compared with height and period results from analysis of the nearest ERS1 SAR satellite image obtained on a closest point of approach 6 hours

and 50nm distant. Though the results for the single example may be fortuitous, the technique does present a robust way to approach the problem; more sophisticated wave representations such as spreading and multiple wave systems are relatively easily incorporated.

Saito & Maeda (1999) give a further approach based on a minimisation procedure. There is a proper treatment of the following seas problem, but a 'correction factor' is introduced to help cope with it, and it is limited to prediction of a long crested spectrum. There was good agreement between the average wave spectra deduced from heave and pitch motions and those of a static probe in ship tank tests in following seas. Convincing looking wave spectra were also calculated from the motions of a 275m ship, for two examples, though there is no comparison with spectra measured from other sources. The wave modal periods and significant wave heights from the motion derived wave spectra are compared with the observed parameters for a three week period; periods were predicted fairly well but in general the significant wave height was seriously underestimated. The effect of spreading or bimodal spectra is not discussed, though the author concludes that the method might be further developed to estimate directional wave spectra.

In summary, though the idea of deducing wave spectra from ship motions is attractive and clearly subject to some study over the years, no method has been proposed which is robust and practical to use but successfully deals with the problems which arise in real seas - notably wave spreading and multimodality - and with the following seas problem.

2.5 Sensitivity and error analysis in seakeeping

It was argued in section 2.3 that there is a shortfall in the literature with the reporting of the wave environment; this may be viewed as one aspect of dealing with sensitivity and error analysis of trials and computer predictions. In this section, the topic is expanded and papers discussing sensitivity of the results of trials and software predictions are reviewed. Once again, special attention is given to those papers in which full-scale ship

motion results are given and uncertainty in the wave environment is considered, be it measured or synthesised.

Chryssostomidis & Oakes (1974) show the differences between the ship motions of a destroyer computed for six observed ocean spectra and those resulting from ideal Bretschneider spectra with the same significant height and modal period. Naturally there are differences, of over 10% for some RMS motions, and the authors link this difference with RAO frequency matching to the spectra. Wave spreading and wave fields with both sea and swell are mentioned, and there are some suggestions of how these might be accounted for in the ship design process as operability calculations, but no further examples are given.

McCreight (1998) also considers the effect of spectral formulations on the motions of the examples of a ship and a stationary platform, and in particular discusses the effect of using an (omnidirectional) Ochi-Hubble six parameter spectrum. The effect of directionality is mentioned briefly but the paper concludes by recommending three spectral shapes for limited seakeeping physical or computational modelling. These may be double peaked but are unidirectional nonetheless. Consideration of all relative headings to the waves is likely to give the most excessive possible motions, but the probability of such sea conditions is not represented.

Clarke, Price & Temarel (1984) describe time domain simulations of warship motions in two alternative idealised spectra intended to represent a single measured seaway, with and without $\cos^2$ and $\cos^4$ spreading. Half hour wave amplitude realisations were made, and the results demonstrate considerable variation in the predicted ship responses due to the different wave definitions.

Webster & Trudell (1981) consider the effect of speed and heading on the wave spectra encountered by a Liquefied Natural Gas carrier, with the aim of synthesising motion time histories. They demonstrate how wave spreading can smooth following seas encounter spectra that would have sharp peaks in long crested seas. The authors write from the point of view of creating motion time histories with the correct statistical and spectral

properties (for idealised spectra) and the next step of quantitatively discussing the motions in realistic spread or bimodal short crested seas is not taken.

Guedes Soares & Trovão (1991) consider the sensitivity of ship motion predictions to the wave climate. Several sea areas and ship types were considered, and wave spreading was modelled, with wave atlas type data from several sources - for example Bales et al (1981). The authors calculated extreme motions at 10^{-8} probability, and found that the results in one sea area due to wave climate data from different sources could vary by around ±40% about the mean. The probability of bimodal sea states was not considered.

Juszko & Graham (1997) applied a 10 parameter wave model (already mentioned in 2.1) with full treatment of spread, multimodal seas to the RAOs of a destroyer to compute the RMS roll, pitch and heave motions. They compared the motions predicted for 144 hindcast spectra (covering 42 days), with those for 10 parameter fitted directional spectra, and Bretschneider spectra with $\cos^2$ spreading. The 10 parameter model results were very close to those of the hindcast spectra, for 97% of the cases, whereas the Bretschneider model only worked well for 75% of the cases - where the seaway was predominantly unimodal.

Crossland & Johnson (1999) propose a treatment of spreading and directionality from the point of view of ship trials where analysis will assume long crested seas. The sensitivity of a frigate to a wide variety of wave conditions is investigated. This work forms the basis of Section 3 of this thesis.

Maggi (1998) is a rare paper giving a treatment of the error bands recorded by his instruments in seakeeping trials, which are traced through to error bars on the ordinates of the motion spectra. However, long crested waves are assumed when the wave spectra suggest bimodal seas, and this is likely to give rise to a large part of the discrepancy between predicted and calculated RAOs which is beyond the range of the error bars.

This section therefore concludes that there is a lack of sophistication in the naval architecture community in the area of error reporting, and moreover the sensitivity of results to subtle changes in ship design and environment. The ITTC has a specialist

committees to address this shortfall, but there is no compulsion for recommendations to be followed, and indeed results reported in naval architecture papers are rarely subject to any uncertainty analysis. Though such parameters as ship load condition and sea state are often stated, for example, error bands for these parameters in general are not.

2.6 Directions for Research

This literature review has given a background to the issues that must be addressed when considering the behaviour of ships at sea. A theme running through the review has been that in general the seakeeping trials and the process of comparing with computer predictions is not carried out with proper consideration to all the variables that have a bearing on the results.

The main source of uncertainty appears to be the directional nature of the seaway, be it spreading of the waves or the presence of several systems simultaneously. Clearly there is scope to develop methodology for trials that can account for this complication, and furthermore to account for it in the software that the trials are being conducted to validate.

The development of parameterised spectra for long crested and short crested unimodal random seas is well established, with a less mature extension to bimodal and greater seas.

This thesis will highlight the effects of the sophistication of wave models on the responses of ships in the seaway. Techniques for assessing the effects of directional spectra on ship motions will be demonstrated, including the effects of spreading and directionality. Examples will be made of from full-scale ship trials and numerical models.

Ship motion software typically only considers the ship behaviour in long crested, unidirectional waves, or in short crested, multidirectional but still unimodal waves. For the construction of the ship motion responses in short crested waves, linear superposition of the waves and hence the ship motions is invariably assumed. Linear superposition in directional waves (as opposed to summation of waves to create a random but long

crested wave train) appears not to have been well validated with full-scale trials. A recommended direction of research is therefore the gathering of trials data with good quality measurement of the wave field. Demonstration that the seakeeping theory can deal with the trials results, with proper treatment of the wave directionality, could prove the validity of linear superposition in this respect.

There are also avenues open for research in accounting for other areas of uncertainty and the sensitivity of predicted results. This might include the ship condition itself, and the sensitivity to such basic parameters as metacentric height. Other aspects of the waves, such as selection of which of the available idealised wave spectra are most appropriate for a particular situation, would also be worthy of study.

Some of the lack of drive to properly account for the seaway directionality must be due to the resources available to the naval architect when considering the operability of his designs at sea. The typical wave data source is the wave atlas, describing wave height and period by season, sometimes with principal direction, but not with description of spreading and multimodality; this lack of long term quantitative data giving the directional spectra for the worlds oceans is one of the main barriers to their routine application in naval architecture. Though extensive wave measurement programs are underway in equatorial regions to study the 'El Niño' phenomenon, the data storage of measured wave spectra presents a problem, and condensation of the data into an easily digestible atlas form is not easy given the many possible scenarios. Perhaps adoption of the 10 parameter spectrum (2.1.3) would be an efficient way to gather long term data efficiently.

Gathering of objective long term data would be one application of using the ship motions to deduce directional wave spectra. This field has not seen a robust and practical tool developed which deals with the following seas problem and is able to predict spread or multimodal spectra. This field is also clearly a worthy subject for research.

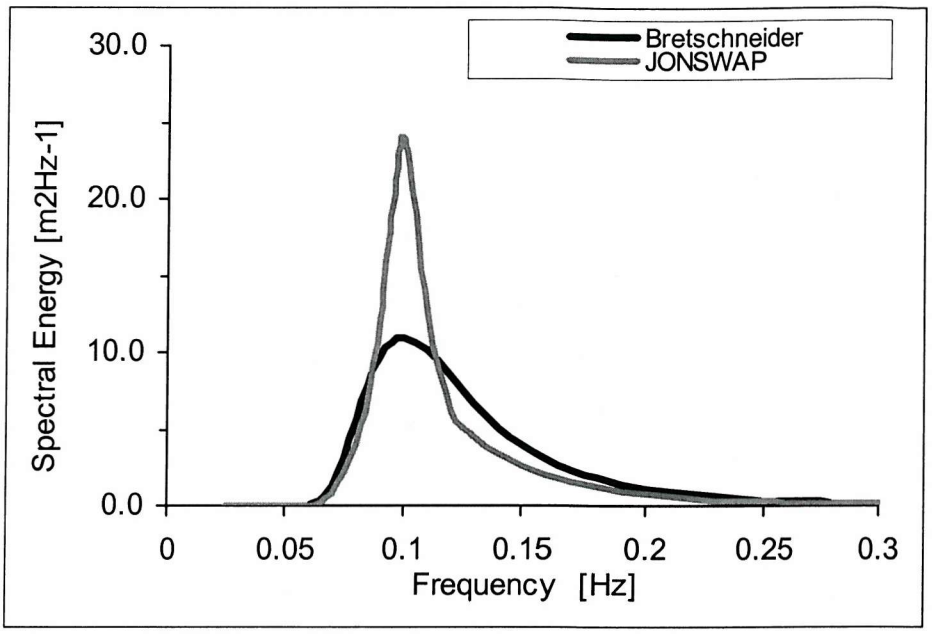

Figure 2.1 Idealised wave spectra (unidirectional), $H_{1/3}$=3.5m, T_m=10.0s

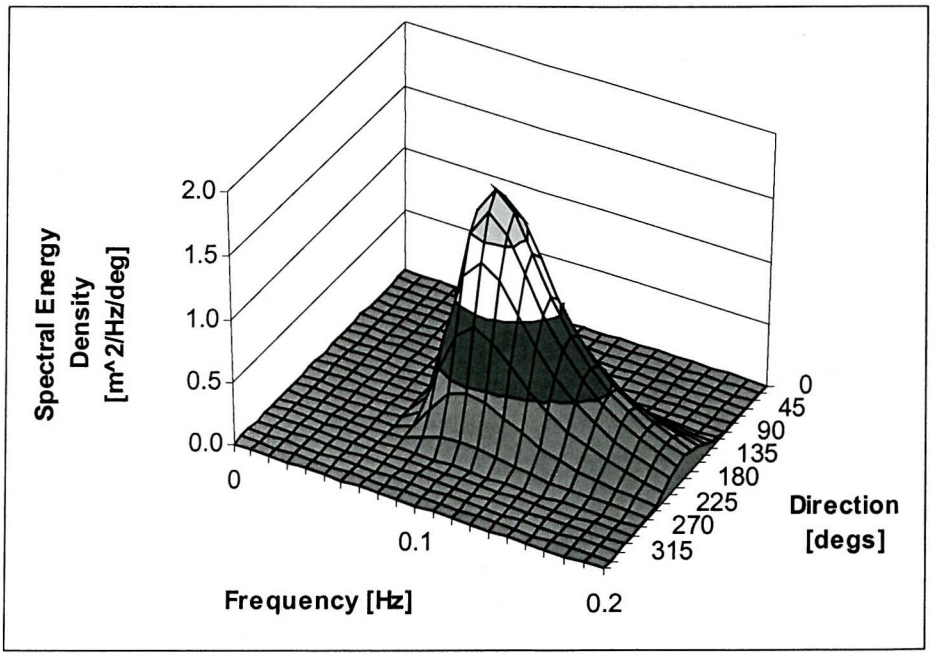

Figure 2.2 Idealised wave spectrum (directional): Bretschneider spectrum with $\cos^2$ spreading, $H_{1/3}$=3.5m, T_0=10.0s

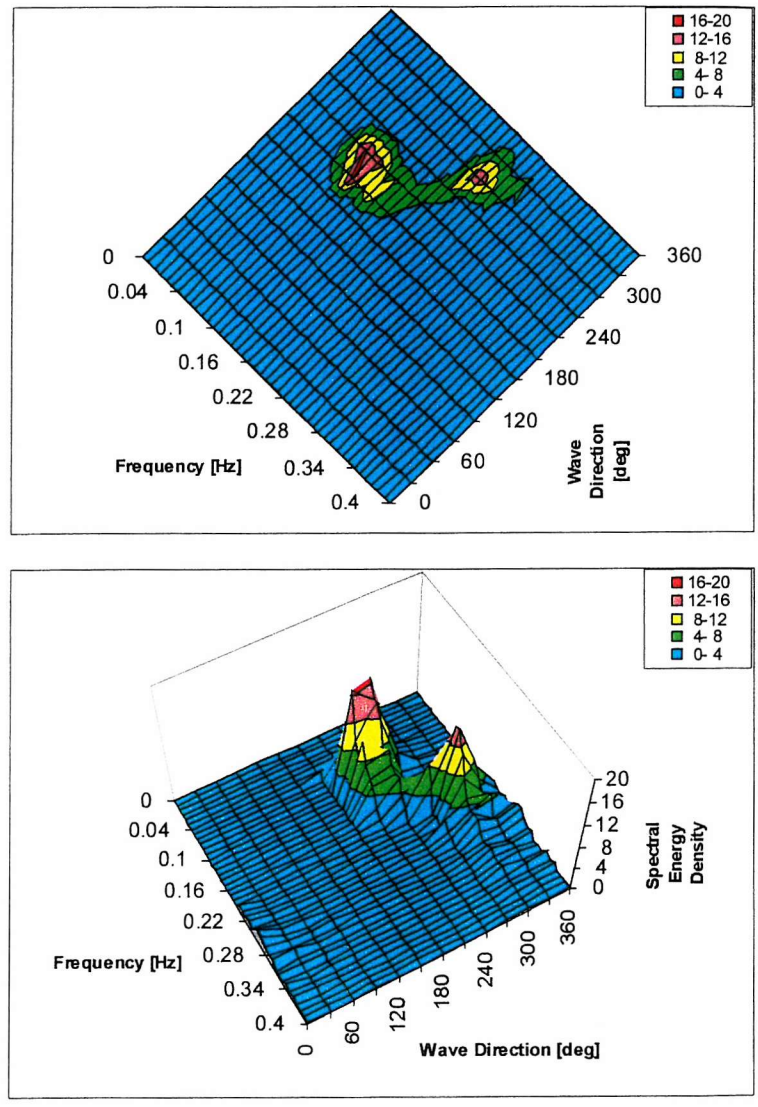

Figure 2.3 Example bimodal directional wave spectrum, measured in UK waters

Figure 2.4 MIROS Wavex system

Right: Radar system

Left: PC showing extracted radar picture, directional wave spectrum, and derived parameters (2.5m wave height)

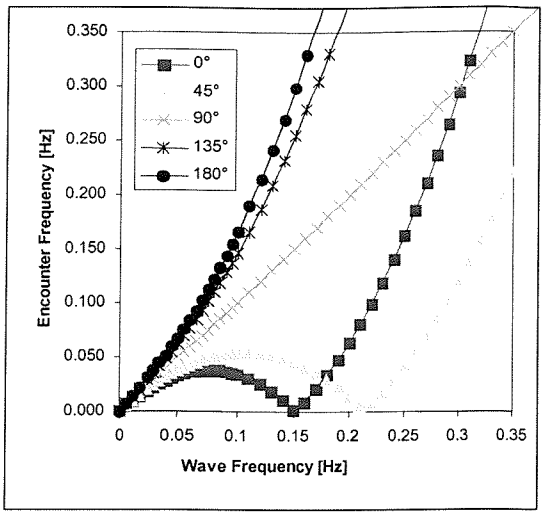

Figure 2.5 Change in encounter frequency with heading relative to the waves 180° is head seas. 20 knots in 200m water depth.

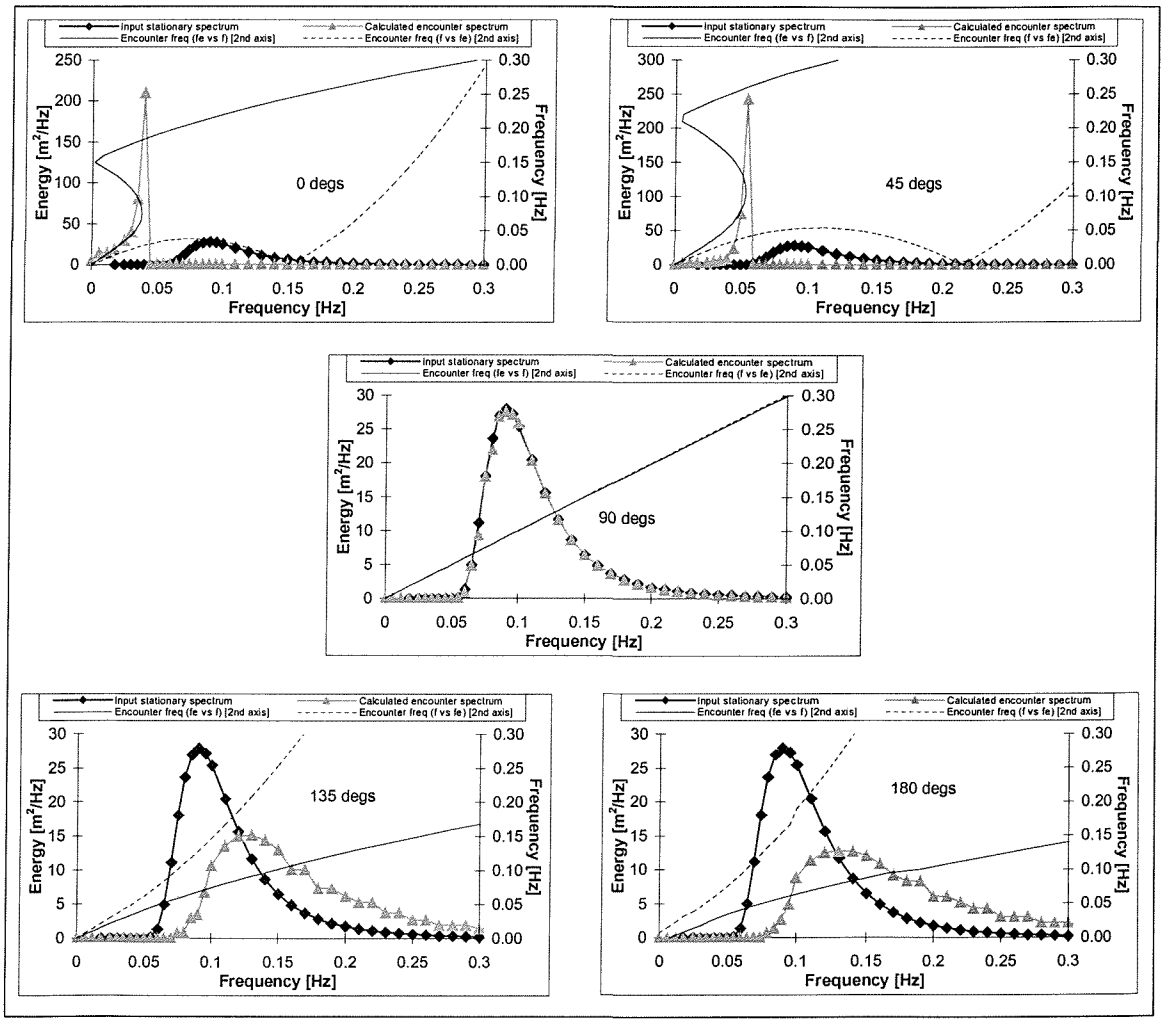

Figure 2.6 Change in encounter spectrum with heading relative to the waves 180° is head seas. 20 knots in 200m water depth.

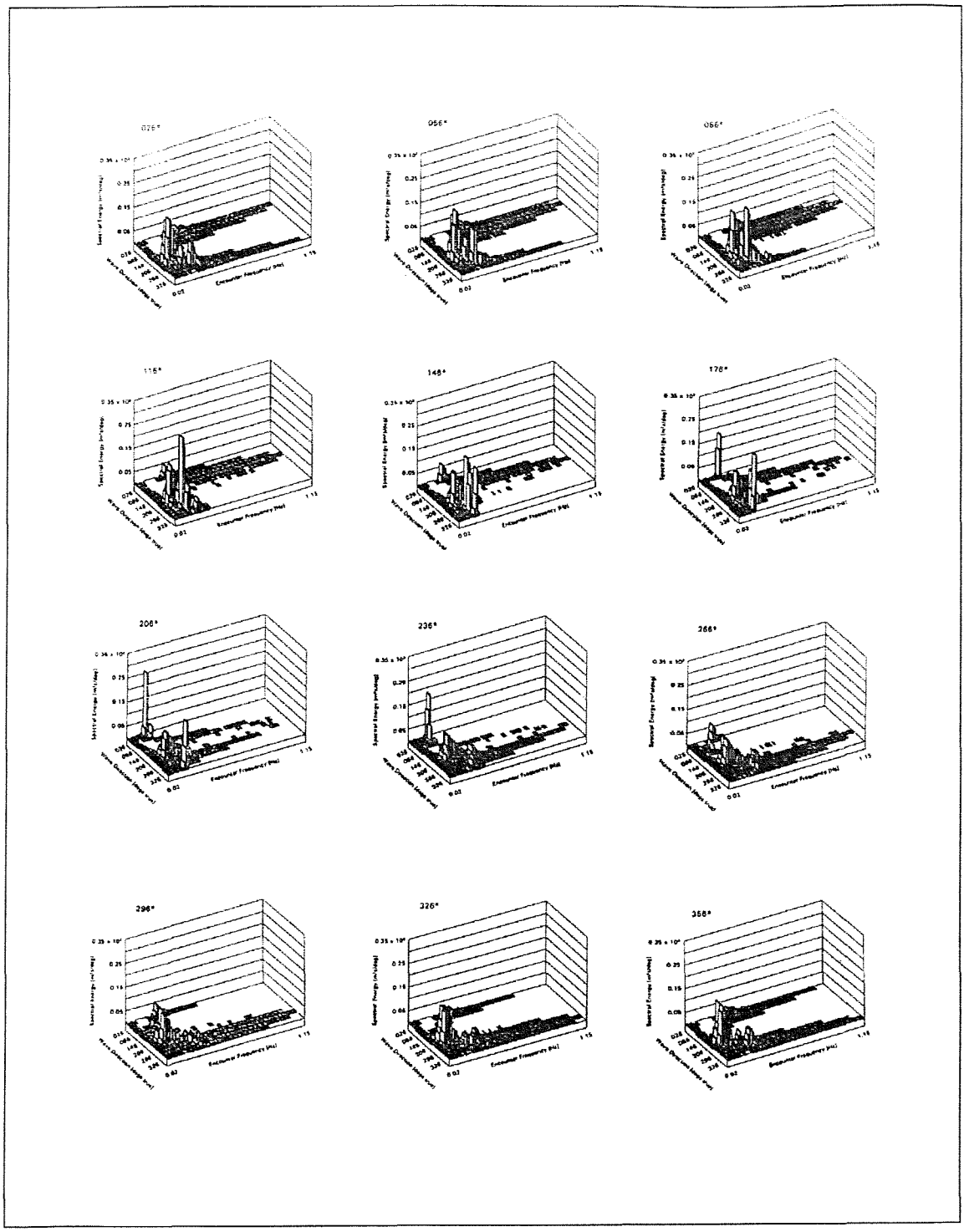

Figure 2.7 Directional encounter spectra transformed from moored waverider spectrum

3. THE STAR TRAJECTORY

3.1 Description

The choice of the ship trajectory to be steered in seakeeping trials is an important one. It is desirable to achieve the trials in a timely fashion as analysis is made easier if the wave spectrum is stationary, and a single spectrum can be assumed to give the ship motions on all headings. A large number of headings relative to the waves is also necessary to achieve a good understanding of the ship behaviour - though these are conflicting requirements since a minimum time on each leg is necessary to obtain a statistically significant exposure to the seaway. When a waverider buoy is used, it is also desirable to stay in its vicinity to be sure that the spectrum the buoy measures is the same one that the ship is experiencing.

Many texts recommend a simple trajectory of five legs, covering head, beam and following seas, and bow and starboard quartering seas (Figure 3.1). However, it will be demonstrated in later chapters that seas with spreading and some multidirectional nature have a great effect on the ship motions, and the simple trajectory shown in Figure 3.1 is not sufficient to fully account for the effect of the seaway on the ship motions. Eight legs at 45° compass intervals is suggested as a minimum - making an octagonal trajectory an attractive option. Better definition by relative heading is achieved with legs at 30° compass intervals, giving a 12 sided 'octagon' trajectory, as shown in Figure 3.2. Figure 5.1 will show the actual path achieved in a ship trial attempting to make this trajectory, illustrating the practical difficulties involved in making seakeeping trials - there was a large gap between the fourth and fifth runs for operational reasons - however the ship still completed the trial with all target headings to the waves sampled.

The 'octagon' trajectory has the advantage of minimising the time spent in turns, and being very easy to perform (involving a series of 30° or 45° turns), but the disadvantage that it may have a large diameter. It is very easy for the ship to end up travelling a long way from the waverider buoy, even if efforts have been made to place the buoy at the centre of the pattern - legs of the order of half an hour may be required at higher speed in following seas. In this time the ship might travel over ten miles – a waverider buoy only transmits a strong radio signal for

a radius of this distance, and should the signal be lost can take up to an hour to synchronise again.

This thesis proposes a 'star' trajectory for seakeeping trials as the optimum choice. With the star pattern, the ship makes a 330° turn after each leg, and repetition ensures that all headings of the compass with 30° degree intervals are covered. Figure 3.3 shows the pattern that might be used in well spread, bimodal, or in seas of unknown directional composition. The star pattern better ensures that the ship stays in the same region of sea as the buoy compared with an 'octagon' type trajectory. In seas of unknown composition, or clearly directionally bimodal character, the amount of time on each leg can practically be made equal, since it will be difficult to tell which compass directions might be head or following seas for which part of the directional spectrum.

Normally less time is required in head seas, and more in following seas in order to encounter a statistically significant number of waves. Figure 3.4 shows a modified star pattern that may be used when there is some confidence that the seaway is largely unimodal. This is essentially the same pattern as Figure 3.3, but the time spent on each leg is adjusted according to relative heading to the waves in order to reduce the overall time necessary to complete the entire pattern. Less time is required in head seas than following seas (since the encounter frequency is higher). Head sea runs might require around 15 minutes whereas following sea runs require at least 30 minutes running in order for the ship to make a significant number of motion cycles.

Figure 3.4 shows a further advantage of the star pattern over an octagon style trajectory; the full pattern may be regarded as two stars, one drawn with grey lines and one with striped lines, with the dashed long following sea run common to both stars. A (short) extra head sea run at the end is necessary for the second star. The advantage is that if the trial is curtailed after halfway through, or the wave conditions change drastically, analysis of either or both stars separately may still be meaningful. The pattern gives the nominal sea direction alternately on the starboard then port side, and so systematic error due to any 'noise' wave systems is reduced when considering either star separately.

3.2 Speed, currents and tides

A problem immediately faced when conducting a seakeeping trial is the decision on whether to take the ship nominal speed as "speed over ground" as reported by GPS based instruments or "speed through the water" as reported by EM (electromagnetic) log devices.

The difference between these speeds is mainly due to local currents and tidal currents in the trials area. The EM log measures the resultant of speed components due to the ship speed and current speed – and thus reports speed in the resultant direction rather than the speed through the water in the direction the ship is pointing.

EM logs may suffer problems of accuracy where there are considerable vertical and lateral motions, as these effectively form a component of ship speed to which the log is not sensitive. Additionally EM logs may be subject to local flow effects such as viscous eddy formation, unless carefully sited on the keel.

For this reason speed over the ground as reported by GPS systems is recommended as the most objective measure of ship speed. Progress is clearly charted in only two dimensions and the weather, tides or local flow effects do not alter the quality of the measurement. Moreover, the speed over the ground has a clearer relationship with the constant speeds simulated in time or frequency domain computer models and tow tank tests.

Intimately related with the question of selecting the best measure of speed is consideration of how currents affect the waves that the ship is travelling through during the trial. Currents certainly change the steepness of waves by changing the orbits from near circular (in deep water) to elliptical. The waves can be flattened by a current running in the same direction, or steepened by currents running in the opposite direction. Taken to extremes, a famous example is the Agulhas current running down the south east coast of Africa, where the current can cause steepening of large waves up to breaking point, and the region is notorious for ship losses.

Wave steepening by current is effectively a refraction effect whereby the frequency is maintained but the wavelength and phase velocity change (wavelength decreases and phase velocity increases). Not only is the wave spectrum encountered by the ship modified, but this also affects the shape of wave spectra seen by a moored buoy. Correction of buoy spectra for comparison with spectra measured directly with radar appears to be a complex process not solved satisfactorily and rarely attempted by dedicated oceanographers (Tucker 1991). For the ship scientist, the advice must be to perform trials only in areas of low current activity where these effects will be minimised.

The effect of currents on wave spectra, their measurement, and the resulting effect on the ship motions has not been considered explicitly in this thesis. Until a more advanced treatment is made, it is suggested that this is effectively incorporated as an uncertainty in the ship speed when transforming stationary wave spectra into encounter spectra.

The impact of the tidal currents, which have a periodicity of around 12 hours, on a ship trial will also be related to the duration and conduct of the trial. Slack water occurs every 6 hours at high and low tides. A short trial of less than 3 hours is bound to have an effective systematic error due to these effects unless the trial is carefully planned to take place at slack water. The star pattern trajectory put forward in this thesis has the advantage of leading to longer trials of over 6 hours that are much more likely to include slack water and currents in both directions. With headings to the waves performed in a staggered order (as opposed to 'octagon' patterns) the currents effectively become a random rather than systematic error when the motions are considered a function of relative heading. Examples of trials results of ships performing a 'star' trajectory are given in Chapter 5.

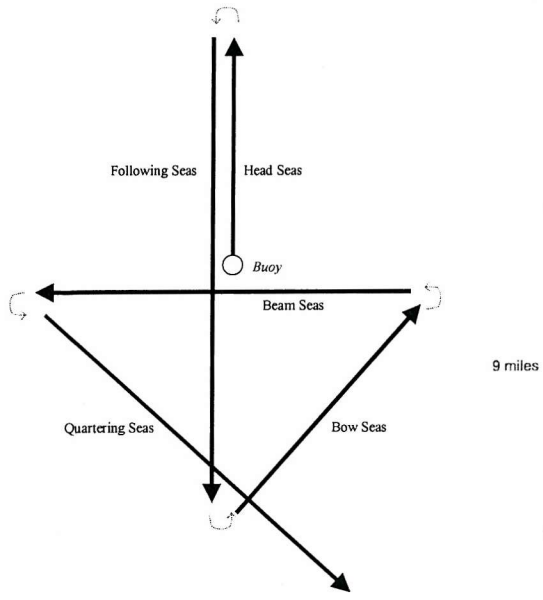

Figure 3.1 Simple trajectory for trials [after Lloyd (1989)]

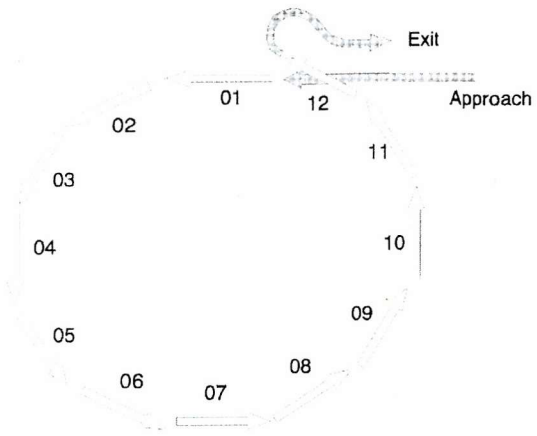

Figure 3.2 Octagon trajectory for trials

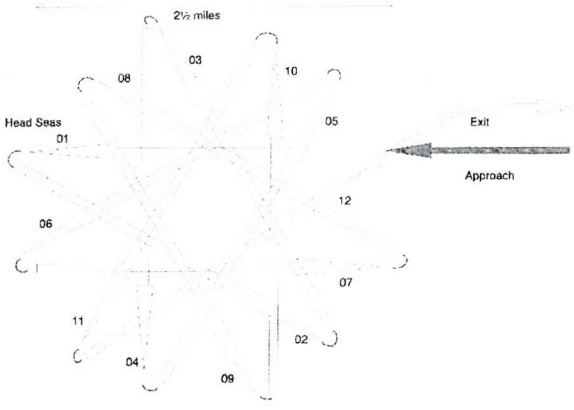

Figure 3.3 'Star' trajectory for trials

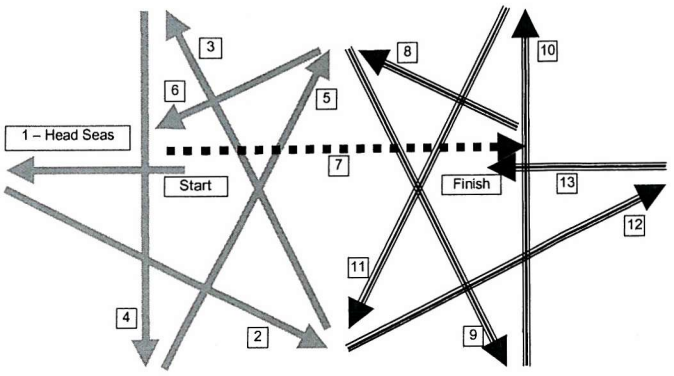

Figure 3.4 Modified 'star' trajectory for near symmetric seas

4. LIMITS OF WAVE DIRECTIONALITY FOR TRIALS

4.1 Rôle of Sea Trials

The performance of a ship design may be derived from computer simulations, model tests or directly by full-scale trials.

Sea trials on a delivered ship should be carried out to establish the actual seakeeping behaviour in a real seaway whenever possible, in order to demonstrate that the performance meets the design or indeed contract requirements.

Full-scale trials present problems as the sea environment encountered on the trial will rarely be that specified in the requirements. Establishing the link between the trials and contract sea conditions, and hence the ship responses, is a crucial step. Analysis of trials results is particularly difficult as the sea surface is spatially and temporally random. Chapter 2 showed that the description of the seaway in terms of parameters such as significant height and wave spreading is a science in itself.

Trials analysis involves calculation of the linear 'response amplitude operators' or RAOs of the ship motions. These transfer functions can be applied either to a range of design wave conditions for comparison with criteria or as input into a full operability analysis. This exercise will illustrate whether the ship meets the design or contractual requirements.

There has been some progress in developing methods to obtain the linear transfer functions from the response of the ship in spread sea conditions, and this is the subject of the next section of this thesis, but it is not considered that these advanced techniques are yet in a fully developed form which can be applied readily and reliably. The simplest analysis, and that almost universally applied, assumes that there is no wave spreading i.e. the waves are long crested.

Given that analysis will be by the simple, long crested method, this section continues to investigate, by example, what trial wave conditions are suitable for determining RAOs with acceptable accuracy.

It is assumed that trials will consist of runs in an octagonal or star trajectory so that motions are stimulated at a range of headings relative to the predominant waves. In particular, the questions considered are:

(i) What is the maximum wave spreading possible so that the spectrum may be considered long crested as far as the ship motions are concerned ?

(ii) What is the minimum wave height required to give acceptably large ship motions?

4.2 Maximum wave spreading

Wind generated seas are often not long crested, and usually they show considerable spreading about the dominant wind/wave direction. This has consequences for the rigid body motions of a ship - for example in short crested head seas there will be some roll, whereas there should be no roll in long crested head seas. Typically the maximum responses are smaller than for long crested seas of the same energy and the minimum responses are larger. Figure 4.1 illustrates this point.

A method to assess the allowable level of spreading in trials has been developed, and this will be described alongside supporting calculations. The calculations simulate a frigate performing trials at 20 knots in a wide range of possible sea states in the North Atlantic. The ship motion calculations have been performed using a 'strip theory' model.

Table 4.1 gives annual wave statistics derived for the North Atlantic [Bales et al. (1981)], in terms of the percentage probability of seas for possible combinations of modal wave period and significant wave height. Only the 95% most probable wave conditions are considered so that the most extreme seas are excluded.

There are several ways of describing the spreading of wave spectra. For modelling purposes, the usual approach is to multiply a long crested spectrum by a spreading function that distributes energy in other directions besides the principal one. Advanced models use a frequency dependent function but a common approach adopted by the naval architect is spreading with an even power of the cosine function, Equation 2.9. The energy present in a long crested spectrum is distributed in the range ±90° about the principal direction. Cosine squared spreading is typically applied for well spread short crested seas, but higher powers may be used when one direction becomes more dominant. Figure 4.2 shows how energy is concentrated in the primary wave direction as the cosine power increases.

The rigid body motions (at the centre of gravity) of the frigate have been calculated for a full set of relative headings for each of the wave height/period 'bins' of Table 4.1, with a range of spreading from none (long crested seas) to cosine squared. Table 4.2 gives an example of the results for just one of these. For each set of results a second table has been constructed where the RMS response due to spreading has been effectively 'non-dimensionalised' by dividing by the long crested seas RMS response. For some headings, the non-dimensionalisation is not possible; this occurs when there is no response in long crested waves e.g. roll in head seas.

The non-dimensionalised RMS motion results are grouped and plotted by type and heading for each wave condition; Figure 4.3 gives the example of heave motion at 180° relative heading. The X-axis is given in terms of spreading angle rather than cosine spreading power, to give a linear axis.

The plot includes extra horizontal lines at 0.95 and 1.05 – indicating where the RMS motion in spread seas differs from the RMS motion in long crested seas by ±5%. This is considered to be an acceptable accuracy for RMS motion results of trials.

A 5% allowable error in RMS motions is a useful guideline, but since this is related to the area under the motion spectrum, and not directly to the frequency distribution of energy, the accuracy of RAOs obtained is not guaranteed. Indeed ±5% allowable error in RMS motion arises from a possible ±10% error in the overall motion spectral area

(1.05^2). Furthermore, individual lines in the response spectrum could be more than 10% in error, though in this study and in nature relatively smooth wave spectra prevail which negate this possibility.

Figure 4.3 shows that the non-dimensionalised motions have weak dependence on wave height (which one would expect with a linear system) but strong dependence on wave period. It is the shortest period, higher frequency wave spectra for which spreading causes the largest effect i.e. cause exceedance of the ±5% acceptable error bands for the lowest amount of spreading.

This is quite surprising as high frequency wave components alone have little effect on ship motions. It is suggested that the reason is to do with encounter frequency of the spread waves; high frequency waves have a much greater Doppler shift of frequency than low frequency waves when ship speed and relative direction is taken into account. There may be considerable energy in the high frequency 'tail' of the wave spectrum which can accumulate at unfavourable frequencies for ship motion when changing relative wave directions due to spreading are taken into account.

Considering RMS responses outside the ±5% band to be unacceptable, one may read off from Figure 4.3 the maximum allowed spreading. Results here are based on the calculated points only, but more sophisticated analysis could involve interpolation. Table 4.3 summarises the results obtained for the frigate for a full set of figures like 4.3, for five motion types and five relative headings. It can be seen that there is wide variation, with roll and sway limiting at some headings in a spectrum with only very slight spreading.

These show that trial results will only be guaranteed to be suitable for determining RAOs with a simple long crested approach, for fully long crested seas only. This is a relatively rare situation. More spreading might be allowed by removing the contribution of the low period waves, which usually limit the allowable spreading. Table 4.4 summarises the effect of ignoring the contribution of the 6.3s and 7.5s wave period data, and clearly there is some improvement in the limiting spreading. However, Roll in quartering seas is still limited by a very small amount of spreading, and sway in bow quartering seas is also

sensitive to spreading. The 6.3s and 7.5s modal wave periods are present approximately 18% of the time in the North Atlantic (Table 4.1).

Recognising that bow and stern quartering seas give errors for some motions, $\cos^{60}$ spreading gives acceptable error in all but 2 of the 17 cases possible in Table 4.4. So a spreading function equivalent to $\cos^{60}$ or less, combined with wave periods greater than 7.5s, is recommended as a practical criterion for ship trials with this frigate at 20 knots. $\cos^{60}$ spreading may also be described as a wave spreading angle of 17°.

4.3 Minimum wave height

The data generated for the Atlantic wave conditions reported in the previous section may also be used to investigate a possible minimum wave height specification for trials. The data applies to the motions of the example frigate ship at 20 knots operating in the North Atlantic.

Locally generated wind seas may often be superposed onto swell waves arriving in the area from a distant storm. Swell waves characteristics are difficult to predict in the same way as wind waves, but generally they have periods of more than 10 seconds and at any one time the swell wave spectrum is narrow banded.

For this study, the wind generated wave spectrum was considered to be the primary system, and swell waves to be noise corrupting the ship responses due to the primary wave system.

Ship motions for each entry of Table 4.1 were calculated as the primary responses, with long crested seas or $\cos^{90}$ spreading allowed. The responses due to 0.5m significant height waves with periods greater than 10 seconds (10.9s, 12.4s, 13.8s, 15s, 16.4s) were superposed to model a swell 'noise' system. These swell waves were allowed to arrive from 13 possible directions in the range 0°-180° relative to the simulated wind sea. All the waves were assumed to follow the Bretschneider spectral form. For swell waves an

even more narrow banded representation might make a better model, though this has not been attempted.

The ship motions due to the joint effect of wind and swell waves may be combined as follows:

The ship motion prediction program calculates the encountered wave spectra and motion RAOs to determine encounter motion spectra for five of the six rigid body motions (surge is ignored). The RMS motion is given by the square root of the area under the encounter motion spectrum (Lloyd (1989) pp.155).

Consider the RMS Response R due to a multidirectional sea state; the motion spectral area is A. Area A may be set as the superposition of responses in two separate wave systems A_1 (primary system) and A_2 (noise system). The RMS response for A_1 is R_1 and for A_2 is R_2.

$$R=\sqrt{A} \qquad \ldots(4.1)$$

$$A=A_1+A_2 \qquad \ldots(4.2)$$

$$R_1=\sqrt{A_1} \quad R_2=\sqrt{A_2} \qquad \ldots(4.3)$$

$$R=\sqrt{(R_1^2+R_2^2)} \qquad \ldots(4.4)$$

Thus the RMS response may be expressed in terms of the RMS responses due purely to the component wave systems.

Allowing a 5% 'error' increase in R as a result of R_2 affecting R_1 gives the condition:

$$R < 1.05\ R_1 \qquad \ldots(4.5)$$

and rearranging the previous equation gives

$$R_2=\sqrt{(R^2-R_1^2)} \qquad \ldots(4.6)$$

Substituting for R with the 5% allowed error gives

$$R_2 < \sqrt{(1.05^2-1^2)}\ R_1 \qquad \ldots(4.7)$$

$$\boxed{R_2 < 0.32\ R_1} \qquad \ldots(4.8)$$

So the RMS motion due to the noise wave system must be less than about a third of that due to the primary system.

This is applied to the frigate data by looking for the maximum value of R_2/R_1 for any combination of sea and swell as follows:

- select one of the long crested wave systems e.g. 10.9s/0.5m
- find the maximum RMS response over all headings in this system (ignoring zero magnitude responses, so for sway and roll used range 30°-150°, for yaw 30°-60° and 120°-150° and for pitch 0°-60° and 120°-180°)
- find the minimum RMS motion R_1 over all headings in all the possible sea state bins 6.3s/1.5m, 7.5s/0.5m etc.
- calculate the ratio R_2/R_1 to find which sea/swell combinations satisfy $R_2 < 0.32\ R_1$ even in the worst combination of relative headings.

Table 4.5 illustrates this result for heave motions of the frigate. The table relates to one condition of swell, and shows the ratio R_2/R_1 for all the height period bins possible from Table 4.1. At the bottom of each table, there is a linear interpolation for the significant height at which the condition $R_2/R_1 < 0.32$ is exceeded.

Results for the set of tables like 4.5 at each of the 'swell' conditions are plotted for five degrees of freedom on Figures 4.4-4.8. The significant wave height and modal period on the X and Y axes relate to the primary wave system. The points indicate the limiting wave heights interpolated from tables like 4.5.

In most cases, mid sea state 5 (3.5m significant wave height) is sufficient to ensure that the effect of swell waves always satisfies the condition $R_2<0.32R_1$, so that the effect on the overall RMS motion is less than 5%. This is a somewhat high sea state, and reflects that the calculation is limited by allowing the 'noise' swell systems to have a relatively large 0.5m wave height; this was the smallest height for which wave atlas information was available.

The exceptions are sway and roll, as in Section 4.2, and very high and improbable sea states indeed are required to satisfy the 5% condition, where the ship would not be

operable! The reason is that roll motions, for example, can be highly tuned to a particular frequency, and even small amounts of energy in 'noise' wave spectra are sufficient to stimulate large responses when the conditions of speed and heading conspire to place the wave energy at the roll natural frequency.

Finding the worst case R_2/R_1 for each possible relative heading combination of the wind and swell waves is perhaps a little pessimistic but was taken in the interests of finding a result covering all eventualities. One might attempt to specify directions relative to the primary wave system from which swell should not be allowed for trials purposes, for example, less than 45° difference in relative direction. It would be difficult to apply this generalisation, since there is always likely to be a condition at which the swell is encountered at an unfavourable frequency.

Summarising this section, a method for assessing the effect of secondary wave systems on ship trials has been demonstrated. For a frigate example, it has been shown that a full set of acceptable rigid body motion results is extremely difficult to obtain in trials by 'long crested' analysis methods with a secondary 'noise' system of 0.5m present.

4.4 Summary

This chapter has reviewed the limiting conditions for acceptance trials of full-scale ships. It has been demonstrated that the directional nature of sea waves has a profound effect on the rigid body ship motions, particularly roll and sway. It is therefore essential that directional wave spectral information be measured at the trial site, preferably before the trials begin, to allow rejection of unfavourable conditions.

The most straightforward analysis of trial results involves the assumption that the waves are long crested. For 0.5m 'noise' waves, it has been shown that this assumption is tenable for a frigate if the wave modal period is greater than 7.5s and the wave spreading is less than $\cos^{60}$. It has not been possible to recommend a minimum sea state, but clearly the higher the better. A recommendation might be achieved by using smaller 'noise'

waves, a limitation of the wave data used here, or relaxing the criterion of 5% allowable error at Equation 4.5 to 10%.

This chapter has used the example of a single type of ship operating at certain speeds in a certain sea area. A large number of similar calculations for different sized ships at their operating speeds and in other sea areas could establish trends in the criteria for acceptable spreading, with possible relation to the gross ship properties like length and displacement. The spreadsheet approach used here would be unsuitable for a more extensive study, but assuming linear responses, a dedicated program could generate the data quickly given previously calculated RAOs.

	Modal Period [s]										
Hsig [m]	6.3	7.5	8.8	9.7	10.9	12.4	13.8	15.0	16.4	18.0	*sum*
0.5	4.2	4.3	3.0	3.7	2.0	2.0	0.9	1.0	0.5	0.0	*21.6*
1.5	3.0	5.1	4.2	4.1	2.8	2.6	1.2	1.3	0.7	0.4	*25.4*
2.5	-	1.7	4.2	4.4	2.9	2.3	1.2	1.0	0.6	0.3	*18.6*
3.5	-	-	0.6	3.5	3.0	2.6	1.1	0.8	0.5	-	*12.1*
4.5	-	-	-	0.5	2.4	2.6	1.0	0.8	0.4	-	*7.7*
5.5	-	-	-	-	0.5	2.3	1.0	0.8	0.4	-	*5.0*
6.5	-	-	-	-	-	1.0	0.8	0.7	0.3	-	*2.8*
7.5	-	-	-	-	-	-	0.6	0.6	0.3	-	*1.5*
8.5	-	-	-	-	-	-	-	0.5	-	-	*0.5*
9.5	-	-	-	-	-	-	-	-	-	-	*0.0*
sum	*7.2*	*11.1*	*12.0*	*16.2*	*13.6*	*15.4*	*7.8*	*7.5*	*3.7*	*0.7*	*95.2*

Table 4.1 North Atlantic 95% most likely wave probabilities [Bales et al.1981]

Bretschneider	RMS Heave							NON-DIMENSIONALISED BY LONG CRESTED RMS						
6.3s/1.5m	cos2n spread							cos2n spread						
Heading	long	90	60	30	14	8	2	long	90	60	30	14	8	2
0	0.016	0.016	0.016	0.016	0.017	0.020	0.043	1.00	1.01	1.02	1.04	1.11	1.25	2.75
15	0.017	0.017	0.017	0.018	0.020	0.025	0.059	1.00	1.01	1.03	1.07	1.21	1.48	3.48
30	0.022	0.023	0.024	0.027	0.034	0.045	0.091	1.00	1.04	1.09	1.22	1.53	2.03	4.10
45	0.040	0.042	0.045	0.052	0.067	0.084	0.124	1.00	1.05	1.13	1.30	1.68	2.10	3.10
60	0.084	0.089	0.095	0.108	0.126	0.139	0.152	1.00	1.06	1.13	1.29	1.50	1.65	1.81
75	0.181	0.184	0.188	0.194	0.196	0.193	0.172	1.00	1.02	1.04	1.07	1.08	1.07	0.95
90	0.287	0.282	0.274	0.258	0.239	0.223	0.182	1.00	0.98	0.95	0.90	0.83	0.78	0.63
105	0.246	0.244	0.243	0.238	0.229	0.217	0.181	1.00	0.99	0.99	0.97	0.93	0.88	0.74
120	0.154	0.157	0.161	0.169	0.176	0.179	0.170	1.00	1.02	1.05	1.10	1.14	1.16	1.10
135	0.093	0.095	0.098	0.105	0.117	0.129	0.149	1.00	1.02	1.06	1.13	1.26	1.39	1.61
150	0.051	0.052	0.054	0.063	0.075	0.086	0.122	1.00	1.02	1.04	1.10	1.23	1.41	2.00
165	0.047	0.048	0.048	0.050	0.054	0.060	0.095	1.00	1.01	1.03	1.06	1.15	1.28	2.01
180	0.043	0.044	0.044	0.045	0.048	0.052	0.082	1.00	1.01	1.02	1.04	1.10	1.20	1.89

Table 4.2. Calculation of ship motion in spread waves

20 knots					
Relative Heading	Heave	Sway	Roll	Pitch	Yaw
0	30	-	-	30	-
45	90	60	LONG	60	30
90	60	60	90	-	-
135	90	LONG	90	30	90
180	30	-	-	30	-

Table 4.3 Limiting cosine spreading

20 knots					
Relative Heading	Heave	Sway	Roll	Pitch	Yaw
0	30	-	-	8	-
45	60	60	LONG	8	60
90	30	14	60	-	-
135	30	90	60	14	30
180	14	-	-	14	-

Table 4.4 Limiting cosine spreading, but ignoring low periods

13.8s/0.5m										
Tm / Hsig	6.3	7.5	8.8	9.7	10.9	12.4	13.8	15	16.4	18
0.5	23.99	8.99	4.45	3.23	2.39	1.87	1.61	1.47	1.35	-
1.5	8.01	3.00	1.48	1.08	0.80	0.63	0.54	0.49	0.49	0.42
2.5	-	1.80	0.89	0.64	0.48	0.38	0.32	0.29	0.27	0.25
3.5	-	-	0.63	0.46	0.34	0.27	0.23	0.21	0.19	-
4.5	-	-	-	0.36	0.27	0.21	0.18	0.16	0.15	-
5.5	-	-	-	-	0.22	0.17	0.15	0.13	0.12	-
6.5	-	-	-	-	-	0.14	0.12	0.11	0.10	-
7.5	-	-	-	-	-	-	0.11	0.10	0.09	-
8.5	-	-	-	-	-	-	-	0.09	-	-
Hinterp				4.87	3.79	3.01	2.52	2.36	2.27	2.10

Table 4.5. Limiting primary wave height calculation for 0.5m/13.8s secondary waves

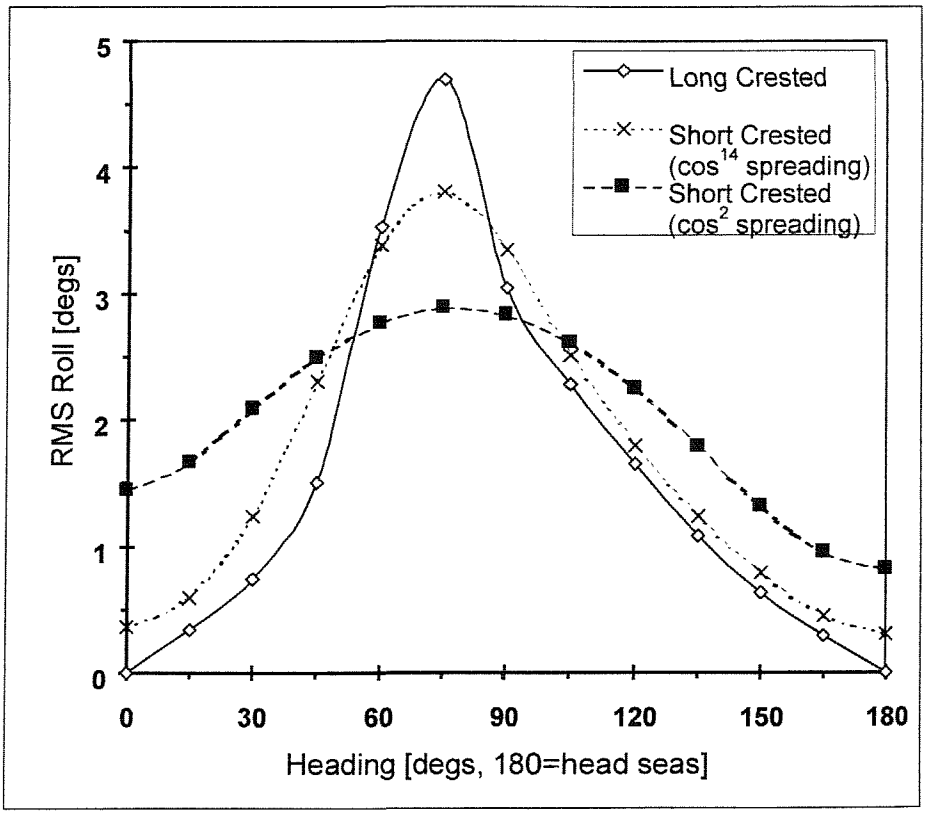

Figure 4.1 RMS roll of frigate in long and short crested seas (Bretschneider 3.5m/8.8s)

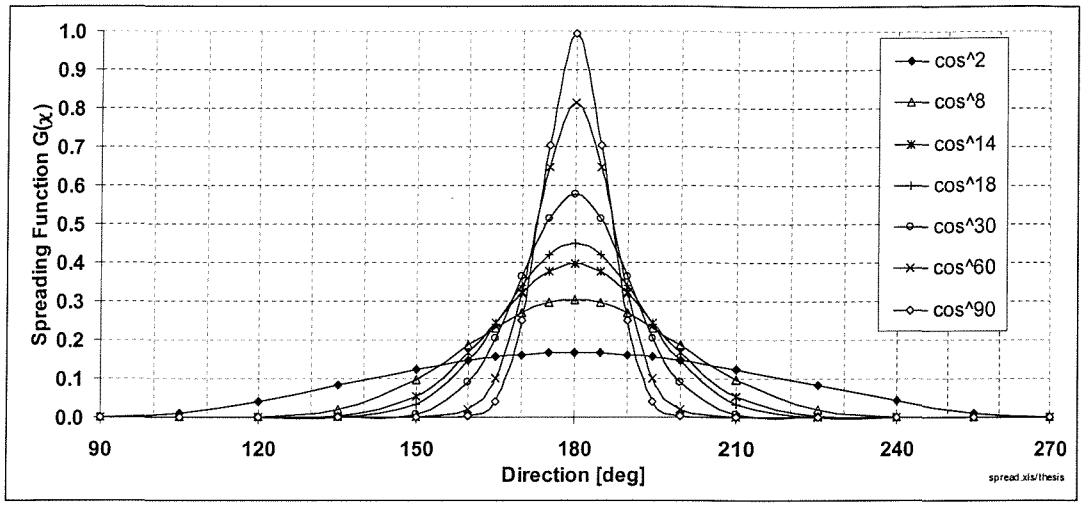

Figure 4.2 Cosine even power spreading functions (15° steps)

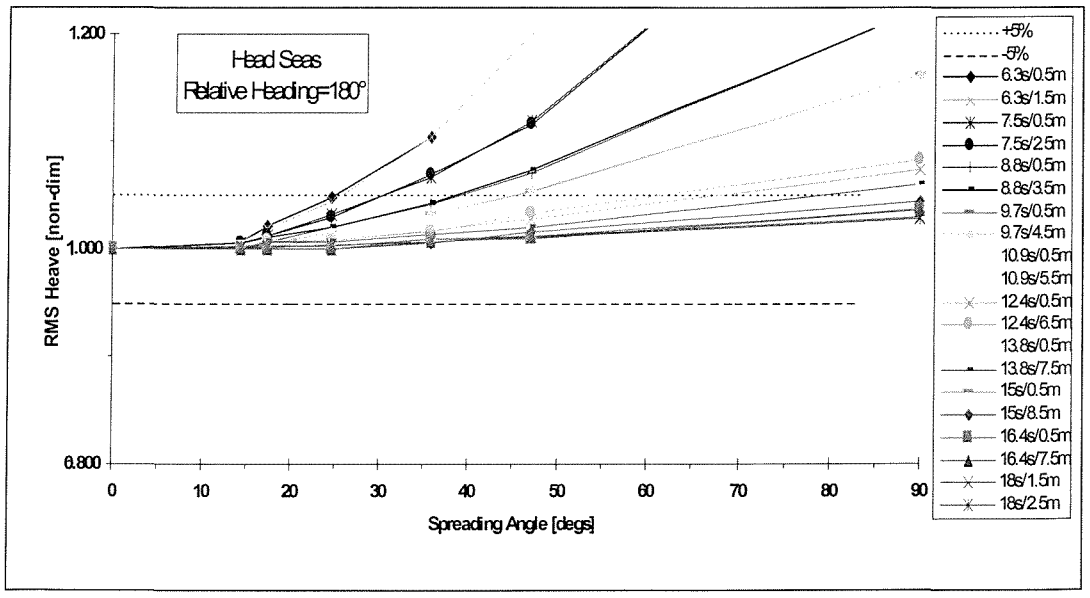

Figure 4.3. Plot of motion in Spread Waves

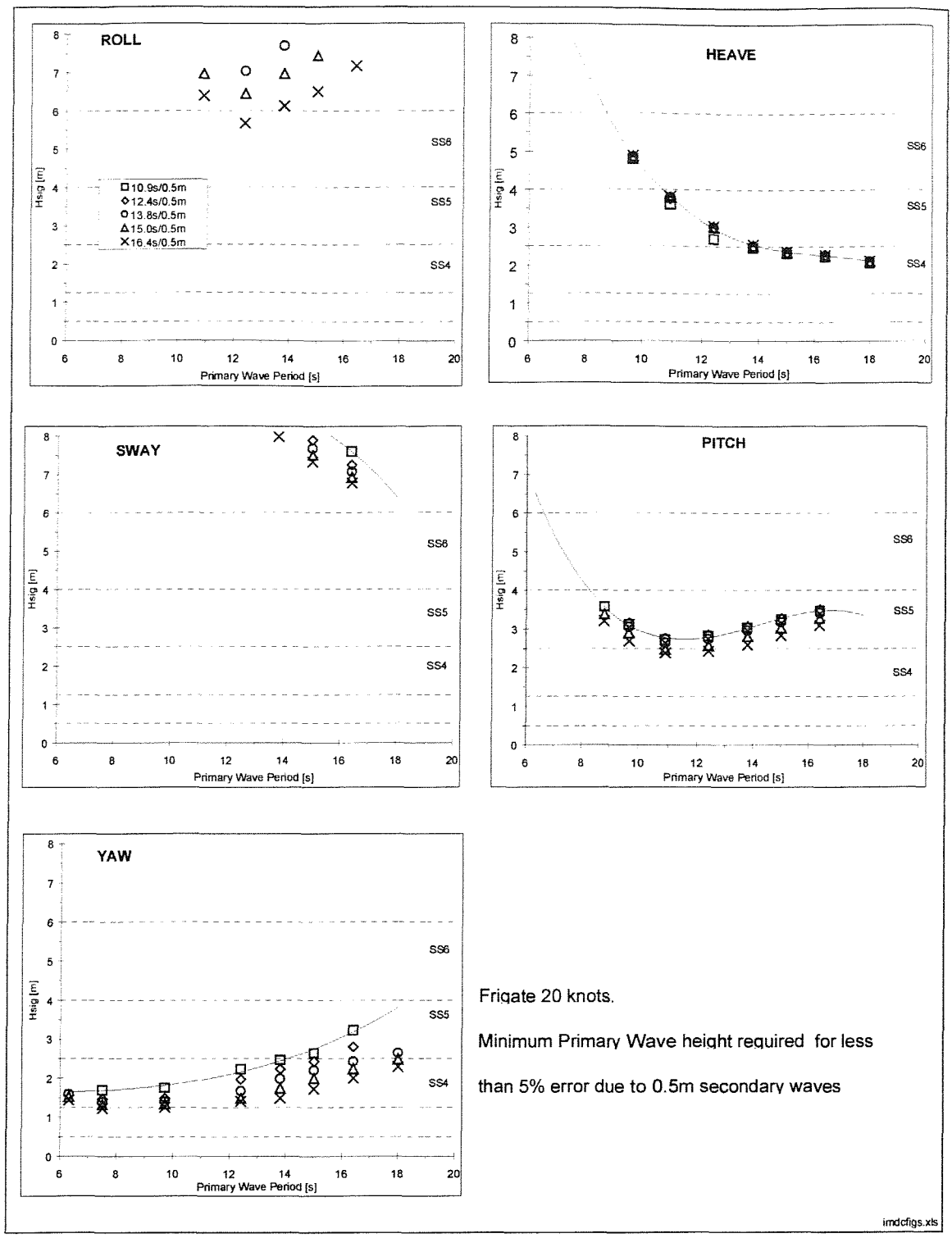

Figures 4.4-4.8 Minimum wave height

5. EFFECTS OF WAVE DIRECTIONALITY – SHIP TRIALS

5.1 Introduction

This section will demonstrate how wave spreading and directionality has a great effect on the results and interpretation of seakeeping trials. Data presented here is from four dedicated seakeeping trials aboard vessels with a range of sizes. These trials are all distinguished in that concurrent directional wave data was measured with a Datawell Waverider buoy, and in one case with additional instruments.

In general, ship motions were measured in six degrees of freedom using tri-axial accelerometer packs to measure the linear motions and gyros to measure the angular motions. The seakeeping trials consisted of runs at a constant speed at various headings to the waves.

The ship motions and wave data are analysed and reported here in some detail. The characteristics of the seaway and the subsequent ship response are discussed, as is the suitability of the trial for the purposes of seakeeping software validation. In some cases, this process is illustrated further by comparing the trial results with results calculated from a suite of programs PAT-95 [Montgomery & Crossland (1995)]. This is a 'strip theory' program based largely on the formulation by Gerritsma & Beukelman (1967).

5.2 Trials with Frigate

The trial was performed with a 4000 Tonne naval frigate in the Lyme Bay area of the Southern coast of England. The frigate performed an 'octagon' type evolution, nominally similar to Figure 3.3, in order to obtain motion data at all headings to the wave field, at a resolution of 30°. Figure 5.1 shows the actual trajectory achieved. There was a gap in between the fourth and fifth runs as the ship headed north to remain within the Captain's overnight 'box'.

Runs were all performed at a nominal speed of 5 knots through the water; Table 5.1 gives the mean compass headings for each run and the mean speeds. Data was acquired at a sample rate of 12Hz for 12 minutes each leg of the pattern. This was chosen as it gives just over 2^{13} points; a power of 2 number of points makes for efficient data spectral analysis by FFT techniques.

At 12 minutes, the run time for each leg of the run pattern was rather short, but necessary to complete the trial in the allotted time. 100 motion periods are usually considered necessary to give stable statistics (Lloyd (1998)). If the motion periods are equated with the peak wave frequency 0.12 Hz in Figure 5.2, the number of waves encountered in head, beam and following seas are 102, 86 and 70 respectively.

The accelerations were measured with a tri-axis accelerometer pack mounted on 2 deck towards the aft of the ship. Roll, pitch and heading were extracted from the ship's own gyro compass system outputs. The accelerations have not been corrected for the effects of angular motions; the RMS roll was less than 2 degrees and the RMS pitch was less than 0.3 degrees, so these corrections should be negligible (significant error would only occur for peak angular motion of 10 degrees or greater).

The directional wave field was recorded by a Datawell waverider buoy positioned relative to the ship trajectory as shown in Figure 5.1. The water depth in this region is around 45m. The buoy transmitted wave data hourly, based on the previous half hour's wave measurements. For run by run analysis, linear interpolation has been used to give the wave conditions at the mid point of each run.

The run by run development of the wave environment can be seen in Figure 5.2. The seaway was clearly bimodal throughout the trial, though there was some diminishment in energy as shown in the reduction in significant height in Table 5.1. The NATO sea state definition by significant wave height is given in Table 5.2; the sea state diminished from lower Sea State 4 to upper Sea State 3 during the course of the trial.

An example interpolated wave spectrum is given in Figure 5.3, including information on wave direction and spreading. The spreading angle increases significantly at 0.2Hz as this

effectively comprises components from both wave systems which were approaching diametric opposition by the end of the trial. The directional spectrum given in Figure 5.4 has been constructed from this data.

The wave system present consisted of a low frequency swell component of period 8-10s coming from a South Westerly direction approximately 210° true i.e. from the North Atlantic Ocean, and also a locally wind generated component of period 4-5s which veered from Westerly (300°) to Northerly (20°) during the course of the trial. This corresponded with a similar change in wind direction recorded manually during the trial.

Figure 5.5 shows the RMS responses of the frigate in six degrees of freedom plotted against the nominal relative heading. The sea direction is assumed to stay constant as the direction of the first – head seas – run, 286°. Comparison with the wave data such as Figure 5.3 indicates that this heading was chosen as directly into the swell waves rather than the wind sea. The trial was conducted at night, and these would be the most distinguishable waves. By day the sea surface would have appeared somewhat confused.

Figure 5.5 co-plots the complementary relative headings on the same axes (e.g. 120° and 240°). In a symmetrical seaway, the responses from the port and starboard sides would be identical, as indicated previously in Figure 4.1. Clearly in Figure 5.5 this is not the case. The bimodality of the seaway is mainly responsible for the asymmetry, and it is likely that the diminishing seaway is also a factor – in general the 0°-180° results are generally slightly higher than the 180°-360° ones.

The results around 90° to 120° relative heading on Figure 5.5 are particularly interesting. In nominally beam seas, one would expect high lateral plane and low vertical plane motions, but there is a large difference shown in these results for the nominal port and starboard sides of the ship facing the waves. For example, a captain turning to 090° (nominal relative heading) expecting high roll angles due to near beam seas would actually find minimal roll, whereas on the complementary heading 240° he would find maximised roll. This confusing situation supports the case for directional wave information (or its consequences) to be made available on the bridge where the decisions made may ultimately affect the safety of passengers or crew.

5.3 Trials with fishing vessel

These trials were performed with Research Vessel Colonel Templer, a 49m converted fishing vessel displacing 1300 Tonnes. The trials area was Veryan Bay, off the Cornish coast of the southern UK. The water depth in this area is around 70m, which exceeds the rule of thumb criterion for deep water of half a ship length. The ship is equipped with a flume tank stabilisation system, but this was emptied for the trial.

Linear motions were measured with a tri-axial accelerometer pack mounted close to the expected ship Centre of Gravity. Angular motions were measured with two instruments, a Humphrey gyro, supplemented for roll by a 'Hippy' gyro in the ship's laboratory. For analysis, the accelerations were not corrected for the effects of the angular motions.

The ship performed a star pattern trajectory of runs at all headings to the compass in 30° steps similar to that shown in Figure 3.3, at a nominal speed of 5 knots. The directional wave field was recorded with a Datawell waverider buoy; Table 5.3 summarises the run data and wave conditions.

Once again the buoy measured wave conditions hourly, and linear interpolation has been used to give the wave conditions at the mid point of each run. The hourly interpolated wave spectra are given in Figure 5.6, and a more detailed example for Run 6 is given in Figure 5.7, showing the wave direction and spreading parameters for each frequency point. The sea state remained fairly constant at around 5.4m for the duration of the trials, corresponding to mid Sea State 6. These were severe wave conditions for the ship to attempt all the headings required for the 'star' pattern, and indeed the Master requested that one of the runs (in quartering seas) be aborted.

There is some evidence of bimodality in the wave spectrum recorded. Unfortunately, evidence of the wind direction from the ship is not available, which makes it difficult to identify which component was locally wind generated and which was arriving from elsewhere. The largest waves appear well developed, having a modal period about 12s and coming from direction 240°. The smaller wave system came from a direction approximately 150°, i.e. South south Easterly, with a modal period around 8.5s. Given

the reduced fetch in this direction, it is likely that these were locally generated wind waves, with the larger system being recent storm waves arriving from the Atlantic. For calculation of the relative headings shown in Table 5.3, the wave spectra were subjected to a calculation of the 'weighted mean direction'. The direction of each frequency component of the spectrum was averaged but with a weighting according to the magnitude of the energy spectral ordinate.

The RMS responses of the vessel measured on the trial are plotted against this heading relative to the waves in Figure 5.8. In general, the trial points show less confusing trends than the frigate data, and the roll plot for example is much closer to the classic form for well spread waves of Figure 4.1.

Some comparison with the seakeeping software has been attempted in Figure 5.8 (the points labelled 'PAT' and 'PCG'). The computer modelling assumed symmetrical but spread spectra at the relative headings in Table 5.3, and used the individual wave spectra calculated for each run. The models met with mixed success; pitch appears reasonably well predicted, but roll and heave are over predicted. This could well be due to the simplicity of the software in assuming a symmetrical spectrum; the trial spectra are dominated by the low frequency component but the higher frequency component from the South East may be significant – better results might be obtained with a more advanced approach accounting for the directionality of the wave spectra.

5.4 Trials with two launches

Trials with two different craft are presented together in this section as they perform similar roles, and the trials were performed in an identical trials area (Holyhead Bay) on consecutive days.

'Launch A' is a steel hulled craft of 24m length and displacing 70 tonnes. 'Launch B' is an older, wooden hulled craft of length 19m and 28 Tonnes displacement. Again, motions were measured in 6 degrees of freedom (at convenient points on the vessels rather than the anticipated Centre of Gravity), and a star trajectory was carried out about

a moored directional waverider buoy. The modified star pattern shown in Figure 3.4 was used as the seaway appeared relatively long crested, with runs of 14 or 28 minutes depending on the heading to the waves. Runs were made at 7 knots nominal speed for both craft.

For Launch A, the wave conditions were subjectively reported as high sea state 3, stationary, fairly long crested and from direction 310° magnetic. For the trial with Launch B, the waves were estimated as low sea state 3, from direction 270° magnetic, but diminishing significantly by the end of the trial. Average directional wave data for the two trials are given in Figure 5.9. For Launch B, the average was taken only over the first half of the wave data, when the conditions were reasonably stationary. The energy in the seaway, related to the square of the significant wave height, on the second day (for Launch B) was roughly half that of the first day. The wave data are summarised in Table 5.4. These spectra are much more closely symmetrical and unimodal than for the previous two ships. This can be seen visually and also by examination of the skewness points in Figure 5.9; the values are close to zero (a skewness of 6 represents severe asymmetry).

Figure 5.10 and 5.11 give the RMS motions (at the instrument locations) for Launch A and Launch B respectively. The results from complementary headings port and starboard are clearly very consistent with each other, in marked contrast to the ships reported in section 5.2 and 5.3. This is the effect of the much more long crested, symmetrical wave spectra.

Results using the PAT-95 strip theory code are also included on the plots. The correlation with trials results appears much better for Launch 1 than Launch 2. Again the wave definition could play a part as the code accepts a smooth average spectrum with constant spreading only. The shape of Launch B may also play a part, with hard chines that may increase roll damping but that will not be accounted for in the calculation.

5.5 Trials with trimaran ship

This candidate was privileged to be nominated Seakeeping Trials Officer for trials of the trimaran warship demonstrator RV Triton. Launched in 2000, RV Triton is the world's only large steel hulled, powered trimaran ship. She is 90m on the waterline and around 1350 Tonnes in displacement. The seakeeping trials, aimed at providing full-scale RAOs, form a critical part of the seakeeping software model development process because the existing ship motion theories and tools for multihulls are immature. The techniques proposed in this thesis have been applied for the trials.

Some thirty star patterns of trials runs have been performed for the ship with concurrent directional wave buoy data, at various speeds, displacements, loading conditions and both stabilised and unstabilised. Trials were carried out in the western English Channel in a water depth of 95m. The ship is instrumented with around 300 data channels, including seven tri-axial accelerometer packs.

Two star pattern examples will be presented here complementing the results already given for monohull ship trials. The linear motions are reported for the most centrally located accelerometer pack, nominally at the ship Centre of Gravity.

For the first example, the directional wave spectrum in Figure 5.12 shows strong bimodality in a similar way as the frigate data but at mid Sea State 5 this is a much larger seaway. There are strong wind and swell components that are almost opposed to each other in directions approximately 70° and 270° respectively. The star pattern was performed with 270° as the nominal head sea direction. The ship responses in this wave environment, in Figure 5.13, show some confusion as for the frigate trial; roll for example shows a peak in one of the nominal 150° directions and a low roll angle in one of the nominal beam sea directions.

For the second example, Figure 5.14 shows a beautifully long crested and unimodal high Sea State 5 spectrum, of classic fully developed shape. The wave spreading at the peak is low at around 15°, and the symmetry is shown in the skewness plot which is close to zero for all wave frequencies. This purity follows through onto the plots of RMS

motions vs. nominal relative heading in Figure 5.15. Save for one rogue point in Yaw, the port and starboard results on complementary headings are almost coincidental, and there is only a slight sawtooth effect in the plots.

The magnitudes of the responses in beam seas compared with head and following seas in Figure 5.15 is interesting; roll does not approach zero in nominal head and following seas and pitch does not approach zero in beam seas, but they remain around one half their peak values. For the computed monohull roll of example Figure 4.1, this ratio is close to one third even for the most highly spread (cosine squared) seas. The trimaran may be relatively more dynamically stable than the monohull in beam seas, and/or relatively less stable in head and following seas. The monohull example in Figure 5.15 was at 18 knots; more substantial comparison should consider speed as Froude number.

5.6 Summary

This section has demonstrated the conduct of seakeeping trials using the trajectories discussed in Chapter 3 using five different vessels. Performing trials at all compass headings is clearly beneficial in understanding the effect of the wave environment on the ship. The example presenting the most difficulty for the seaman with regards to sea confusion, the frigate trial, had a strongly bimodal seaway and if thinking of the seas in a conventional way, the ship motions showed inconsistency about the nominal relative headings. This trial clearly requires advanced techniques to extract meaningful RAO information.

In contrast, the final example of a trial conducted in a strongly unimodal seaway showed corresponding symmetry in the complementary nominal relative headings. Whilst this data is much more suitable for extraction of RAO information by making the assumption of unidirectional seas, the non-zero pitch response in beam seas for example suggests that a more in depth analysis is still necessary to deduce the RAOs. This thesis presents one such approach in Chapter 7.

Run	Start Time	Mean ship Heading	Nominal Relative Heading	Log Speed	Significant Wave Height
		deg True	deg	knots	m
1	22:20	286	180	5.1	1.48
2	22:42	256	150	5.2	1.37
3	22:59	228	122	5.2	1.34
4	23:15	199	93	5.5	1.34
5	23:52	166	60	4.9	1.32
6	00:08	136	30	5.6	1.31
7	00:24	105	359	5.5	1.30
8	00:42	75	329	5.3	1.28
9	01:05	46	300	5.1	1.25
10	01:22	16	270	5.3	1.22
11	01:38	346	240	5.2	1.18
12	02:01	316	210	5.4	1.14

Table 5.1 Run details: frigate 'octagon'

Sea State Number	Significant Wave Height [m]
0 – 1	0 - 0.1
2	0.1 - 0.5
3	0.5 – 1.25
4	1.25 – 2.5
5	2.5 – 4
6	4 – 6
7	6 – 9
8	9 – 14
>8	>14

Table 5.2 NATO Sea State definition (Bales et al. 1981)

Run	Mid Time	Mean ship Heading	Significant Wave Height	Wave Modal Period	Weighted Mean Wave Direction	Relative Heading [0°-360°]	Relative Heading [0-180°]
		deg True	m	s	deg True	deg	Deg
1	12:36	6	5.28	11.1	208	338	22
2	13:04	215	5.25	11.8	206	189	171
3	13:33	63	5.18	11.8	203	164	164
4	14:03	274	5.45	11.8	201	253	107
5	14:31	124	5.47	11.8	202	102	102
6	14:53	337	5.13	11.1	204	313	47
7	15:40	185	5.50	11.1	201	164	164
8	15:59	34	5.45	10.5	203	11	11
9	16:27	245	5.36	11.8	202	223	137
10	17:01	93	5.45	10.5	203	70	70
11	17:15	305	5.45	10.5	203	282	78
12	17:35	155	5.33	11.1	199	136	136

Table 5.3 Run details: Fishing vessel star

	Time	$H_{1/3}$ [m]	T_0 [s]	T_{peak} [s]	Weighted Mean Direction [deg True]	Weighted Mean Spreading Angle [deg]
Launch A	14:36	1.28	4.3	5.6	332	43
	15:36	1.27	4.1	5.6	346	40
	16:36	1.18	3.9	5.3	322	35
	17:36	1.40	4.0	5.3	321	32
	18:36	1.26	4.3	5.6	315	41
	19:36	1.21	4.7	5.9	304	37
Launch B	10:06	0.78	3.8	4.5	266	36
	11:06	0.87	3.8	4.5	274	38
	12:06	0.79	3.6	4.5	283	37
	13:36	0.83	3.4	4.3	300	42
	14:36	0.72	3.3	4.3	294	27
	15:36	0.67	3.4	4.0	295	24
	16:36	0.53	3.2	4.0	326	54

Table 5.4 Wave details: Launch A and Launch B stars

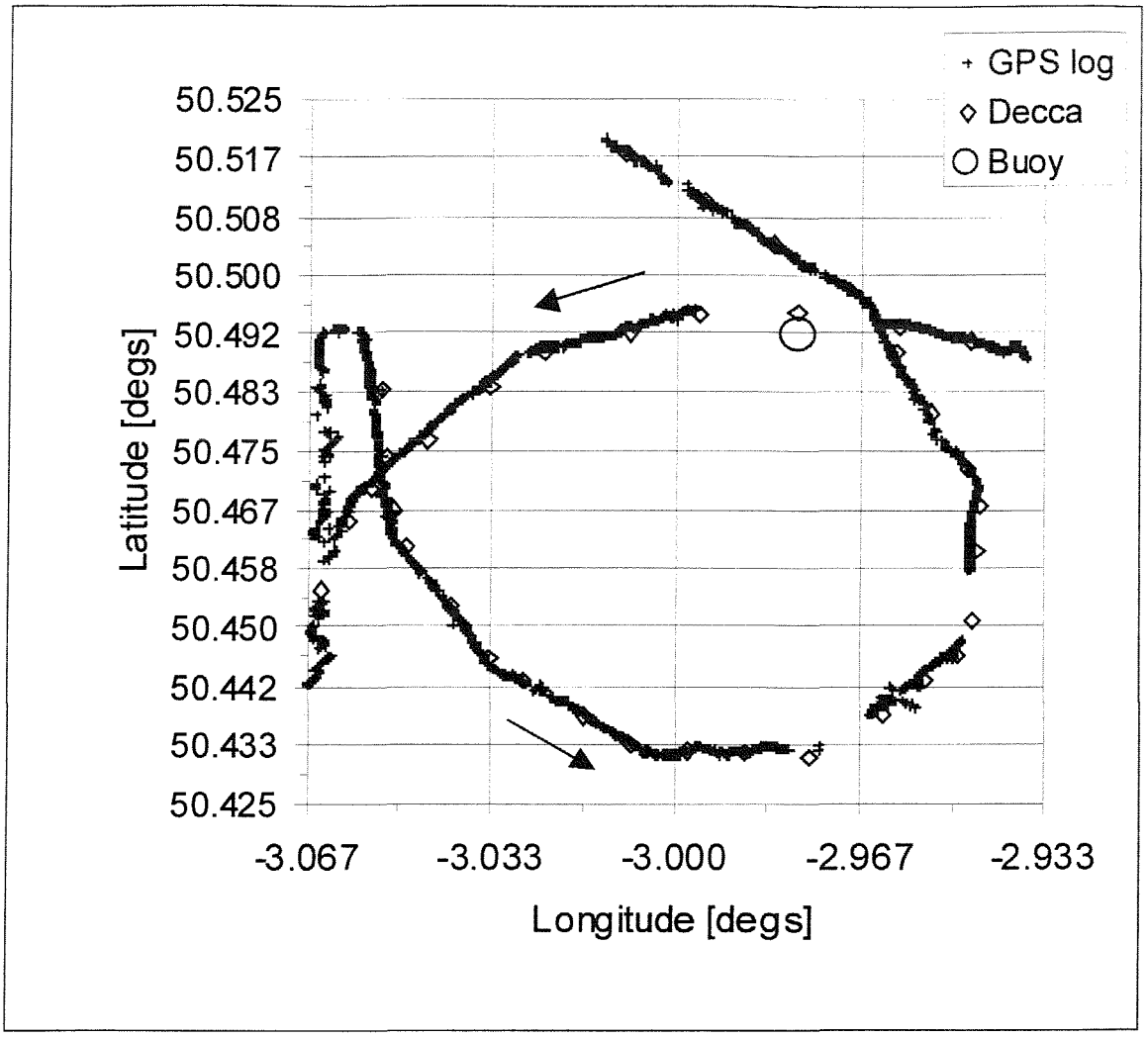

Figure 5.1 Ship trajectory during dedicated trial

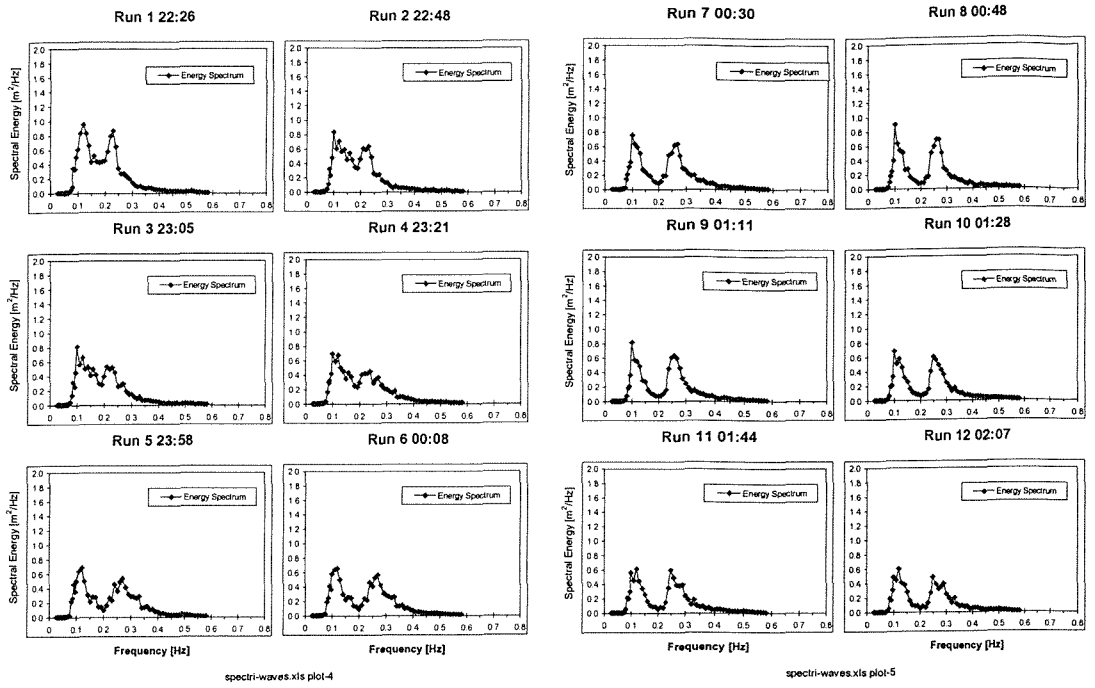

Figure 5.2 Frigate waves summary

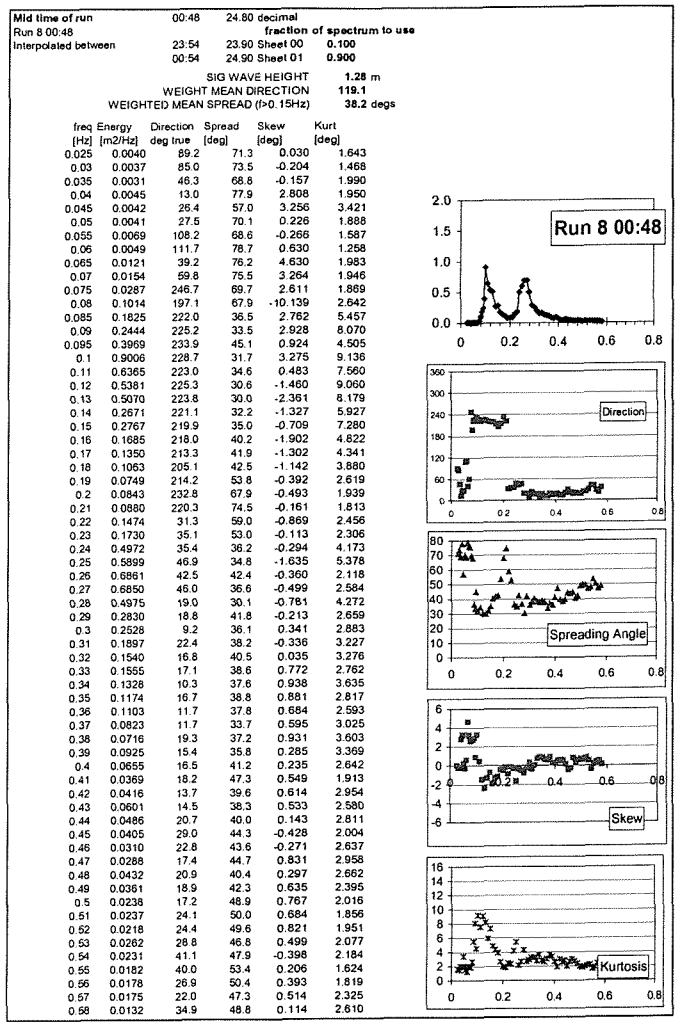

Mid time of run 00:48 24.80 decimal
Run 8 00:48 fraction of spectrum to use
Interpolated between 23:54 23.90 Sheet 00 0.100
00:54 24.90 Sheet 01 0.900

SIG WAVE HEIGHT 1.28 m
WEIGHT MEAN DIRECTION 119.1
WEIGHTED MEAN SPREAD (f>0.15Hz) 38.2 degs

freq [Hz]	Energy [m2/Hz]	Direction deg true	Spread [deg]	Skew [deg]	Kurt [deg]
0.025	0.0040	89.2	71.3	0.030	1.643
0.03	0.0037	85.0	73.5	-0.204	1.468
0.035	0.0031	46.3	68.8	-0.157	1.990
0.04	0.0045	13.0	77.9	2.808	1.950
0.045	0.0042	26.4	57.0	3.256	3.421
0.05	0.0041	27.5	70.1	0.226	1.888
0.055	0.0069	108.2	68.6	-0.266	1.587
0.06	0.0049	111.7	78.7	0.630	1.258
0.065	0.0121	39.2	76.2	4.630	1.983
0.07	0.0154	59.8	75.5	3.264	1.946
0.075	0.0287	246.7	69.7	2.611	1.869
0.08	0.1014	197.1	67.9	-10.139	2.642
0.085	0.1825	222.0	36.5	2.762	5.457
0.09	0.2444	225.2	33.5	2.928	8.070
0.095	0.3969	233.9	45.1	0.924	4.505
0.1	0.9006	228.7	31.7	3.275	9.136
0.11	0.6365	223.0	34.6	0.483	7.560
0.12	0.5381	225.3	30.6	-1.460	9.060
0.13	0.5070	223.8	30.0	-2.361	8.179
0.14	0.2671	221.1	32.2	-1.327	5.927
0.15	0.2767	219.9	35.0	-0.709	7.280
0.16	0.1685	218.0	40.2	-1.902	4.822
0.17	0.1350	213.3	41.9	-1.302	4.341
0.18	0.1063	205.1	42.5	-1.142	3.880
0.19	0.0749	214.2	53.8	-0.392	2.619
0.2	0.0843	232.8	67.9	-0.493	1.939
0.21	0.0880	220.3	74.5	-0.161	1.813
0.22	0.1474	31.3	59.0	-0.869	2.456
0.23	0.1730	35.1	53.0	-0.113	2.306
0.24	0.4972	35.4	36.2	-0.294	4.173
0.25	0.5899	46.9	34.8	-1.635	5.378
0.26	0.6861	42.5	42.4	-0.360	2.118
0.27	0.6850	46.0	36.6	-0.499	2.584
0.28	0.4975	19.0	30.1	-0.781	4.272
0.29	0.2830	18.8	41.8	-0.213	2.659
0.3	0.2528	9.2	36.1	0.341	2.883
0.31	0.1897	22.4	38.2	-0.336	3.227
0.32	0.1540	16.8	40.5	0.035	3.276
0.33	0.1555	17.1	38.6	0.772	2.762
0.34	0.1328	10.3	37.6	0.938	3.635
0.35	0.1174	16.7	38.8	0.881	2.817
0.36	0.1103	11.7	37.8	0.684	2.593
0.37	0.0823	11.7	33.7	0.595	3.025
0.38	0.0716	19.3	37.2	0.931	3.603
0.39	0.0925	15.4	35.8	0.285	3.369
0.4	0.0655	16.5	41.2	0.235	2.642
0.41	0.0369	18.2	47.3	0.549	1.913
0.42	0.0416	13.7	39.6	0.614	2.954
0.43	0.0601	14.5	38.3	0.533	2.580
0.44	0.0486	20.7	40.0	0.143	2.811
0.45	0.0405	29.0	44.3	-0.428	2.004
0.46	0.0310	22.8	43.6	-0.271	2.637
0.47	0.0288	17.4	44.7	0.831	2.958
0.48	0.0432	20.9	40.4	0.297	2.662
0.49	0.0361	18.9	42.3	0.635	2.395
0.5	0.0238	17.2	48.9	0.767	2.016
0.51	0.0237	24.1	50.0	0.684	1.856
0.52	0.0218	24.4	49.6	0.821	1.951
0.53	0.0262	28.8	46.8	0.499	2.077
0.54	0.0231	41.1	47.9	-0.398	2.184
0.55	0.0182	40.0	53.4	0.206	1.624
0.56	0.0178	26.9	50.4	0.393	1.819
0.57	0.0175	22.0	47.3	0.514	2.325
0.58	0.0132	34.9	48.8	0.114	2.610

Figure 5.3 Frigate waves: detailed example

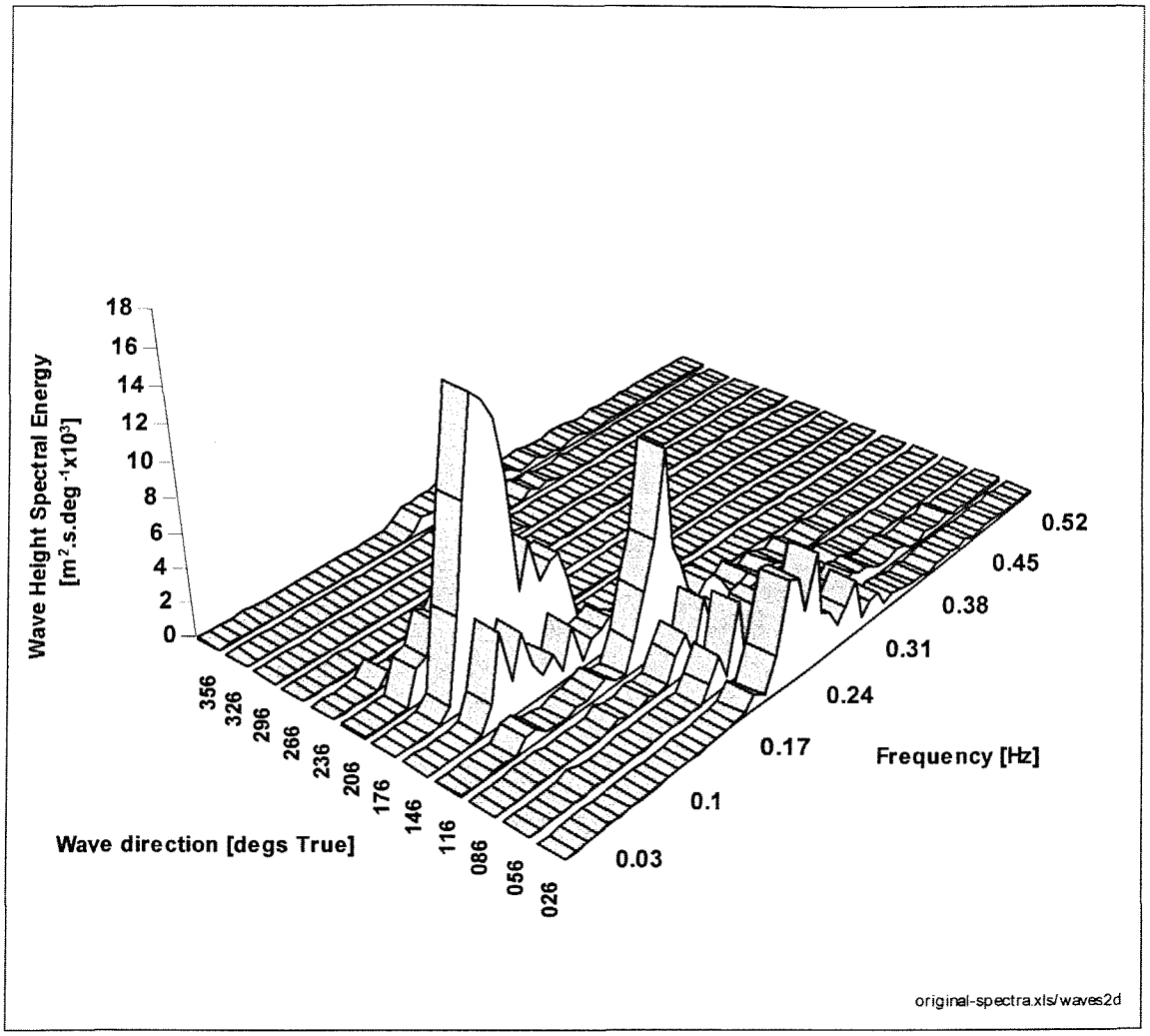

Figure 5.4 Directional spectrum recorded during trial

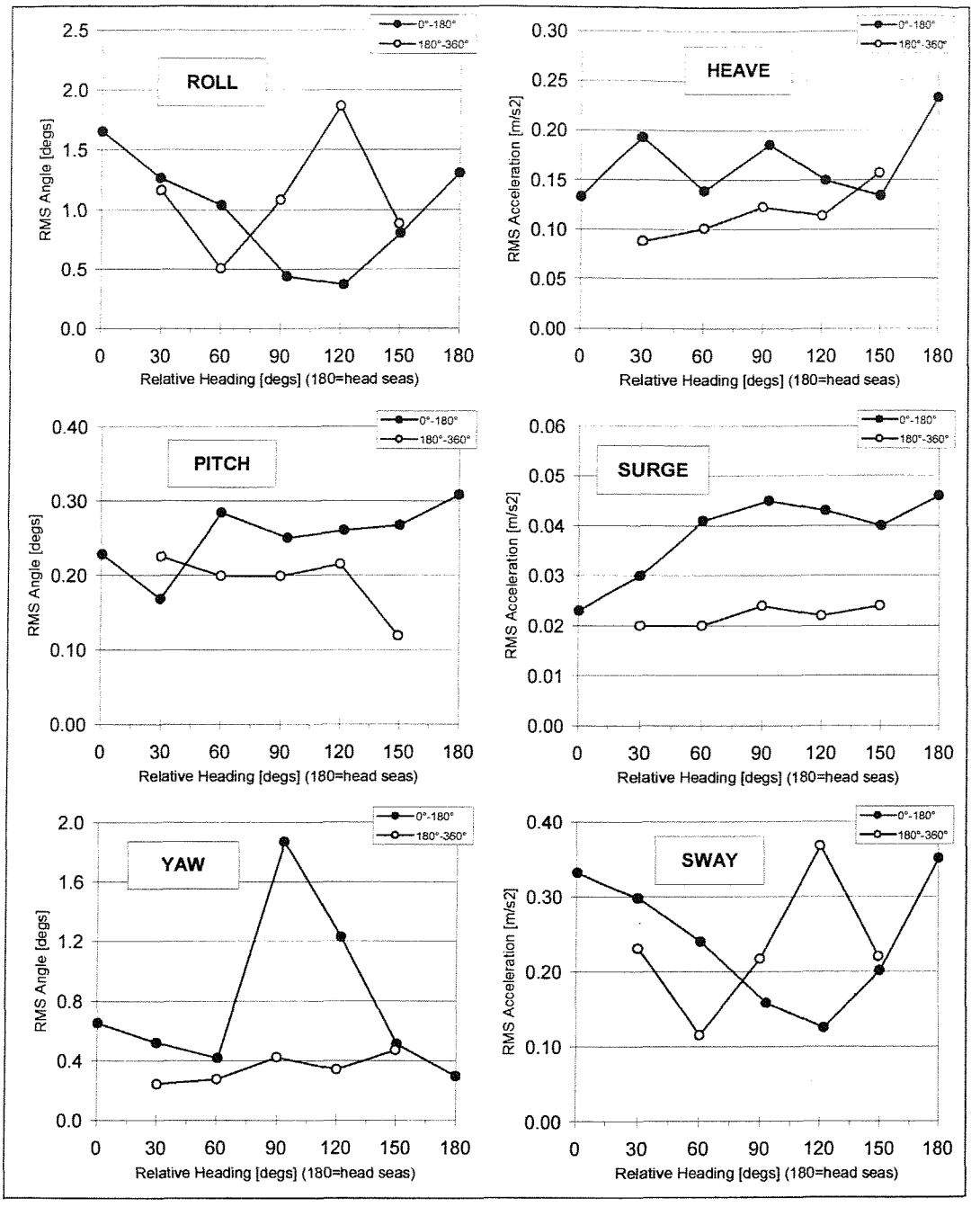

Figure 5.5 Frigate RMS motions

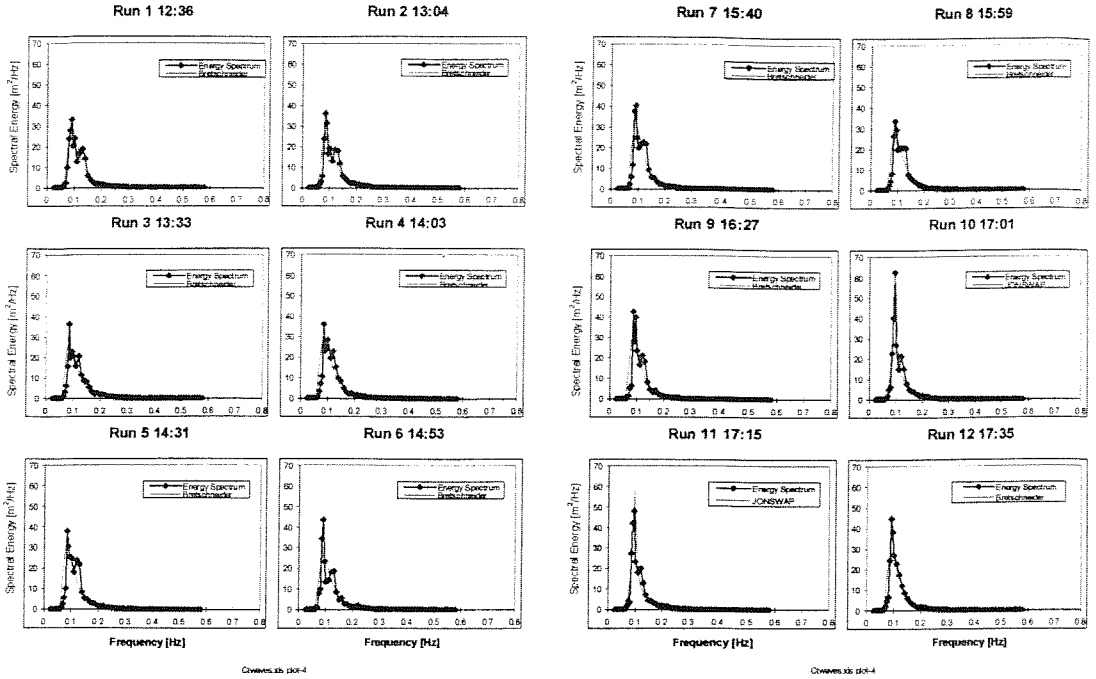

Figure 5.6 Fishing vessel waves summary

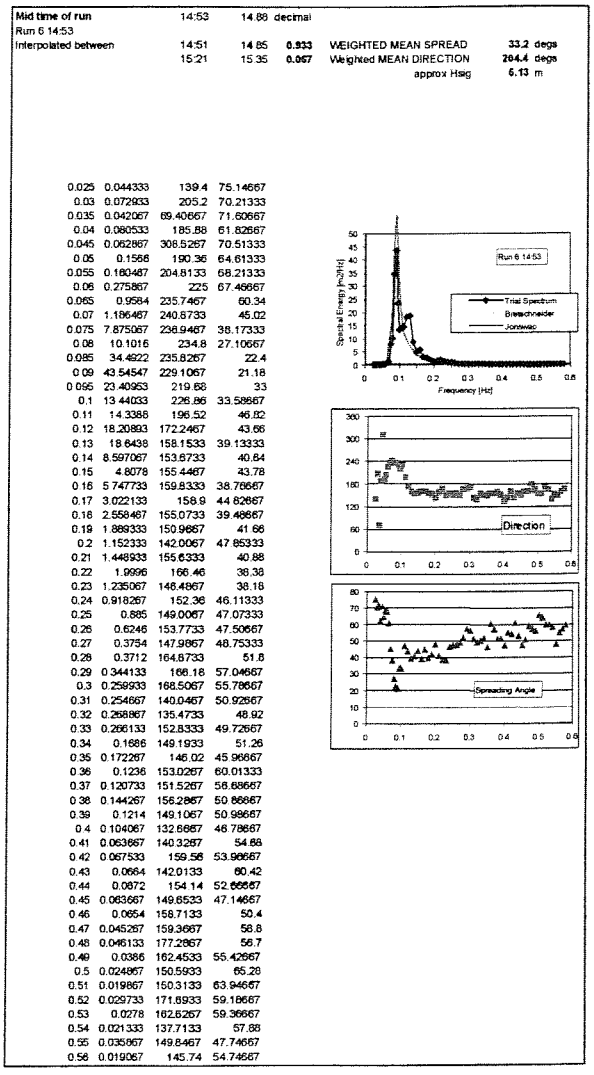

Mid time of run		14:53	14.88	decimal			
Run 6 14:53							
Interpolated between		14:51	14.85	0.833	WEIGHTED MEAN SPREAD	33.2	degs
		15:21	15.35	0.867	Weighted MEAN DIRECTION	204.4	degs
					approx Hsig	6.13	m
0.025	0.044333		139.4	75.14667			
0.03	0.072933		205.2	70.21333			
0.035	0.042067		69.40667	71.60667			
0.04	0.080533		185.88	61.82667			
0.045	0.062867		308.5267	70.51333			
0.05	0.1568		190.36	64.61333			
0.055	0.160467		204.8133	68.21333			
0.06	0.275867		225	67.46667			
0.065	0.9584		235.7467	60.34			
0.07	1.186467		240.8733	45.02			
0.075	7.875067		236.9467	38.17333			
0.08	10.1016		234.8	27.10667			
0.085	34.4922		235.8267	22.4			
0.09	43.54547		229.1067	21.18			
0.095	23.40953		219.68	33			
0.1	13.44033		226.86	33.58667			
0.11	14.3388		196.52	46.82			
0.12	18.20893		172.2467	43.66			
0.13	18.6438		158.1533	39.13333			
0.14	8.597067		153.8733	40.84			
0.15	4.8078		155.4467	43.78			
0.16	5.747733		159.8333	38.78667			
0.17	3.022133		158.9	44.82667			
0.18	2.558467		155.0733	39.48667			
0.19	1.889333		150.9667	41.66			
0.2	1.152333		142.0067	47.85333			
0.21	1.448933		155.6333	40.88			
0.22	1.9996		166.46	36.38			
0.23	1.235067		148.4867	38.18			
0.24	0.918267		152.36	46.11333			
0.25	0.885		149.0067	47.07333			
0.26	0.6246		153.7733	47.50667			
0.27	0.3754		147.9867	48.75333			
0.28	0.3712		164.8733	51.8			
0.29	0.344133		166.18	57.04667			
0.3	0.259933		168.5067	55.78667			
0.31	0.254667		140.0467	50.92667			
0.32	0.268867		135.4733	48.92			
0.33	0.266133		152.8333	49.72667			
0.34	0.1686		149.1933	51.26			
0.35	0.172267		146.02	45.96667			
0.36	0.1236		153.0267	60.01333			
0.37	0.120733		151.5267	58.68667			
0.38	0.144267		156.2867	50.86667			
0.39	0.1214		149.1067	50.98667			
0.4	0.104067		132.6667	46.78667			
0.41	0.063667		140.3267	54.66			
0.42	0.067533		159.56	53.96667			
0.43	0.0664		142.0133	60.42			
0.44	0.0872		154.14	52.66667			
0.45	0.063667		149.8533	47.14667			
0.46	0.0654		158.7133	50.4			
0.47	0.045267		159.3667	56.8			
0.48	0.046133		177.2867	56.7			
0.49	0.0386		162.4533	55.42667			
0.5	0.024867		150.5933	65.28			
0.51	0.019867		150.3133	63.94667			
0.52	0.029733		171.6933	59.18667			
0.53	0.0278		162.6267	59.36667			
0.54	0.021333		137.7133	57.88			
0.55	0.035867		149.8467	47.74667			
0.56	0.019067		145.74	54.74667			

Figure 5.7 Fishing vessel waves: detailed example

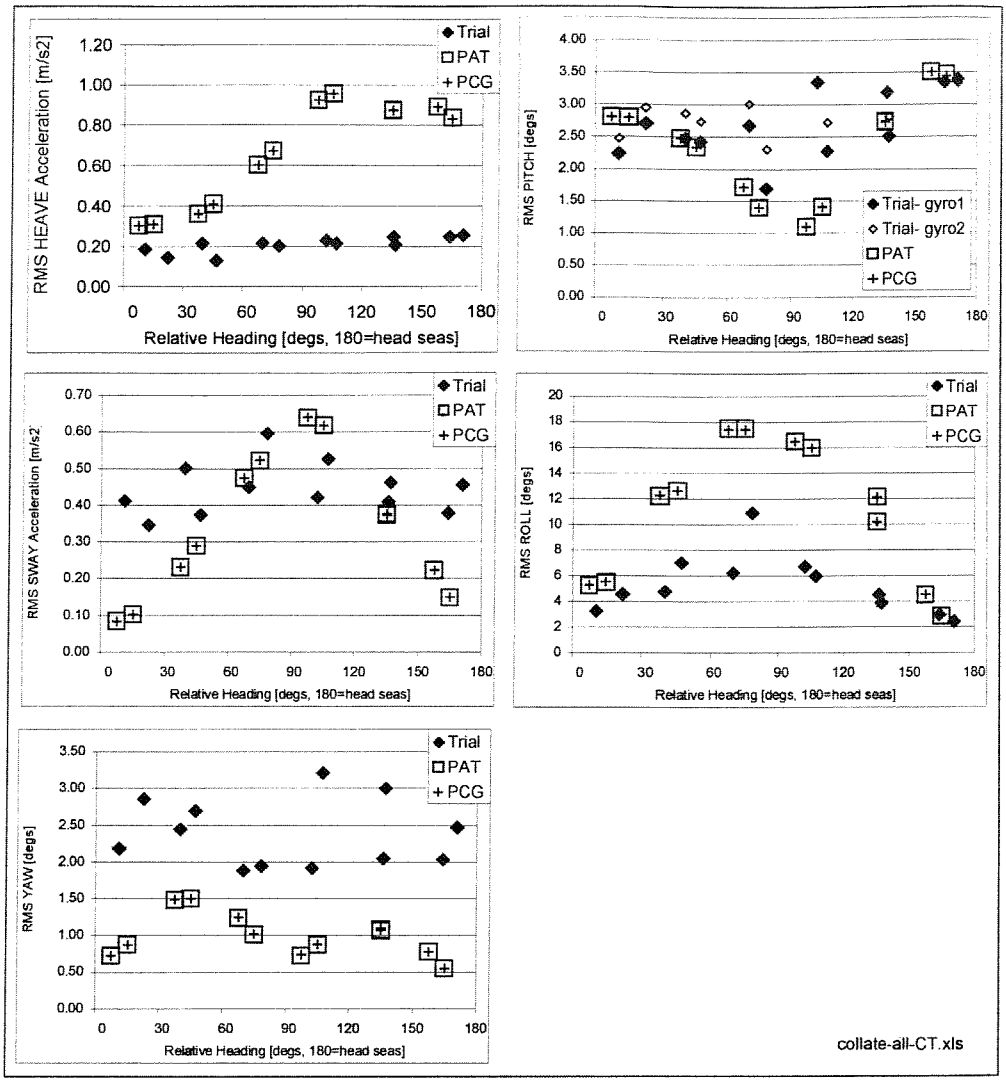

Figure 5.8 Fishing vessel RMS motions

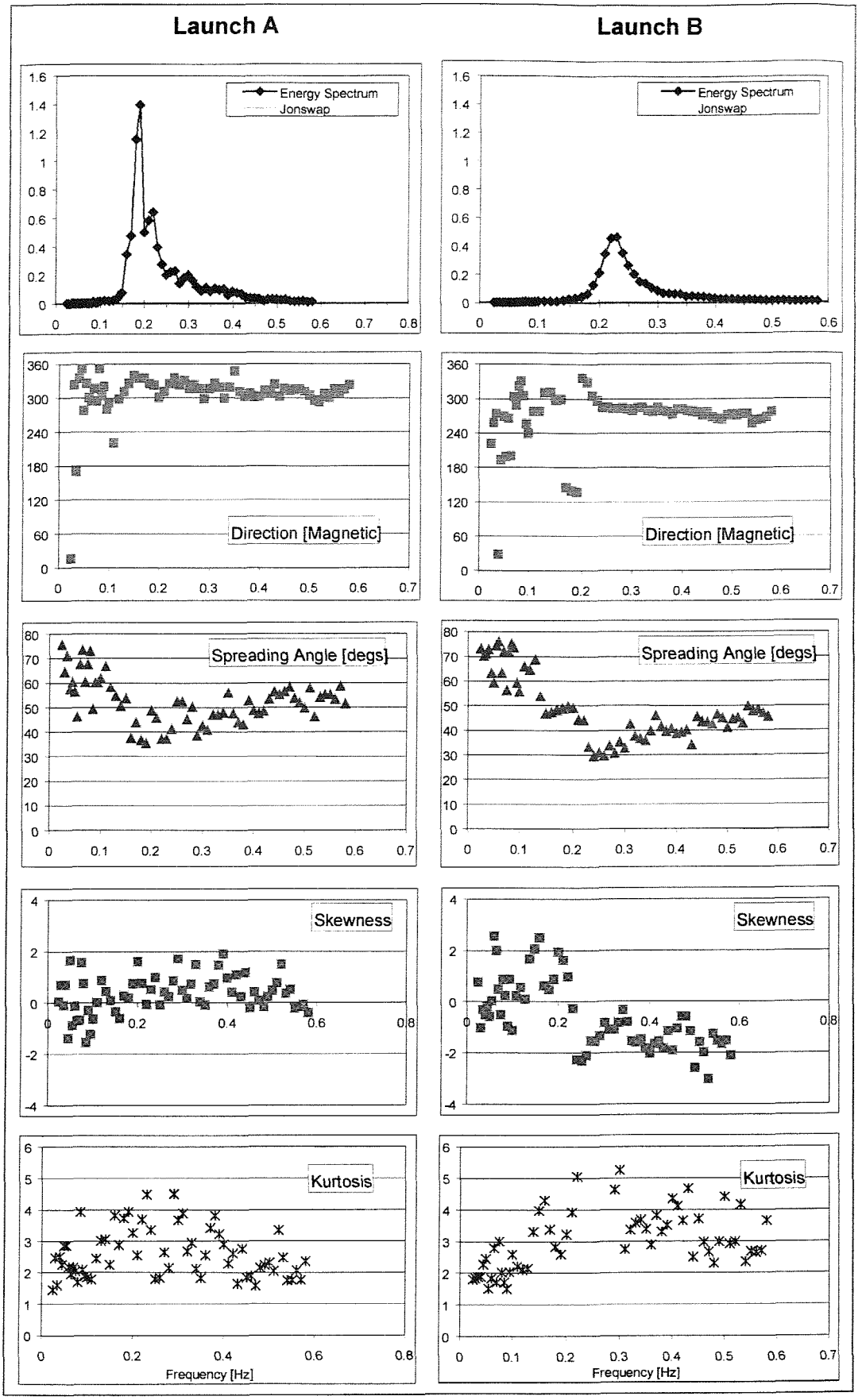

Figure 5.9 Average wave parameters for trials with Launch A and Launch B

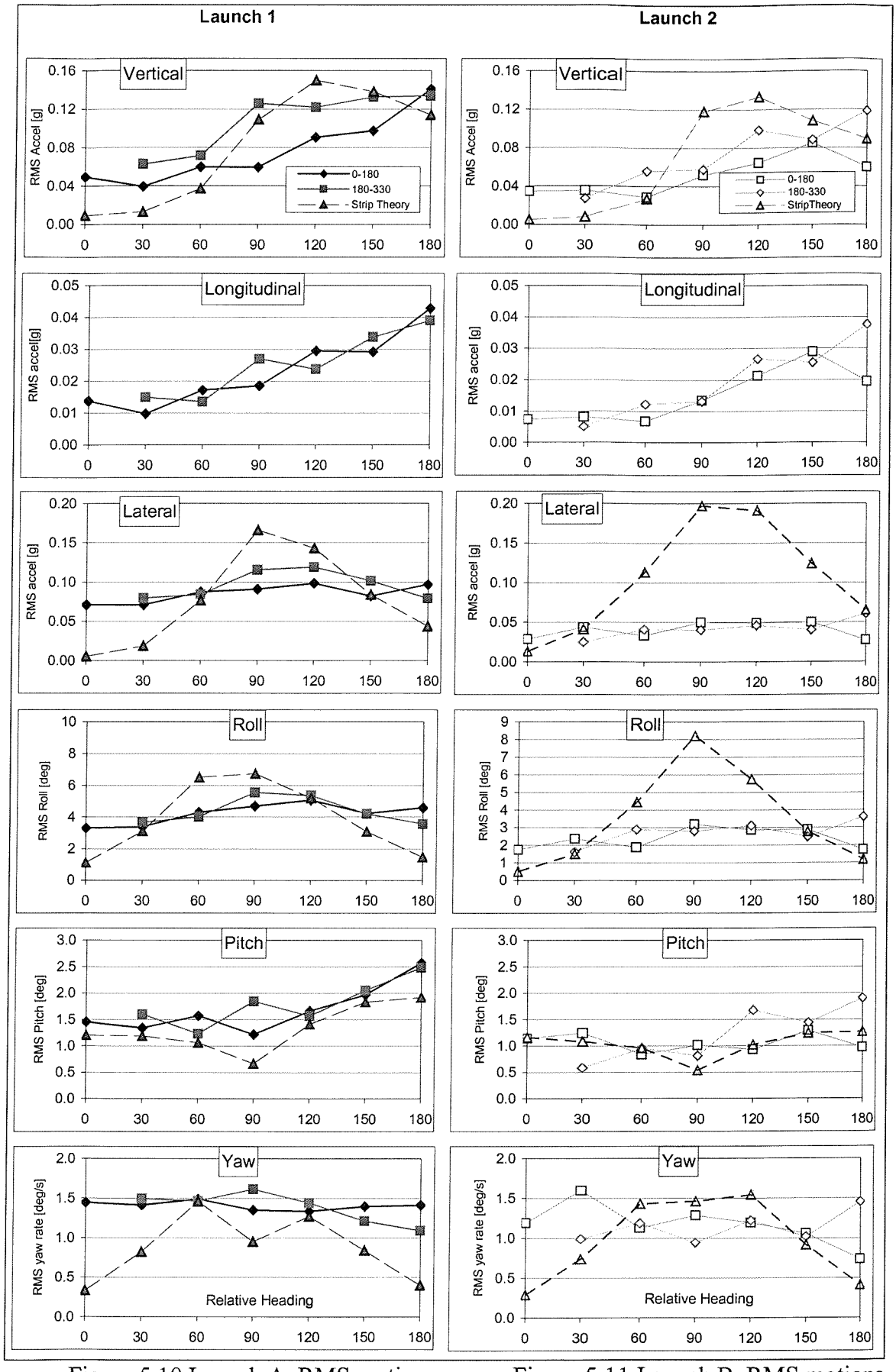

Figure 5.10 Launch A RMS motions

Figure 5.11 Launch B RMS motions

7	transmission no
230	sig height (cm)
6.451613	Tz [s]
9.508569	max S(m) [m2/Hz]
25.3	Sea surface temperature (deg C)
10.95	Ref (dummy) temperature
7	Battery condition 0-7
-0.2475	Vertical accel offset [m/sec2]
0.065	X accel offset [m/sec2]
0.04375	Y accel offset [m/sec2]
4.21875	Compass heading [deg],
64.6875	Magnetic field inclination [deg]

Freq [Hz]	Energy (m2/Hz)	Direction (true)	Spreading	Skewness	Curtosis
0.025	0.005	149	75.6	0.197	1.539
0.03	0.013	328	70.7	-1.605	2.147
0.035	0.016	23	69.4	2.509	2.241
0.04	0.033	343	68.9	-0.171	1.786
0.045	0.022	238	68.0	1.404	2.161
0.05	0.066	280	57.7	-0.697	1.666
0.055	0.087	156	79.2	-0.144	1.519
0.06	0.122	228	71.2	-1.143	1.634
0.065	1.661	278	38.0	-2.337	6.660
0.07	4.866	263	34.5	-3.652	9.025
0.075	9.509	271	27.3	1.182	7.616
0.08	3.429	257	29.5	-2.376	8.856
0.085	3.885	270	36.7	-0.746	5.201
0.09	1.737	259	36.3	-0.066	3.948
0.095	1.703	260	34.9	-1.182	6.353
0.1	1.313	259	28.2	-0.410	8.791
0.11	0.713	253	56.4	-0.620	3.130
0.12	1.141	58	63.6	-2.650	2.786
0.13	2.253	66	33.6	0.913	9.397
0.14	2.453	73	20.1	3.849	20.089
0.15	2.219	75	22.8	0.000	14.657
0.16	1.387	70	27.8	1.690	9.669
0.17	1.408	75	25.5	1.753	8.251
0.18	1.086	72	28.2	1.316	4.797
0.19	1.182	76	26.4	1.391	6.712
0.2	0.630	79	31.8	0.905	4.748
0.21	0.578	76	30.9	0.815	4.513
0.22	0.567	75	30.4	1.135	5.738
0.23	0.418	83	36.7	0.676	2.696
0.24	0.293	80	40.3	0.684	3.041
0.25	0.270	97	41.2	-0.039	2.591
0.26	0.382	97	36.7	-0.563	3.809
0.27	0.335	87	34.0	0.960	3.426
0.28	0.230	100	38.0	-0.332	2.884
0.29	0.167	105	42.5	-0.150	2.627
0.3	0.206	96	34.5	-0.199	5.446
0.31	0.096	103	46.1	-0.915	2.861
0.32	0.107	90	43.4	-0.415	2.464
0.33	0.067	94	52.4	-0.367	1.878
0.34	0.065	87	51.9	0.089	1.928
0.35	0.092	84	42.1	0.071	2.421
0.36	0.091	84	47.9	0.053	2.108
0.37	0.049	94	50.6	-0.216	1.788
0.38	0.044	96	47.9	-0.242	2.684
0.39	0.052	114	48.8	-0.544	2.545
0.4	0.041	110	46.1	-1.143	3.084
0.41	0.032	83	56.0	0.149	1.531
0.42	0.028	83	57.7	0.167	1.757
0.43	0.033	94	51.0	0.116	1.963
0.44	0.031	114	44.3	-1.081	3.019
0.45	0.030	107	42.5	-0.702	3.091
0.46	0.017	107	54.6	-0.408	1.847
0.47	0.013	118	54.6	-1.078	2.245
0.48	0.014	113	54.6	-0.684	2.415
0.49	0.015	128	53.7	-1.523	2.872
0.5	0.010	124	54.2	-1.254	2.950
0.51	0.018	115	47.0	-1.322	3.218
0.52	0.012	111	55.1	-0.536	2.133
0.53	0.010	108	61.3	-0.185	2.015
0.54	0.016	127	47.4	0.107	3.474
0.55	0.010	128	50.6	-0.390	2.586
0.56	0.007	136	55.1	-0.731	2.334
0.57	0.007	122	54.6	-1.007	2.529
0.58	0.005	120	60.4	-1.047	2.081

Filename	01152042
Date	15-Jan-2001
Time	8:42 PM

Significant Height	2.3 m
Sea State	4.75
Peak Direction	271 degs
Spreading at peak	27 degs

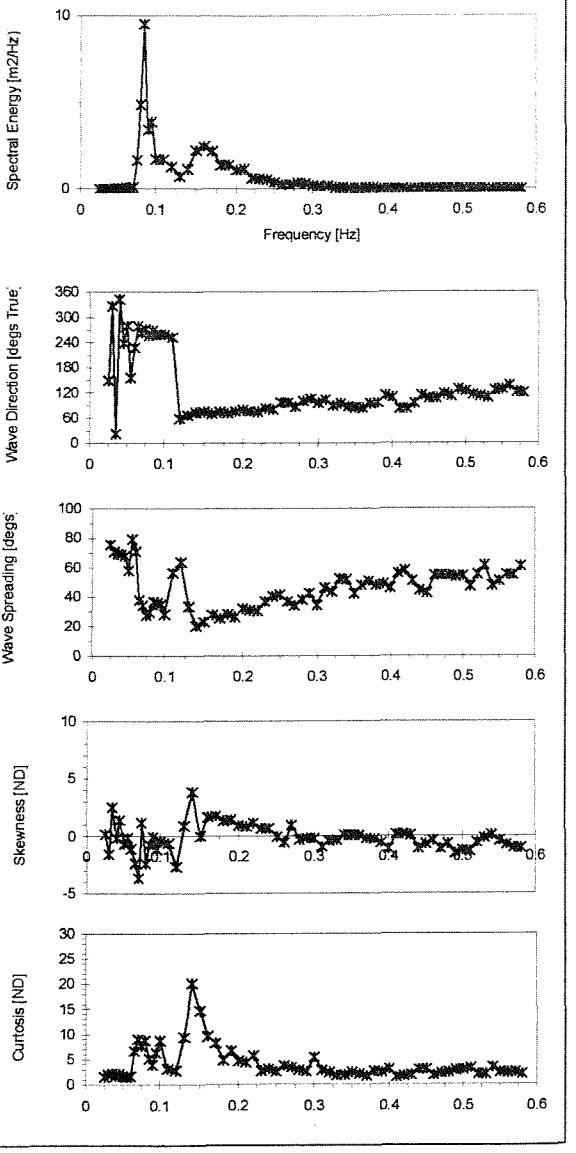

Figure 5.12 Trimaran trial: First example directional wave spectrum file

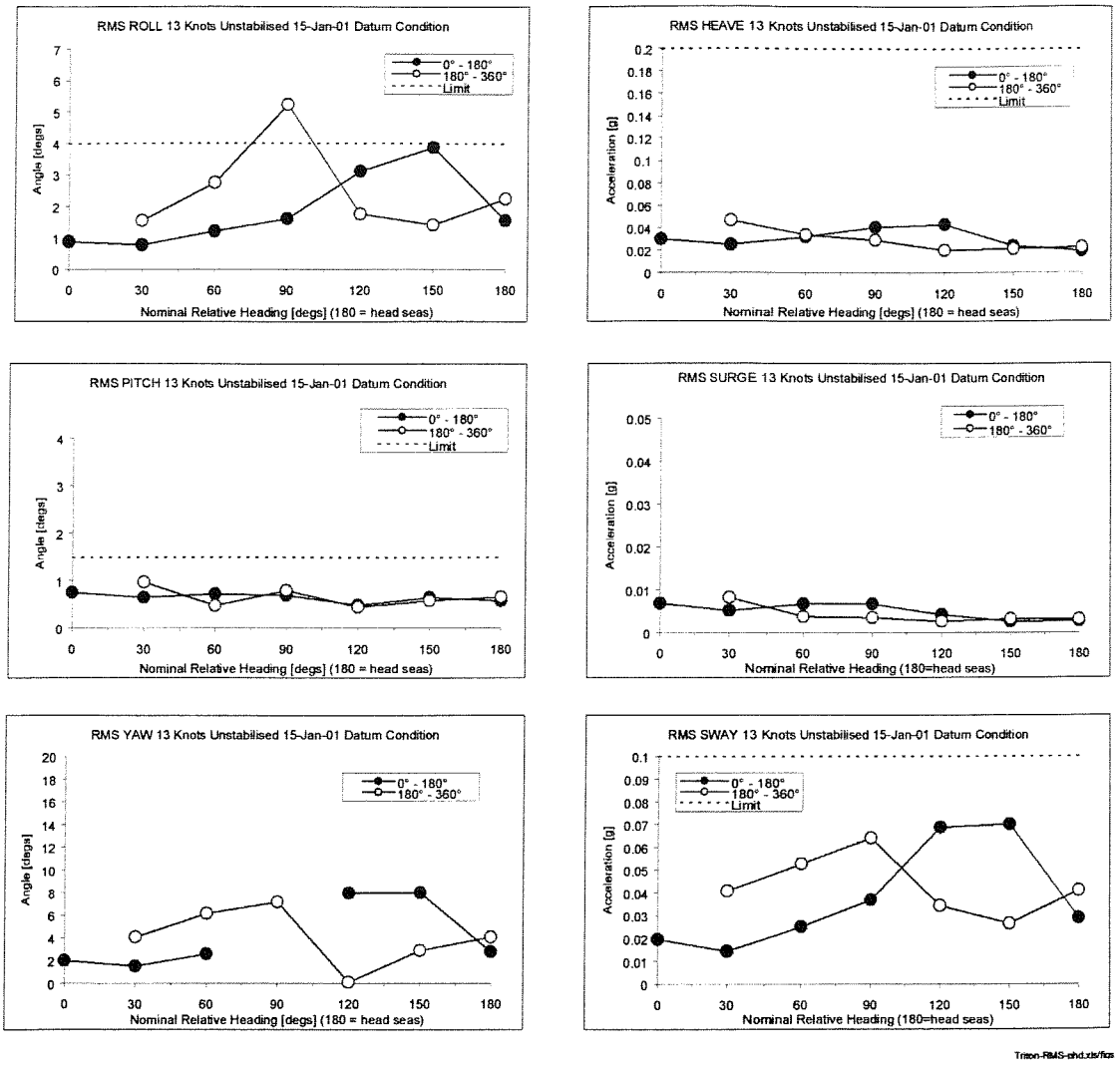

Figure 5.13 Trimaran trial: RMS Motions in first example seaway

7	transmission no
387	sig height (cm)
7.692307	Tz [s]
23.3873	max S(m) [m2/Hz]
25.3	Sea surface temperature (deg C)
13	Ref (dummy) temperature
7	Battery condition 0-7
-0.22125	Vertical accel offset [m/sec2]
-0.21125	X accel offset [m/sec2]
-0.34375	Y accel offset [m/sec2]
223.5938	Compass heading [deg],
64.6875	Magnetic field inclination [deg]

Filename	12051448
Date	05-Dec-2001
Time	2:48 PM

Significant Height	3.87 m
Sea State	5.75
Peak Direction	278 degs
Spreading at peak	17 degs

Freq [Hz]	Energy (m2/Hz)	Direction (true)	Spreading	Skewness	Curtosis
0.025					
0.03					
0.035	0.050	335	75.6	-1.167	1.554
0.04	0.074	300	60.9	-0.134	2.354
0.045	0.072	315	70.7	-1.874	1.818
0.05	0.115	280	66.7	-0.449	1.948
0.055	0.145	257	63.6	0.236	1.744
0.06	0.378	312	49.7	-1.003	2.943
0.065	1.628	290	46.6	-0.426	2.904
0.07	5.431	280	21.5	-3.935	12.642
0.075	13.697	281	13.4	-4.355	41.749
0.08	13.493	288	15.2	3.079	19.028
0.085	23.387	278	16.6	-7.111	27.730
0.09	16.730	277	19.2	-0.665	9.680
0.095	15.835	285	15.7	-0.551	11.573
0.1	12.088	284	26.4	-1.445	5.327
0.11	7.669	285	29.1	-0.840	3.998
0.12	4.793	281	38.0	-0.650	2.803
0.13	4.514	276	40.7	-0.700	2.348
0.14	3.659	264	39.4	0.163	2.518
0.15	3.213	269	38.0	0.381	1.920
0.16	3.087	276	38.5	0.125	2.420
0.17	1.998	276	39.4	-0.214	3.497
0.18	1.929	281	47.9	-0.352	2.332
0.19	1.387	290	47.0	-0.839	2.425
0.2	1.333	277	45.2	-0.292	2.434
0.21	1.387	278	43.4	-0.089	1.991
0.22	0.655	283	45.2	-0.620	2.878
0.23	0.850	278	40.3	0.150	2.337
0.24	0.439	300	49.2	-1.296	2.208
0.25	0.457	285	51.5	-0.458	1.958
0.26	0.335	305	53.3	-1.064	2.223
0.27	0.351	305	52.4	-1.134	2.281
0.28					
0.29	0.287	283	51.9	-0.249	1.952
0.3	0.293	298	46.1	-0.918	2.339
0.31	0.220	283	44.3	-0.189	3.325
0.32	0.177	281	47.9	0.037	2.812
0.33	0.119	290	59.5	-0.628	1.734
0.34	0.125	301	53.3	-0.866	2.097
0.35	0.107	304	51.0	-0.340	2.659
0.36	0.094	316	51.9	-0.242	2.670
0.37	0.076	288	56.4	0.101	1.865
0.38	0.042	297	61.8	-0.431	1.741
0.39	0.066	297	61.8	-0.315	1.649
0.4	0.033	326	60.9	-0.916	2.011
0.41	0.073	314	51.5	-1.259	2.653
0.42	0.065	294	52.4	0.105	2.236
0.43	0.042	304	59.5	-0.552	1.681
0.44	0.033	312	63.1	-0.694	1.864
0.45	0.039	312	57.3	-0.739	2.266
0.46	0.025	295	59.5	0.059	1.855
0.47	0.020	315	60.4	-1.290	2.118
0.48	0.022	325	55.1	-0.748	2.793
0.49	0.025	301	60.9	-0.348	1.765
0.5	0.014	333	59.1	-0.832	2.242
0.51	0.010	342	69.8	-0.811	1.765
0.52	0.018	322	59.5	-0.540	2.204
0.53	0.016	281	65.8	0.528	1.694
0.54	0.013	319	64.5	0.144	1.727
0.55					
0.56					
0.57					
0.58	0.007	338	64.5	-0.664	2.273

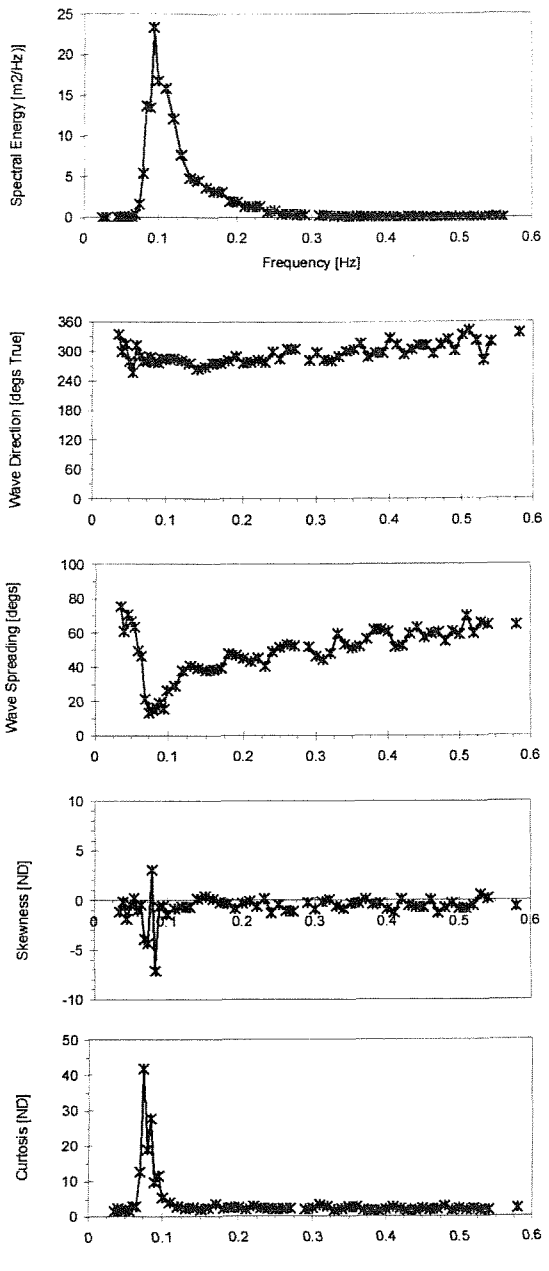

Figure 5.14 Trimaran trial: second example directional wave data

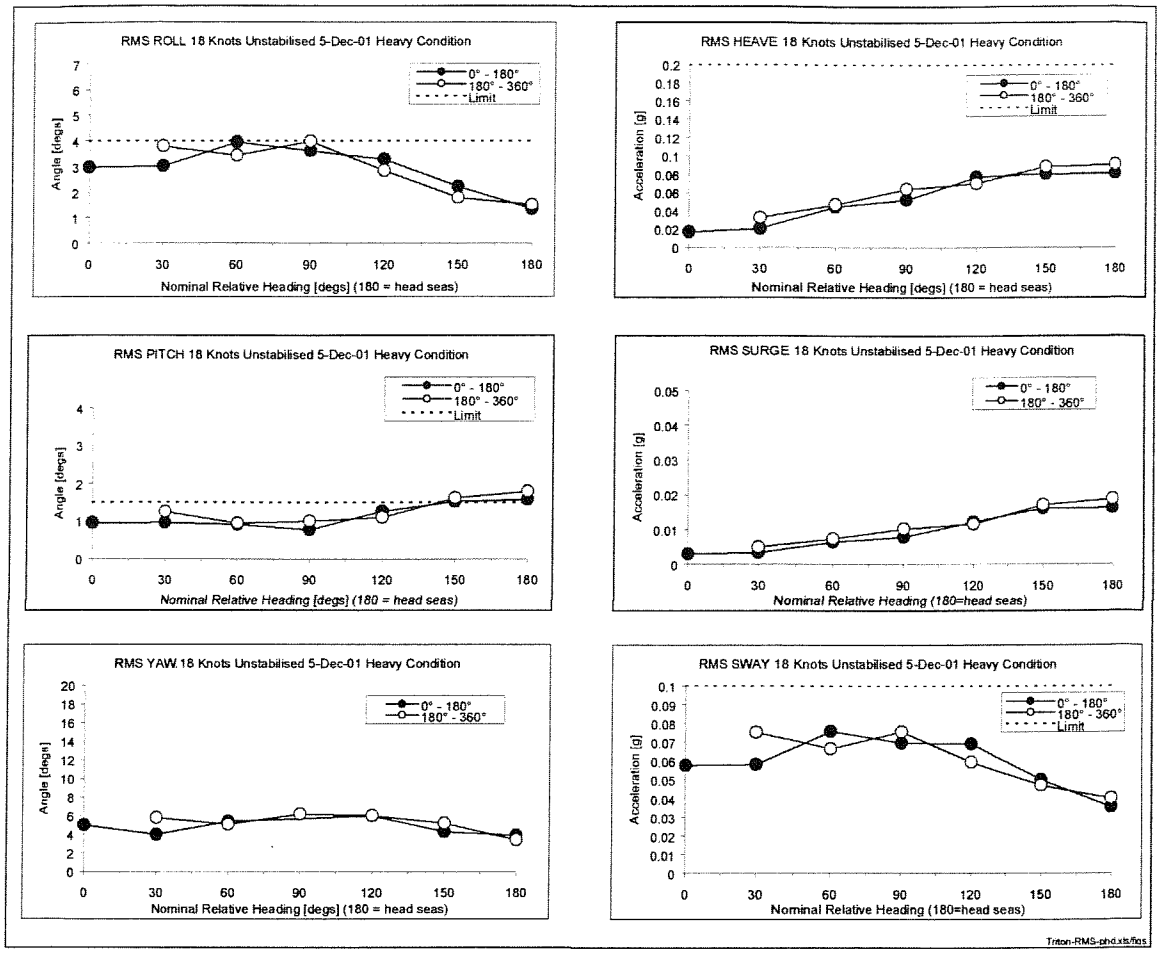

Figure 5.15 Trimaran trial: RMS motions in second example seaway

6. SHIP MOTION CODES - COMPARING WITH TRIALS DATA

6.1 Introduction

The process of validating ship motion theories is usually to compare with results of scale model tests, but full-scale trials represent the ultimate test of the theory. Chapter 3 demonstrated a controlled approach to such trials, and Chapter 5 illustrated the benefits of using this approach. A full-scale trial naturally has a large capital cost, a large associated logistical effort, and of course is at the mercy of the weather – will the sea state be within the desired severity during the allotted time frame? With these pressures on delivering good quality trials data, it is understandable that the effort placed on the use and interpretation of the ship motion code in question often has a less clear focus. This chapter demonstrates the problems encountered when trying to compare ship motion codes directly with trials data, and goes on to suggest general methods to meaningfully compare the trials and computed results.

6.2 Ship trial results

6.2.1 Ship data

The data used in this chapter was for the same frigate as in section 5.2, but was recorded the day before the dedicated trial. The ship had already been rigged with a tri-axial accelerometer pack, and angular motions were measured concurrently, and the opportunity was taken to gather ship motion information whilst the ship went about her daily business. Figure 6.1 shows the ship trajectory on this day; the top left shows how the ship made her entrance and exit to the harbour through different places in the breakwater. The ship speed and heading were at the Captain's discretion.

Seven portions of the trajectory, identified by thick lines on Figure 6.1, have been identified as trials 'runs' where constant speed and heading were maintained. Basic information on these runs is given in Table 6.1. Run 2 is of rather short duration and so

the motion statistics may not be fully representative, and Run 5 is also rather short. The sea state was larger than during the dedicated trial, so here the accelerations measured have been corrected for the effects of roll, pitch, and yaw (the accelerometers respond to components of g when rotated); Table 6.2 gives all the measured and calculated ship motion data.

A further transformation of the data was made to project the motions (measured near the hangar) back to the expected values at the ships centre of gravity (CG). The data was now in 'Earth axes' at the CG, which is the typical format used by ship motion prediction codes, and indeed comparison with a strip theory program is made later in this chapter.

6.2.2 Wave data

A directional waverider buoy was moored in the English Channel some 20 miles to the west of the ship location during the opportunity runs. It has been assumed that the wave spectrum would be similar at this site, as the waves were south westerly and there would be a clear fetch between the two locations. However, the water depth in this region was around 30m, somewhat lower than the 45m at the buoy location, and some of the lower frequencies may have attenuated.

Figure 6.2 gives an example directional energy spectrum recorded at the time of the trial. Half-hourly waverider buoy results were interpolated to give the spectra at the mid times of the 'runs'. Bretschneider and JONSWAP idealised spectra (see Chapter 2) have been fitted to these by a least squares method, for illustrative purposes, and are shown in Figure 6.3(a). The fitted spectra are directional in that they allow $\cos^{2n}$ spreading, but are unimodal.

There appear to have been two wave systems present in the area at the time, a wind system with an energy peak at 0.13Hz from a direction approximately 230°, and some underlying small magnitude swell waves from around 290°. The wind system dominates the total energy at the start of the time window considered here, but diminishes somewhat by the end, as seen in Figure 6.3(b).

The wave conditions during this trial are summarised in Table 6.3. The bimodal character of the seaway makes assessment of the sea direction difficult. At the start of the trial, the peak at 0.13Hz dominates, and the direction of these waves is clearly head seas. By the end of the trial, this direction still looked to be the principal direction, but the seas appeared more confused.

Table 6.3 therefore includes two measures of wave principal direction and spreading angle. The first one is a 'weighted mean', where an average direction and spreading were computed, but with weighting according to the energy present at each frequency in the spectrum. The second measure is the energy peak direction only, with the spreading angle reported by the buoy at the energy peak frequency.

6.3 Comparing trials and computed data

6.3.1 Conventional computer simulation

Most seakeeping codes have two separate aspects of their use, a ship 'geometry' definition giving the ship shape and detailing its appendages, and a 'control' definition where the ship and environmental conditions are specified. For the example given here, the geometry definition is assumed accurate, and the main task for the program user is to set the values of parameters for control of the program. For simulation of the frigate trial runs these were:

- Average ship speed on each run
- Ship displacement approximately 4200 Tonnes
- KG typically 6.05m
- GM typically 1.0m
- Trim between perpendiculars typically 0.6m by stern
- Autopilot with unknown parameters
- Headings relative to the waves for each run
- Wave energy spectrum or significant height and modal period

- Wave spreading $\cos^{32}$ equating to a spreading angle 28 degrees

Note that whilst some of these values can reasonably be measured e.g. draughts giving trim between perpendiculars and displacement, several must remain 'typical' or estimated unless detailed consultation is made with hydrostatic models of the ship, or indeed dedicated trials are made. Financial resources are not usually available to explore these parameters in great detail.

For definition of waves, the usual approach would be to assume long crested waves with an idealised spectrum of significant height and modal period as given in Table 6.3. For the program used here, a slightly more sophisticated representation of the waves can be made - the wave spectrum as reported by the waverider buoy can be input, with a cosine even-power spreading function. Though a welcome advance on a simple idealised long crested approach, this still does not reflect the observed dependence of spreading on wave frequency noted in Chapter 2 and evident in Figure 6.2, or the definition of more than one principal wave direction.

The process of defining the principal wave direction presents the user choices in deciding the relative headings to specify in the computer code. Table 6.4 shows the relative headings possible from the data of Table 6.3 by two methods already mentioned. i.e. taking the principal wave direction as an average weighted according to the energy present at each frequency, or taking it simply as the direction of the waves at the frequency with the highest energy. Without using a directional buoy, it is likely that the second option would bear the strongest resemblance to the visually observed wave direction.

Figure 6.4 compares the trials and predicted motions for all the runs of Table 6.1 in a bar chart format, using both methods for assessing the principal wave direction mentioned above. At first sight the computer code does not appear to perform at all well with this basic presentation. An alternative presentation for the slower speed data is given in Figure 6.5, giving more information - computed values at a range of relative headings showing that in general the computer code follows similar trends as the trial data. The

computer code still does not appear to be performing well, with trials data clearly not lying close to the computed data, but it is impossible to draw firm conclusions without some representation of the uncertainty to be expected in either the trials or computed results.

6.3.2 Introduction of uncertainty into computed results

This section suggests two possible approaches to improving the comparison between computed ship motion data and trials data. The specific example of the trial data presented above is used, but the techniques have general application.

6.3.2.1 Maximum uncertainty method

Ship motion codes are sometimes subject to a 'sensitivity study', where the effects of varying a single parameter are evaluated. In this section it is suggested that variation of a large number of parameters can be used to assess the range of results to be reasonably expected from the program.

First, some estimate of the upper and lower possible variation of the parameters is required, and for the same list of variables in 6.3.1 these are:

- Speeds between 4 knots and 6 knots (±1 knot about nominal trial value)
- Displacement 3800 and 4400 tonnes (±200T about estimated trial value 4200T)
- KG 5.55m and 6.55m (±0.5m about default 6.05m)
- GM 0.7m and 1.3m (±0.3m about default 1.0m)
- Trim level and 1.2m by stern (±0.6m about default 0.6m by stern)
- Two different autopilots
- Heading subject to error ±10 degrees
- Wave spreadings between $\cos^{28}$ (47°) and $\cos^{70}$ (16°). (~±15° about measured average from the wave data $\cos^{32}$ (28deg))

- ±10% error in wave height, with corresponding range of modal period from a wave atlas e.g. Bales et al. (1981): 2.83m/8.18s and 2.31m/7.4s. The trials average was 2.57m/7.8s.

For this example, the choice of some of these ranges is somewhat arbitrary and has depended on the experience and judgement of the user to specify realistic values. However, the ranges could equally be set from uncertainties more formally derived.

The suggested method now involves computation of the ship motions using all possible combinations of these input parameters. With 10 parameters, there are therefore 2^{10} (1024) combinations which might be explored. This is relatively simple to program, and a batch file was made to compute results for all these combinations with the strip theory code used as the example under examination here.

The mean motion response over all 1024 runs can then be taken as a central value, but some measure of the spread of results is needed. Using the minimum and maximum motions found over all results is certainly an option, but would give a rather pessimistic view of the accuracy of the software. The standard deviation σ of the results has been chosen to give upper and lower limits. These lower and upper bounds of the computed data are plotted as dashed lines on Figure 6.6.

Selecting the standard deviation as a measure of dispersion in the data is most appropriate if the underlying distribution of data is Gaussian, but choosing extreme values for the uncertain parameters as suggested in this section ought to lead to a non-Gaussian distribution of the data. Figure 6.7 examines the distribution of data for three examples of ship motions computed for the 1024 cases described; indeed the distributions are not Gaussian in shape, and for the vertical plane motion examples given, there is a concentration towards the extremes of the data range. Nevertheless, for the heave, roll and pitch examples in Figure 6.7, the standard deviation (0.034m, 1.6° and 0.092° respectively) still represents a sensible measure of the typical range of values to be expected from the software prediction.

As a small digression, the data contributing to distributions in Figure 6.7 has been examined further to ascertain its nature. Figures 6.8 and 6.9 plot all the results, but the points are separated according to whether they are from the low or high end of the range of each controlling parameter. The shape of these graphs shows the dependence of the prediction on each parameter – a square shape indicates low sensitivity, whereas a diagonal shape indicates strong sensitivity. Figure 6.8 shows a strong dependence on the wave height/modal period parameter for the heave motion example, and a weaker dependence on wave spreading angle. The roll motion example in Figure 6.9 shows a strong sensitivity to ship displacement and GM as well as the wave height parameter.

Figure 6.6 also represents an improvement over Figure 6.5 as error bars have been included for the trials data. The heading error bars represent the uncertainty in the relative heading arising from the two definitions of principal wave direction above. The motion error bars used here have been set as dependent on the duration of the run, so there are large error bars for the short runs 2 and 6 of Table 6.1.

A rather different conclusion may therefore be drawn from Figure 6.6 compared with Figure 6.5 even though the data represented is essentially the same. With the exception of yaw motions, and pitch to a lesser extent, the range of possible values expected from the method outlined above in general overlaps the error bars of the trials data on Figure 6.6, suggesting that the computer code is actually performing adequately.

6.3.2.2 Random uncertainty method

The method to introduce error bars for computed data, in the example given for 10 parameters and thus 1024 runs, might be considered intensive both in terms of computational time and post-processing time required. A more efficient method to generate a similar result was therefore sought.

Standard practice in physical experiments to measure fixed quantities is to repeat measurements of the quantity at least six times. Systematic errors are not accounted for, but random errors are quantified by taking the mean value of the six measurements as the best estimate of the true value, and the standard deviation as an expression of the

uncertainty in this value. The underlying assumption is that the measurements are samples from a normally distributed population.

It is suggested that a similar technique can be applied to computer simulation of ship motion results. The approach is:

- select parameters for which there is uncertainty
- estimate the range of uncertainty for each parameter
- for each parameter, select a value randomly within this range
- compute ship motion results with this randomised input data
- repeat this computation at least six times (with different random parameter values)
- calculate statistics for the ship motions averaged over the six or more runs

This technique has been applied to the simulation of frigate trials data, using the same ten input parameters used in 6.3.2.1, and values randomly selected from the ranges previously stated.

A much smaller number of computer runs was made, just 27 have been used to construct the histograms in Figure 6.10. With randomly selected parameters, a more Gaussian distribution of results should be expected this time, and the normal distribution function has been co-plotted with the motion results on Figure 6.10. These ideal distributions have the same mean and standard deviation as the histogram data.

With such a small number of runs, the motion distributions do not follow the normal distribution perfectly, but are close enough to encourage further analysis based on this premise.

Figure 6.11 gives results computed by this method (the trials data is identical to that of Figure 6.6). The range of values used to calculate the lower and upper bound of the strip theory results - the dashed lines – are based on the mean and standard deviation of just seven randomised runs. Very similar mean and standard deviation values were derived using three other groups of six or seven randomised runs of the total 27 made.

The lower and upper bands of the theory dashed lines in Figure 6.11 are plotted at the mean value ±2σ. This larger band has been selected with the idea that the results of the efficient 'random uncertainty' method should match those of the 'maximum uncertainty' method as a target. Using a larger error band at ±2σ merely reflects the desirability of taking a more conservative view of the performance of the theory in question, as revealed by the fuller analysis in the previous section, rather than to shed the theory in a better light *per se*.

6.4 Summary

Full-scale seakeeping data has been reported in this section, for a frigate operating in sea state 4, and modelling of the full-scale results was made with current 'strip theory' seakeeping software packages.

This chapter initially demonstrates the difficulties in modelling ship motions in natural seas. The sea state for the trial showed a bimodal nature, which presented some difficulty of representation within the seakeeping code which lacks this sophistication. One approach to overcoming this difficulty would therefore be to improve the spatial and directional representation of the wave nature within the code. Another would be to negate the effect of the waves on the ship motions by comparing results at the transfer function level, and this is dealt with in Chapter 7. A parallel approach is to make some estimation of the errors to be expected in the computed results due to these factors, and it is this which was explored in this chapter.

This chapter illustrates ways to take account of the variation in possible results from the example seakeeping code. The manner of presentation alone is clearly very important to the assessment process. With a conventional comparison of the trial ship motion results against the seakeeping code prediction using the best single estimate of the conditions, the results are inconclusive, with correlation between the two sources hard to discern.

Using error bars for the trials results has an immediate helpful effect, and two ways are proposed to also include error bounds for predicted results. The first method, the

'maximum uncertainty' method, essentially comprises calculation of the range of results when input parameters are forced to take values at the extremes of their expected range. The second 'random uncertainty' method requires a smaller number of calculations; computer runs are instead made with input parameters randomly selected from within their expected range, and it is shown the dispersion of these results for the purposes of plotting error bounds can be taken as two standard deviations about the mean.

Getting consistent results from seakeeping codes that can be compared with trials results in a fair manner is not a trivial process. The ship and the environment are invariably not simple, stationary, accurately known quantities, and therefore the computed results should not be expected to be so either. The methods established here help in understanding the consequences of these uncertainties, and it is recommended that the naval architecture community adopts them.

Run	Mid Time of Run	Duration	Ship Heading	Speed over ground
	(hh:mm)	(min)	(deg)	(knots)
1	14:42	18.0	100	10.7
2	15:01	3.6	220	3.8
3	15:13	11.4	80	12.2
4	15:34	22.8	260	3.7
5	16:10	5.8	240	4.4
6	16:21	11.4	270	5.2
7	16:35	13.8	330	6.8

compare-all.xls /compare

Table 6.1 Run details: frigate opportunity data

Run	1		
Number_of_points=	13210		
Run_Time_[s]=	1100.75		
Channel	Mean	Std.Dev	
Speed	**10.72236**	0.30781	knots
Heading	**103.8962**	**3.29205**	degs
Roll	-2.98765	**2.58266**	degs
Pitch	0.08895	**0.70744**	degs
Vertical Accel -raw	0.01784	*0.24646*	m.s-2
Longitudinal Accel-raw	0.01704	*0.04339*	m.s-2
Lateral Accel -raw	0.46717	*0.6416*	m.s-2
Heave-Corrected for g	-0.00618	0.23756	m.s-2
Surge-Corrected for g	0.00181	0.14475	m.s-2
Sway-Corrected for g	10.72236	0.27645	m.s-2
Heave -calc at CG	-0.00615	**0.22724**	m.s-2
Surge -calc at CG	0.00181	**0.13931**	m.s-2
Sway -calc at CG	-0.04326	**0.20829**	m.s-2

Run	5		
Number_of_points=	4148		
Run_Time_[s]=	345.58		
Channel	Mean	Std.Dev	
Speed	**4.42698**	0.25739	knots
Heading	**-119.487**	**0.5073**	degs
Roll	-1.48435	**0.70789**	degs
Pitch	0.04036	**0.84534**	degs
Vertical Accel -raw	-0.00806	*0.27347*	m.s-2
Longitudinal Accel-raw	0.02926	*0.12855*	m.s-2
Lateral Accel -raw	0.21191	*0.23016*	m.s-2
Heave-Corrected for g	-0.01316	0.27358	m.s-2
Surge-Corrected for g	0.02235	0.26761	m.s-2
Sway-Corrected for g	4.42698	0.13563	m.s-2
Heave -calc at CG	-0.01336	**0.16707**	m.s-2
Surge -calc at CG	0.02237	**0.24733**	m.s-2
Sway -calc at CG	-0.04195	**0.09848**	m.s-2

Run	2		
Number_of_points=	2593		
Run_Time_[s]=	216		
Channel	Mean	Std.Dev	
Speed	**3.76858**	0.42654	knots
Heading	**-140.049**	**1.58262**	degs
Roll	-2.8172	**1.07831**	degs
Pitch	0.04834	**1.04005**	degs
Vertical Accel -raw	0.01091	*0.32148*	m.s-2
Longitudinal Accel-raw	0.02816	*0.16277*	m.s-2
Lateral Accel -raw	0.44053	*0.34405*	m.s-2
Heave-Corrected for g	-0.0043	0.31771	m.s-2
Surge-Corrected for g	0.01989	0.33389	m.s-2
Sway-Corrected for g	3.76858	0.1921	m.s-2
Heave -calc at CG	-0.00578	**0.20818**	m.s-2
Surge -calc at CG	0.02004	**0.30879**	m.s-2
Sway -calc at CG	-0.04123	**0.1271**	m.s-2

Run	6		
Number_of_points=	8209		
Run_Time_[s]=	684		
Channel	Mean	Std.Dev	
Speed	**5.17181**	0.97748	knots
Heading	**-89.4401**	**0.73456**	degs
Roll	-0.39033	**0.97567**	degs
Pitch	0.03906	**0.99743**	degs
Vertical Accel -raw	-0.00864	*0.38406*	m.s-2
Longitudinal Accel-raw	0.03113	*0.14807*	m.s-2
Lateral Accel -raw	0.02885	*0.34469*	m.s-2
Heave-Corrected for g	-0.01177	0.38443	m.s-2
Surge-Corrected for g	0.02445	0.31216	m.s-2
Sway-Corrected for g	5.17181	0.20917	m.s-2
Heave -calc at CG	-0.01162	**0.26938**	m.s-2
Surge -calc at CG	0.02443	**0.28764**	m.s-2
Sway -calc at CG	-0.03793	**0.15835**	m.s-2

Run	3		
Number_of_points=	8209		
Run_Time_[s]=	684		
Channel	Mean	Std.Dev	
Speed	**12.19539**	0.45875	knots
Heading	**80.97552**	**4.36624**	degs
Roll	-1.78659	**3.01555**	degs
Pitch	0.08832	**0.5361**	degs
Vertical Accel -raw	0.01257	*0.13389*	m.s-2
Longitudinal Accel-raw	0.01392	*0.04056*	m.s-2
Lateral Accel -raw	0.25592	*0.64923*	m.s-2
Heave-Corrected for g	-0.0062	0.12534	m.s-2
Surge-Corrected for g	-0.00119	0.11826	m.s-2
Sway-Corrected for g	12.19539	0.16754	m.s-2
Heave -calc at CG	-0.00616	**0.11922**	m.s-2
Surge -calc at CG	-0.0012	**0.11632**	m.s-2
Sway -calc at CG	-0.04935	**0.12381**	m.s-2

Run	7		
Number_of_points=	9937		
Run_Time_[s]=	828		
Channel	Mean	Std.Dev	
Speed	**6.80011**	0.16072	knots
Heading	**-25.5574**	**2.18252**	degs
Roll	2.41859	**2.1452**	degs
Pitch	0.07564	**0.57143**	degs
Vertical Accel -raw	0.00691	*0.50515*	m.s-2
Longitudinal Accel-raw	0.02347	*0.0823*	m.s-2
Lateral Accel -raw	-0.44365	*0.56773*	m.s-2
Heave-Corrected for g	-0.00919	0.49454	m.s-2
Surge-Corrected for g	0.01053	0.16918	m.s-2
Sway-Corrected for g	6.80011	0.37219	m.s-2
Heave -calc at CG	-0.00905	**0.46755**	m.s-2
Surge -calc at CG	0.01051	**0.15717**	m.s-2
Sway -calc at CG	-0.02995	**0.35138**	m.s-2

Run	4		
Number_of_points=	16397		
Run_Time_[s]=	1366.33		
Channel	Mean	Std.Dev	
Speed	**3.69689**	0.45077	knots
Heading	**-98.9598**	**1.69062**	degs
Roll	0.60005	**1.06478**	degs
Pitch	0.02756	**1.17866**	degs
Vertical Accel -raw	-0.00819	*0.36256*	m.s-2
Longitudinal Accel-raw	0.03514	*0.16638*	m.s-2
Lateral Accel -raw	-0.14455	*0.32267*	m.s-2
Heave-Corrected for g	-0.0125	0.36191	m.s-2
Surge-Corrected for g	0.03042	0.36033	m.s-2
Sway-Corrected for g	3.69689	0.16906	m.s-2
Heave -calc at CG	-0.01232	**0.21454**	m.s-2
Surge -calc at CG	0.0304	**0.33314**	m.s-2
Sway -calc at CG	-0.04183	**0.11553**	m.s-2

getdata3.xls / trial

Table 6.2 Measured and Calculated Ship Motion Data

			Weighted mean		Energy Peak	
			Wave	Wave	Direction	Spreading
Run	$H_{1/3}$	T_0	Direction	Spreading	of Peak	at Peak
	m	s	deg	deg	deg	deg
1	2.57	7.80	234	28	222	18
2	2.53	7.56	237	28	221	18
3	2.48	7.57	238	29	221	19
4	2.40	7.32	241	31	220	21
5	2.30	7.14	245	32	219	23
6	2.28	7.21	245	32	219	23
7	2.26	7.29	245	32	218	23

Nor-waves.xls /compare

Table 6.3 Wave summary

Run Number	Ship heading	Ship Relative Heading (using weighted mean wave direction)	Ship Relative Heading (using energy peak wave direction)	Difference between alternative definitions of relative heading
	deg (0-360)	deg (0-180)	deg (0-180)	deg
1	100	50	62	12
2	220	163	179	16
3	80	23	40	17
4	260	160	139	21
5	240	175	159	17
6	270	154	128	26
7	330	90	64	27

Nor-waves.xls /compare

Table 6.4 Ship heading relative to waves

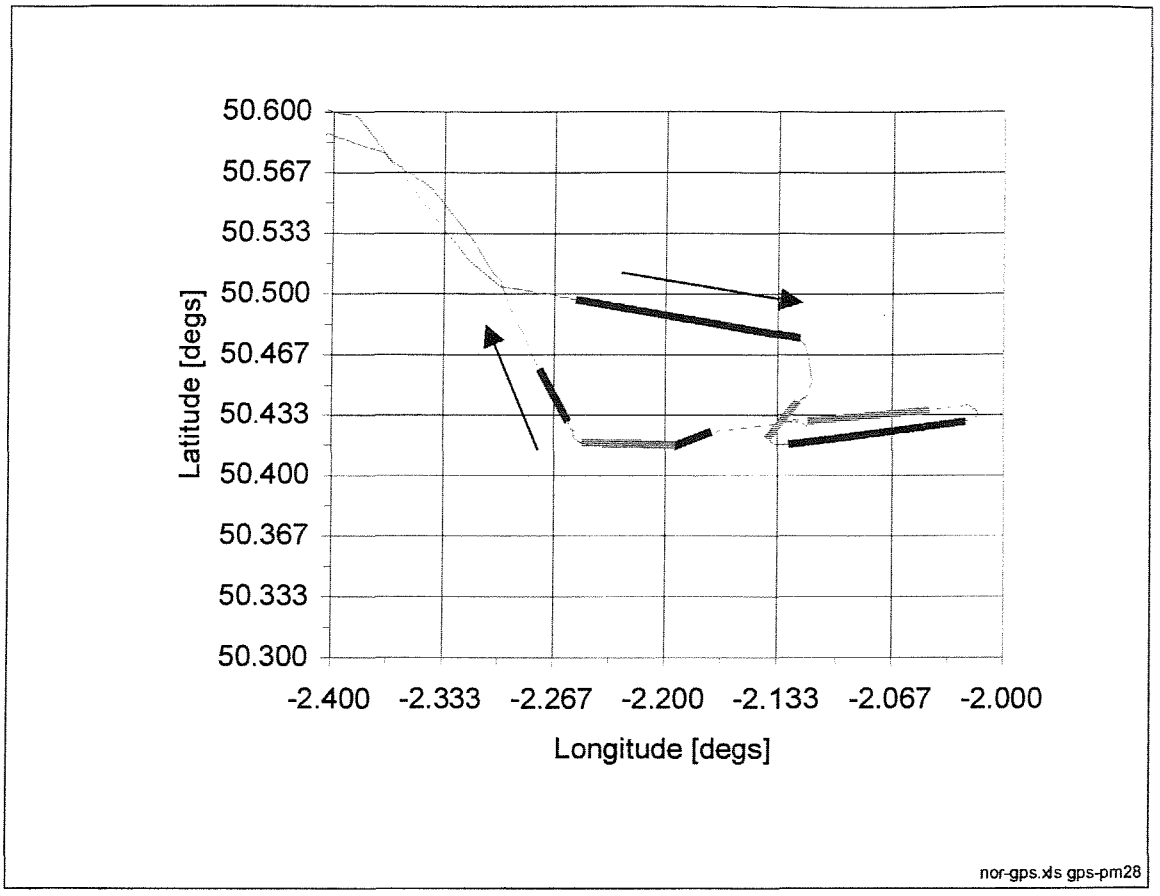

Figure 6.1 Ship trajectory for frigate opportunity data

SIGNIFICANT WAVE HEIGHT **2.57** m
WEIGHTED MEAN DIRN **234.0** degs
WEIGHTED MEAN SPREAD **28.0** degs
for f=>0.15Hz

freq [Hz]	Energy [m2/Hz]	Direction deg true	Spread [deg]	Skewness [deg]	Kurtosis [deg]
0.025	0.0173	70.4	71.4	0.657	1.960
0.03	0.0187	310.6	67.5	-2.287	2.229
0.035	0.0236	209.0	67.1	0.269	1.998
0.04	0.0150	276.8	58.7	-0.314	2.258
0.045	0.0102	279.3	67.1	-0.767	2.020
0.05	0.0186	233.2	62.3	0.694	2.135
0.055	0.0335	237.7	58.8	-0.769	2.237
0.06	0.0138	250.1	59.2	-0.688	2.303
0.065	0.0270	262.8	52.8	-0.997	3.380
0.07	0.0187	233.2	60.1	-0.110	2.654
0.075	0.0479	234.6	52.7	-0.919	2.375
0.08	0.0778	192.4	62.5	0.134	2.181
0.085	0.1122	242.5	50.0	-2.396	3.676
0.09	0.3497	228.7	40.7	-0.922	3.669
0.095	0.5301	206.5	39.6	-0.373	2.782
0.1	0.8394	213.8	35.2	-0.877	4.856
0.11	3.0616	215.2	30.3	-2.262	9.504
0.12	4.4009	220.8	21.5	-2.338	12.400
0.13	6.7834	221.7	18.1	-2.674	14.644
0.14	4.3444	222.0	15.7	-1.781	16.127
0.15	2.3007	225.9	18.7	-0.570	14.492
0.16	2.0674	223.7	21.5	-0.544	9.266
0.17	1.7352	223.7	27.3	-0.079	4.442
0.18	2.1010	223.4	25.0	0.689	5.695
0.19	1.5981	232.1	29.2	0.427	4.283
0.2	1.2057	250.9	37.2	-0.149	2.701
0.21	1.0963	258.0	41.4	-0.388	2.343
0.22	1.1599	266.7	42.8	-0.551	1.998
0.23	1.3258	270.3	39.7	-0.816	2.052
0.24	0.9626	272.3	39.6	-1.028	2.827
0.25	0.6796	259.4	42.8	-0.181	2.259
0.26	0.6512	261.6	44.5	0.106	2.301
0.27	0.5699	279.1	41.7	-1.150	2.555
0.28	0.3689	278.2	45.0	-1.310	2.874
0.29	0.2984	278.8	44.4	-1.155	3.065
0.3	0.2515	275.4	50.8	-0.975	2.217
0.31	0.2374	279.3	42.5	-1.040	3.108
0.32	0.1903	273.2	46.6	-0.625	2.212
0.33	0.1316	282.2	48.8	-0.936	2.475
0.34	0.1637	280.8	48.9	-1.036	2.301
0.35	0.1619	273.2	46.5	-0.496	2.080
0.36	0.1237	289.2	48.1	-1.080	2.420
0.37	0.1177	279.1	45.4	-0.304	2.913
0.38	0.1031	272.6	47.6	-0.843	2.718
0.39	0.0868	267.3	46.6	-0.334	2.233
0.4	0.0867	280.2	45.0	-1.385	3.295
0.41	0.0722	288.3	46.6	-1.239	2.733
0.42	0.0673	279.9	52.6	-0.485	2.151
0.43	0.0512	291.4	53.4	-0.939	2.140
0.44	0.0588	290.6	46.0	-0.498	2.667
0.45	0.0602	287.2	45.0	-0.360	2.537
0.46	0.0474	283.3	54.0	-0.449	1.794
0.47	0.0542	285.8	45.4	-0.743	2.417
0.48	0.0517	282.7	49.9	-0.341	1.930
0.49	0.0575	292.0	47.8	-1.061	2.256
0.5	0.0322	299.3	49.7	-1.500	2.483
0.51	0.0300	295.7	49.1	-1.243	2.800
0.52	0.0317	281.0	52.3	-0.172	1.740
0.53	0.0246	273.7	52.7	-0.243	1.664
0.54	0.0269	283.8	46.4	-0.326	2.386
0.55	0.0262	283.3	44.3	-0.161	2.227
0.56	0.0152	304.1	52.2	-1.021	2.394
0.57	0.0206	297.1	49.9	-0.612	2.049
0.58	0.0143	237.9	37.2	-0.618	2.151

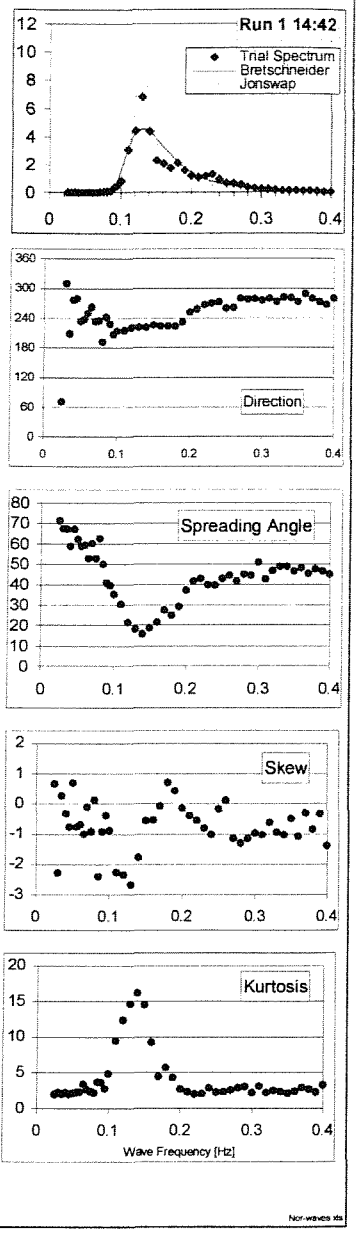

Figure 6.2 Example wave spectral information

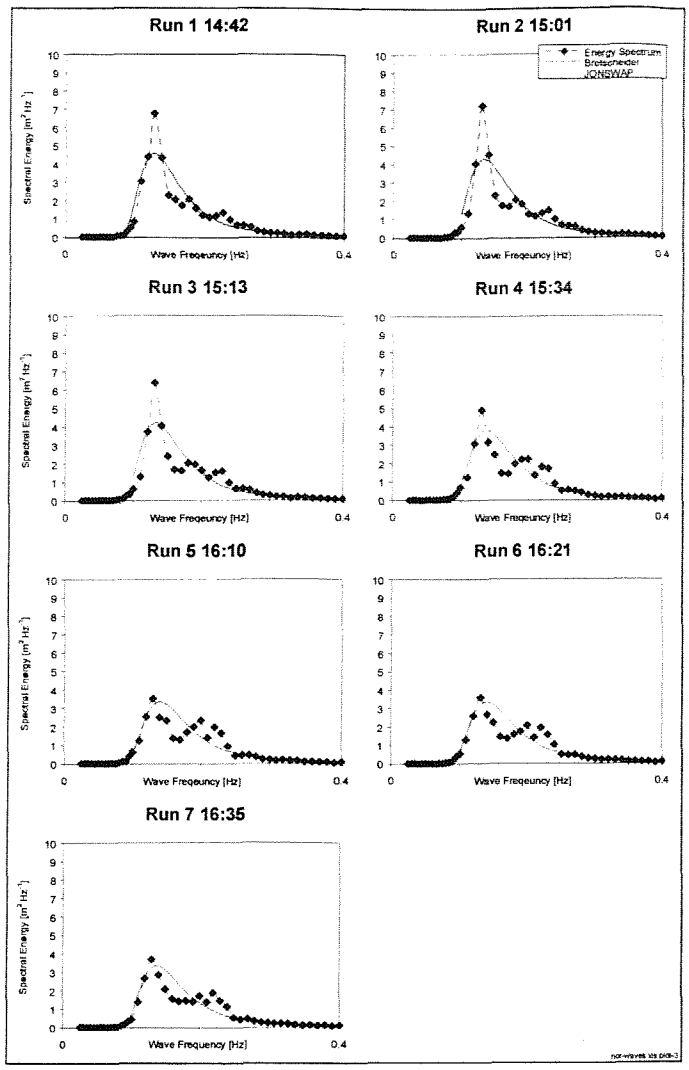

Figure 6.3(a) Wave spectral development (individual spectra)

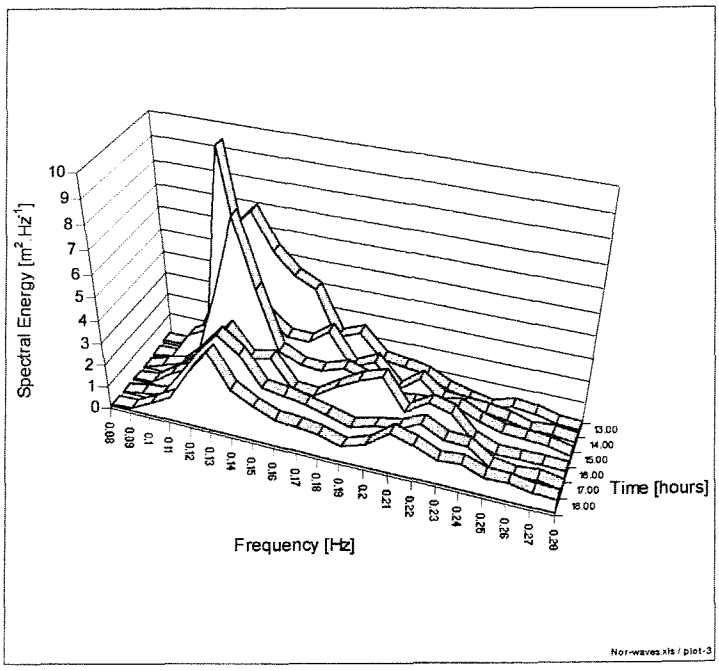

Figure 6.3(b) Wave spectral development (group)

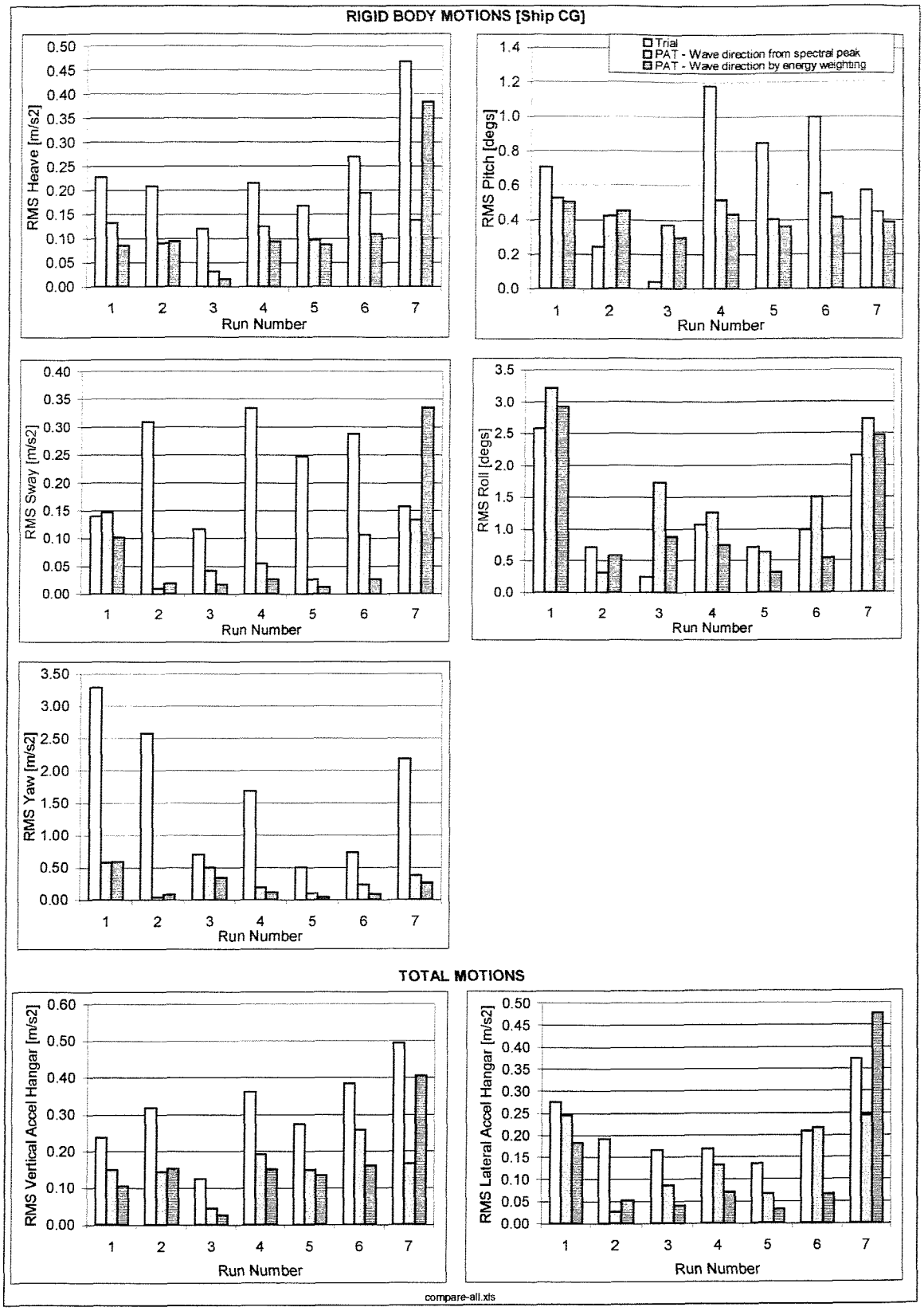

Figure 6.4 Trial and predicted data: bar chart presentation

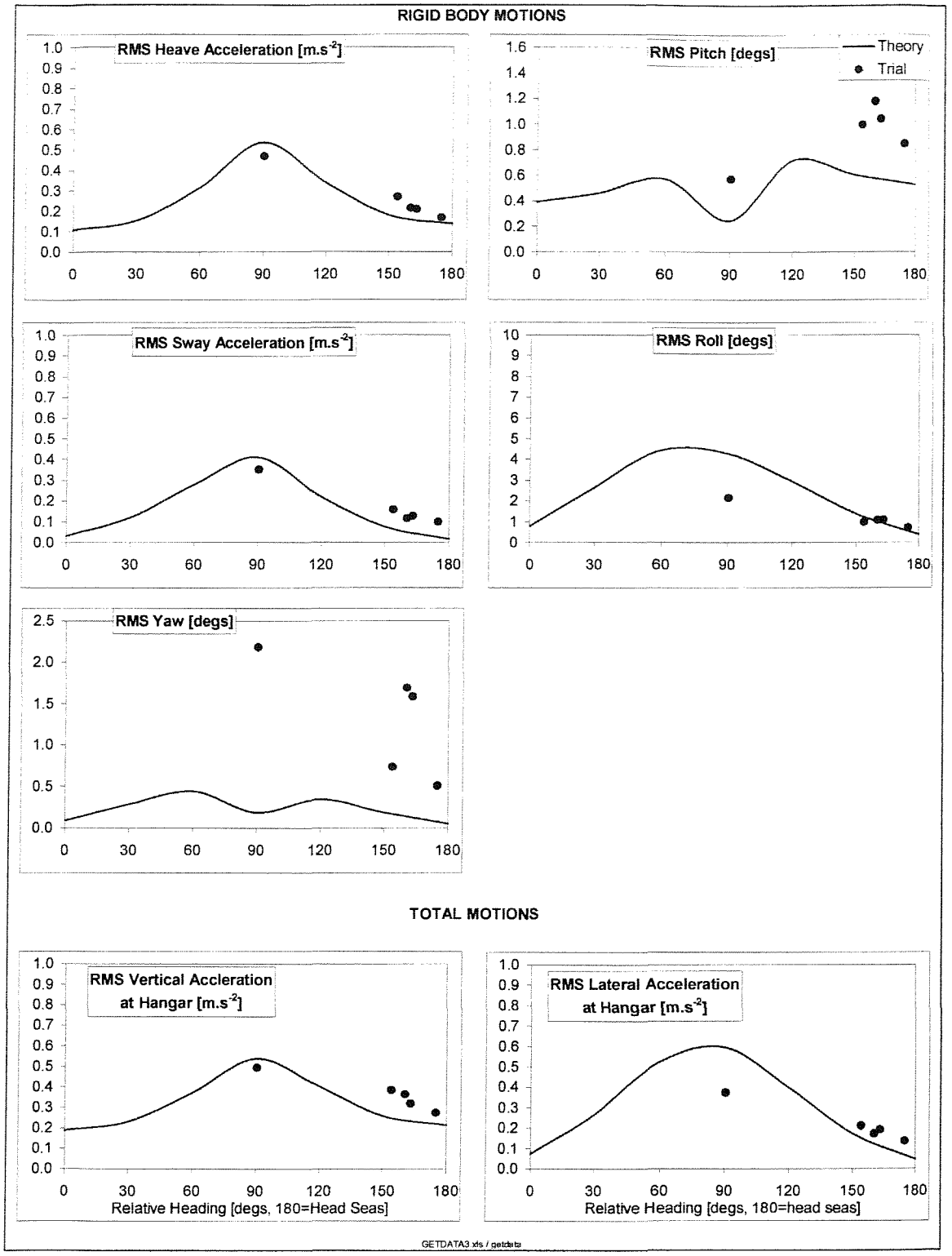

Figure 6.5 Trial and predicted data: simple presentation

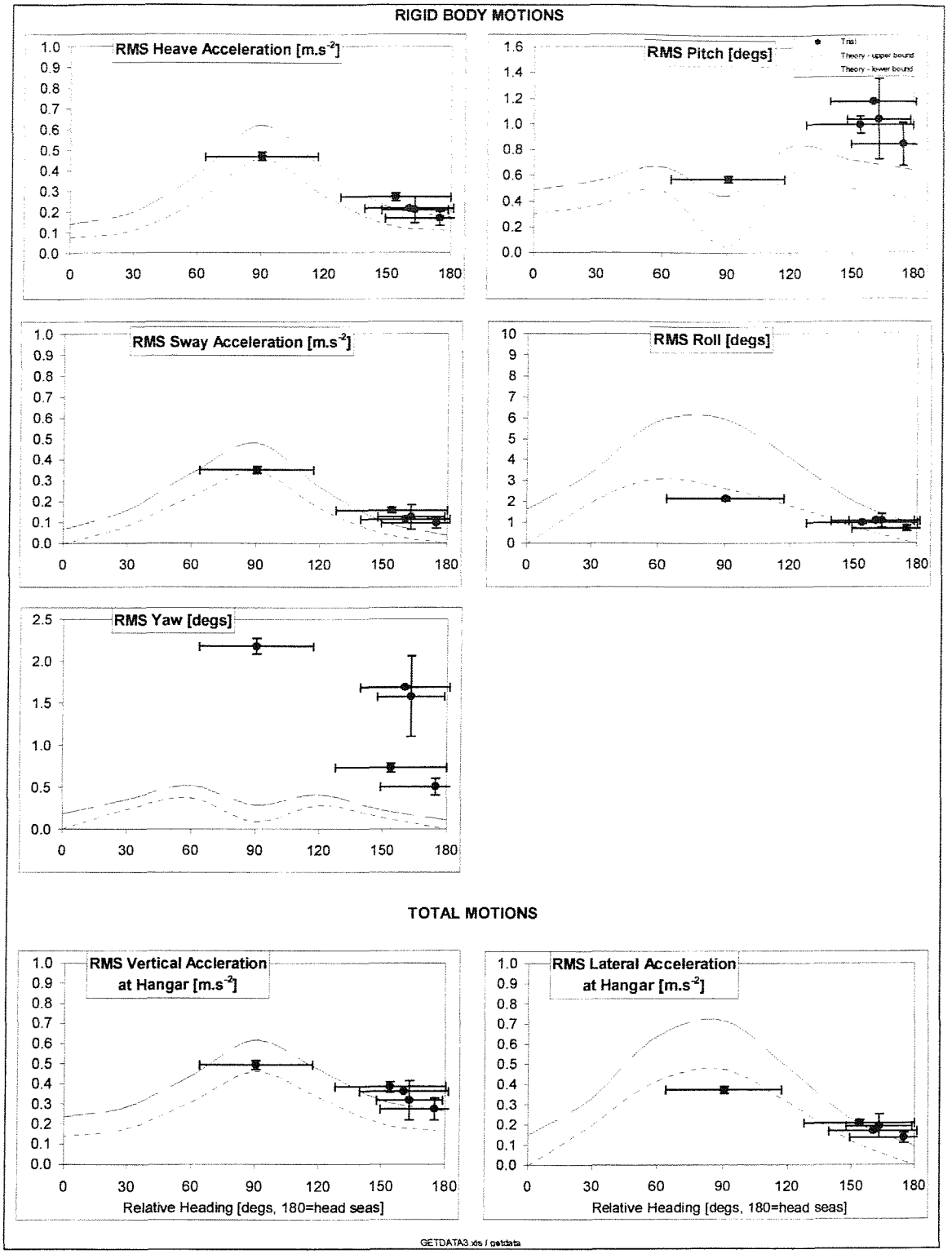

Figure 6.6 Trial and predicted data: improved presentation (maximum error method)

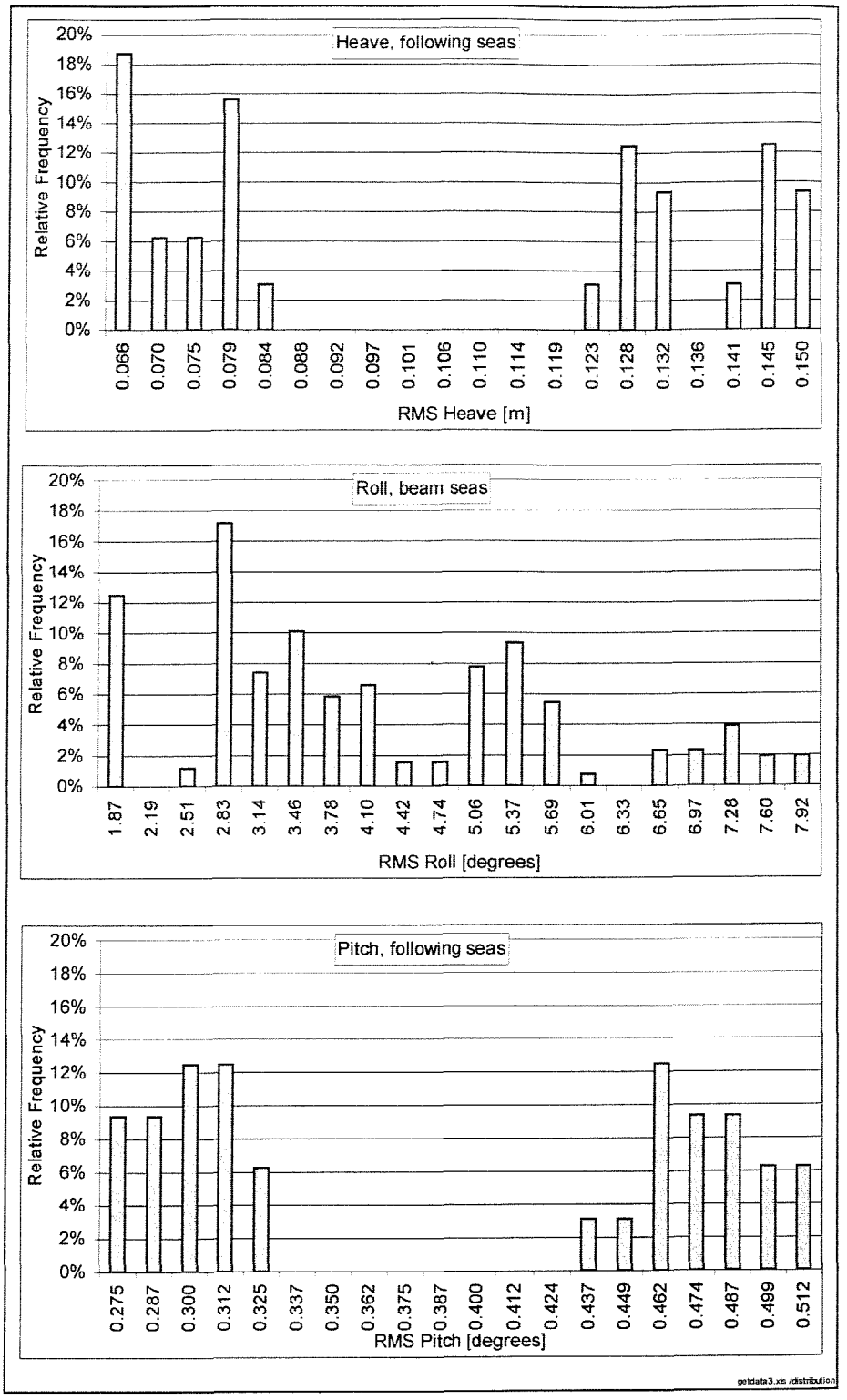

Figure 6.7 Data distribution (1024 runs, maximum uncertainty method)

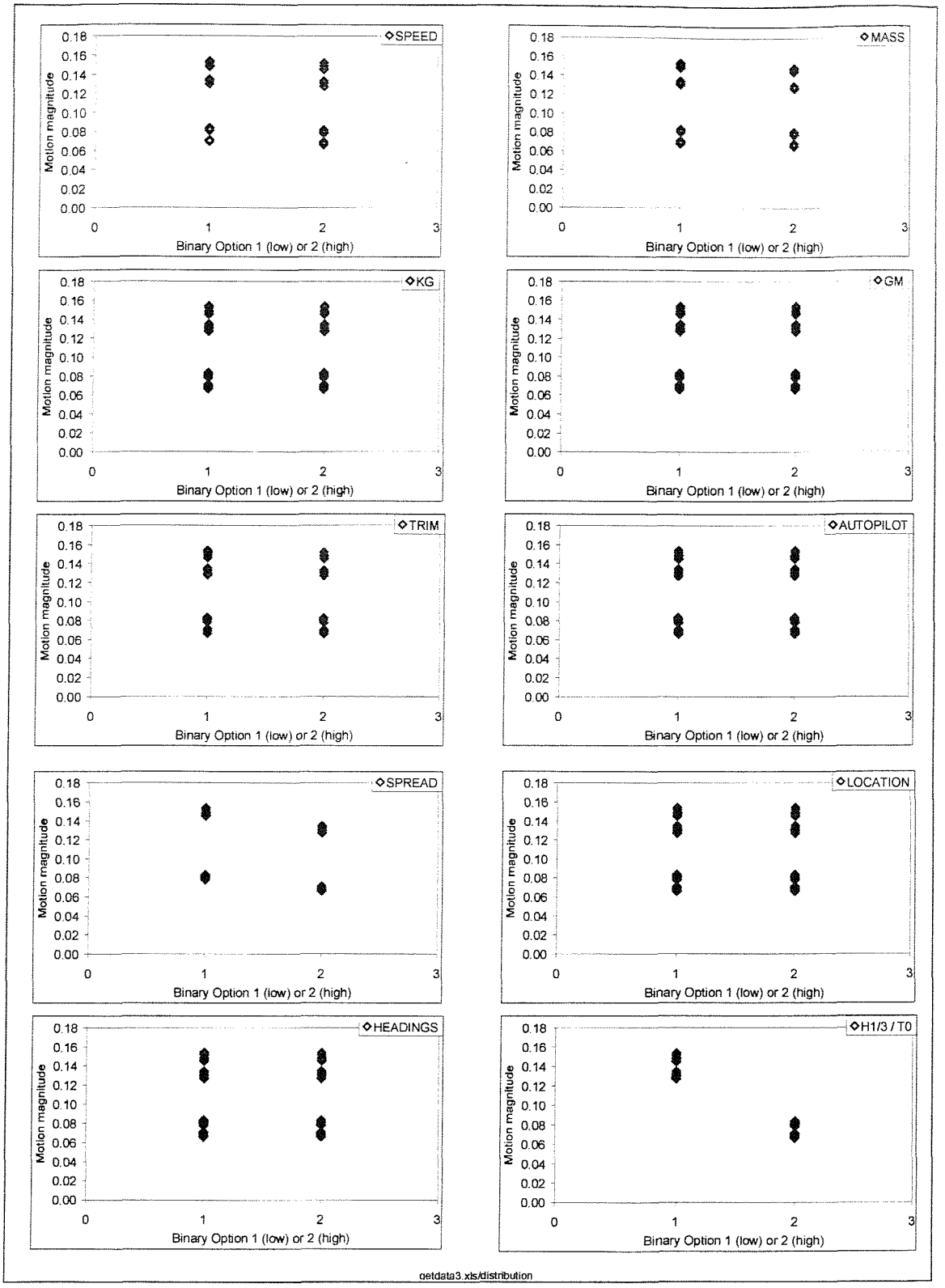

Figure 6.8 Dependence of data distribution on parameter (heave, following seas)

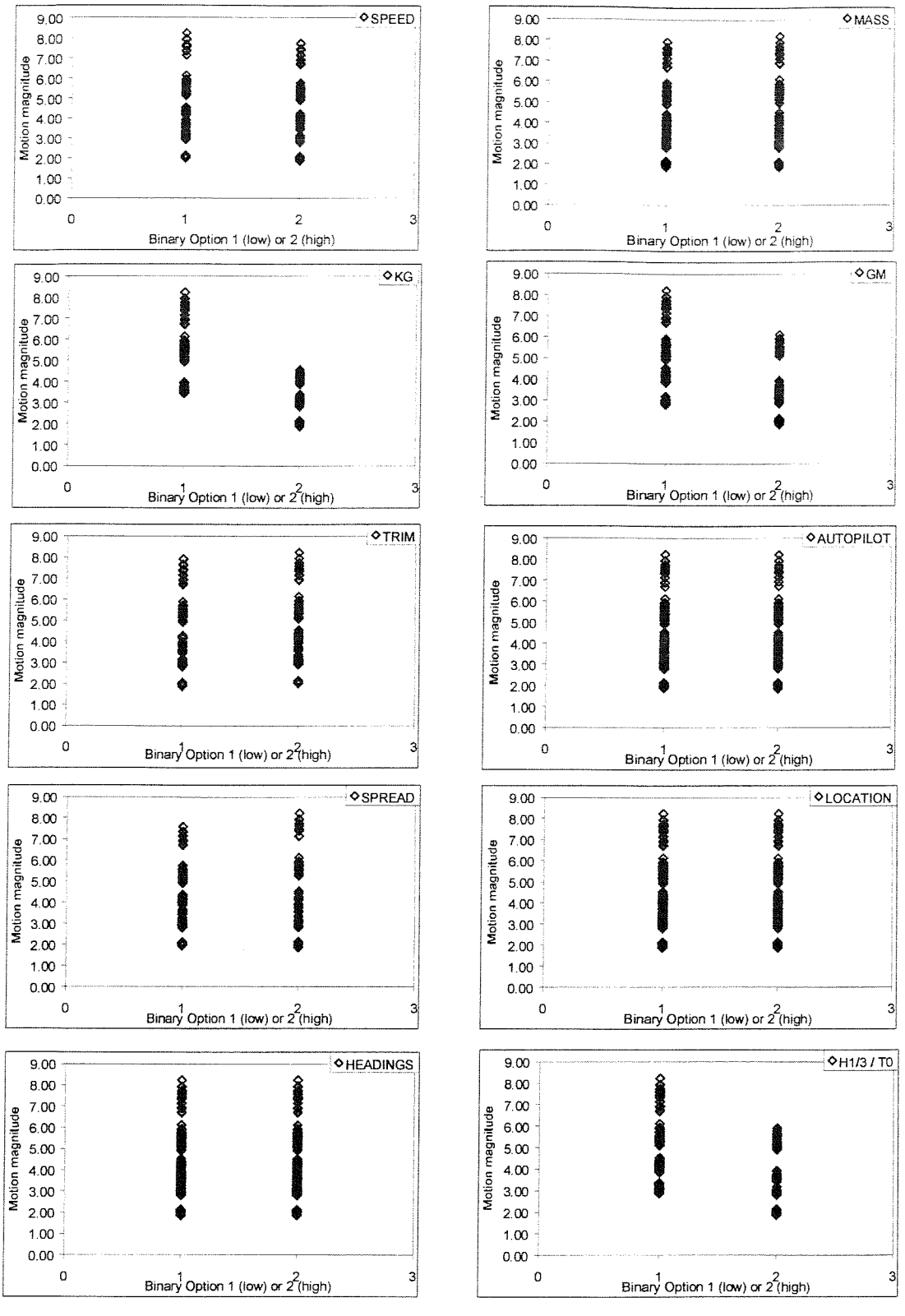

qetdata3.xls/distribution

Figure 6.9 Dependence of data distribution on parameter (roll, beam seas)

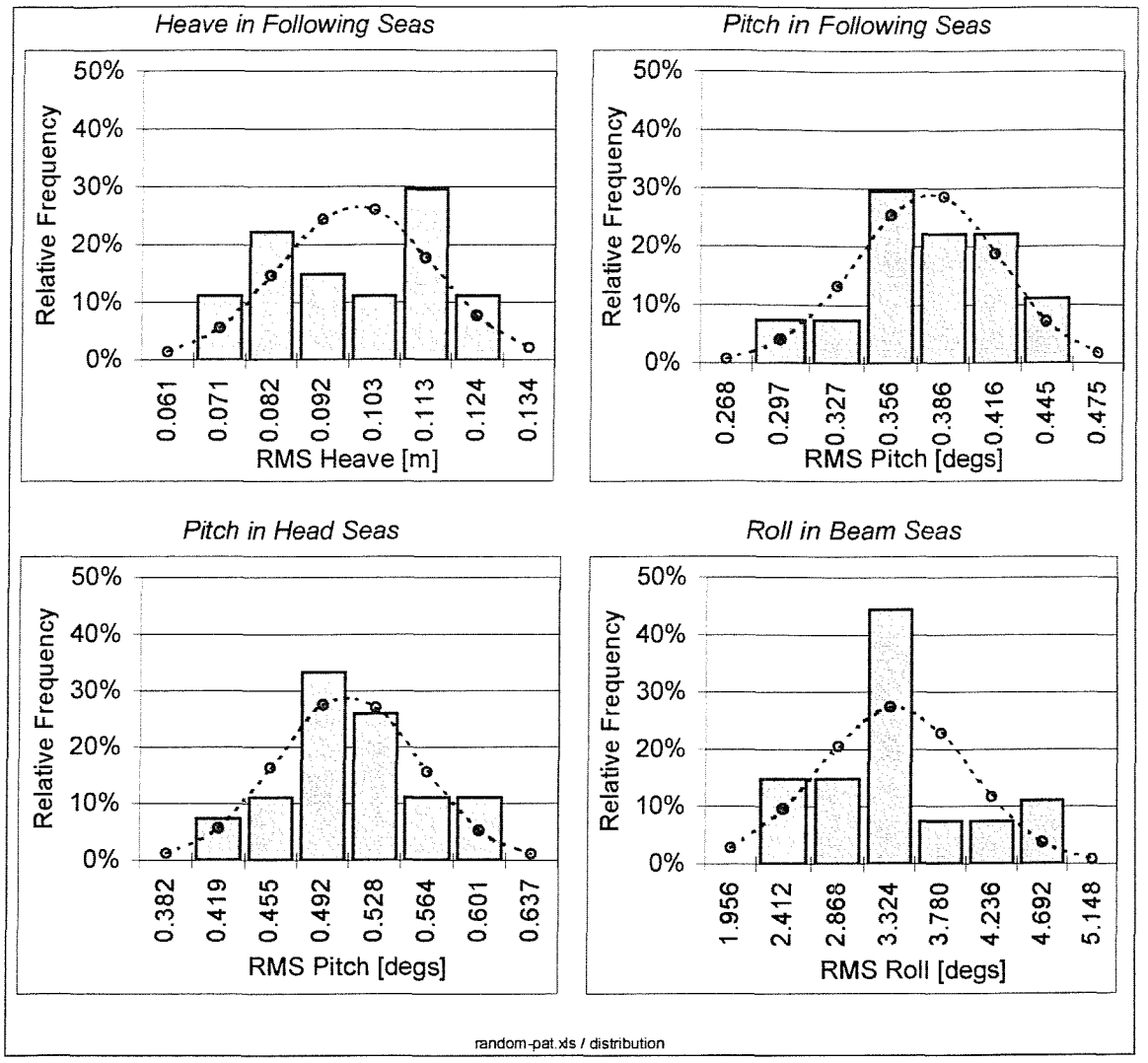

Figure 6.10 Data distribution (27 runs, randomised method)

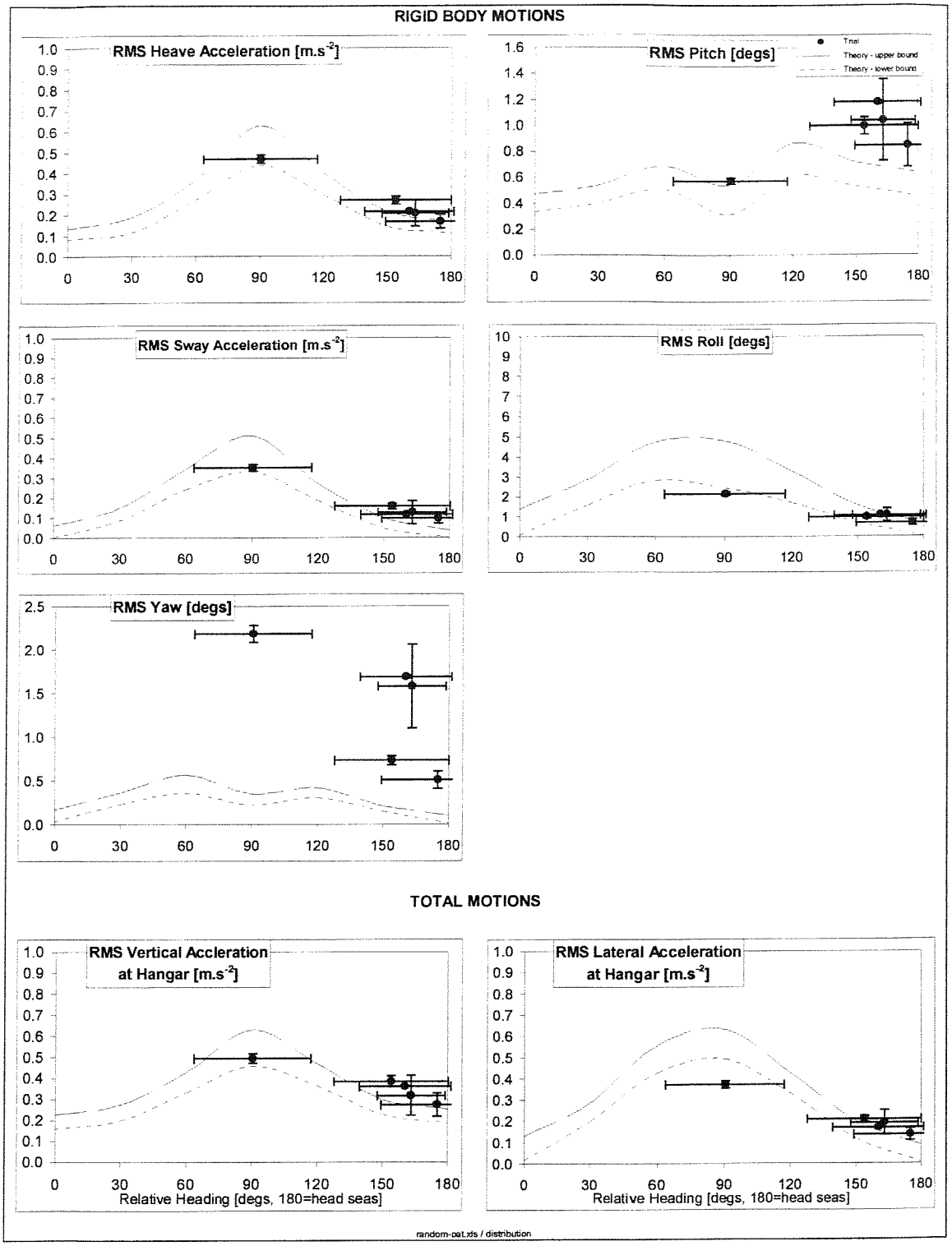

Figure 6.11 Trial and predicted data: improved presentation (randomised method)

7. TRIALS DATA - COMPARING WITH SHIP MOTION CODES

7.1 Introduction

Chapter 5 demonstrated the difficulties posed when trying to interpret results from seakeeping trials of ships in naturally occurring seaways, where spreading and wave confusion are common. This affects two of the principal aims that trials may aim to achieve - to validate ship motion codes, and to give data suitable for calculation of the ship RAOs. In this section, the theory proposed by Fryer (1991) and Fryer et al. (1994) is implemented, which treats the directionality of the waves comprehensively, and is used to calculate RAOs for a ship in such a seaway, showing directional spreading and bimodality.

Fryer et al. (1994) used the example of a SWATH trial in a sea loch, showing wave spreading but unimodal seas. The lack of a RAO prediction code at the time meant that the results obtained could not be validated in any way against theory. This section reports a similar analysis but for a new data set involving sea trials of the Royal Navy frigate introduced in Chapter 5, operating in bimodal seas. As a conventional monohull, comparison with predicted RAOs is possible. Some of the detailed measures required to achieve the RAO results in practice, and not reported in Fryer et al. (1994), are also described here.

7.2 Analysis for transfer functions

7.2.1 Background

The Fryer (1991) theory is applied here to results of the frigate trial with ship motions recorded at all points of the compass, at 5 knots in a bimodal seaway. The salient feature of the theory is the solution of a linear system of simultaneous equations, which it is convenient to express in matrix form; a solution for $\underline{R}^2$ in the matrix equation $\underline{M}=\underline{S}.\underline{R}^2$ at each encounter frequency interval is required, which is written in full:

$$\begin{pmatrix} Me_A \\ Me_B \\ Me_C \\ Me_D \\ Me_E \\ Me_F \\ Me_G \\ Me_H \\ Me_I \\ Me_J \\ Me_K \\ Me_L \end{pmatrix} = \begin{pmatrix} S_{e\,A,0} & S_{e\,A,30} & S_{e\,A,60} & S_{e\,A,90} & S_{e\,A,120} & S_{e\,A,150} & S_{e\,A,180} & S_{e\,A,210} & S_{e\,A,240} & S_{e\,A,270} & S_{e\,A,300} & S_{e\,A,330} \\ S_{e\,B,0} & S_{e\,B,30} & S_{e\,B,60} & S_{e\,B,90} & S_{e\,B,120} & S_{e\,B,150} & S_{e\,B,180} & S_{e\,B,210} & S_{e\,B,240} & S_{e\,B,270} & S_{e\,B,300} & S_{e\,B,330} \\ S_{e\,C,0} & S_{e\,C,30} & S_{e\,C,60} & S_{e\,C,90} & S_{e\,C,120} & S_{e\,C,150} & S_{e\,C,180} & S_{e\,C,210} & S_{e\,C,240} & S_{e\,C,270} & S_{e\,C,300} & S_{e\,C,330} \\ S_{e\,D,0} & S_{e\,D,30} & S_{e\,D,60} & S_{e\,D,90} & S_{e\,D,120} & S_{e\,D,150} & S_{e\,D,180} & S_{e\,D,210} & S_{e\,D,240} & S_{e\,D,270} & S_{e\,D,300} & S_{e\,D,330} \\ S_{e\,E,0} & S_{e\,E,30} & S_{e\,E,60} & S_{e\,E,90} & S_{e\,E,120} & S_{e\,E,150} & S_{e\,E,180} & S_{e\,E,210} & S_{e\,E,240} & S_{e\,E,270} & S_{e\,E,300} & S_{e\,E,330} \\ S_{e\,F,0} & S_{e\,F,30} & S_{e\,F,60} & S_{e\,F,90} & S_{e\,F,120} & S_{e\,F,150} & S_{e\,F,180} & S_{e\,F,210} & S_{e\,F,240} & S_{e\,F,270} & S_{e\,F,300} & S_{e\,F,330} \\ S_{e\,G,0} & S_{e\,G,30} & S_{e\,G,60} & S_{e\,G,90} & S_{e\,G,120} & S_{e\,G,150} & S_{e\,G,180} & S_{e\,G,210} & S_{e\,G,240} & S_{e\,G,270} & S_{e\,G,300} & S_{e\,G,330} \\ S_{e\,H,0} & S_{e\,H,30} & S_{e\,H,60} & S_{e\,H,90} & S_{e\,H,120} & S_{e\,H,150} & S_{e\,H,180} & S_{e\,H,210} & S_{e\,H,240} & S_{e\,H,270} & S_{e\,H,300} & S_{e\,H,330} \\ S_{e\,I,0} & S_{e\,I,30} & S_{e\,I,60} & S_{e\,I,90} & S_{e\,I,120} & S_{e\,I,150} & S_{e\,I,180} & S_{e\,I,210} & S_{e\,I,240} & S_{e\,I,270} & S_{e\,I,300} & S_{e\,I,330} \\ S_{e\,J,0} & S_{e\,J,30} & S_{e\,J,60} & S_{e\,J,90} & S_{e\,J,120} & S_{e\,J,150} & S_{e\,J,180} & S_{e\,J,210} & S_{e\,J,240} & S_{e\,J,270} & S_{e\,J,300} & S_{e\,J,330} \\ S_{e\,K,0} & S_{e\,K,30} & S_{e\,K,60} & S_{e\,K,90} & S_{e\,K,120} & S_{e\,K,150} & S_{e\,K,180} & S_{e\,K,210} & S_{e\,K,240} & S_{e\,K,270} & S_{e\,K,300} & S_{e\,K,330} \\ S_{e\,L,0} & S_{e\,L,30} & S_{e\,L,60} & S_{e\,L,90} & S_{e\,L,120} & S_{e\,L,150} & S_{e\,L,180} & S_{e\,L,210} & S_{e\,L,240} & S_{e\,L,270} & S_{e\,L,300} & S_{e\,L,330} \end{pmatrix} \begin{pmatrix} R^2_{e\,0} \\ R^2_{e\,30} \\ R^2_{e\,60} \\ R^2_{e\,90} \\ R^2_{e\,120} \\ R^2_{e\,150} \\ R^2_{e\,180} \\ R^2_{e\,210} \\ R^2_{e\,240} \\ R^2_{e\,270} \\ R^2_{e\,300} \\ R^2_{e\,330} \end{pmatrix}$$

...(7.1)

The suffices 0 to 330 represent the relative headings for which the transfer function solution is required. The suffices A to L index the actual headings that the ship took on each run as the trial was performed.

The points in vector $\underline{M}$ represent the ship motions measured at each ship heading at this frequency. For any one ship heading, the motion at this frequency is stimulated by the wave energy from all directions that is *encountered* at this frequency.

The encounter spectral ordinate in the $\underline{S}$ matrix $S_{e\,G,120}$, for example, represents the energy in the *encounter* wave spectrum at the frequency in question which is originating from a direction 120° relative to the ship heading direction G. Twelve different encounter spectra were calculated from the average directional wave spectrum measured by the waverider buoy.

In practice, it is necessary to create wave encounter spectra for every ship heading A-L. The $\underline{S}$ matrix contains elements from all twelve encounter spectra: Each row of $\underline{S}$ originates from the strip of data at the frequency in question in each of the 3D encounter spectra shown previously of Figure 2.3. A rotation of the order of these points is also necessary when they are placed in $\underline{S}$, so that the relative headings are correct and the row is populated properly.

Most of the calculations performed in this report used the range of relative headings 0°-330°, but they do not have to have a regular interval or cover a complete range of headings for a meaningful calculation to be performed.

Solution of the matrix equation at each frequency allows the construction of the squared transfer function in the encounter frequency domain. Taking the square root and transforming back to the wave frequency domain gives the standard transfer function.

Where seas originate from one general direction for a particular frequency, the encounter frequency matrix is typically populated by a swathe of values about one of the diagonals when the runs are placed in order of heading. The actual diagonal depends on which heading is taken as the datum. In perfectly long crested seas, only the diagonal itself is populated, and the same diagonal is populated in the $\underline{S}$ matrix at all frequencies.

The datum direction from which to calculate relative headings should be chosen with care. Roll transfer functions, for example, are narrow banded, and even in short crested seas, the motion is likely to be stimulated by the waves from one predominant direction which are encountered close to the natural roll frequency for a particular heading. It is quite possible to set up the matrix equation so that the roll transfer function is calculated from head or following seas rather than from beam seas, and in doing so it is likely that the results would be flawed.

The encounter frequency matrix $\underline{S}$ often has a rank less than the number of ship headings (12 for this trial). This occurs when entire rows or columns of the matrix have zero magnitude elements. These arise due to the effective expansion or contraction of zero magnitude zones when creating the daughter encounter spectra from the parent directional spectrum - low frequencies are not favoured when the relative heading is 180°, whilst high frequencies are depopulated when the relative heading is 0°. In this case the problem may be simplified, as the fully zero populated rows/columns may be ignored and the sizes of $\underline{R^2}$, $\underline{S}$ and $\underline{M}$ may be reduced. Dummy values need to be introduced into the appropriate places of the full (12 element) solution so that these directions are ignored when post processing.

Linear displacement transfer functions may be calculated where $\underline{S}$ contains the encounter wave *amplitude* spectral ordinates. Angular motion transfer functions may be calculated if encounter wave *slope* spectral ordinates are used.

The solution of the matrix equation is by no means straightforward. In Fryer et al. (1994) the method used was to calculate the inverse of the wave encounter spectrum matrix (the determinant of $\underline{S}$ multiplied the transpose of the matrix of cofactors of $\underline{S}$) and multiplying by the motion column vector to obtain the transfer function column vector. This method involves mathematical computations in which rounding errors may magnify, and to the creation of very large and very small numbers which are difficult to deal with successfully.

Hosking et al. (1981) describe the solution of $\underline{A}.\underline{X}=\underline{B}$ by the Gaussian elimination method, with the refinement of 'partial pivoting' to reduce errors due to rounding. The method requires fewer operations and is generally more appropriate for all but the smallest size matrices. It is the technique which has been used to obtain the results in this thesis (and is implemented in the MATGAU module described later), after the inverse method indeed proved unsatisfactory.

7.2.2 Software modules

Data analysis was performed in the DATS signal processing environment marketed by Prosig Computer Consultants Limited, Fareham, UK. This contains data processing tools in a modular format with the advantage that user written modules can be incorporated into the suite. Modules are written in FORTRAN with calls to DATS subroutines linked in. DATS does not nominally handle matrix computations and modules were written from scratch to allow the RAO calculations.

Besides typical matrix operations such as multiplication and transposition, some of the modules have rather specialised functions.

The MATDIA module finds the most populated diagonal of a square matrix, and returns an index number (e.g. 1 for the leading diagonal). There are two modes of operation; Mode 1

returns the diagonal which has the greatest sum of points; Mode 2 returns the diagonal which has the greatest number of non-zero points. For example, the following matrix:

$$\begin{pmatrix} 3 & 0 & 0 & 0 & 0 \\ 0 & 5 & 0 & 0 & 1 \\ 0 & 0 & 4 & 1 & 0 \\ 0 & 0 & 1 & 0 & 0 \\ 0 & 1 & 0 & 0 & 0 \end{pmatrix}$$

has the leading diagonal [3,5,4,0,0] returned with mode 1 (sum 12) but the diagonal [3,1,1,1,1] (with sum 7) returned for mode 2.

MATSDI creates a square matrix file which has zero magnitude points except along a specified diagonal; the values placed in the diagonal are the sum of the elements in each row of the input square matrix. For example, with the leading diagonal specified, the matrix

$$\begin{pmatrix} 0 & 5 & 3 & 0 & 0 \\ 2 & 3 & 0 & 0 & 0 \\ 0 & 6 & 0 & 0 & 0 \\ 0 & 0 & 0 & 3 & 0 \\ 0 & 0 & 0 & 0 & 1 \end{pmatrix}$$ leads to an output matrix $$\begin{pmatrix} 8 & 0 & 0 & 0 & 0 \\ 0 & 5 & 0 & 0 & 0 \\ 0 & 0 & 6 & 0 & 0 \\ 0 & 0 & 0 & 3 & 0 \\ 0 & 0 & 0 & 0 & 1 \end{pmatrix}$$

MATRED reduces the size of a square matrix and associated vector file by deleting any rows and columns that are fully populated by zero magnitude elements. For example, the following matrix:

$$\begin{pmatrix} 0 & 1 & 2 & 3 & 4 \\ 0 & 5 & 6 & 7 & 8 \\ 0 & 9 & 8 & 7 & 6 \\ 0 & 0 & 0 & 0 & 0 \\ 0 & 5 & 4 & 3 & 2 \end{pmatrix}$$ is reduced to an output matrix $$\begin{pmatrix} 5 & 6 & 8 \\ 9 & 8 & 6 \\ 5 & 4 & 2 \end{pmatrix}$$

The eliminated rows/columns of the original matrix are reported to the user. Note that it is still possible that the resultant matrix has linearly dependent rows/columns (which could produce a zero row/column following row operations).

MATGAU solves $\underline{A}.\underline{X}=\underline{B}$ where $\underline{A}$ is a square matrix and $\underline{B}$ is a column vector by the Gaussian elimination method with partial pivoting [Hosking et. al. (1981)]. The augmented matrix is reduced to upper triangular form, and then the elements of $\underline{X}$ are calculated in turn by back substitution.

7.2.3 Wave data manipulation

The frigate trial described in Chapter 5 has been used for the analysis in this chapter. The mean wave spectrum (Figure 5.4) from the waverider buoy during the trials period was used, which was bimodal, and the energy was redistributed from bins of 5° x 0.01 Hz into bins of 30° x 0.01 Hz. A mean 3D wave *slope* spectrum was also calculated from this spectrum, by multiplying amplitude spectral ordinates by ω^4/g^2 as described in Lloyd (1998).

These mean 3D wave amplitude and slope spectra were taken in a stationary frame of reference. The analysis technique requires the computation of the spectra that are 'seen' by the moving ship, the 'encounter spectra'. On any heading, waves from forward of the beam appear at higher than actual frequency, whilst those from abaft the beam appear at lower frequency.

A DATS procedure was written to calculate these encounter spectra at the ship speed over the range of headings of the trial. The energy ordinates in each 30° direction segment are treated as separate spectra for this purpose. The technique in Fryer et al. (1994) is used to distribute energy in the encounter frequency range. The upper and lower limits of the actual frequency bin are calculated using the formulae (recast from Equations 2.29-2.31):

$$f_e = \left(c - U.\cos\psi_r\right)\frac{f}{c} \qquad \ldots(7.2)$$

$$c^2 = \left(f\lambda\right)^2 = \frac{g\lambda}{2\pi}\tanh\left(\frac{2\pi d}{\lambda}\right) \qquad \ldots(7.3)$$

The second equation requires solution for λ (and hence f) by iteration, though initial values given by the deep water or shallow water approximations for wavelength often lead to few iterations being necessary. The general equation (Equation 2.3) for phase velocity was used as the water depth was not great compared with the ship length for this trial. Energy from the actual frequency bin is then apportioned between all the corresponding encounter frequency bins (of constant but user selected frequency width) within these limits. The encounter frequency limits may fall entirely within a single encounter frequency output bin, or span two or more bins.

As described in Chapter 2, actual frequencies do not map to encounter frequencies with a one to one relationship when the waves are abaft beam on to the ship. Noticeably for following seas there is effectively a maximum encounter frequency for seas abaft of the beam, and a 'reflection' in encounter frequency may take place as the actual frequency range is stepped through - see Figure 2.6. The energy output in one encounter frequency bin may thus originate from two or three separate actual frequencies.

An encounter frequency range of 0.02Hz to 1.15Hz with ±0.005Hz bins was selected for the output files. This spanned the entire possible encounter frequency range and allowed checking that all energy had been accounted for.

7.2.4 Motion data manipulation

The angular motion time histories were converted from degrees to radians, and acceleration measurements (in body axes) were converted to earth axes and then to the equivalent acceleration at the ship CG. The accelerations were then integrated twice in order to obtain linear displacements at the CG. Auto spectra of the time histories were then taken, with windowing such that the output frequency range and step were the same as the wave encounter spectra. The agreement of the frequency base for the motion and wave spectra was necessary before solution of the matrix equation $\underline{M}=\underline{S}.\underline{R}^2$

7.2.5 Transfer function calculation

Using the motion spectra and encounter spectra obtained by the methods outlined above, calculation of transfer functions for all six degrees of freedom was then performed using a new DATS procedure.

A large part of this program is taken up with extraction of the information required to set up the $\underline{S}$ and $\underline{M}$ matrices for each frequency step. There are six degrees of freedom, each of which requires an $\underline{M}$ matrix. The two $\underline{S}$ matrices for encounter wave amplitude and slope spectral elements must be extracted from 12 separate files each, and then the order of the elements in each row must be rotated in order to ensure they fall into the correct place according to the relative heading of the wave component.

Having set up the $\underline{S}$ wave matrix and $\underline{M}$ column vector, the MATRED module is used to remove any all zero rows or columns in the $\underline{S}$ matrix and the corresponding rows in the $\underline{M}$ vector. Without this precaution, rows/columns full of zeros would cause the calculation to fail because there are effectively more unknowns than simultaneous equations.

The matrix equation is then solved for $\underline{R^2}$ using the MATGAU module. Despite using the MATRED module, it is still possible (though unlikely) that there are linearly dependent rows/columns in the equation, and in this case dummy values are output into $\underline{R^2}$ to prevent the program from halting.

In practice, the solution for $\underline{R^2}$ often yields negative values; though mathematically possible these have no physical meaning. This is a problem of ill conditioning of the matrix equation, discussed further in 7.3, and in this case the negated square root of the absolute value is saved and the problem flagged in a text file.

7.3 Results

Figures 7.1 to 7.16 give a selection of results of the transfer function calculations, concentrating on heave and roll as examples of linear and angular motion respectively. The

results presented differ in the detailed way in the way simplification has been attempted and in the direction which has been used as the reference direction in each case.

All the transfer functions have been left in the encounter frequency domain, but could have been transformed to a stationary reference frame. The solid lines are the results of a transfer function calculation provided for comparison, using the PAT suite of 'strip theory' seakeeping prediction code [Montgomery & Crossland (1995), based on Gerritsma & Beukelman (1967)]. The symbols show the results of the matrix transfer function calculations. Each graph is labelled with the appropriate relative headings; for symmetrical headings eg.90°/270°, both data sets are included on the same graph, but 'o's refer to relative headings 0°-180° and 'x's to 210°-330°.

The strip theory calculations are generally considered reasonable except for stern quartering seas calculations (30° and 60° in this case).

The scales on Figures 7.1 to 7.16 have been selected so that scatter in the results is demonstrated, and all have a Y-axis extended below the origin so that 'negative' transfer function ordinates may be seen. In general, if negative points arise at a particular frequency on one relative heading, it is likely that points at the same frequency on the other (simultaneously calculated) headings are in error also.

Figures 7.1 to 7.3 give the results using the complete set of motion data and the mean wave spectra over the entire trial period. The matrices for these calculations were aligned so that the relative headings 0°/180° were in the direction of the low frequency swell waves of Figure 4.2, whereas alignment with the wind generated waves was used for the Figure 7.4-7.6 matrices. The former appears to be the better result in terms of lower scatter of points and correspondence with the PAT predictions.

Whilst the solutions at higher frequencies appear good, with transfer function points consistently close to zero, results at the more important lower frequencies - where features in the transfer functions are expected to occur - are much more scattered, as in Figure 7.6 (heave). This is most probably due to ill conditioning of the matrix equations at these frequencies, and will be exacerbated for motions like roll which have a narrow band width

and hence few significant motion spectrum points. The results for roll in Figure 7.1 show this scatter, but points on the resonance peak are clear, especially in the 90° case.

Figures 7.7 to 7.10 give results of a repeat solution for the same data as the previous figures, but using the MATSDI module to simplify the matrix equations according to the diagonal advised by MATDIA. Condensing energy into one diagonal of the encounter wave matrix $\underline{S}$ effectively enforces a long crested seas calculation at each frequency. The operative wave encounter spectra then appear in a form similar to the spectrum in Figure 7.17, with only one direction associated with each frequency. The spectrum in Figure 7.17 is a stationary spectrum, and has been calculated from the spectrum of Figure 5.4, but does not form part of the analysis and is included for illustration only.

The diagonal in which to condense energy is determined using the MATDIA module. The two modes of operation for MATDIA are effectively two different ways of interpreting the nature of energy distribution in the $\underline{S}$ matrix. With mode 1, it is assumed that the predominant diagonal is the one in which the total energy is greatest, whereas with mode 2 the distribution is considered the best indicator of the dominant diagonal irrespective of energy. In long crested seas there is no ambiguity, because all the energy occurs in only one diagonal - mode 1 and mode 2 would both reference this diagonal.

This lack of ambiguity between the two calculation modes is shown in similar results for high frequencies, but there are differences at lower frequencies. Consider roll at 180° (Figure 7.7 and 7.9); mode 1 gives virtually zero roll as expected, and the position of resonance peaks on the other headings is relatively well defined in 7.7, but with mode 2 there is a peak at 180° and reduced peaks on the other headings. Simplification with MATDIA mode 1 thus appears to be more successful than with mode 2.

The heave results in Figures 7.8 and 7.10 are very similar, and the simplification appears to have reduced the scatter found with the full solution and give more convincing transfer functions. There is also encouraging correlation between points obtained from symmetrical headings.

It was mentioned in Chapter 4 that the sea state reduced during the trial, and in an attempt to improve the transfer function results, calculations have also been performed using only the first seven ship runs for motion data. The stationary wave spectrum was averaged over a correspondingly reduced length of time before calculation of the directional spectra. The variation in the sea state and ship motions over this period should be less, and so ill conditioning of the matrix equations should also be reduced. Restricting the number of runs to seven also restricts the number of transfer function directions which can be calculated to seven. With the wave encounter spectrum matrix 'aligned' for the sea swell, the seven directions are those between 90° and 270° relative headings.

Figures 7.11 and 7.12, with a full matrix solution, do indeed show an improvement over the corresponding graphs of Figure 7.1 and 7.3, with a greater number of solved points, reduced scatter and better agreement with the strip theory predictions. Figures 7.13 to 7.16 are the results with the same data but simplified as before by MATSDI modes 1 and 2 respectively. Again, mode 1 gives the more authentic results, and the solutions for heave transfer function look convincing.

7.4 Discussion

7.4.1 Present calculations

Success of the technique used in this chapter is dependent on reducing the degree of `ill conditioning' of the wave matrix and vectors system: mathematical texts show that for $\underline{A}.\underline{X}=\underline{B}$ small changes in the square matrix $\underline{A}$ can lead to large changes in the solution $\underline{X}$. There are several potential sources of error which may lead to ill conditioning of the matrix equation $\underline{M}=\underline{S}.\underline{R}^2$ used here.

The main analysis reported here assumes the trial took place in a constant sea state, but it is known that the sea state reduced during the trial. The process of taking the mean spectrum over the trials period is a source of ill conditioning of the $\underline{S}$ matrix; the mean spectrum might best represent the wave conditions for the middle runs of the trial, but the effect on the other

runs is difficult to determine. The change in sea state noted was significant - the direction of waves of frequency greater than 0.2 Hz changed by 90° for example.

Other sources of ill conditioning for the matrix equation could be:

- The nominal ship speed used for calculating wave encounter spectra was 5 knots through the water; the actual ship speed varied by up to half a knot about this so that the encountered wave spectra could be slightly different from those actually used.
- The wave amplitude spectra measured at the wave buoy are themselves calculated from the buoy's motion time history and subject to uncertainty. In addition, the data is recorded for a few minutes each hour, and it is assumed but not certain that these samples are representative of the sea state.
- Ship motion measurement is always difficult in seas abaft of the beam, where the difference between ship speed and wave speed may be small and encounter frequencies are correspondingly low. This leads to low acceleration measurements. Accelerometers are usually set up to cover a wide range of acceleration, so these low measurements may be subject to significant digitisation error (visible as 'stepping' in the time history).
- For this trial, there is more statistical uncertainty as the run length was constrained to 11½ minutes for each leg. Considering a desirable number of 100 wave encounters [Lloyd (1998)], the minimum encounter frequency meeting this condition is 0.14 Hz. This ship responds particularly to frequencies below 0.1 Hz, so the run time was rather low. The worst case occurs in following seas. The vector $\underline{M}$ is therefore likely to introduce ill conditioning for the data used here.
- The MATRED module used to eliminate zero populated rows and columns may lead to loss of integrity in the $\underline{S}$ matrix. Since $\underline{S}$ must be square, if MATRED deletes a row/column then the equivalent column/row must also be deleted. It is assumed that the contributions are small, but potentially important data is lost which might be included in the computation by a more advanced technique.

7.4.2 Possible improvements

Many of these points may essentially be seen as uncertainties about a central best estimate value, and as such could be subject to an error analysis as introduced in Chapter 6, to give error bars on the individual points. Of course, the strip theory transfer functions used for comparison can also be given this treatment to reflect uncertainty in these results due to ship displacement, trim etc.

Additionally, using a single 3-D wave spectrum, averaged over the whole trial, is not strictly necessary. If a full set of encounter spectra had been calculated for each hourly spectrum recorded at the wave buoy, matrix equations could have been set up where the ship motions were linked with these individual encounter energies rather than the averaged energies. Logistically this calculation would be more demanding to construct, but the potential for improved results makes this well worth attempting in further studies.

The matrix solution of linear simultaneous equations is well documented in advanced numerical analysis texts. Schendel (1989), for example, indicates iterative methods of solution e.g. Gauss-Seidel, which might be useful for larger matrices - more ship headings and greater wave direction resolution in this case - but which converge on the solution calculated directly by the Gauss elimination method used here.

Watkins (1991) discusses methods for estimation of the ill-conditioning of the $\underline{A}.\underline{X}=\underline{B}$ system and its sensitivity to errors like those mentioned above. This is particularly useful, as eliminating the ill-conditioned portion of data at each frequency step should lead to improved solutions for the remaining data, and improved calculation of the transfer function. The use of least squares methods are also discussed, which may be used where repeat runs have been used or to effectively combine results on port/starboard symmetrical headings eg.150°/210°. Application of these techniques could be investigated in future development of the technique.

These techniques may also have application to manoeuvring basin and tank testing of models. Seakeeping tests are usually performed with the aim of conducting the model run in long crested unidirectional waves. For random waves in particular, the need to avoid reflected waves requires complex control software, but even so the useful length of a ship tank may be

less than half of its physical length. In conjunction with measurements from a directional wave probe, the methods reported here could be used to calculate transfer functions without this restriction; the motions due to direct and reflected (and radiated) waves are accounted for simultaneously.

Seakeeping experiments are usually very time consuming to perform, because of the number of runs required (especially if the useful tank length is small) and also because of the time needed between runs for waves to decay (so that the next set of waves generated will be practically unidirectional). Using the new techniques, there would be no need to wait between runs as all waves can be included in the calculations, and the run lengths themselves may be longer. There is thus a considerable cost saving potential.

Success would depend on the reliability of the information recorded at the directional wave probe. In a manoeuvring basin, a single stationary wave probe would provide a wave spectrum from which encounter spectra could be easily calculated, but would not have measured exactly the same wave system that the model encountered. In a ship tank, the exact encounter wave spectrum that the model encountered would be measured, but determination of wave propagation direction may be more difficult because the probe is moving.

7.5 Summary

RAOs were calculated using the method proposed by Fryer (1991) for a frigate, based on a dedicated seakeeping trial where ship motions were measured in sea states 3 to 4. The trial was notable as the prevalent sea state was measured in terms of its direction as well as its wave height and frequency content. The sea state was composed of swell and wind generated components which originated from very different directions.

The calculated transfer functions have been compared with those predicted by strip theory calculation. The trial transfer functions are correctly calculated in essence, but show a large degree of scatter. The uncertainty in the results is seen as being principally due to 'ill-conditioning' of the matrix equation; sources of this uncertainty are suggested, in particular the reducing sea state during the trial. Methods of improving the results are suggested. These

methods could also be further validated using results from alternative trials where directional wave spectra were measured, like those reported in Chapter 5.

There is also a possible application of this technique to tank testing of models for RAOs. The need to experiment in a unidirectional environment currently restricts both the duration of a run, and imposes a time interval between tests of some 15 to 30 minutes for waves to die down. If the directional wave spectrum in the tank were measured using an array type device (section 2.2.1), reflected as well as direct waves from the wavemaker could be accounted for when calculating the model RAOs. The efficiency of testing programmes could be vastly improved.

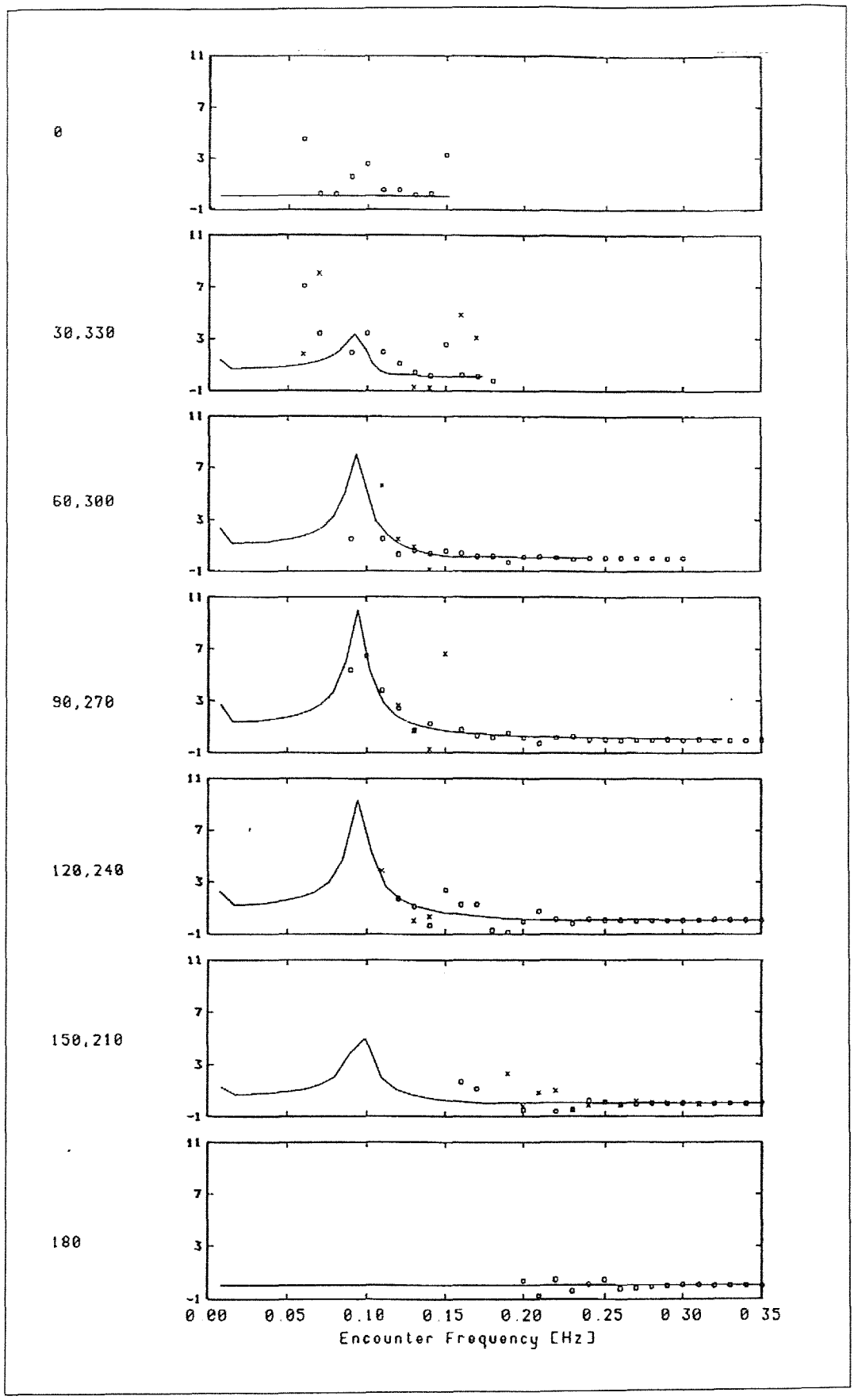

Figure 7.1 Roll RAO, all trial, aligned with swell

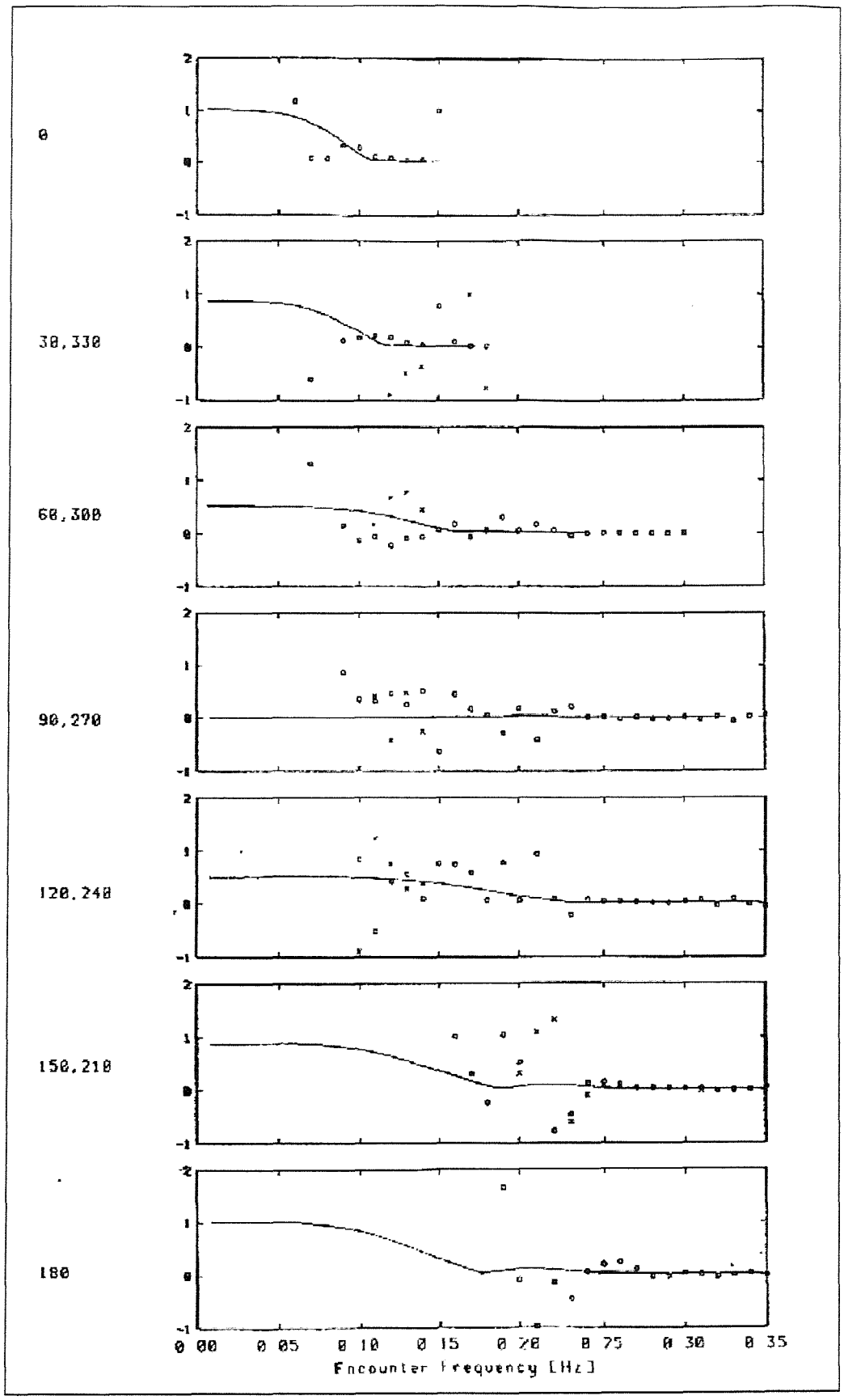

Figure 7.2 Pitch RAO, all trial, aligned with swell

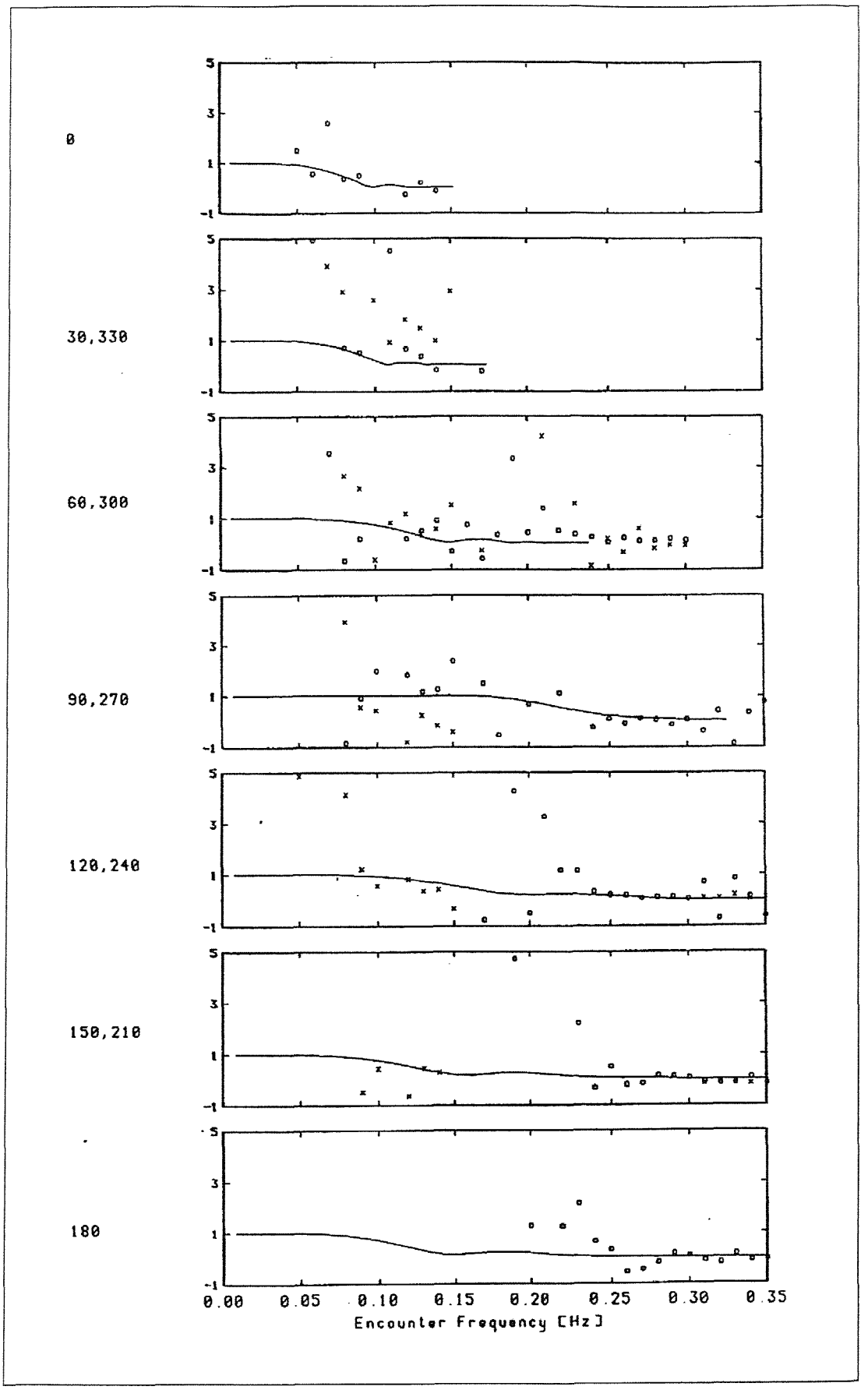

Figure 7.3 Heave RAO, all trial, aligned with swell

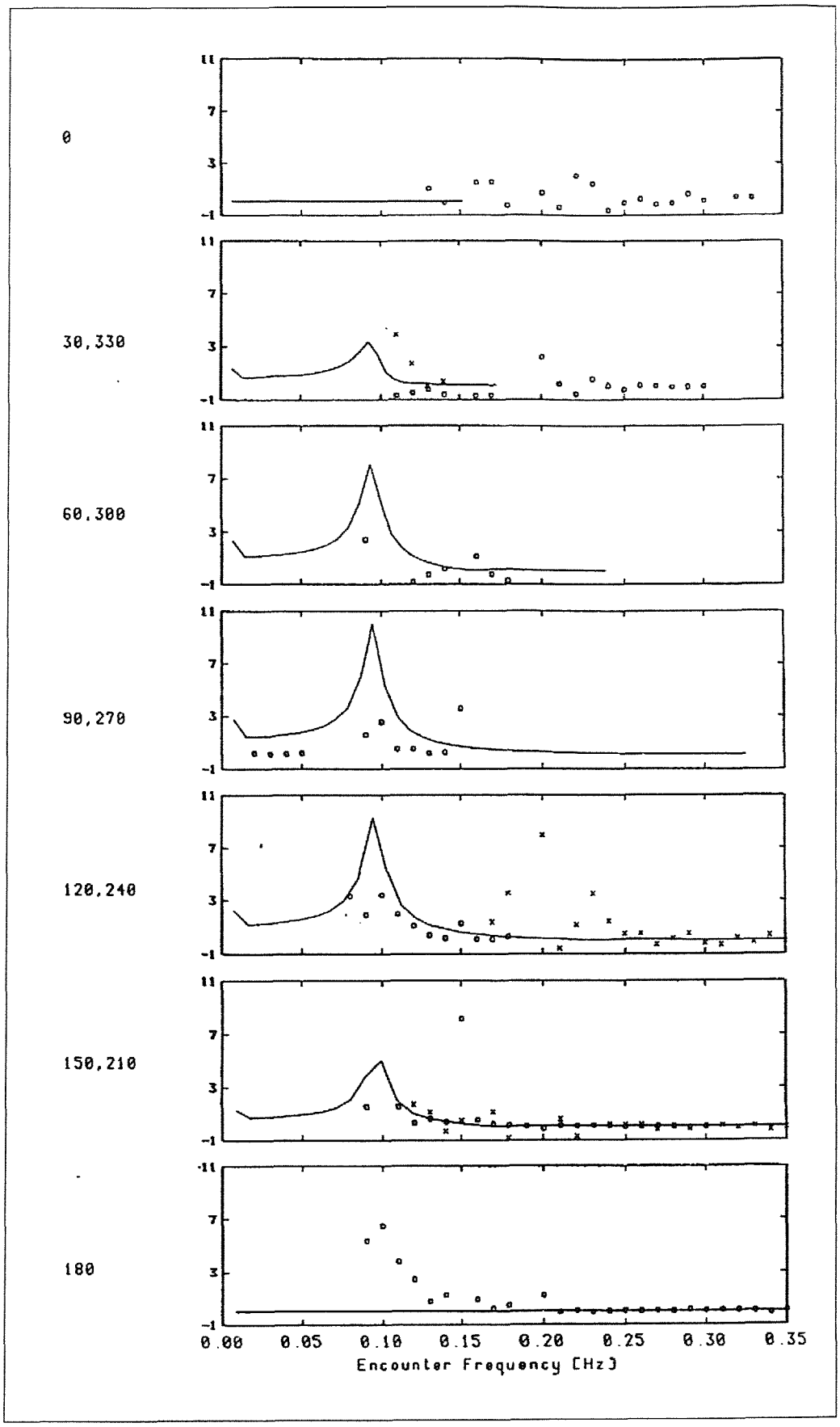

Figure 7.4 Roll RAO, all trial, aligned with wind

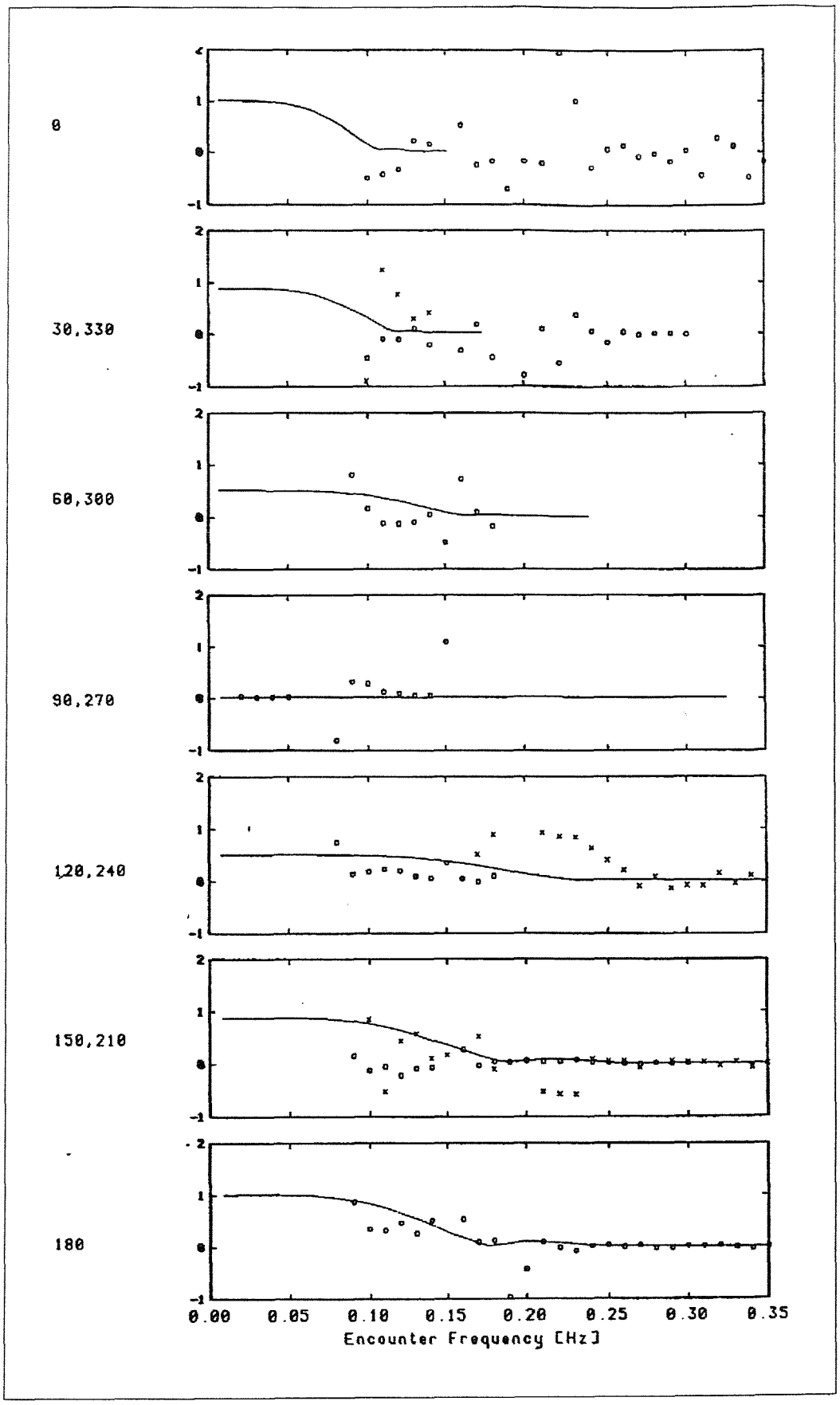

Figure 7.5 Pitch RAO, all trial, aligned with wind

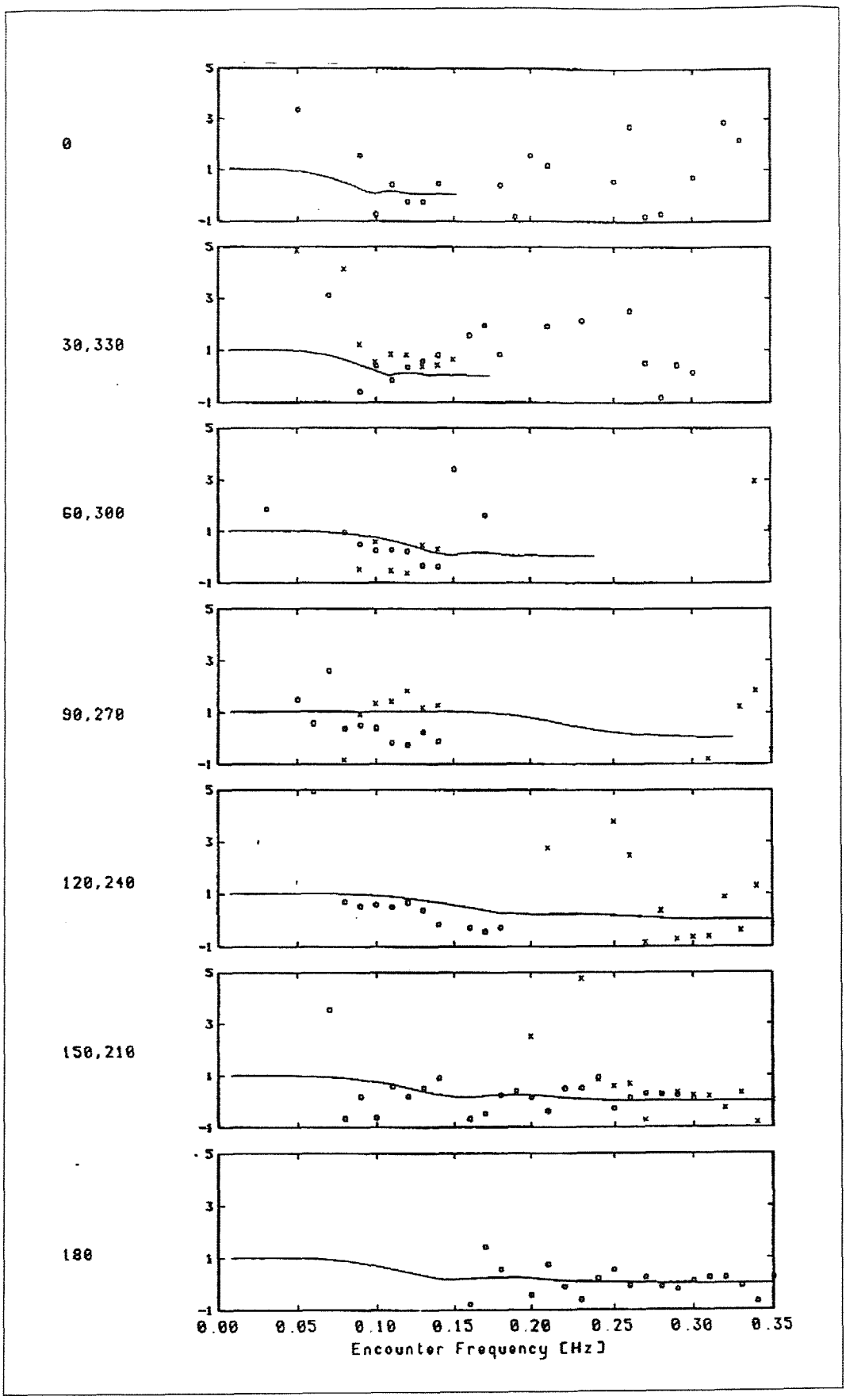

Figure 7.6 Heave RAO, all trial, aligned with wind

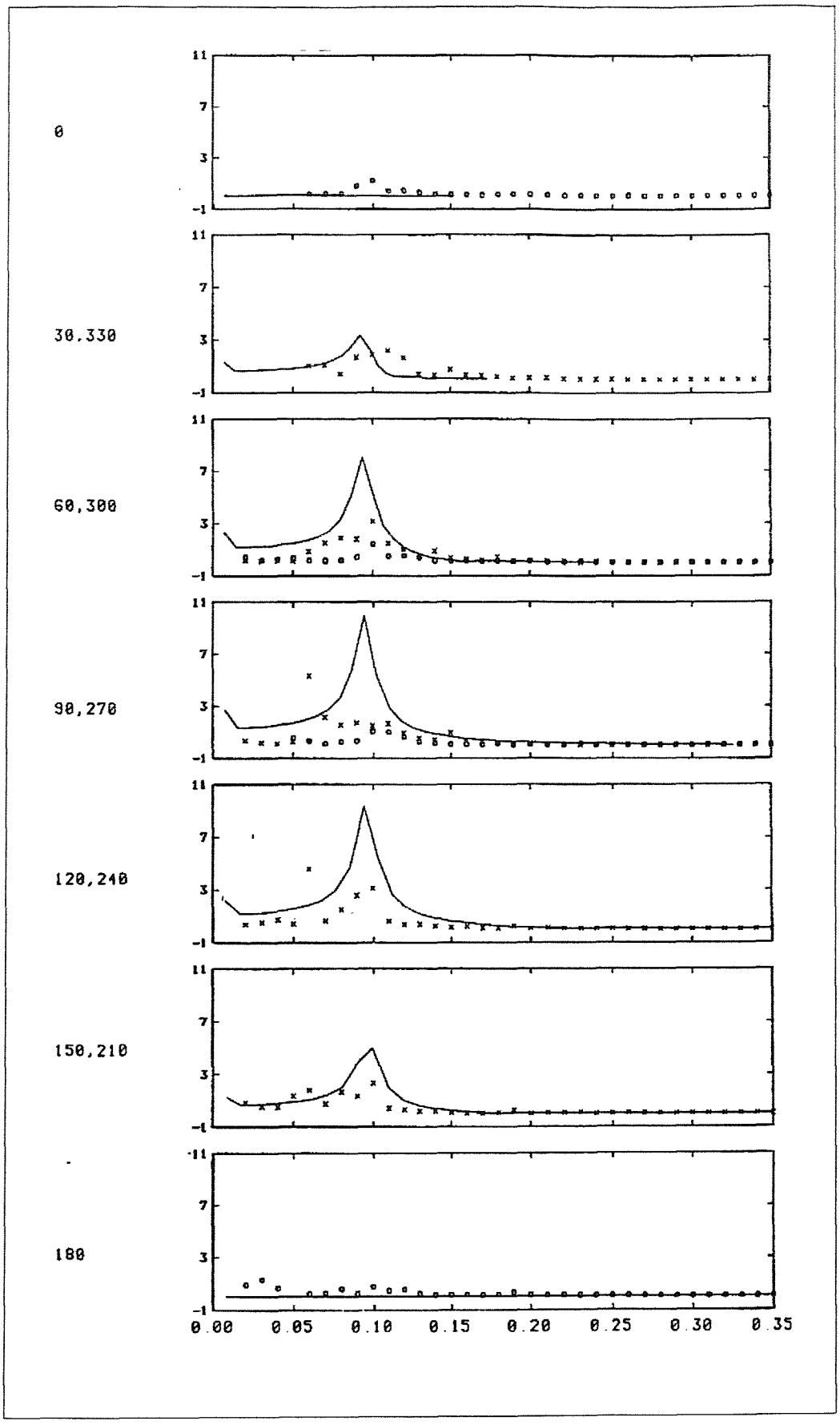

Figure 7.7 Roll RAO, all trial, MATDIA mode 1

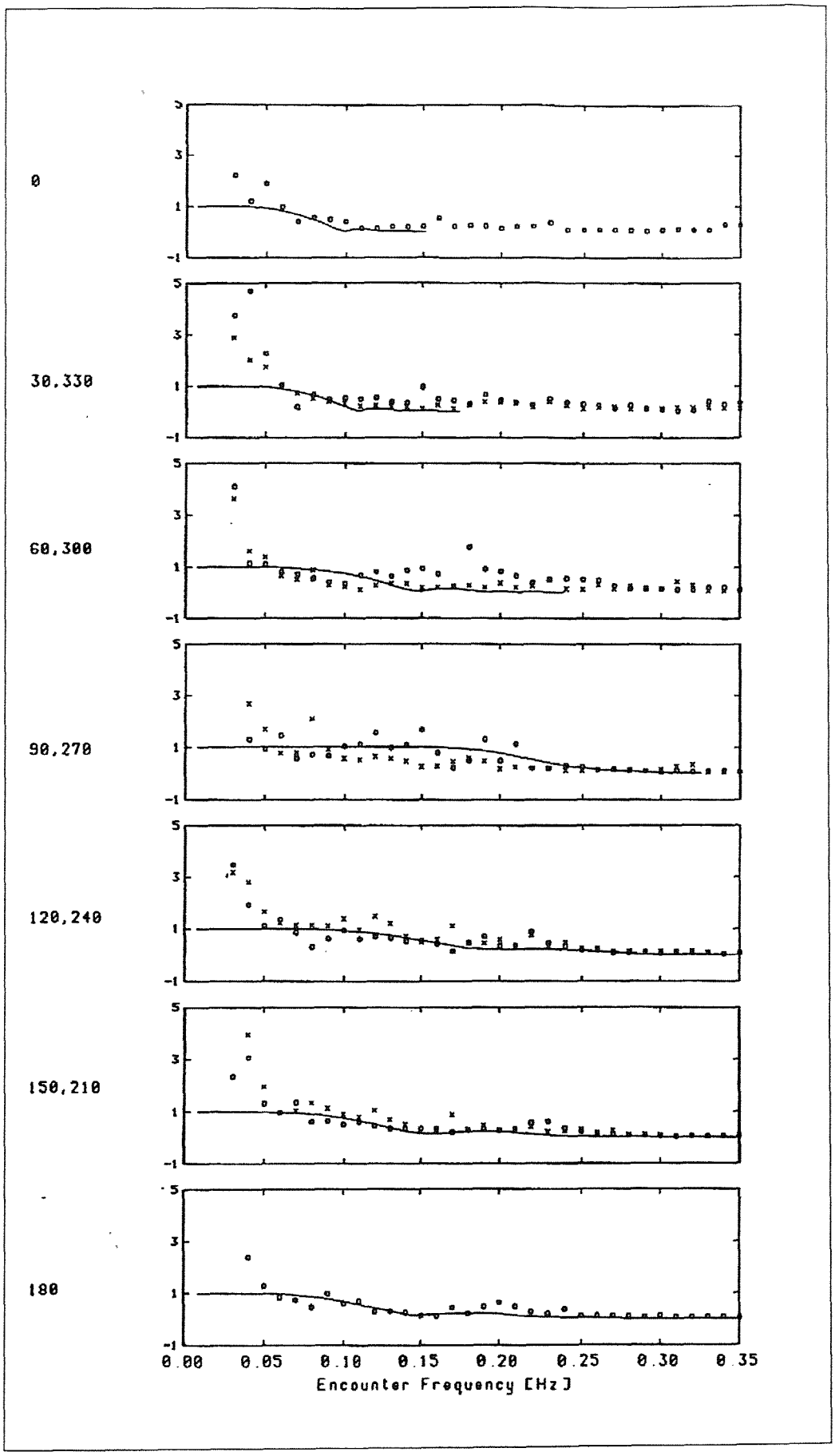

Figure 7.8 Heave RAO, all trial, MATDIA mode 1

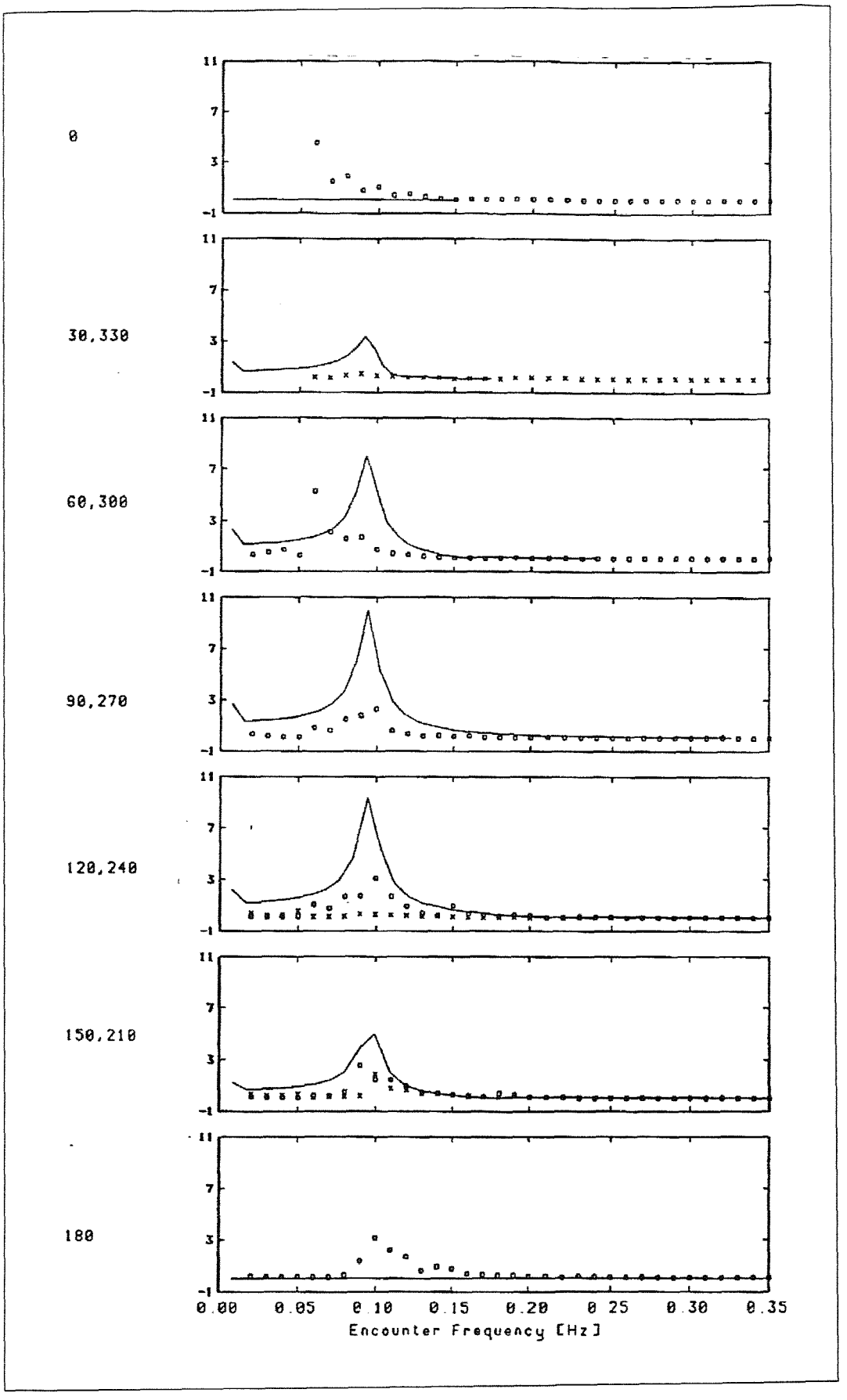

Figure 7.9 Roll RAO, all trial, MATDIA mode 2

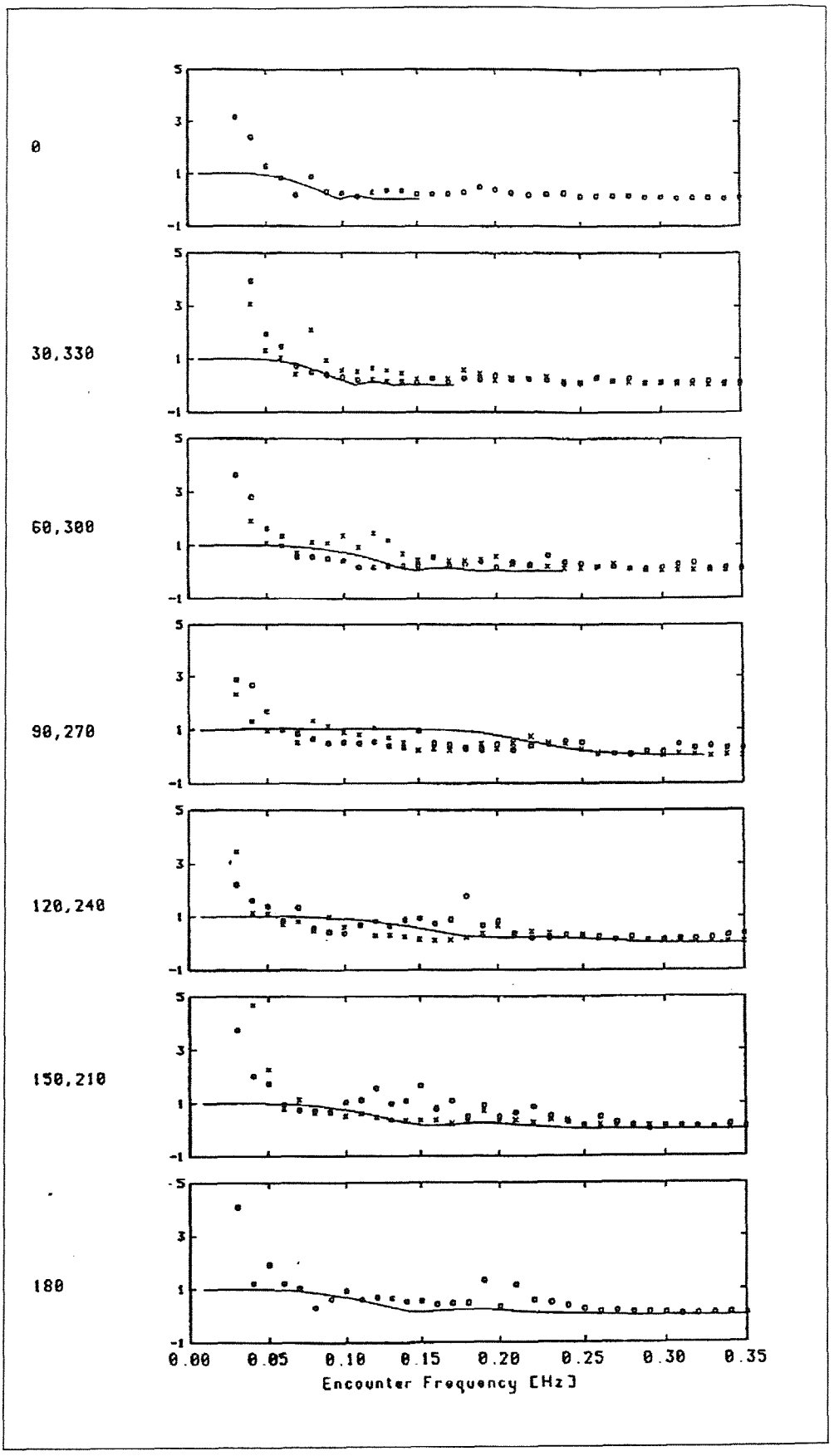

Figure 7.10 Heave RAO, all trial, MATDIA mode 2

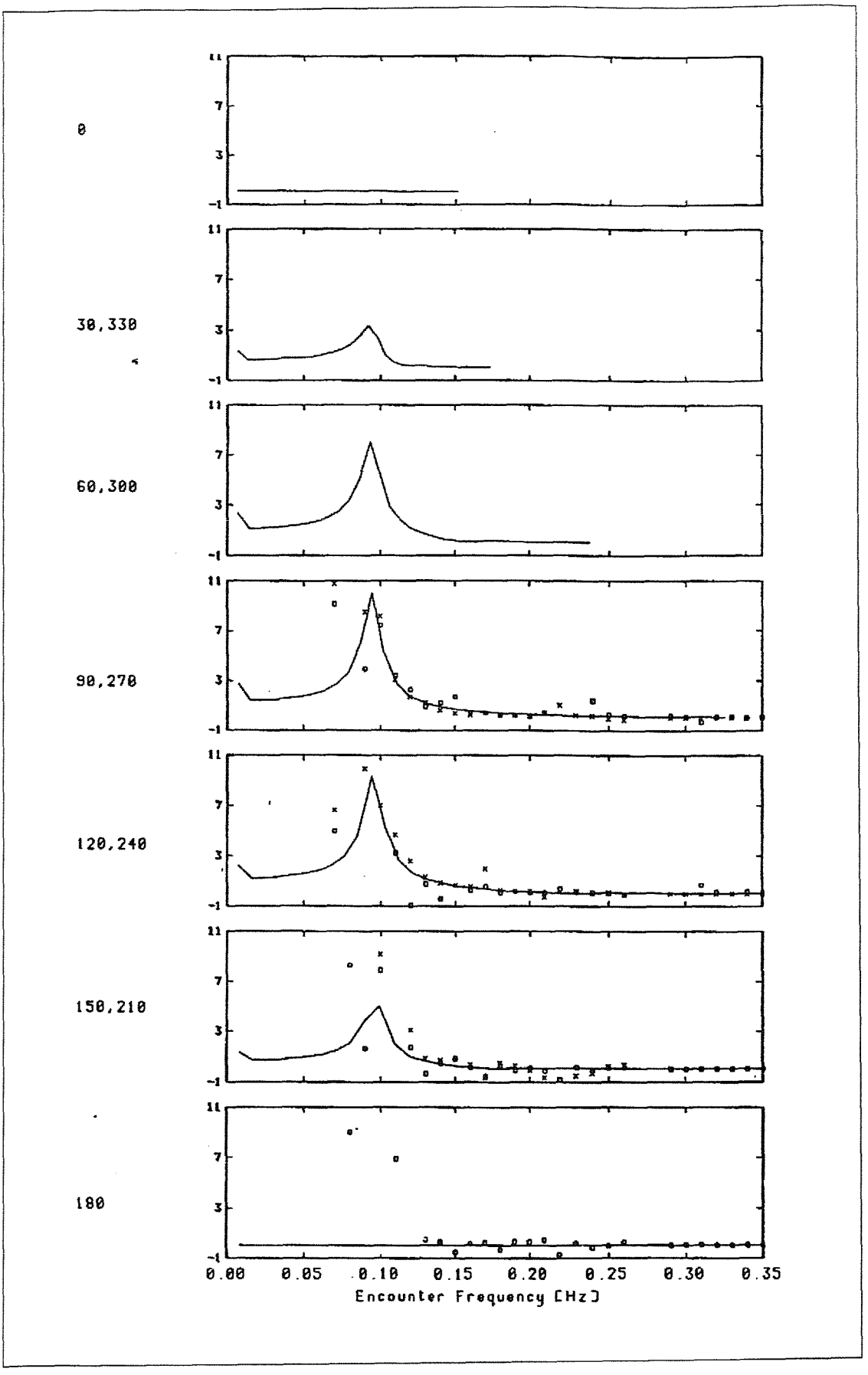

Figure 7.11 Roll RAO, first half of trial

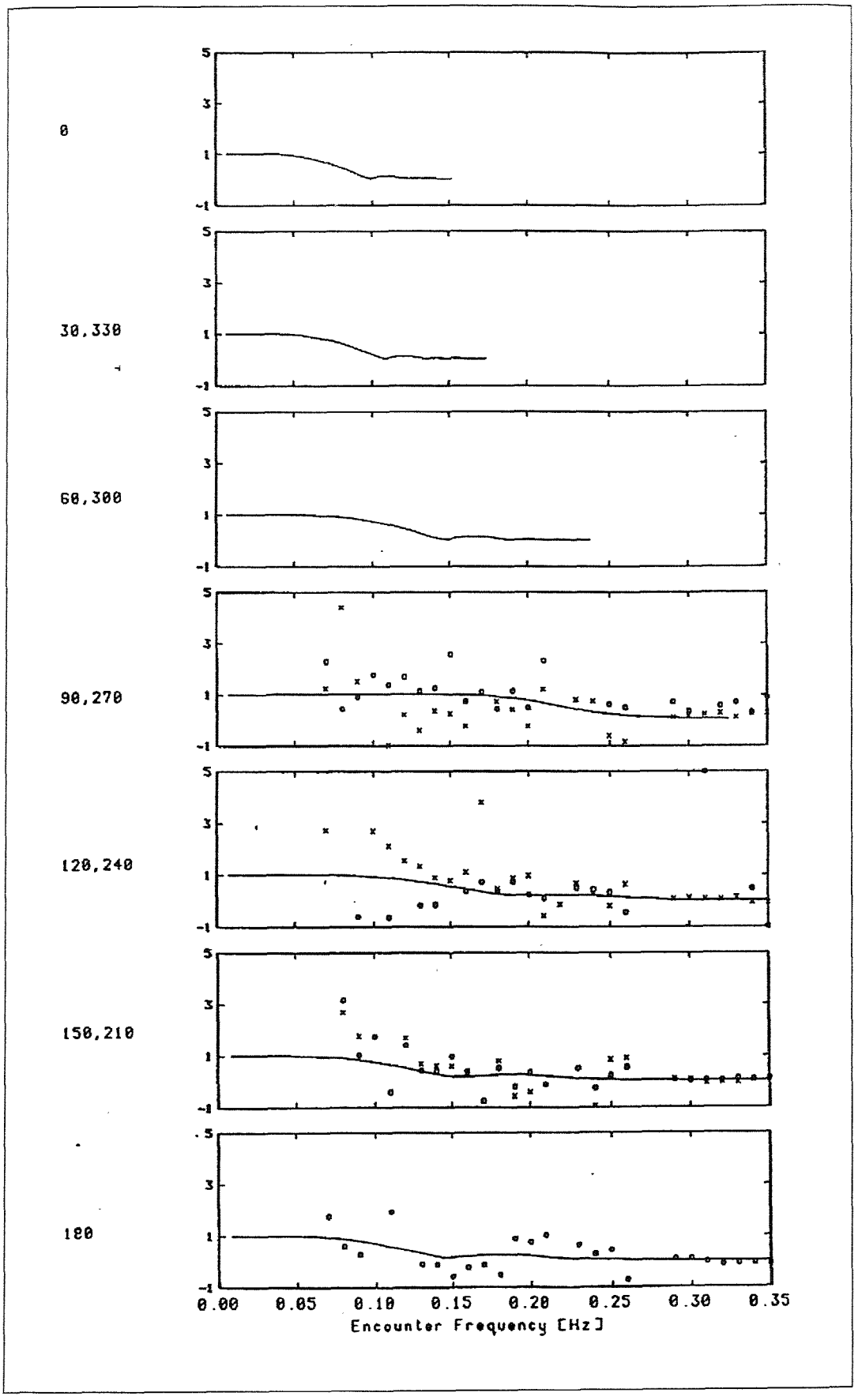

Figure 7.12 Heave RAO, first half of trial

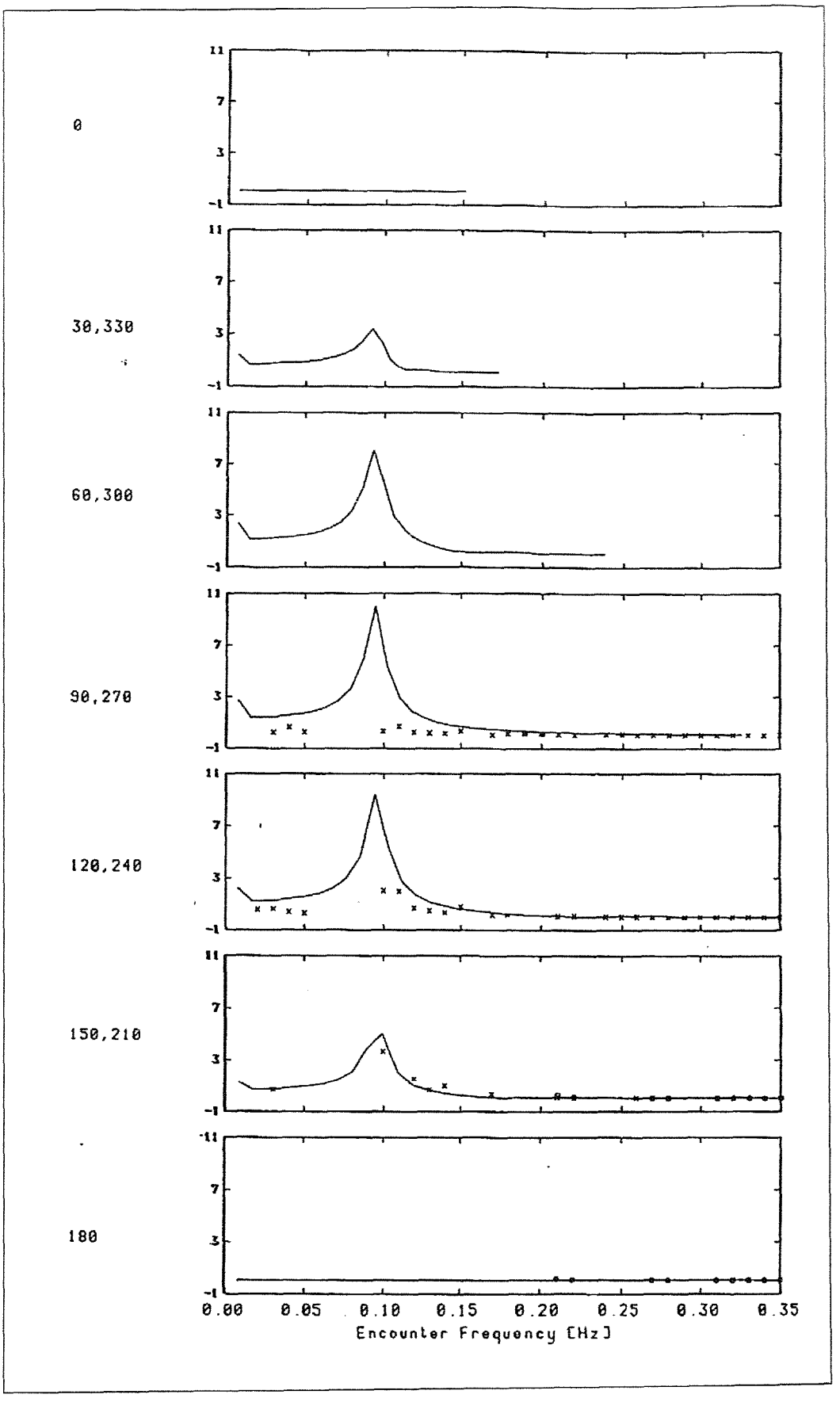

Figure 7.13 Roll RAO, first half of trial, MATDIA mode 1

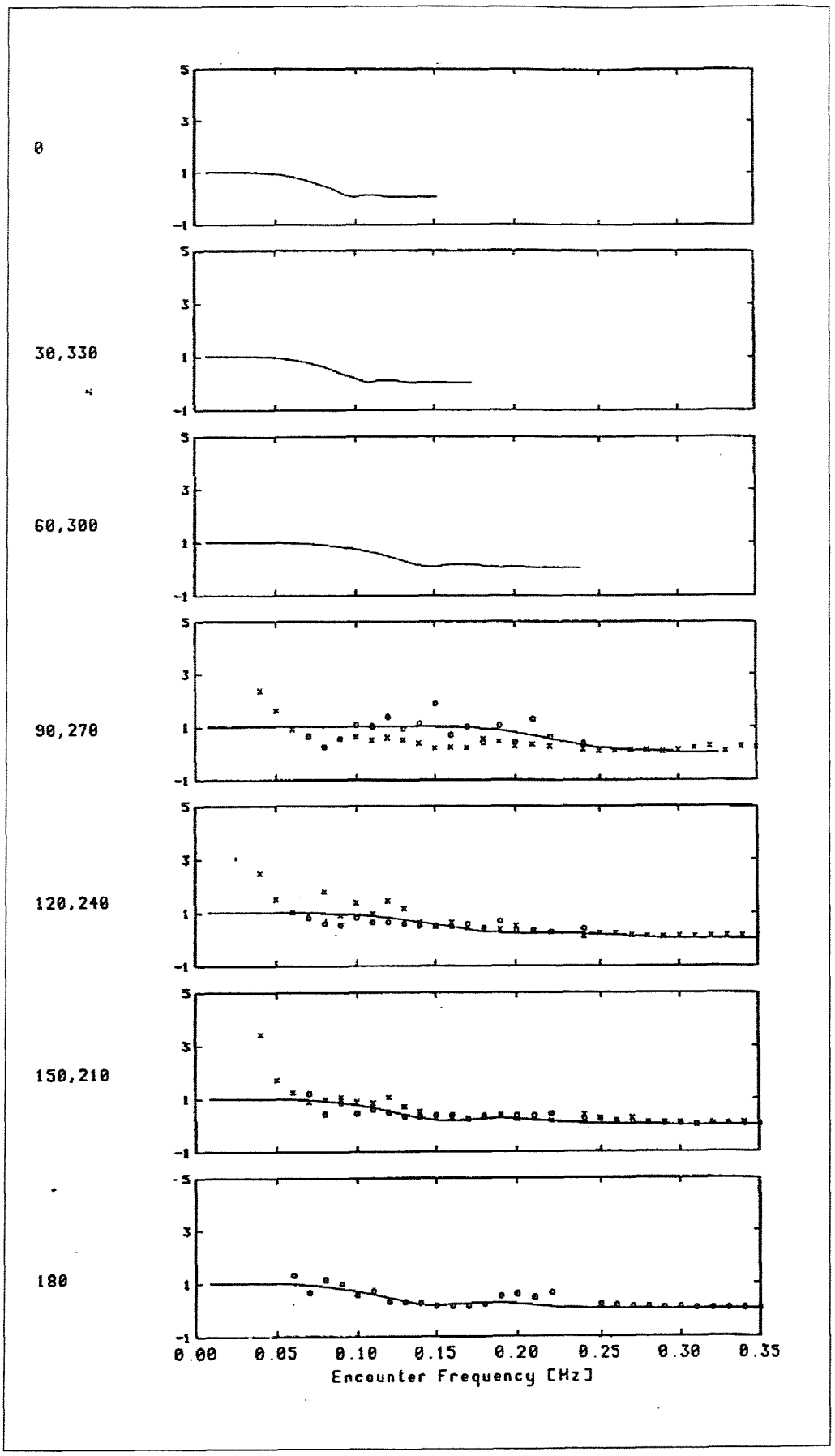

Figure 7.14 Heave RAO, first half of trial, MATDIA mode 1

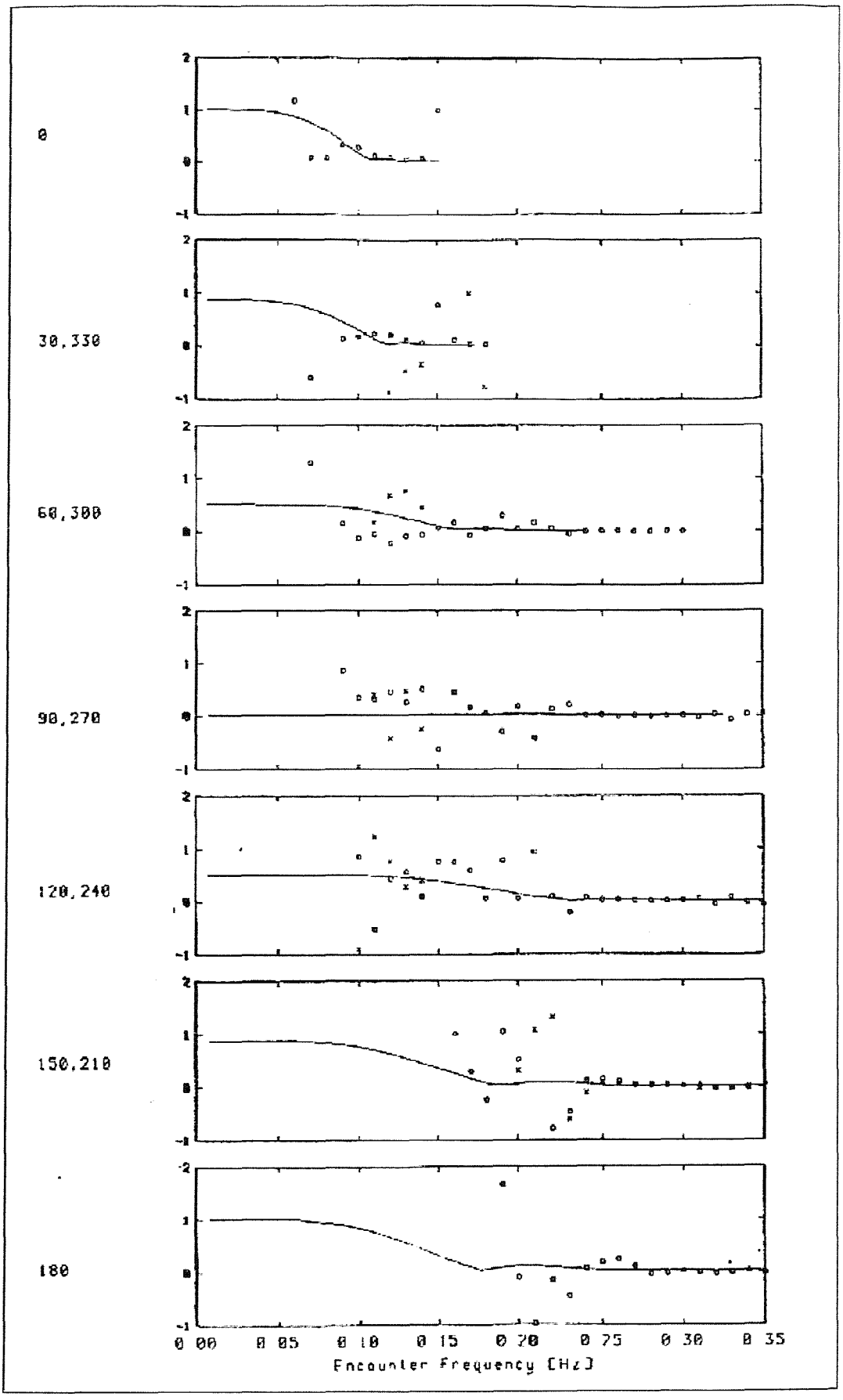

Figure 7.15 Roll RAO, first half of trial , MATDIA mode 2

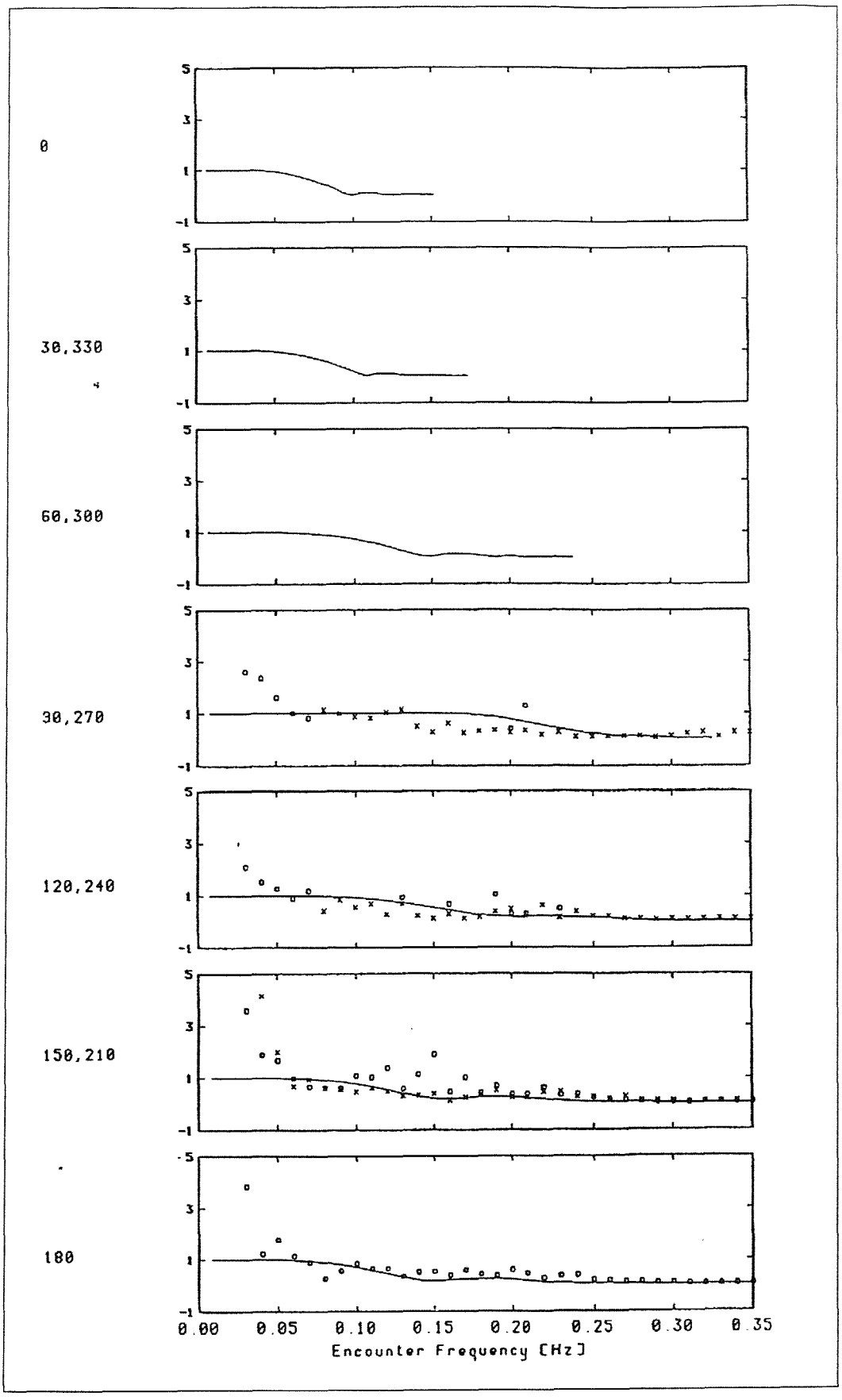

Figure 7.16 Heave RAO, first half of trial, MATDIA mode 2

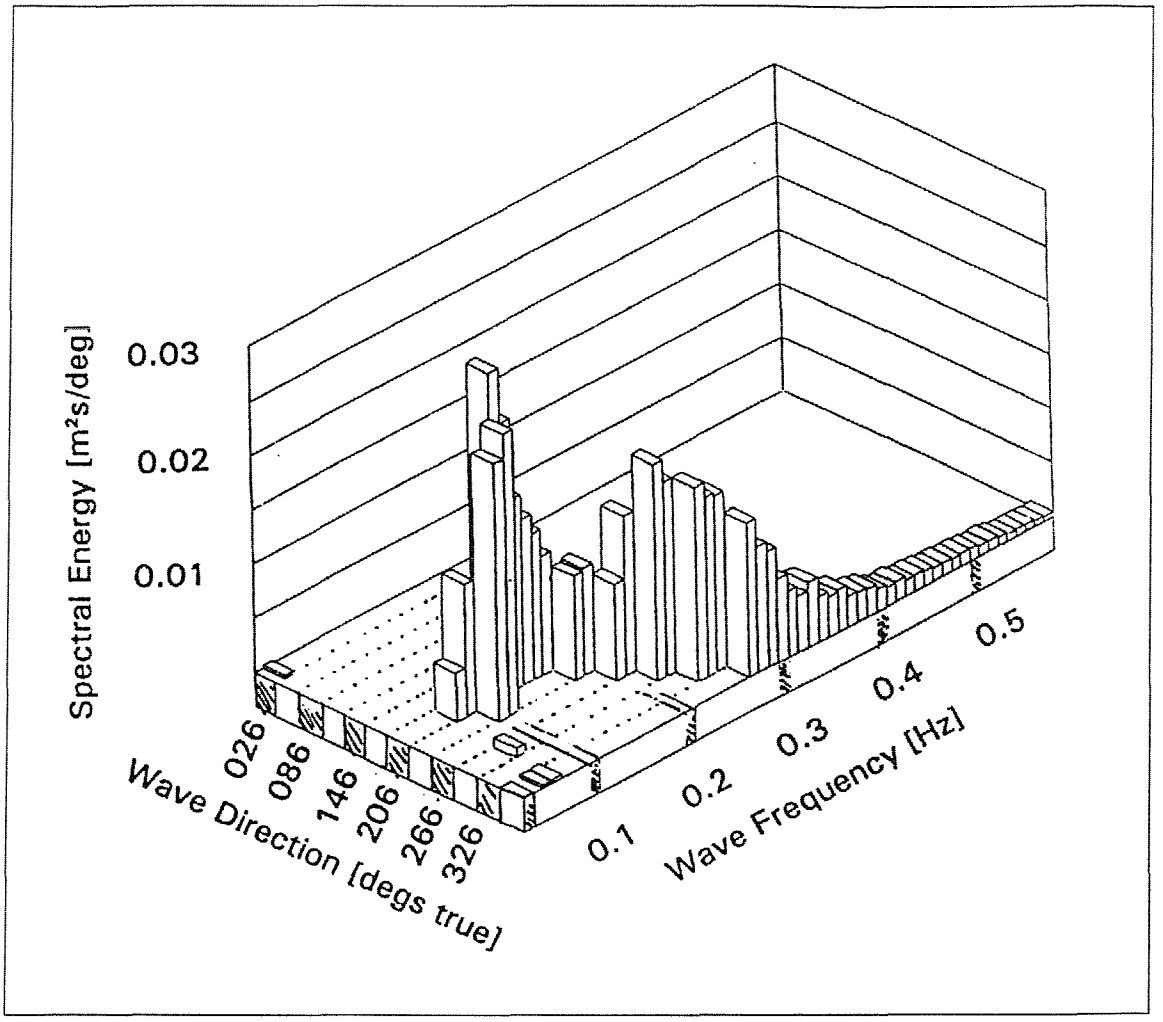

Figure 7.17 Manipulated wave spectrum with artificial long crestedness

8. ESTIMATING SEA STATE FROM SHIP MOTIONS – STATISTICAL METHOD

8.1 Introduction

Determining the prevalent sea state, with a full description in terms of frequencies and directions, is highly desirable for a ship in rough weather. If the sea state is known, then in conjunction with modern ship motion prediction programs, which are both reliable and quick to run, the ship motions on alternative headings and at different speeds can be calculated. A shipboard advisory system is envisaged in which these motions are evaluated against criteria for specific ship operations; examples might be helicopter recovery for warships, or some motion based passenger comfort index on ferries. The system could also be used to calculate the corresponding motions of other ships in the vicinity, which may assist in establishing a mutually comfortable speed under escort, for example. Section 2.4 showed that there has been interest in this subject over the years, but concluded that no reliable and robust method has been reported that can deal with the complexities of real seas.

In the Chapter 9, the matrix techniques developed in Chapter 7 for predicting transfer functions will be applied in a reverse calculation to obtain sea state information given the ship motions and known transfer functions. Before that, an investigation is made in this chapter of what accuracy can be achieved in deducing the significant wave height given the ship motions from a purely statistical point of view. A large data set of trials results made with the 'star' patterns of Chapter 3 has been used. Though an estimate of the significant wave height may be made based on the ship motion, this approach does not give directional information about the waves.

8.2 Statistical approach – linear regression

The trials with the trimaran ship introduced in Chapter 5 have provided an unusually extensive data set for examination. The trials were conducted with a number of ship displacements, in a number of loading conditions, at various speeds, and at with a full set

of headings relative to the waves given by the 'star' pattern as given in Chapter 3. Many of the star patterns were repeated so that the whole data set covers a wide range of sea states, and furthermore nearly all the trials were made in the vicinity of a waverider buoy providing a reliable measure of the seaway characteristics. Table 8.1 summarises the range of data used in this study.

8.2.1 Preliminary calculations

The first linear regression fit was to all 236 runs making up the 'star' trajectories summarised in Table 8.1, irrespective of the differences due to speed, relative heading, stabilisation etc. The runs were between 14 and 56 minutes duration. With such a wide range of variation in responses, a regression model giving an accurate calculation of the underlying significant wave height is not likely. However, it is useful to describe the process because an identical method has been used later on when presenting results for which the full data set was divided into more sensible subsets e.g. all runs in head seas only.

Figure 8.1 shows the RMS motion responses (strictly standard deviation σ rather than RMS) measured on the ship for each run, plotted against the mean significant wave height recorded by the waverider buoy for the star (the heights given in Table 8.1). The right hand set of graphs repeat the results of the left hand set of graphs, but with the axes reversed so the RMS responses appear rather unnaturally on the X-axes.

A linear regression fit to these graphs gives a rudimentary formula for significant wave height given the ship motion. Of course, there is a great deal of scatter in these results as a large number of ship conditions are covered, and errors of over 100% are possible if any one of these formulae were used alone.

The motions roll and pitch were used, and vertical, longitudinal and transverse accelerations measured near the ship centre of gravity.

Yaw motions were not used, as these are likely to be strongly affected by the rudder and autopilot characteristics of the ship. Yaw is also more difficult to report 'live' at the bridge as it is typically derived from compass heading; this channel is subject to effectively large jumps in magnitude at the boundary between 0° and 360°. Any system calculating the RMS yaw based on a few minutes of data must take account of this subtlety.

The accelerations reported are not platform stabilised, and therefore contain components due to the angular motion of the ship e.g. roll will affect the measured transverse acceleration. With high angular motions, these accelerations will be significantly different from the orthogonal, earth referenced axes usually predicted by ship motion software. For the purposes of this work this refinement is not relevant because it is being attempted to predict the seaway characteristics from the output of the instruments *as recorded* rather than as notionally desired.

The results reported here strictly apply only to the instruments installed on the trimaran demonstrator ship though one would expect similar conclusions to be drawn for any ship. For the rest of this section, the motions are therefore referred to by their channel name on the trimaran ship data instrumentation system as follows:

- ROLL Average roll angle measured by three instruments where available, *ROLLHMP Humphrey gyro unit, WATROLL Watson unit, AGPSROLL, Attitude GPS instrument.*
- PITCH Average pitch angle *ditto for {PITCHMP, WATPITC, AGPSPITC}*
- CGVACC vertical acceleration *measured by Colombia instrument at nominal CG*
- CGLACC Longitudinal (Forward) acceleration *ditto*
- CGTACC Transverse acceleration *ditto*

A multiple linear regression was performed using all 5 channels simultaneously, using the LINEST function in Microsoft Excel. The option of forcing the regression to zero at the origin was selected (since zero wave height should result in zero motion). The statistics reported by Excel are shown in Table 8.2 and standard statistical tests may be applied to these results. The F values suggest that the relationship between significant wave height and the five motion channels is not by chance, since F=23 is greater than the critical F

value of 3.34 at the 1% level for example. Also Student's T test suggests that all five channels make a significant contribution to the overall regression since the observed T values (standard error in m / m) are all greater than the critical value of 2.5 at the 1% level.

Table 8.2 suggests that, for the trimaran ship, at any time the significant wave height might be predicted by (to two significant figures):

$$H_{1/3} = 1.6\,\sigma_{PITCH} - 0.31\,\sigma_{ROLL} - 83\,\sigma_{CGLACC} + 39\,\sigma_{CGTACC} + 14\,\sigma_{CGVACC} \qquad \ldots(8.1)$$

with $H_{1/3}$ in metres, angles in degrees and acceleration units of g.

The results of calculation of the significant wave height in this way for each of the source data runs are plotted on Figure 8.2 against the significant wave height measured by the waverider buoy, together with results using for the individual motion channels. With perfect correlation the data would appear on a straight diagonal line on this figure.

As suggested above, there is a great deal of scatter in this data as the set covers all the variables such as ship heading and condition. Using a multiple regression technique, there is a strong improvement on the significant height predicted by the individual ship motions, and despite the range of variables present, the significant height is still given with an error of around ±45% (indicated by the straight lines about the diagonal on Figure 8.2).

8.2.2 Refinement of calculations

The regression fits obtained above would obviously be improved by splitting up the data into groups reflecting the individual conditions tested: stabilised or unstabilised, 5, 13 or 18 knots, one of 6 ballast conditions, and by heading. Potentially, a regression fit might be made for all of these individual cases. This would still be a difficult undertaking even with the large amount of trials data available here. Firstly, between one and three stars only were made in each one of the speed/stabilisation/ballast conditions, so that even for

these extensive trials it would be difficult to draw reliable statistics for the individual cases. Secondly, this would rather defeat the object of drawing general expressions for the significant height without relying on a large number of variables or test conditions.

The data have therefore been split into groups for comparison with the results of the global data given above, to illustrate which boundaries are sensitive and must be preserved and which are insensitive and where generalisations might be made. The results are summarised in Tables 8.3 to 8.7. Each line of these tables report the slice of data tested, the regression correlation coefficient, approximate percentage error, and the best fit line coefficients (the top line of regression statistics similar to Table 8.2).

Table 8.3 shows the effect of separating the data by speed, for comparison with the global data on the top line. The 18 knots data shows an improved correlation coefficient and reduced uncertainty, the 13 knots data shows a worse correlation coefficient and marginally improved error, and the 5 knots data a negative correlation coefficient but much improved per cent error. The separation of the 5 knots data is flawed because the 26 runs represent only two stars, and both were performed in seaways of very similar seaway, and this is responsible for the negative correlation coefficient – a constant significant wave height would be the best fit to this limited data set. The results for 13 and 18 knots are likely to be related to relative heading and stabilisation effects rather than speed *per se*: the 13 knot data has a lot of scatter as this contains both stabilised and unstabilised data. At 18 knots, the ship is naturally more dynamically stable, and might be regarded as effectively stabilised at all times. The speed would also serve to even out the effects of heading relative to the waves, compared with the 13 knots case, so there is less scatter, and more consistent motion results. The global data is in effect the average of the 13 and 18 knot data, hence it has an intermediate correlation coefficient.

Table 8.4, separating results of stabilised and unstabilised data directly, interestingly shows improved correlation and uncertainty compared with the global data, for the unstabilised slice of data rather than the stabilised set. Perhaps generally increased lateral plane motions are a good indicator of the seaway, and the regression fit can successfully place more weight on these motions? Comparing the changes in the forward and vertical acceleration coefficients, and the roll and lateral acceleration coefficients compared with

the global data, the largest changes are actually with the vertical plane motions. The converse therefore appears to be true, the generally larger lateral plane motions can more effectively be ignored by the regression fit and greater weight placed on the vertical plane motions.

The effect of ship ballast condition is considered with reference to Table 8.5. The data is separated into a 'datum' – typical ship condition, 'heavy' – about 6% heavier, and '2sRP', a condition with much increased roll period achieved with a great deal of ballast placed high in the ship. The '2sRP' data shows the same flaw as the 5 knots data above, the runs were performed in very similar sea states and hence the negative correlation coefficient. The heavy condition results are more successful than the datum and global data, but this is hard to explain. The number of runs contributing to the data set is rather less for the heavy condition, perhaps by chance the seaways were more long crested and the ship responses were more linear in general. The biggest change in the regression coefficients is for the lateral plane motions, perhaps a similar effect as suggested for the stabilised/unstabilised data suggested above can take place.

The heading relative to the waves should rather obviously have an effect on the success of the regression fits, as vertical plane motions dominate in head and following seas, whereas the lateral plane motions will dominate in beam and quartering seas. Given the clear effect of stabilisation on this technique, Table 8.6 and Table 8.7 give results separating the global data into groups by nominal relative heading to the waves and by stabilisation.

There is a large improvement in the significant wave height prediction, with the uncertainty in $H_{1/3}$ reducing from 45% for the global data to around 17% on average for the unstabilised data and around 23% for the stabilised data.

To help clarify the data in Table 8.6 and Table 8.7, example results are shown in Figures 8.3 and 8.4. Numerically, these results are:

For head seas, unstabilised, with uncertainty of 16%

$$H_{1/3} = 0.55\ \sigma_{PITCH} + 0.59\ \sigma_{ROLL} - 32\ \sigma_{CGLACC} - 4.9\ \sigma_{CGTACC} + 31\ \sigma_{CGVACC} \quad \ldots(8.2)$$

For head seas, stabilised, with uncertainty of ±19%

$$H_{1/3} = 2.3\ \sigma_{PITCH} - 0.48\ \sigma_{ROLL} - 19\ \sigma_{CGLACC} + 56\ \sigma_{CGTACC} - 13\ \sigma_{CGVACC} \quad \ldots(8.3)$$

8.3 Assessment of heading relative to waves

The results above suggest that $H_{1/3}$ can be estimated within around 20% error using the RMS ship motions and the ship heading relative to the waves. The RMS motions can be measured directly, but with the exception of shipboard wave radar systems, the relative heading cannot be measured with instruments directly. In the daytime, the relative heading can be estimated visually, but this would defeat the desire for an automatic system requiring no human input.

There is often a strong correlation between the wind direction (which is universally measured onboard ship) and the principal wave direction but this is not always the case. This section explores whether the relative wave direction might be determined from the same ship motion data channels as for the previous analysis.

Figure 8.5 shows the relationships between each of the five RMS rigid body motions and the nominal relative heading; this is same data as in section 8.2.1.1, covering a wide range of sea states, ship speeds, loading conditions, and stabilisation for the trimaran ship. The spots represent trials data and the line, a quartic fit, is included to show the trend.

For a good identification of relative heading, high weight should be placed on those motions showing a narrow spread of data at any heading, and with a one to one relationship between the motion and heading. Longitudinal acceleration meets these requirements at the following seas 'end' of the scale, but less successfully at the head seas end where the data has a large spread and the spread for 150 degrees and 180

degrees is similar. Additionally it can be seen that RMS longitudinal acceleration of 0.005g could potentially arise from any relative heading.

Figure 8.5 demonstrates that roll and pitch are less good to identify the relative heading. The data shows both a wide spread e.g. RMS roll of 1.5-3 degrees possible at any heading, and a many to one relationship with relative heading shown by the trend lines having a peak or trough. Even if the data was less well spread, similar roll and pitch levels can be expected at both 90° and 30° headings - which would be correct?

Several different combinations of RMS motions and functions of the RMS motions were plotted against the nominal relative heading from the trials to find a better indicator, and these are shown in Figure 8.6. Roll/Pitch did not give a one-to-one trend. CGVACC*CGLACC/CGTACC showed little spread of values in following seas, and Ln(CGVACC*CGLACC/CGTACC) showed a nearly linear trend. CGTACC/CGVACC and CGTACC/CGLACC showed some promise but largely due to the vertical plane CGVACC and CGLACC rather than the lateral plane CGTACC. The combination finally chosen was CGVACC*CGLACC as shown in the bottom right hand graph of Figure 8.6.

At first sight, logarithmic functions of the RMS motions giving relative heading are the best fit to the data, however in practice it was found that for a logarithmic function only very small RMS motion differences covered the range of headings 0°-60°, and 0° was hardly ever identified correctly. So the relationship

$$\Psi_r = 146881\ (\sigma_{CGLACC} \cdot \sigma_{CGVACC}) \qquad \ldots(8.4)$$

was adopted for indication of the relative heading, derived on Figure 8.6. Detection of relative heading prediction greater than 180° or less than 0° degrees is necessary:

$$\begin{aligned} \psi_r &\xrightarrow{\psi_r < 0} 0 \\ \psi_r &\xrightarrow{\psi_r > 180} 180 \\ \psi_r &\xrightarrow{0 < \psi_r < 180} \psi_r \end{aligned} \qquad \ldots(8.5)$$

and the result must be rounded for use with the tables derived in 8.4. to give Ψ_r in multiples of 30°:

Ψ_r=ROUND(Ψ_r/30,0)*30 in Excel terminology ...(8.6)

or equivalently

Ψ_r=NINT(Ψ_r/30)*30 in FORTRAN ...(8.7)

The next section shows the results of applying this technique to assess the relative heading and then making significant height calculation by applying the appropriate equation from Table 8.6 and Table 8.7.

8.4 Demonstration of wave height calculation with 'blind' data

The sections above gave the elements required to evaluate the wave significant height for a particular ship at sea based on calculation of heading relative to the waves, and then application of a formula to give the significant height, based on the RMS ship motions only. In this section the technique is validated against a further three sets of data for the trimaran ship, representing three different sea states.

For these trials, the ship performed 'star' pattern trajectories in the ocean, but a wave measuring buoy was not present. The ship did have two radar systems operating, a MIROS Wavex wave radar and a TSK wave radar (see Chapter 2). In addition, at the start of each run, a visual estimate of the wave height was made by observing the motions of the ship mast at the stem, and of the wave length by comparing with the length of the ship. Visually reported wave heights are known to correspond with significant wave height. In this case the visually reported wave height was the wave *amplitude* rather than peak-peak height (and indeed significant wave height is also strictly an amplitude).

The computed significant wave height by the technique in this chapter is compared against these three sources, and in addition the significant wave height and direction derived directly from the wind recordings on the ship.

The derivation of significant height and direction from the wind recordings is as follows:

- Figure 8.7 and 8.8 show the relationship between significant wave height and modal period with the steady wind speed, for the North Atlantic [Bales et al. 1981]. The error bars show the 95% confidence data range given in Bales et al., and the curved lines represent a regression fit with error bands.

- The relationships required given by the best fit lines are:

  $H_{1/3} = 0.00730\ v^{1.82}$ (±40%) ...(8.8)

  $T_m = 0.00464\ v^2 + 0.153\ v + 5.78$ (±3.5s) ...(8.9)

- It was found that the instantaneous wind speed v is subject to a great deal of fluctuation and the so the speed actually used to derive $H_{1/3}$ and T_m is the mean over the previous 10 minutes.

Following on from the last point for the wind data, by the same token RMS motions must be calculated over some time period. The regression results were obtained by taking RMS motions over the entire length of runs that varied between 14 and 54 minutes. For this section, a nominal time period must also be taken over which to derive the RMS motions, and a time of (the preceding) 10 minutes has been selected. This means that there will effectively be a 'phase lag' of 10 minutes after every ship heading change before the consequences are fully utilised by the equations from which significant height is derived.

With the historical data reported here, it would have been possible to use RMS statistics over a 10 minute period starting 5 minutes before the each time step and ending 5 minutes after, thus reducing the lag effect (but introducing a phase lead effect at the end of the run). RMS over the previous 10 minutes was retained, as this is the data available for any 'live' onboard ship advisory system.

The RMS motion derived relative heading data is given in Figure 8.9 (black lines). This is compared with the trial nominal headings (dashed lines) converted to the range 0°-180°, and with the relative wind direction (grey lines), also converted to the range 0°-180°.

In the first and third parts of Figure 8.9, the determination of relative heading is clearly working well compared with the nominal relative heading. The phase lag effect predicted above is evident, but otherwise the relative headings are typically within 30° of each other. There is also a strong correlation with the relative wind direction in the third part of the figure, but less so with the first part.

The second part of the Figure 8.9 is evidently much less successful and there is little agreement with the nominal relative heading. The vertical accelerations throughout this star pattern were rather low, and hence (bottom right part of Figure 8.6) only relative headings between 0° and 30° were predicted.

Figure 8.10 compares the motion derived significant wave height (black line with error bars), with the visual estimate (black zigzag line), the wind derived $H_{1/3}$ (red line) and $H_{1/3}$ from the Wavex and TSK radar systems (green and blue lines respectively).

For these data sets no one measurement of significant height may be regarded as definitive. The visual estimate is likely to be reasonably good, but was only made at the start of each 6 hour star. On previous trials involving a waverider buoy, the TSK radar was found only to give good readings on headings with low roll motions, effectively meaning that the hourly minima are likely to be correct. Similarly, the Wavex system was found to give good readings above $H_{1/3}$~3.5m, but could be erratic otherwise e.g. the second part of Figure 8.10 for star 16.

The motion derived significant wave height does appear to agree at least as well as the radar results with the visually estimated wave height, and more consistently than the TSK and Wavex radar systems. The first part of Figure 8.10 shows some drop away of the derived significant height from the general trend, but otherwise the results are at a consistent level and with just a few a small discontinuities. Even the second part of

Figure 8.10, where the corresponding part of Figure 8.9 was poorly predicted, shows a good result. Perhaps the analysis in section 8.3 which separated the source data by relative heading might be recast to actually separate it by the vertical motion magnitude – and this may be why for this star, with low vertical magnitude and derived relative headings all between 0° and 30°, the predicted significant height is still good.

8.5 Further possible improvements

8.5.1 Angular Motions

The underlying philosophy behind the statistical approach demonstrated in this chapter is that there is a linear relationship between each motion and the significant wave height of the seaway causing the motions. This is assumed for the rigid body displacements (and hence accelerations) in ship theory, but angular motions are usually assumed proportional to wave slope rather than wave height. For the purposes of this study, the following digression shows that linearity nevertheless is a reasonable model within the error bands of sea statistics and the desired accuracy of the significant wave height from ship motions calculation, but suggests possible improvement.

The previous section introduced Figures 8.7 and 8.8, showing quadratic fits to annualised wave data for the North Atlantic [Bales et al. 1981], where significant wave height and modal period respectively were related to the sustained wind speed. The same reference has also been used to give Figure 8.11 relating significant wave height and wave modal period directly (the error bars show the 95% confidence ranges), and Figure 8.12 showing significant height against the derived wave slope amplitude (at the significant wave height).

For the ship angular motions, the previous analysis has been based on proportionality with the significant wave height – essentially the straight line drawn in grey on Figure 8.12. Clearly a curved line like the dashed grey line in that figure is an improvement.

The wave slope amplitude [Lloyd (1998)] is

$$\alpha_0 = \frac{\pi H}{\lambda} \qquad \ldots(8.10)$$

and in deep water, the wavelength tends to

$$\lambda = \frac{g T^2}{2\pi} \qquad \ldots(8.11)$$

and so

$$\alpha_0 \propto \frac{H}{T^2} \qquad \ldots(8.12)$$

The wave slope amplitude is strongly dependent on the relationship between H and T.

The Pierson-Moskowitz relationship introduced in Chapter 2 relates the significant wave height with the modal frequency:

$$H_{1/3} = \frac{0.1962^2}{f_m{}^2} \qquad \ldots(8.13)$$

so equating H with $H_{1/3}$ and T with T_m the wave slope amplitude of the significant waves in any fully developed seas state would be:

$$\alpha_0 \propto \frac{H_{1/3}}{T_m{}^2} = constant \qquad \ldots(8.14)$$

This constant wave slope has a value 0.08 rad and is plotted as the dotted vertical line on Figure 8.12. This figure gives only the slope of the significant waves, and the extension of Equation 8.14 to other (more commonly less steep) waves is not clear. However, Figure 8.12 does show that constant wave slope as derived in Equation 8.14 is not a good model.

An alternative fit to the Bales et al. (1981) data has been derived, a cubic

$$400 H_{1/3} = T^3 \qquad \ldots(8.15)$$

and this is shown as the dotted line on Figure 8.11. This is apparently a better fit to the north Atlantic data, than the Pierson-Moskowitz relationship in Equation 8.13, passing

more closely to the data points. Equating for wave slope amplitude as above, again taking H to be the significant wave height, leads to the expression:

$$\alpha_0 = \frac{2\pi^2 (400)^{-2/3} H^{1/3}}{g} \approx 0.0371 H^{1/3} \quad \ldots(8.16)$$

$$\Rightarrow \alpha_0^3 \propto H \quad \ldots(8.17)$$

Since the angular motions are considered linearly related to the wave slope amplitude, regression fits for significant wave height given RMS ship motions might therefore be improved by considering the cubes of roll and pitch motions, i.e. an expression of the form

$$H_{1/3} = k_1 \sigma(\text{PITCH}^3) + k_2 \sigma(\text{ROLL}^3) + k_3 \sigma_{\text{CGLACC}} + k_4 \sigma_{\text{CGTACC}} + k_5 \sigma_{\text{CGVACC}} \quad \ldots(8.18)$$

8.5.2 Wind

The strong relation between steady wind speed and significant wave height demonstrated in Figure 8.7 might also be included as an extra parameter. A polynomial regression fit to the data of Figure 8.7 is:

$$H_{1/3} = 0.0032 \overline{\text{VWIND}}^2 \quad \ldots(8.19)$$

(with VWIND the wind speed in knots, and the bar indicating a ten minute average). This could be used to estimate $H_{1/3}$ alone, or the quadratic relationship used to improve the estimate of $H_{1/3}$ including the other motions so that

$$H_{1/3} = k_1 \sigma(\text{PITCH}^3) + k_2 \sigma(\text{ROLL}^3) + k_3 \sigma_{\text{CGLACC}} + k_4 \sigma_{\text{CGTACC}} + k_5 \sigma_{\text{CGVACC}} + k_6 \overline{\text{VWIND}}^2 \quad \ldots(8.20)$$

8.5.3 Motion Periods

Further improvement in the relative heading estimate might be made by also considering the data periodicity – the motions have long periods in following seas and short periods

in head seas. Pitch and roll rate are usually measured directly (most gyros actually measure rates and integrate once to give angles) and are present for the trimaran data set used in this chapter. The periods might be derived from time domain analysis e.g. counting of zero crossings, or frequency domain analysis e.g. finding frequencies with most energy. Alternatively or additionally, Lloyd (1998) also shows that the motion periods can be derived from the statistical moments m_0,m_2,m_4 without recourse to the time or frequency domain analysis.

8.5.4 Wave data simplification

The data set used here also has rather a coarse description of $H_{1/3}$ from the waverider buoy. For the purposes of the study here, only a single representative $H_{1/3}$ was used for each star trajectory series of runs. Waverider data was sampled typically every half hour, so potentially every single run within the star might be assigned an interpolated $H_{1/3}$ value, rather than setting $H_{1/3}$ identically for all 13 runs of the star.

8.6 Summary

The availability of an extensive set of trials data for a particular ship with concurrent waverider buoy results has enabled a broad scope statistical analysis considering the relationship between the wave height seen by the ship and its motions. The statistics have been considered with the aim of producing an accurate but easy to derive formula for the significant wave height given just the RMS motions of the ship.

With no separation of the data at all into groups of similar speed, relative heading, displacement etc., it was shown that the significant wave height could be predicted with a 45% error. This is certainly not a small error, but probably better than would be estimated visually in darkness.

The data was then considered in large groups, and it was shown that separation into groups by relative heading and stabilisation mode only was enough to give significant wave height predictions accurate to around 10%-20%. The significant wave height is calculated purely

from the RMS motions of the ship, with weightings determined by a multiple linear regression. It is shown that the ship heading relative to the waves can be successfully derived purely from the RMS motions surge acceleration and vertical acceleration. Several ways in which the results might be improved further are also suggested.

The results were successfully applied to 'blind' data for the ship, where the significant wave height was not measured by waverider buoy. The method gave consistent results and over the three test trials and was at least as good as propietry radar systems.

Though derived for a particular ship, these methods have general application to different ships. It is required to conduct trials to effectively calibrate the ship motions against a trustworthy wave data source such as a waverider buoy, and for the best results the trials should cover a wide range of sea states including very high sea states. Of course, this is not always feasible, but it might be possible to supplement the full-scale trials motion data with ship motion software derived data results, if there is a great deal of confidence in the code, or with physical model test results.

The ultimate application of these techniques would be in a shipboard advisory system. These depend on an accurate estimation of the current sea conditions, and the approach of deriving formulae for significant wave height and heading relative to the waves presented in this chapter could be performed 'live' quickly and automatically.

This chapter has largely ignored the major theme of this thesis, the effect of directionality of wave in terms of spreading and multiple wave systems. Nevertheless, this work does have a strong relevance. This is a robust method for significant wave height and wave direction, and can be seen as a building block with which a more detailed model of the seaway, including complexities like spreading function, might be built up. Alternatively, these statistically derived results might act as a 'sanity check' for more complicated directional sea spectrum methods, like that presented in the next chapter, where there is more scope for unrealistic - but mathematically possible - results to be arrived at.

Star	Date	Loading Condition	Speed	Stabilised	$H_{1/3}$
-	dd/mm/yy	-	Knots	-	M
1	15/01/2001	Datum	13	Yes	2.40
5	16/01/2001	Datum	13	Yes	1.90
6	22/01/2001	Datum	13	Yes	3.30
8	24/01/2001	Datum	18	Yes	2.50
9	25/01/2001	Datum	18	No	2.75
10	25/01/2001	Datum	18	Yes	2.50
12	31/03/2001	+2 secs RP	13	Yes	3.50
13	01/04/2001	+2 secs RP	5	No	2.55
16	06/04/2001	+2 secs RP	13	No	2.50
17	07/04/2001	+2 secs RP	18	Yes	3.90
21	01/12/2001	Heavy	13	Yes	3.50
22	01/12/2001	Heavy	13	No	3.15
23	01/12/2001	Heavy	5	No	3.05
24	02/12/2001	Heavy	18	Yes	2.40
25	02/12/2001	Heavy	18	No	2.25
26	03/12/2001	Datum	13	No	4.70
27	04/12/2001	Datum	18	No	4.45
28	04/12/2001	Datum	13	Yes	4.05
29	05/12/2001	Heavy	18	No	3.65
30	17/12/2001	Datum	18	Yes	3.10
31	17/12/2001	Datum	5	No	3.00
32	18/12/2001	Empty	13	No	3.25

Table 8.1 Summary of data available for statistical analysis

	Pitch [deg]	Roll [deg]	Longitud Accel [g]	Lateral Accel [g]	Vertical Accel [g]	
M values, intercept c (set to zero)	1.593	-0.313	-83.458	39.294	14.412	0
Standard error in m	0.165	0.103	30.612	5.502	5.374	-
Coefficient of determination, standard error for H1/3	0.335	0.595	-	-	-	-
F value, degrees of freedom	22.955	228	-	-	-	-
Regression sum, residual	40.604	80.661	-	-	-	-

Table 8.2 Statistics of multiple linear regression for $H_{1/3}$ over five motions

								Multiple Regression Coefficients				
Tab name	Speeds	Headings	Stabilisation	Ship Condition	Number of trial runs	Correlation coefficient	Approximate Uncertainty	Pitch	Roll	Forward Accel	Lateral Accel	Vertical Accel
-	5 / 10 / 13 knots or All	0 / 30.../180 or All	Yes / No / Both	Datum / Heavy / 2sRP / all	-	-	[%]	[deg]	[deg]	[g]	[g]	[g]
reg-all-Hsig	All	All	Both	All	233	0.335	45	1.59	-0.31	-83.46	39.29	14.41
all-5kts	5	All	No	All	26	-78.404	17	1.67	0.97	70.25	-38.64	9.96
all-13kts	13	All	Both	All	103	0.129	40	1.84	-0.37	-118.11	41.01	15.23
all-18kts	18	All	Both	All	104	0.753	30	1.65	0.02	-38.20	31.79	3.30

Table 8.3 Effect of speed on regression statistics

								Multiple Regression Coefficients				
Tab name	Speeds	Headings	Stabilisation	Ship Condition	Number of trial runs	Correlation coefficient	Approximate Uncertainty	Pitch	Roll	Forward Accel	Lateral Accel	Vertical Accel
-	5 / 10 / 13 knots or All	0 / 30.../180 or All	Yes / No / Both	Datum / Heavy / 2sRP / all	-	-	[%]	[deg]	[deg]	[g]	[g]	[g]
reg-all-Hsig	All	All	Both	All	233	0.335	45	1.59	-0.31	-83.46	39.29	14.41
all-stab	All	All	Yes	All	128	0.128	45	1.73	-0.28	-89.48	39.04	11.68
all-unstab	All	All	No	All	104	0.505	30	1.57	-0.26	-103.77	33.45	21.58

Table 8.4 Effect of stabilisation on regression statistics

								Multiple Regression Coefficients				
Tab name	Speeds	Headings	Stabilisation	Ship Condition	Number of trial runs	Correlation coefficient	Approximate Uncertainty	Pitch	Roll	Forward Accel	Lateral Accel	Vertical Accel
-	5 / 10 / 13 knots or All	0 / 30.../180 or All	Yes / No / Both	Datum / Heavy / 2sRP / all	-	-	[%]	[deg]	[deg]	[g]	[g]	[g]
reg-all-Hsig	All	All	Both	All	233	0.335	45	1.59	-0.31	-83.46	39.29	14.41
all-heavy	All	All	Both	Heavy	78	0.642	20	1.72	-0.58	-171.51	52.45	27.80
all-2sRP	All	All	Both	2sRP	26	-3.067	21	0.86	-0.10	129.32	36.18	-1.45
all-datum	All	All	Both	datum	116	0.306	43	1.76	-0.31	-141.05	35.83	23.34

Table 8.5 Effect of ship condition on regression statistics

Motion-stats.xls								Multiple Regression Coefficients				
Tab name	Speeds	Headings	Stabilisation	Ship Condition	Number of trial runs	Correlation coefficient	Approximate Uncertainty	Pitch	Roll	Forward Accel	Lateral Accel	Vertical Accel
-	5 / 10 / 13 knots or All	0 / 30.../180 or All	Yes / No / Both	Datum / Heavy / 2sRP / all	-	-	[%]	[deg]	[deg]	[g]	[g]	[g]
0-stab	All	0	Yes	All	9	0.975	9	2.39	0.32	386.57	2.51	-47.27
30-stab	All	30	Yes	All	19	0.774	23	2.64	0.56	-147.43	-15.40	26.49
60-stab	All	60	Yes	All	18	0.736	17	0.36	-0.15	204.14	36.24	2.16
90-stab	All	90	Yes	All	19	0.393	25	1.19	-0.52	-235.59	35.48	55.16
120-stab	All	120	Yes	All	20	0.420	24	0.87	-1.99	-7.06	151.84	-22.54
150-stab	All	150	Yes	All	18	0.710	18	3.21	-0.67	-9.83	47.62	-26.92
180-stab	All	180	Yes	All	20	0.559	19	2.26	-0.48	-19.37	56.40	-13.06

Table 8.6 Regression statistics by heading, stabilised

								Multiple Regression Coefficients				
Tab name	Speeds	Headings	Stabilisation	Ship Condition	Number of trial runs	Correlation coefficient	Approximate Uncertainty	Pitch	Roll	Forward Accel	Lateral Accel	Vertical Accel
-	5 / 10 / 13 knots or All	0 / 30.../180 or All	Yes / No / Both	Datum / Heavy / 2sRP / all	-	-	[%]	[deg]	[deg]	[g]	[g]	[g]
0-uns	All	0	No	All	8	0.977	7	1.13	2.04	1049.12	-82.01	-94.74
30-uns	All	30	No	All	16	0.785	16	2.43	2.44	764.74	-107.30	-104.52
60-uns	All	60	No	All	16	0.745	20	2.07	-0.62	-218.07	25.16	77.01
90-uns	All	90	No	All	16	0.812	15	-0.15	1.22	-20.83	-43.75	44.01
120-uns	All	120	No	All	16	0.760	17	-1.10	0.55	138.80	2.95	21.12
150-uns	All	150	No	All	16	0.876	13	0.92	0.54	-132.83	-12.28	46.15
180-uns	All	180	No	All	17	0.843	16	0.55	0.59	-32.44	-4.88	31.44

Table 8.7 Regression statistics by heading, unstabilised

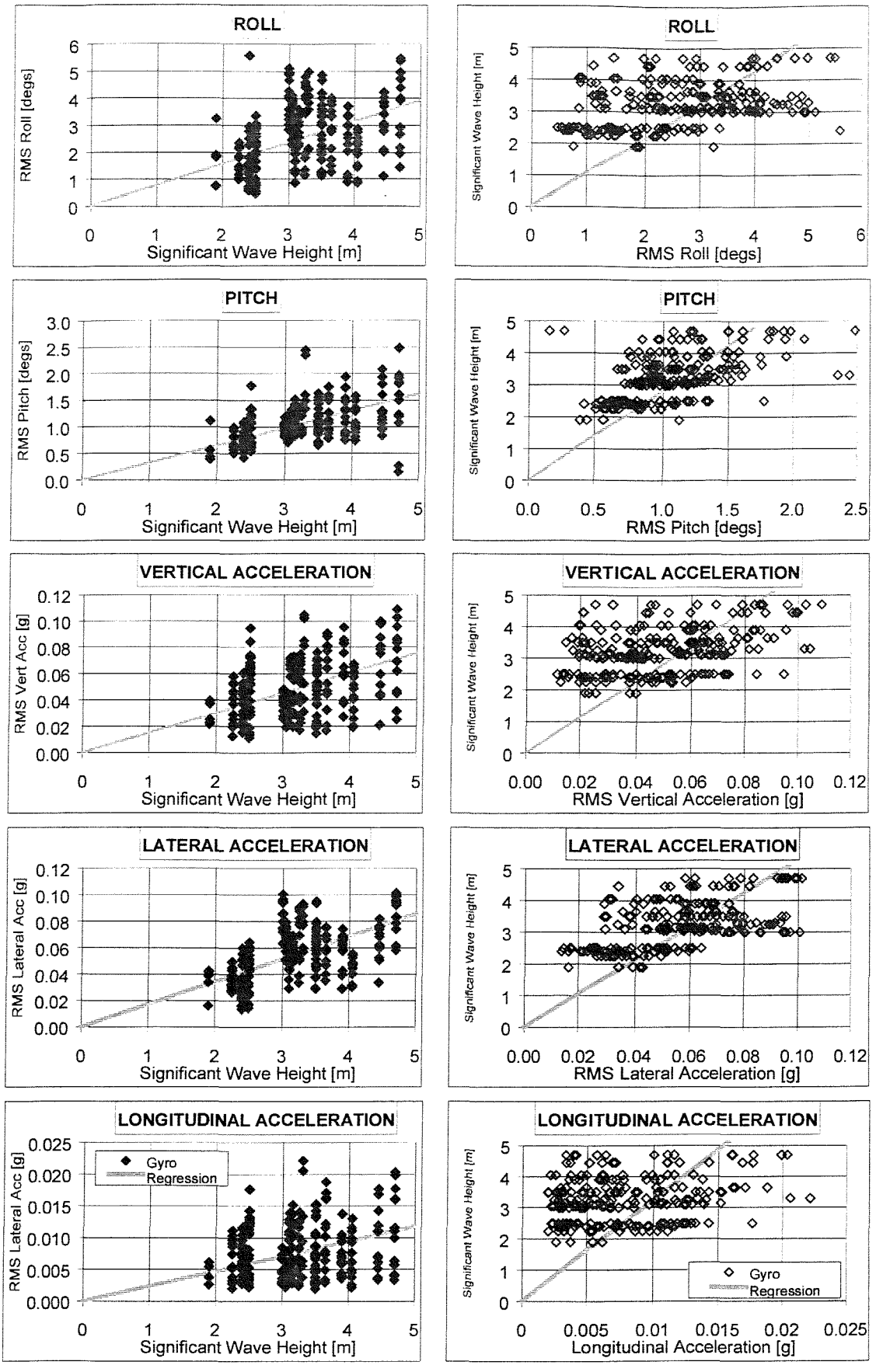

Figure 8.1 Regression results for ship motion channels

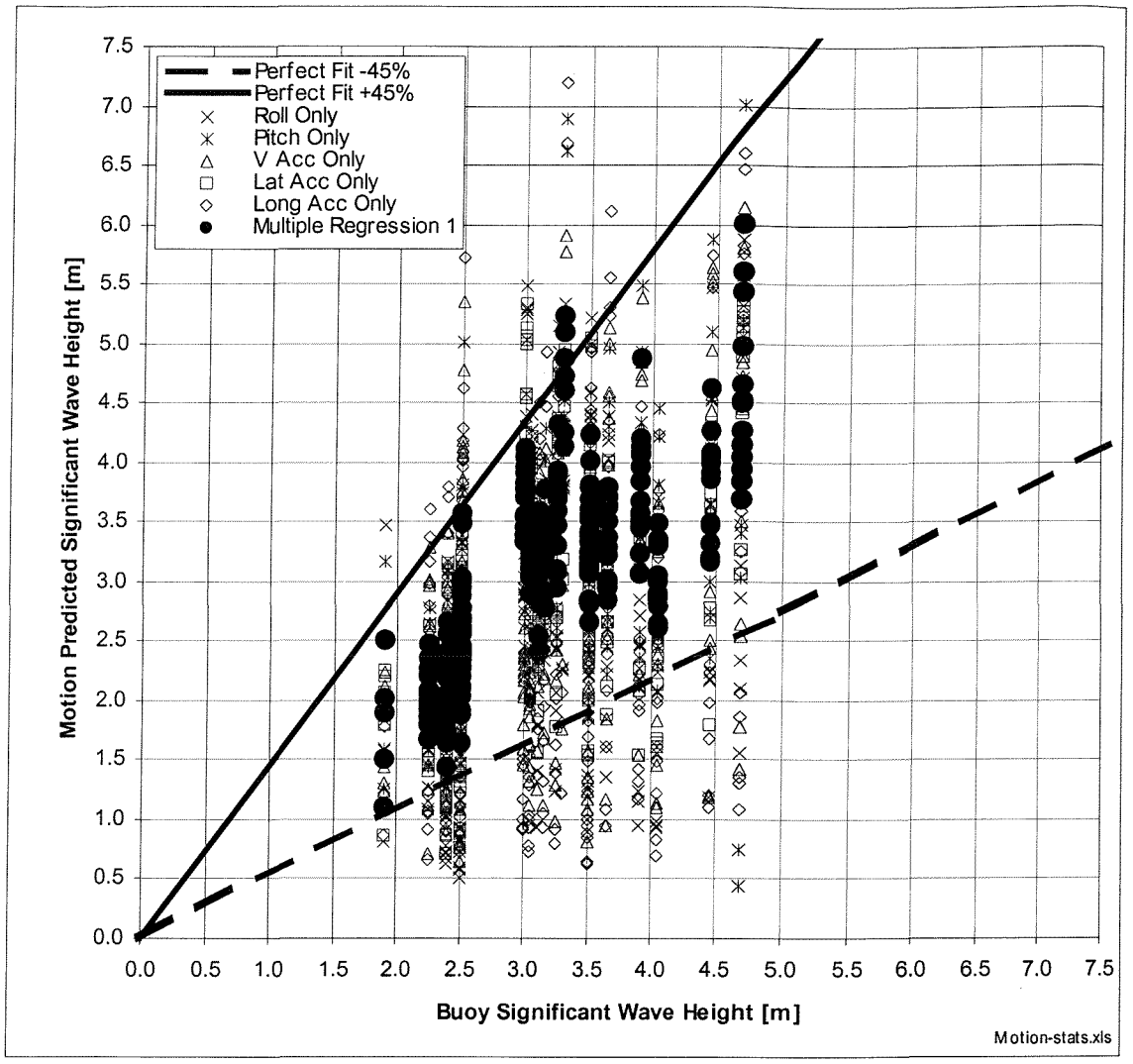

Figure 8.2 Linear regression using entire data set

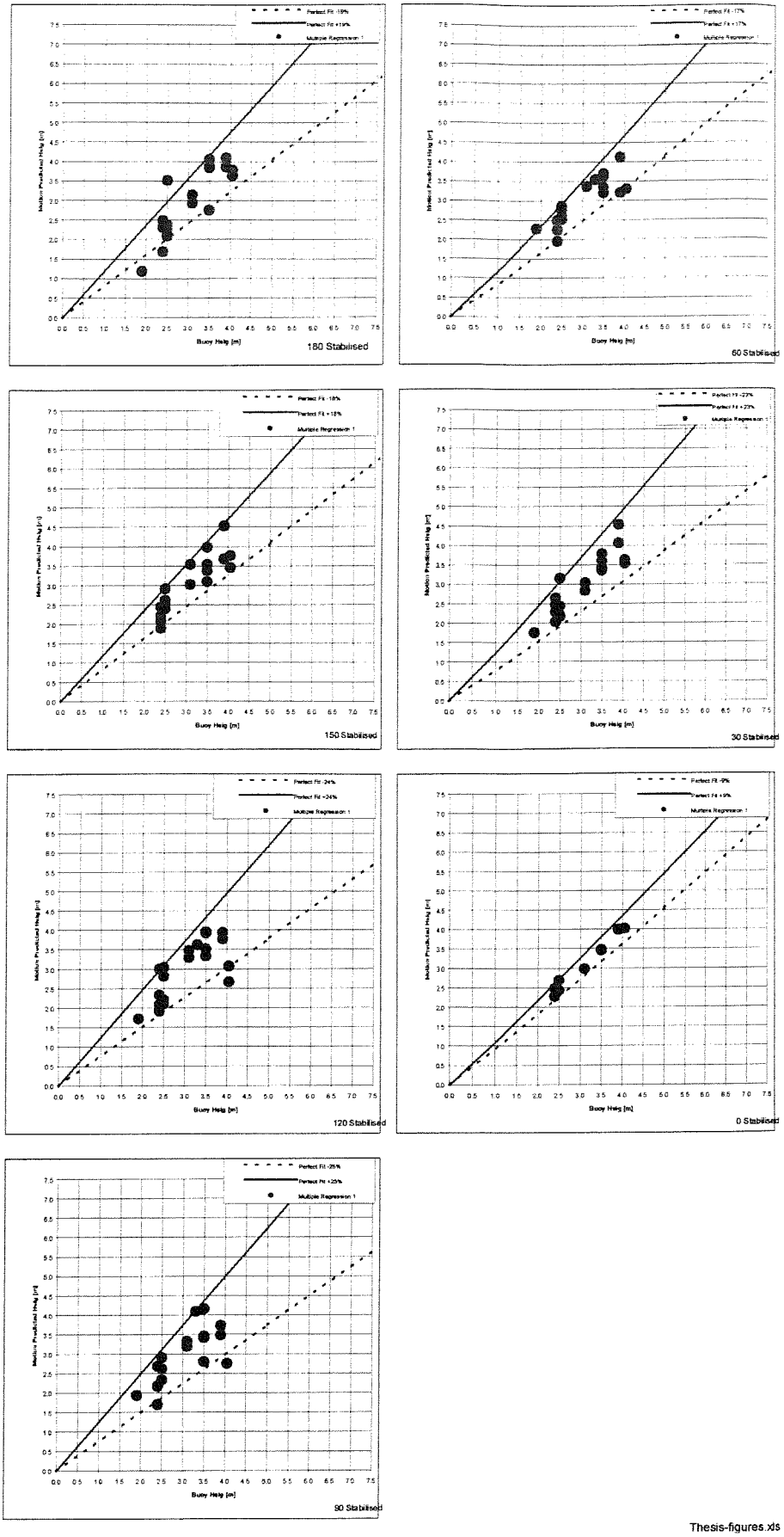

Figure 8.3 Regression results by heading - stabilised

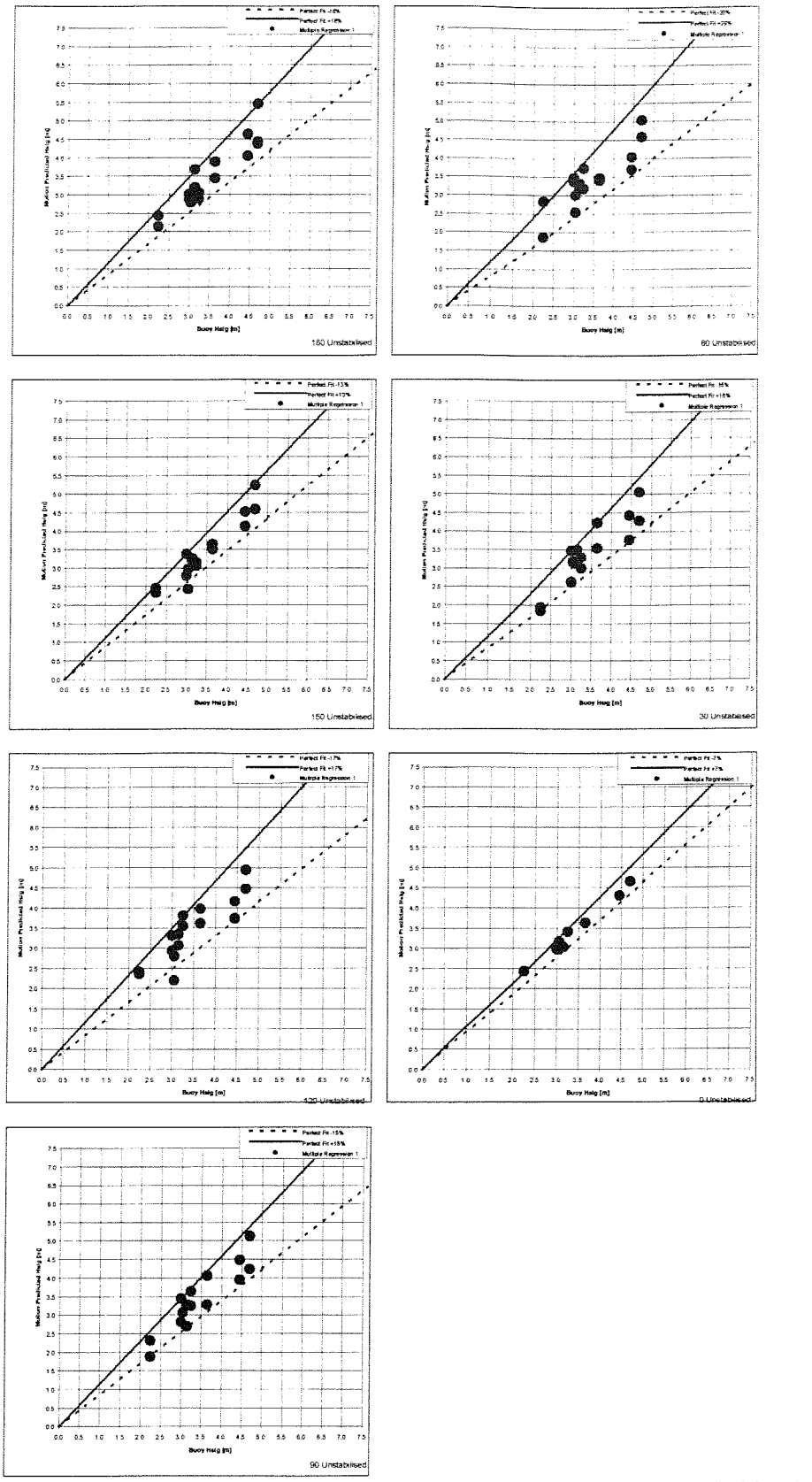

Thesis-figures.xls

Figure 8.4 Regression results by heading – unstabilised

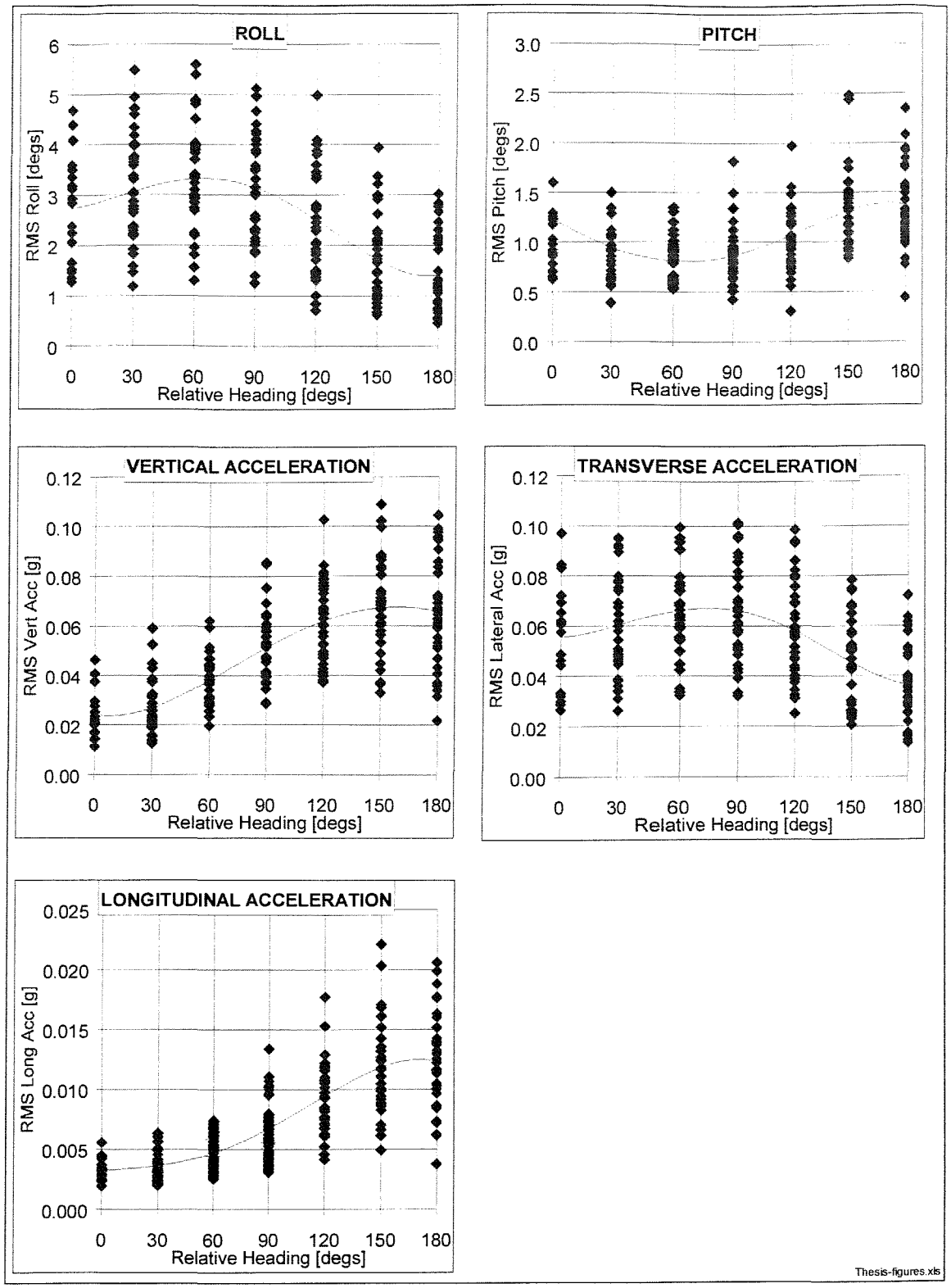

Figure 8.5 Relationship between principal motions and relative heading

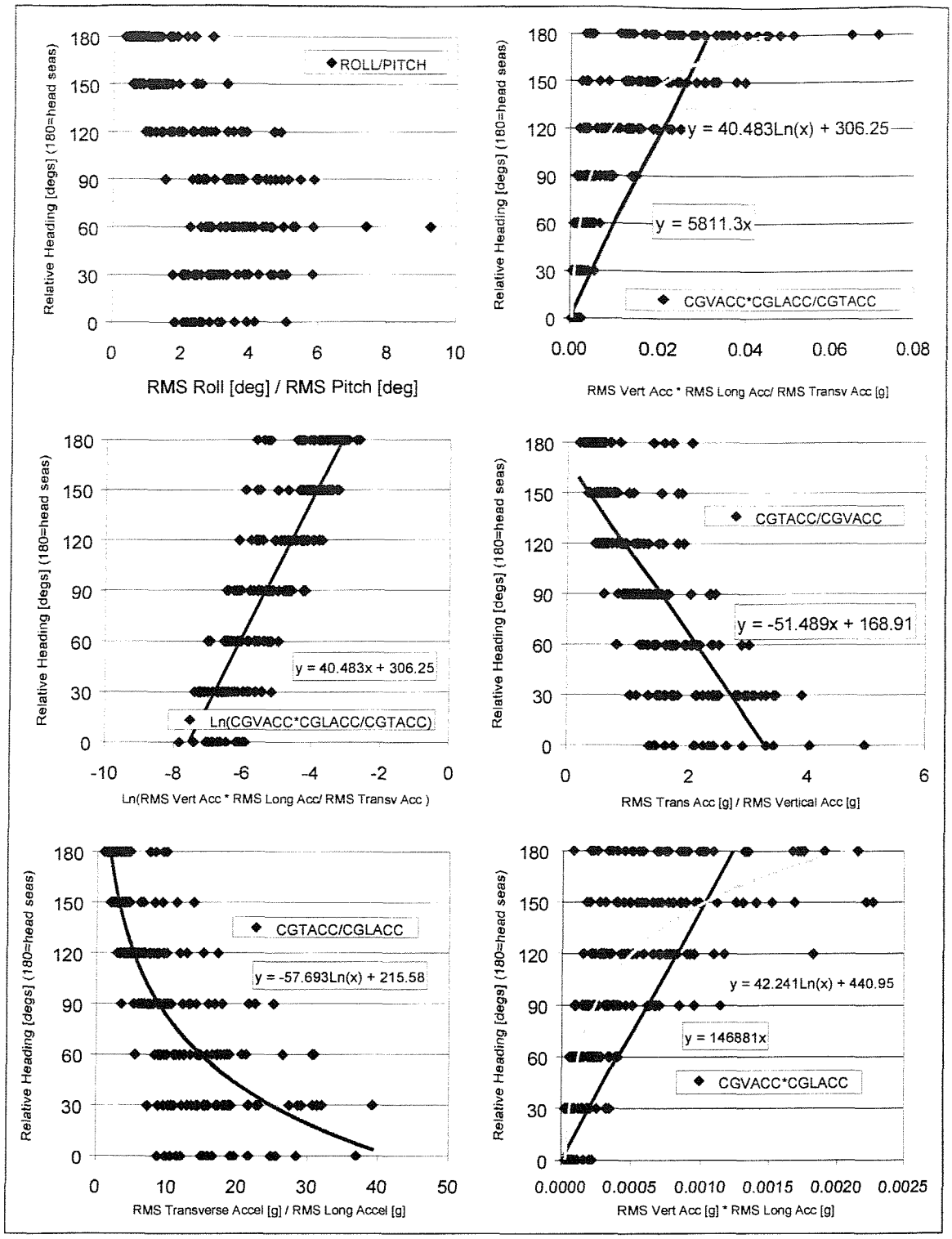

Figure 8.6 Relationship between combinations of principal motions and relative heading

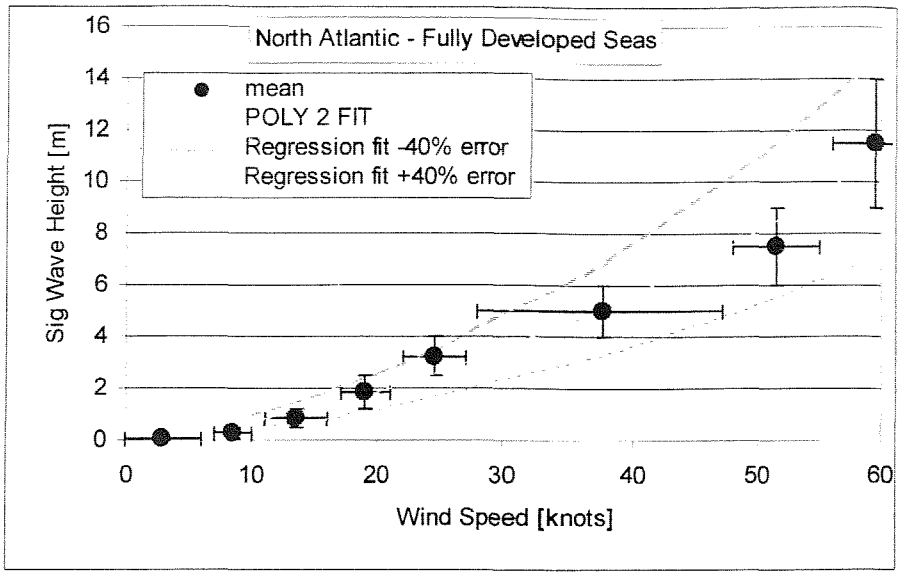

Figure 8.7 Regression fit to North Atlantic significant wave height data

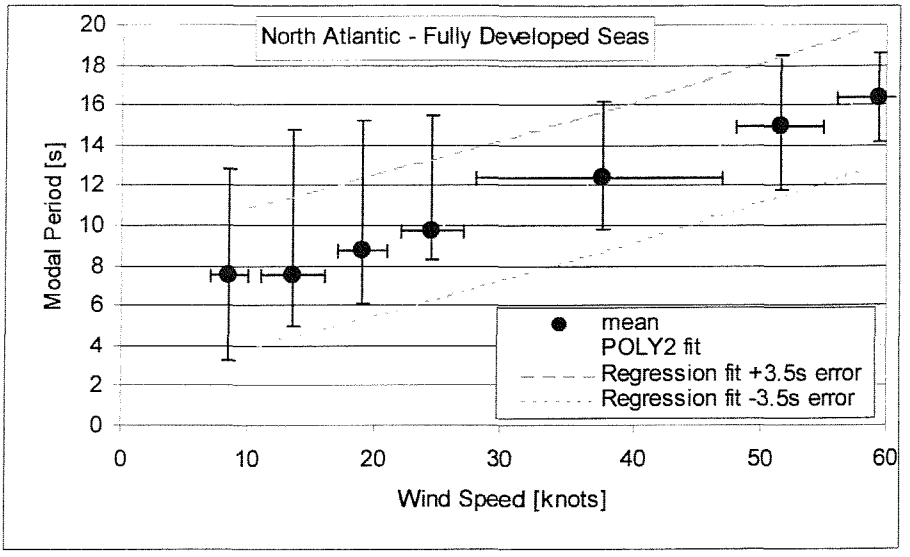

Figure 8.8 Regression fit to North Atlantic modal period data

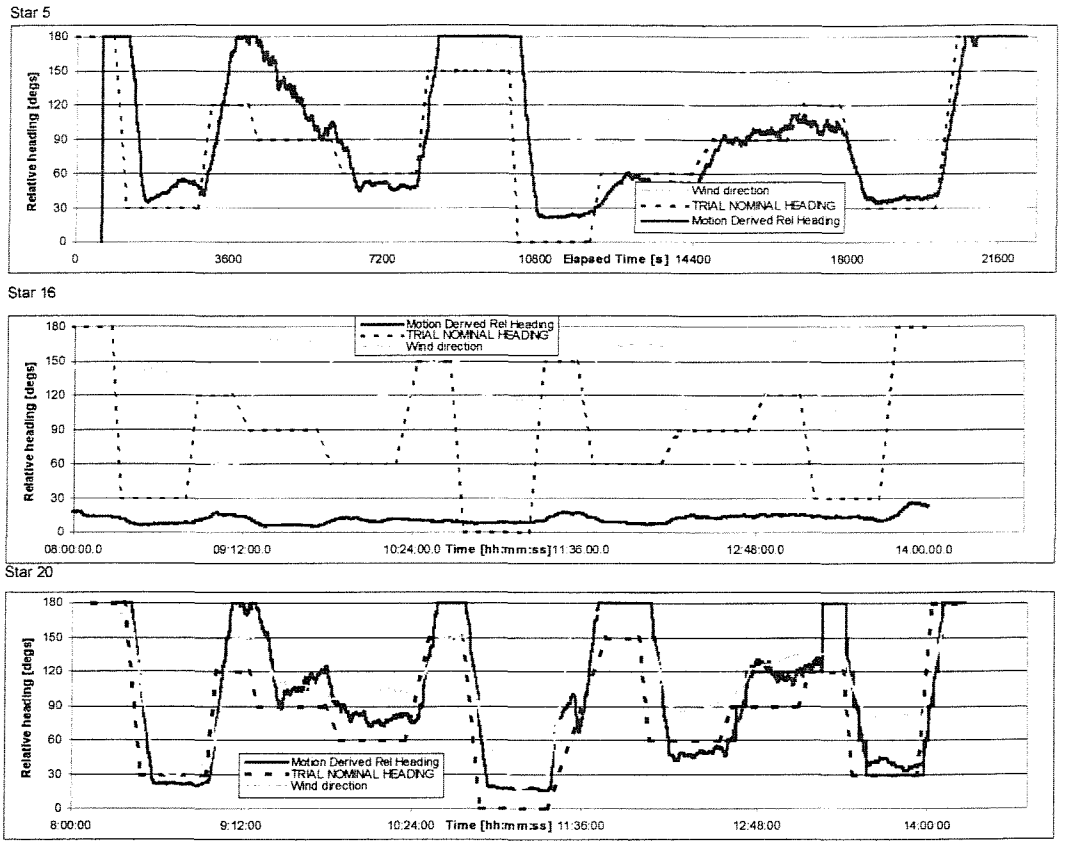

Figure 8.9 Results of relative heading evaluation with 'blind' data

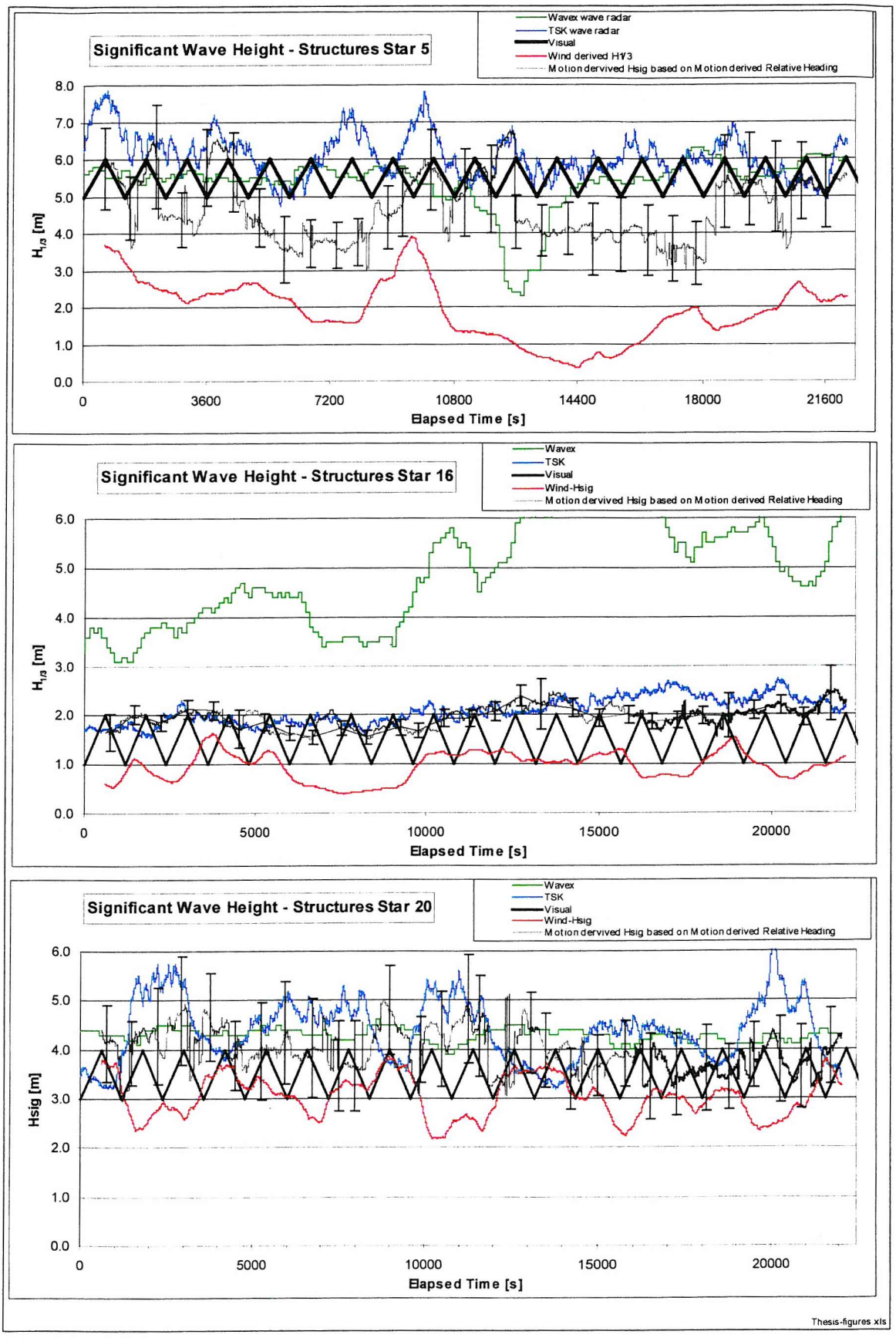

Figure 8.10 Results of significant wave height evaluation with 'blind' data

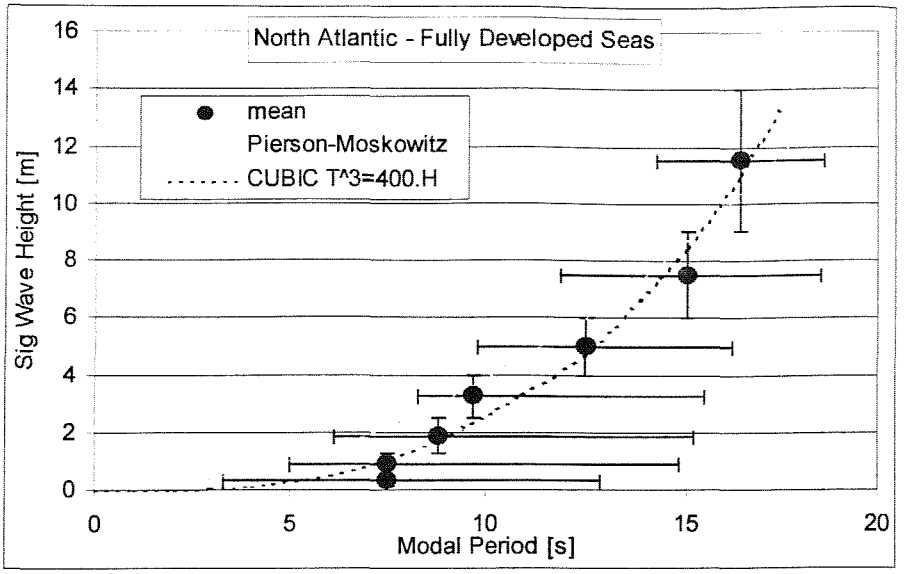

Figure 8.11 North Atlantic wave height and wave period data

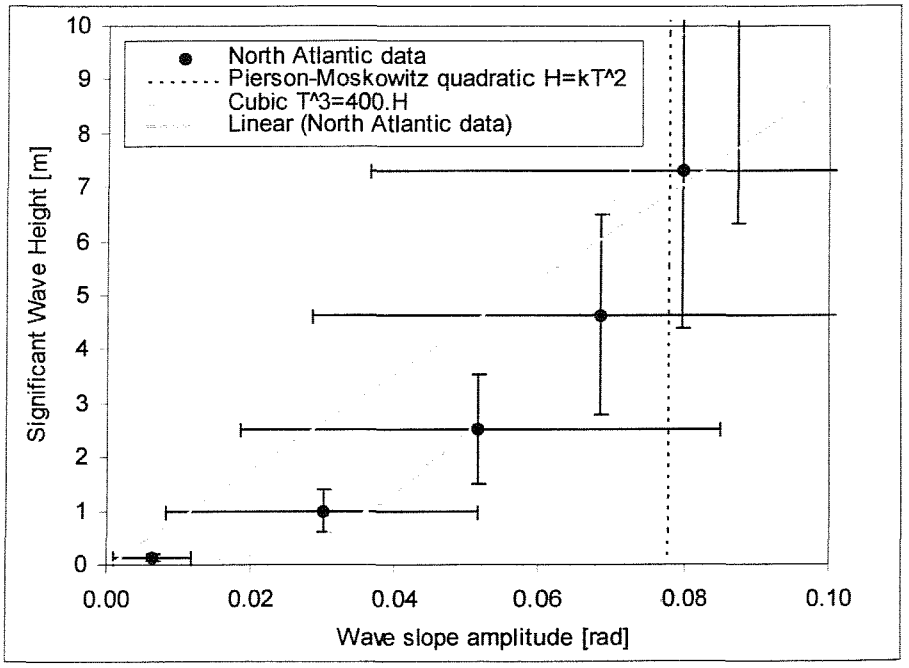

Figure 8.12 North Atlantic wave height and wave slope data

9. ESTIMATING SEA STATE FROM SHIP MOTIONS – MATRIX METHOD

9.1 Introduction

The introduction to Chapter 8 gave reasons why it is very desirable to know in detail the seaway a ship is operating in, and proceeded to demonstrate that information on wave height and principal wave direction can be gleaned from the statistics of the ship motions only. Though a robust method, these results do not give information on the spectral content of the seaway, its directional spreading, or advice on the number of wave systems present.

In this chapter, the matrix techniques developed in Chapter 7 for predicting transfer functions have been applied in a reverse calculation (with the same data) to obtain sea state information given the ship motions and known transfer functions. There are no inherent restrictions on the directional spectrum in terms of its shape, spreading or the number component wave systems with this technique. With buoy data also available for comparison with the results of these calculations, this work potentially represents a considerable advance on much of the previous effort in this area highlighted in Chapter 2.

The trial data set used in Chapter 7 and in this chapter is particularly suitable for validation of such techniques, because detailed sea state information was gathered, and the wave spectrum was strongly bimodal (Figure 2.3). The technique will have been obviously successful if it correctly identifies the two peaks.

9.2 Theory

9.2.1 Full matrix solution

Consider the heave encounter spectral response M_{xe}, for example, for a ship on a heading A in an unknown seaway. The ship heave encounter frequency transfer functions R^2_{xe}, may be calculated from the stationary transfer functions R^2_x for all relative headings at the current ship speed. The response can be written:

$$M_{XeA} = \begin{pmatrix} R^2_{Xea} & R^2_{Xeb} & R^2_{Xec} \end{pmatrix} \begin{pmatrix} S_{ea} \\ S_{eb} \\ S_{ec} \end{pmatrix} \qquad \ldots(9.1)$$

The subscripts a, b and c represent three directions relative to the ship heading A. It is required to solve for S. The same wave amplitude encounter spectrum is simultaneously causing motions in the other two linear degrees of freedom, and the equation can be extended to:

$$\begin{pmatrix} M_{XeA} \\ M_{YeA} \\ M_{ZeA} \end{pmatrix} = \begin{pmatrix} R^2_{Xea} & R^2_{Xeb} & R^2_{Xec} \\ R^2_{Yea} & R^2_{Yeb} & R^2_{Yec} \\ R^2_{Zea} & R^2_{Zeb} & R^2_{Zec} \end{pmatrix} \begin{pmatrix} S_{ea} \\ S_{eb} \\ S_{ec} \end{pmatrix} \qquad \ldots(9.2)$$

The wave amplitude encounter spectra and wave slope amplitude spectra may be related at each frequency ordinate by some transform T (explored in section 9.2.3). The matrix equation may be extended by use of a scaling matrix T with these factors along the leading diagonal, giving:

$$\begin{pmatrix} M_{XeA} \\ M_{YeA} \\ M_{ZeA} \\ M_{\phi eA} \\ M_{\theta eA} \\ M_{\psi eA} \end{pmatrix} = \begin{pmatrix} R^2_{Xea} & R^2_{Xeb} & R^2_{Xec} & R^2_{Xed} & R^2_{Xee} & R^2_{Xef} \\ R^2_{Yea} & R^2_{Yeb} & R^2_{Yec} & R^2_{Yed} & R^2_{Yee} & R^2_{Yef} \\ R^2_{Zea} & R^2_{Zeb} & R^2_{Zec} & R^2_{Zed} & R^2_{Zee} & R^2_{Zef} \\ R^2_{\phi ea} & R^2_{\phi eb} & R^2_{\phi ec} & R^2_{\phi ed} & R^2_{\phi ee} & R^2_{\phi ef} \\ R^2_{\theta ea} & R^2_{\theta eb} & R^2_{\theta ec} & R^2_{\theta ed} & R^2_{\theta ee} & R^2_{\theta ef} \\ R^2_{\psi ea} & R^2_{\psi eb} & R^2_{\psi ec} & R^2_{\psi ed} & R^2_{\psi ee} & R^2_{\psi ef} \end{pmatrix} \begin{pmatrix} 1 & 0 & 0 & 0 & 0 & 0 \\ 0 & 1 & 0 & 0 & 0 & 0 \\ 0 & 0 & 1 & 0 & 0 & 0 \\ 0 & 0 & 0 & T & 0 & 0 \\ 0 & 0 & 0 & 0 & T & 0 \\ 0 & 0 & 0 & 0 & 0 & T \end{pmatrix} \begin{pmatrix} S_{ea} \\ S_{eb} \\ S_{ec} \\ S_{ed} \\ S_{ee} \\ S_{ef} \end{pmatrix} \qquad \ldots(9.3)$$

The $\underline{R^2}$ matrix may be post multiplied by the scaling matrix, so that the problem once again becomes the solution of $\underline{A}.\underline{X}=\underline{B}$, with $\underline{A}$ equating to $\underline{R^2}.\underline{T}$, $\underline{B}$ to $\underline{M}$ and $\underline{X}$ to $\underline{S}$. This may be solved by similar methods to those used in Chapter 7.

9.2.2 Interpretation of matrix solution

It can be seen that the number of separate directional components (here a-f) which can be resolved is related directly to the number of independent motion degrees of freedom that are being measured. With six degrees of freedom, the resolution of an energy spectrum will be limited to 60° for a full 360° calculation.

With calculation at several frequencies, merging the S_e values found for each frequency forms the wave amplitude encounter spectrum. The parent *stationary* spectrum can be calculated by transforming the component encounter spectra back to the frequency in a stationary domain; however, with six direction components considered, there are six possibilities for the parent that would yield this encounter spectrum i.e. there are six datum directions from which the spectrum could originate. If motions are available for only one ship heading, an estimate of the wave direction relative to the ship would be required in order to select the correct stationary spectrum. In beam seas, for example, it would be impossible to tell whether the seas were on the port or starboard beam, as the ship response would be similar in either.

Alternatively, if the calculation is repeated for other headings (B,C...) in the same sea state, further sets of six possible parent spectra are available. The relative wave directions (a-f) should be adjusted by the difference in heading relative to A so that the same datum directions are referred to as for heading A. Each parent spectrum from ship heading A then has its counterpart in the same datum direction at the other headings B, C etc. Sets of candidate parent spectra are thus available for each of the datum directions; for one of these (the correct one), the two or more candidate spectra should all be very similar. Correlation techniques could be employed to identify the group with the most similar spectra. The ambiguity in port/starboard sea direction due to port/starboard ship symmetry would also be removed. The wave amplitude spectrum would have been determined.

Transforming from encounter to 'stationary' domains is not trivial because of the 'following seas problem' mentioned in Section 2.4, and discussion follows in 9.2.3.

9.2.3 Transformation for wave slope spectrum

The calculation of wave slope amplitude in the encounter frequency domain, the transform 'T', needs careful consideration. Figure 9.1 illustrates all the possible transformations between wave height and wave slope, and stationary and encounter frequency domains. Figures 9.2 and 9.3 show the physical situation in terms of speeds, wavelengths and encounter periods.

The transforms T_1 and T_3 of Figure 9.1 are equivalent. These may not be performed analytically for all headings because the relationship between ω and ω_e is non linear (though in deep water Equation 2.32 can be used for seas forward of the beam). The transformation may be performed numerically, e.g. Fryer et al. (1994) taking care to account for the effect of changing ω_e 'bin' width, and for seas abaft the beam where some method to account for energy at a single encounter frequency that may include contributions from up to three separate wave frequencies. This transformation was used to construct the examples in Figures 5.4 and 2.7 (wave amplitude spectra), and Figures 9.5 and 9.6 (wave slope spectra).

The reverse transformations T_2 and T_4 may be performed in a similar way, again except because of the 'following seas problem'; for seas abaft the beam it is not possible to identify the three possible source frequencies. At slow speeds the assumption of 100% contribution from the lowest possible frequency is usually acceptable.

Development of a method to distinguish the frequency content of the actual spectrum when making the transformations T_2 and T_4 would form a valuable feature of further work. One method was outlined by Iseki (1996), as reviewed in Chapter 2. An estimate source spectrum was refined by iteration, comparing the detailed shape of its transform with that of the measured encounter spectrum. If well resolved, advantage can be taken of encounter spectra abaft the beam showing a sharp peak with a step at the local maximum encounter frequency, as shown in Figure 2.6.

The transformation between wave amplitude spectrum and wave slope spectrum T_5 and

T_6 at each spectral ordinate n is given by e.g. Lloyd (1989):

$$S_\alpha(\omega_n) = \frac{\omega_n^4}{g^2} S_\zeta(\omega_n) \qquad \ldots(9.4)$$

Of interest for this chapter are the transforms T_7 and T_8 which have not been detected in the literature, and in particular T_8 for calculation of the wave slope encounter spectrum given the wave amplitude encounter spectrum and shown by the thick arrow.

Lloyd (1989) gives the spectral ordinates of the wave slope spectrum as:

$$S_\alpha(\omega_n) = \frac{\alpha_{n0}^2}{2\delta\omega} \qquad \ldots(9.5)$$

Assigning a similar notation to wave slope amplitude in the encounter domain, the encounter wave slope spectral ordinates are given similarly by:

$$S_\alpha(\omega_{ne}) = \frac{\alpha_{n0e}^2}{2\delta\omega_e} \qquad \ldots(9.6)$$

and equating these expressions:

$$S_\alpha(\omega_{ne}) = \frac{\alpha_{n0e}^2}{\alpha_{n0}^2} \frac{\delta\omega}{\delta\omega_e} S_\alpha(\omega_n) \qquad \ldots(9.7)$$

Incorporating equation 9.4:

$$S_\alpha(\omega_{ne}) = \frac{\alpha_{n0e}^2}{\alpha_{n0}^2} \frac{\omega_n^4}{g^2} \frac{\delta\omega}{\delta\omega_e} S_\zeta(\omega_n) \qquad \ldots(9.8)$$

However, for the transformation T_8 an expression giving $S_{\alpha e}(\omega_e)$ as a function of $S_\zeta(\omega_e)$ is needed, as it is required if possible to work entirely in the encounter frequency domain (and possibly avoid the following seas problem).

Energy must be conserved during transformation of the wave energy or slope spectrum from the stationary to encounter frequency domain and vice versa and so the spectral ordinates are related by (Lloyd (1989)):

$$S_\zeta(\omega_n)\delta\omega = S_\zeta(\omega_{ne})\delta\omega_e \qquad \ldots(9.9)$$

so with substitution into equation 9.8:

$$S_\alpha(\omega_{ne}) = \frac{\alpha_{n0e}^{\ 2}}{\alpha_{n0}^{\ 2}} \frac{\omega_n^{\ 4}}{g^2} S_\zeta(\omega_{ne}) \qquad \ldots(9.10)$$

which is the required form for the transformation T_8.

Consider the meaning of the wave slope amplitude portions of Equation 9.10 with the help of Figure 9.3. The bottom three graphs of this figure show how the wave recorded at a point in the ocean might vary for a regular wave (component of a spectrum). In head seas, the wave appears compressed as the encounter period is reduced, and in following seas it is elongated, but the wave amplitude ζ_0 remains the same.

The top part of Figure 9.3 shows the analogous situation for the wave as if recorded by a line of densely packed wave probes at an instant in time. The ship heading makes no difference to these graphs – even though the encounter period is different, the wave profile remains the same in this regime. There is not an 'encounter wavelength' and, more importantly for this study, the wave slope amplitude is also identical in the stationary and encounter domains:

$$\alpha_0 = \frac{\pi H}{\lambda} = \alpha_{0e} \qquad \ldots(9.11)$$

So equation 9.10 reduces to:

$$\boxed{S_\alpha(\omega_{ne}) = \frac{\omega_n^{\ 4}}{g^2} S_\zeta(\omega_{ne})} \qquad \ldots(9.12)$$

The transformation T_8 between encounter wave height and encounter wave slope is exactly the same as the transformation T_6 between stationary wave height and stationary wave slope given in Equation 9.4.

This result has been validated as shown in Figure 9.4. In this example, a Bretschneider wave spectrum (Equation 2.6) has been converted to a wave slope spectrum using Equation 9.4, and then transformed into the encounter domain using Equation 9.9 – the T_6,T_3 route of Figure 9.1. The resulting encounter wave slope spectrum is identical to a spectrum created by the T_1,T_8 route using Equations 9.4 and 9.12.

The presence of the ω_n term (rather than ω_{ne}) has important consequences for the matrix computations proposed at Equation 9.3. Even though both the wave spectrum and wave slope spectrum are considered to be in the encounter frequency domain, this means that frequency information from the stationary domain is still required. The 'following seas' problem thus operates once again- in seas abaft the beam, ω_n cannot be solved uniquely. The use of the matrix Equation 9.3 is thus severely limited as a general method for identifying directional frequency components of the seaway.

9.2.4 Reduced matrix solution

Mixing wave amplitude and slope spectra in the same set of simultaneous equations as proposed in Equation 9.3 is unlikely to be of great practical use if it must be limited to seas forward of the beam only.

A reduced matrix calculation, just for the linear motions, given by Equation 9.2 is a possibility. Surge motions are relatively difficult to measure and predict however, and this degree of freedom may even be omitted by seakeeping prediction software. Accurately populating the $\underline{R^2}$ matrix could be difficult and there would be consequences for the accuracy of the solved $\underline{S}$ matrix would follow.

An equivalent version of matrix equation 9.2 can be created for the angular motions, employing the encounter wave slope spectral ordinates directly and avoiding the transformation of Equation 9.2:

$$\begin{pmatrix} M_{\phi e A} \\ M_{\theta e A} \\ M_{\psi e A} \end{pmatrix} = \begin{pmatrix} R^2_{\phi e a} & R^2_{\phi e b} & R^2_{\phi e c} \\ R^2_{\theta e a} & R^2_{\theta e b} & R^2_{\theta e c} \\ R^2_{\psi e a} & R^2_{\psi e b} & R^2_{\psi e c} \end{pmatrix} \begin{pmatrix} S_{\alpha e a} \\ S_{\alpha e b} \\ S_{\alpha e c} \end{pmatrix} \qquad \ldots(9.13)$$

All three angular motions are available from the trials data, and transfer function calculations are also available from the seakeeping software used. The solution for $\underline{S}$ yields the wave slope encounter spectrum, which can be transformed back to the stationary wave amplitude spectrum by the methods already discussed.

It has been shown that the resolution achievable by this technique is limited by the number of independent degrees of freedom represented. With only three available, the spectral resolution is potentially limited to 120°, which would make for a very coarse and overly smooth directional spectrum result.

Instead of taking three principal directions (i.e. relative ship headings) for the waves with 120° separation, and a solution that smears the wave energy solution into these coarse bins, an alternative is to select three directions with an arbitrary and smaller separation. The wave energy solution will be forced into these directions only, but if the directions are well chosen, a reasonable representation of the (encounter) directional wave slope spectrum should be possible.

To illustrate this using some real wave data, Figure 9.5 gives a directional wave slope spectrum derived from the bimodal wave energy spectrum (Figure 2.3) for the frigate trial of Chapter 7. In Figure 9.6, these wave slope spectra are converted to the encounter frequency domain for a ship speed of 5 knots. Figure 9.7 shows an encounter spectrum composed of just three directions; this directional spectrum still looks very similar to the 206° data of Figure 9.6 it has been derived from. 71% of the spectral energy is contained in the three most energetic directions. Figure 9.7 has been constructed by setting all directions to zero except these three, which have been increased by a factor of 1/0.71 to maintain the same spectral energy

The technique actually employed to produce the results in the next section is to use a set

of 12 angular motion transfer functions (from headings spaced at 30° all around the compass), but to choose only 3 of these for any one calculation. Calculations were made for a full set of possible combinations of 3 headings from 12 where the order does not matter, i.e. nCr=12!/(12-3)!3!=220 combinations. The order does not matter because this merely effects the order of the components in the resulting $\underline{S}$ matrix. Choosing 3 heading directions in the order 2,4 and 6 would give $\underline{S} = (S_2,S_4,S_6)$ based on those directions, whereas choosing the order 6,2 and 4 would give $\underline{S} = (S_6,S_2,S_4)$; only one of these calculations need be done if the ordering is compensated for in the post processing.

The solution for $\underline{S}$ was repeated for all the random combinations, for results of 12 ship runs, and for each of 114 frequency steps in the motion spectra and transfer function definitions, between 0.02Hz and 1.15Hz.

9.3 Results using reduced matrix computations

The frigate trial of Chapter 7 has been used to test this matrix computation technique. The ship motion column vectors have been constructed from the trials results, and the transfer function matrix from the strip theory predictions. The results can be compared with Figure 9.8, the wave slope encounter spectra derived from the waverider buoy measurements. This is the same data as Figure 9.6, but presented in two dimensions.

Table 9.1 gives an example of the results of the matrix computations as described, for a single ship heading (026°), a single (encounter) frequency (0.07Hz) and for 12 of the 200 or so possible combinations of transfer function data for use in the solution.

Figures 9.9 to 9.17 show the results graphically. The y-axes on these graphs have units $deg^2.Hz^{-1}.deg^{-1}$; the scales are chosen so that they are of a similar relative magnitude as the scales of Figure 9.8 for comparison, and the colours also correspond with those of Figure 9.8. The difference in units is due to the conversion between radians and degrees, so the maximum value of 5×10^{-3} units on Figure 9.8 is equivalent to 16.4 units on Figures 9.9 to 9.17, and the factor is 4.57 vice versa. The graphs have been left in the encounter frequency domain for direct comparison with Figure 9.8.

Section 9.2.4 outlined the method of using all possible random wave direction combinations in order to ensure modelling of the most correct one. The problem remains how best to select this combination. At each frequency step and for each ship heading, the selection here has been based on:

- $\underline{R^2}$ matrix with highest determinant
- Combination with highest sum of $\underline{S}$ elements (negative elements allowed)
- Combination with highest sum of $\underline{S}$ elements (only positive elements allowed)

Each of these options has also been repeated for three 'modes' of calculation (giving a total of nine Figures 9.9 to 9.17). These are 'mode 0' with the $\underline{R^2}$ matrix undisturbed, and 'mode 1' and 'mode 2' with the $\underline{R^2}$ matrix manipulated so elements are forced into the dominant diagonal exactly as described in Section 7.3 for transfer function calculations.

Comparing with Figure 9.8, using the high determinant method does not appear to work well in Figures 9.9 to 9.11. Most results consist of single spikes rather than a continuous trend. Most activity where non-zero solutions are found is in the range 0.2 to 0.4 Hz, which does not correspond with the expected results from Figure 9.8, where the high spectral energy is below 0.2 Hz. Using high determinant as a selection method may not be good as this places a bias on the expected ship motion through $\underline{R^2}$ rather than addressing the nature of the solution $\underline{S}$ directly.

Figure 9.12 is also unconvincing, with very few points being isolated from the analysis, and most of those at 0° relative heading. Data should not be found at a single relative heading for all the ship headings. The behaviour should be as shown on Figure 9.8 where, for example, the high energy peak for relative heading 30° (pink) at ship heading 206 on Figure 9.8 is seen to transfer to 0° (blue) and 330° (red) as the ship turns to 176 and 146 respectively.

Figures 9.13 and 9.14 look very similar to each other, and this is to be expected as the

analysis only differs in the treatment of leading diagonals; with only a 3 x 3 $\underline{R^2}$ matrix, identical results will often be found. The results here look a little better, as energy at the right magnitude and direction is found at around 0.18Hz for ship headings 176 to 236. Unfortunately, energy is found at ship headings 266 to 356 where there are low levels at these headings on Figure 9.8, and little energy is found between 056 and 146 where there are significant peaks on Figure 9.8.

Figure 9.15 shows that insisting all three elements of $\underline{S}$ are positive severely restricts the data that is filtered out from the random possibilities. Not a single spectral point was found by this method with the full matrix solution 'mode 0'. Using the diagonal manipulations 'mode 1' and 'mode 2' for Figures 9.16 and 9.17 gives very similar results as for Figures 9.13 and 9.14; essentially the same data is selected. The results show some activity in the area of principal wave energy at around 0.18 Hz, but in detail are not consistent with the encounter slope spectra calculated from the waverider buoy data in Figure 9.8.

The matrix method for computation of the wave (slope) directional spectrum must therefore be judged a failure. The principal reasons are:

- Difficulty selecting the correct result from many possible solutions
- Difficulty getting physically meaningful results from a purely mathematical solution where negative energies are possible, for example.
- The 0.01 Hz frequency step chosen may be too small; perhaps a larger frequency step would give smoother spectra, though peaks would be less well defined.
- Good conditioning of the matrix equations depends on the source data for the ship motion transfer function data $\underline{R^2}$. Strip theory was used, which in the case of yaw motions depend heavily on the choice of autopilot. Small inaccuracies in this motion transfer function in particular (forming one third of the motions actually used here) may lead to ill-conditioning of the matrix equations and large variations in the $\underline{S}$ values computed.

9.4 Possible improvement of method

Besides addressing the limitations highlighted at the end of section 9.3, a number of further improvements to this method are possible.

It has been shown that the number of directional components available for a calculated wave spectrum is limited by the number of independent ship motion measurements which are available (and for which transfer functions are known). The limitation to just three 'bins' as used above naturally leads to a very coarse spectrum definition, and an improvement would be desirable.

The best approach to improving directional resolution would be to include a greater number of motion measurements in the calculation. Extending the matrix equation in this way requires that the extra lines provided by the transfer functions are linearly independent of the degrees of freedom already included, and that the transfer function can be related to the wave amplitude (or slope) spectrum.

Relative motion is a good candidate as an independent motion but would require specialised instrumentation not normally available on ships. Similarly, structural responses such as midships bending moment would also require installation of dedicated instruments.

The velocities and accelerations of the linear and angular motions might be used, but are linearly dependent on the displacements or angles so do not add to the resolution.

Motion measurements at different locations e.g. bow/stern, port/starboard would yield transfer functions of different magnitudes. The motions themselves will be linearly dependent on the rigid body motions at the CG, and this dependence is also likely to occur for their transfer functions, making them unsuitable for the purpose of improving spectral resolution.

Extra measurements with linear dependence will still be of use, however. In this case, there are more simultaneous equations than unknowns and the system is 'over

determined', and least squares techniques exist to find the solution for the unknowns best satisfying the equations, notably the 'QR decomposition' e.g. Watkins (1991). These mean that the extra measurements can effectively be included in the calculation of the encounter wave spectral ordinates, but the number of directional bins is still limited to the number of linearly dependent motions observed.

9.5 Conclusion

This chapter has described a matrix approach to the problem of solving the problem of sea state estimation based on knowledge of the ship motions and the ship motion transfer functions. There were no prior assumptions about the nature of the seaway, so that multi-modal spectra can be represented.

The initial proposal was that with linear motions dependent on wave height and angular motions on wave slope, a single matrix in five or six degrees of freedom could be formed which expresses the wave spectrum based on simultaneous equations of the ship motion and transfer functions. It was shown that creating encounter wave *slope* spectrum from encounter wave *height* spectrum suffered from the 'following seas problem', and so the matrix computation had to be limited to three degrees of freedom only.

A randomised method of selecting wave directions was employed to achieve reasonable spectral resolution with just three direction components. This led to the problem of selecting the correct solution from all the random possibilities. Various filters were used in an attempt to determine the best solution, and while the correct frequency range for the wave (slope) spectrum was found with one set of results, in general the spectral results were sparse and unconvincing.

Several ways are given in which the solution for the directional wave spectrum might be improved. However, it might be argued that the approach is prone to technical difficulty at heart because independent results are calculated at every frequency step. This means that the detailed properties of the source spectra – the degree of smoothing – come into play and inevitably lead to some ill-conditioning of the matrix computations.

A technique which does not have this limitation, perhaps based on the whole motion spectra or transfer function, rather than individual ordinates, or even discounting the spectral composition and using RMS data only, would give a fundamentally more benign calculation.

Line number	Heading degs true	Frequency Hz	Random List Index	Heading Index #1	Spectral Energy Direction #1	Heading Index #2	Spectral Energy Direction #2	Heading Index #3	Spectral Energy Direction #3	Determinant	Sum of Spectral Energies
67	26	0.07	181	1	0.0001375	8	-0.001019	12	0.001279	-0.0935	0.000398
68	26	0.07	122	6	-1.996E+13	8	1.996E+13	12	0.001209	0.0000	0.001209
69	26	0.07	27	3	0.1973	4	-2.55E+15	10	2.55E+15	0.0000	0.197300
70	26	0.07	100	1	11910	3	6.758E-06	7	-7160	0.0000	4750
71	26	0.07	149	3	2.354E+14	4	0.001699	11	-2.354E+14	0.0000	0.001694
72	26	0.07	150	1	11970	7	-7195	9	0.000006095	0.0000	4775
73	26	0.07	79	1	12020	7	-7228	10	0.000005129	0.0000	4792
74	26	0.07	20	1	0.0001375	6	-0.001019	12	0.001279	-0.0935	0.000398
75	26	0.07	177	4	0.006663	6	-2.496E+14	8	2.496E+14	0.0000	0.006668
76	26	0.07	154	1	12020	4	5.129E-06	7	-7228	0.0000	4792
77	26	0.07	47	1	11880	7	-7142	8	0.00001821	0.0000	4738
78	26	0.07	180	2	2.413E+14	4	0.004123	12	-2.413E+14	0.0000	0.00412

Table 9.1 Example of wave spectrum results

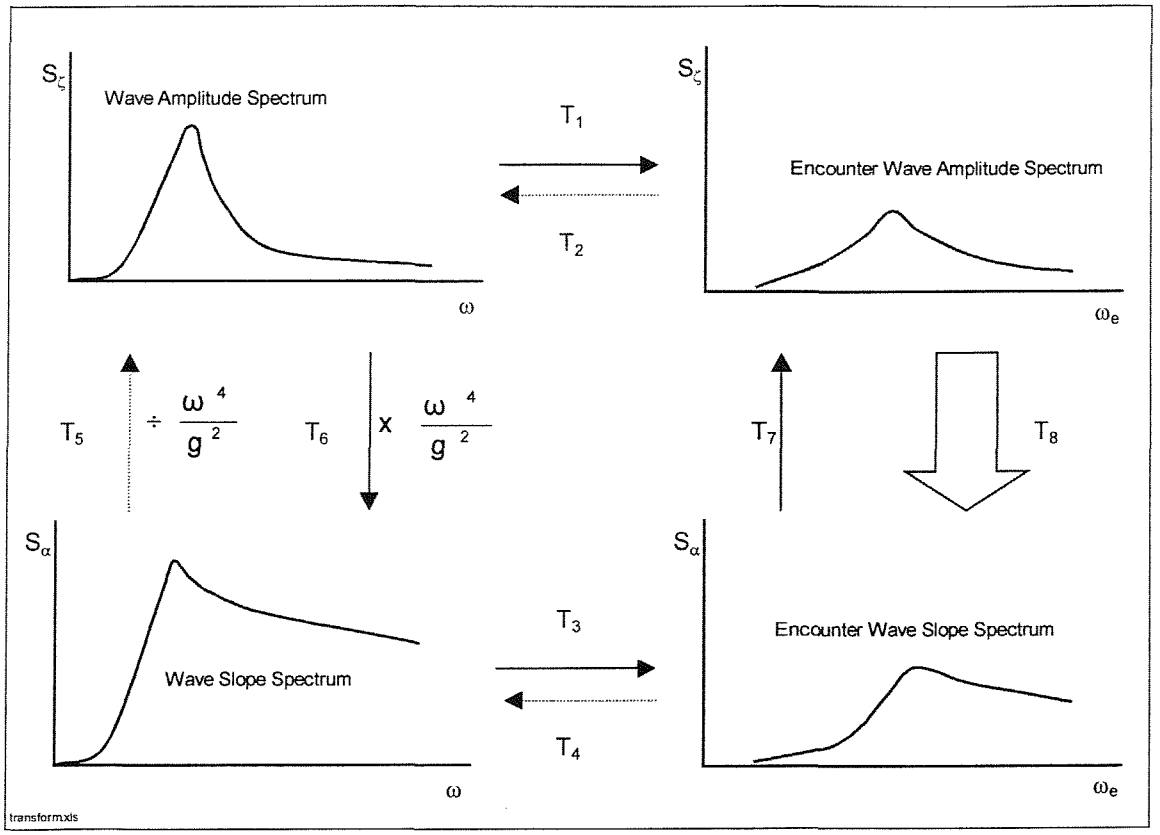

Figure 9.1 Wave amplitude and slope spectral transformations to encounter frequency

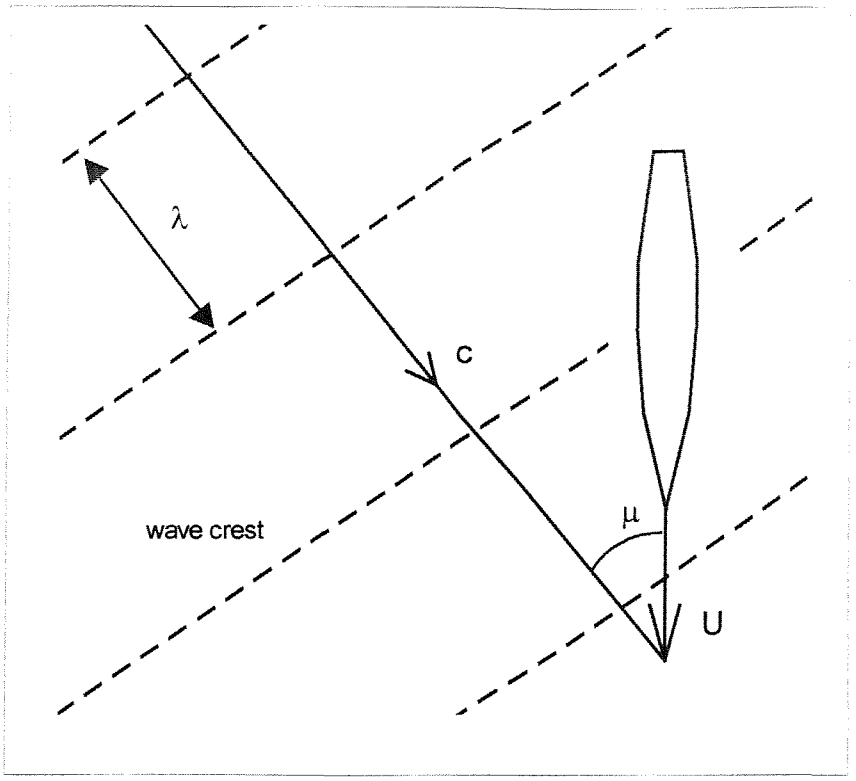

Figure 9.2 Heading angle relative to waves [after Lloyd (1989)]

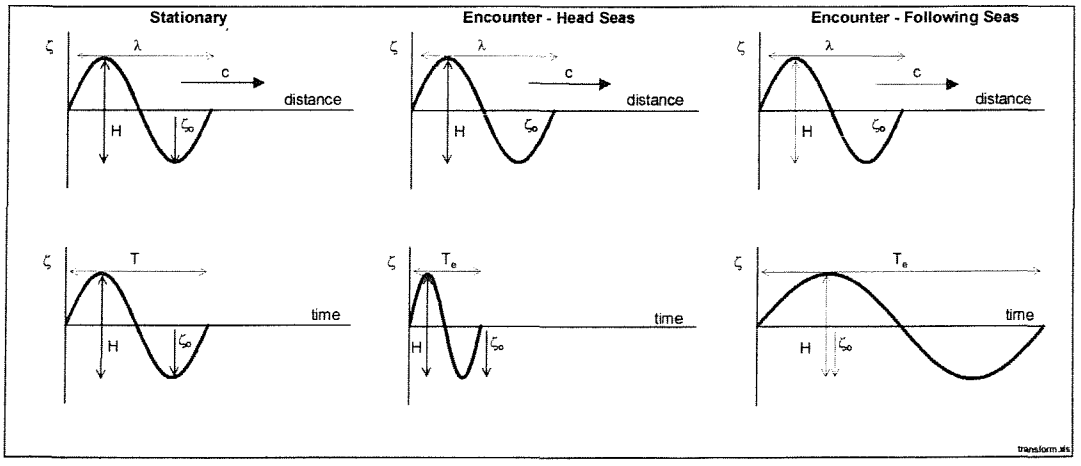

Figure 9.3 Wave amplitude and slope definition

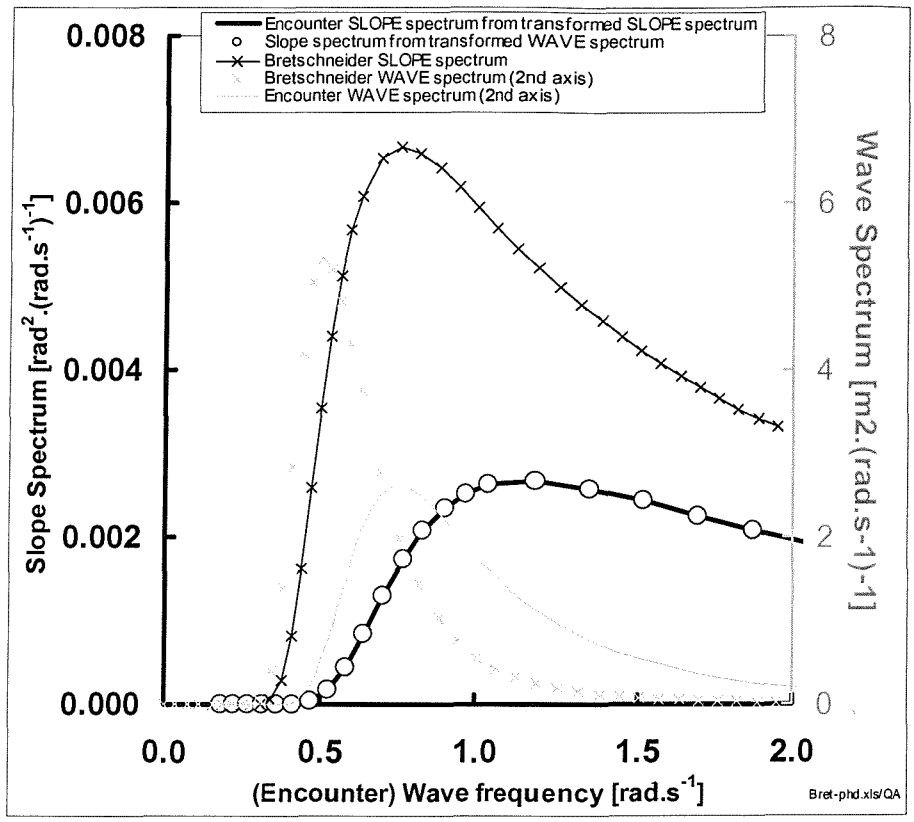

Figure 9.4 Validation of encounter wave slope calculation
(Head seas, deep water, 5.5m 12.4s Bretschneider spectra)

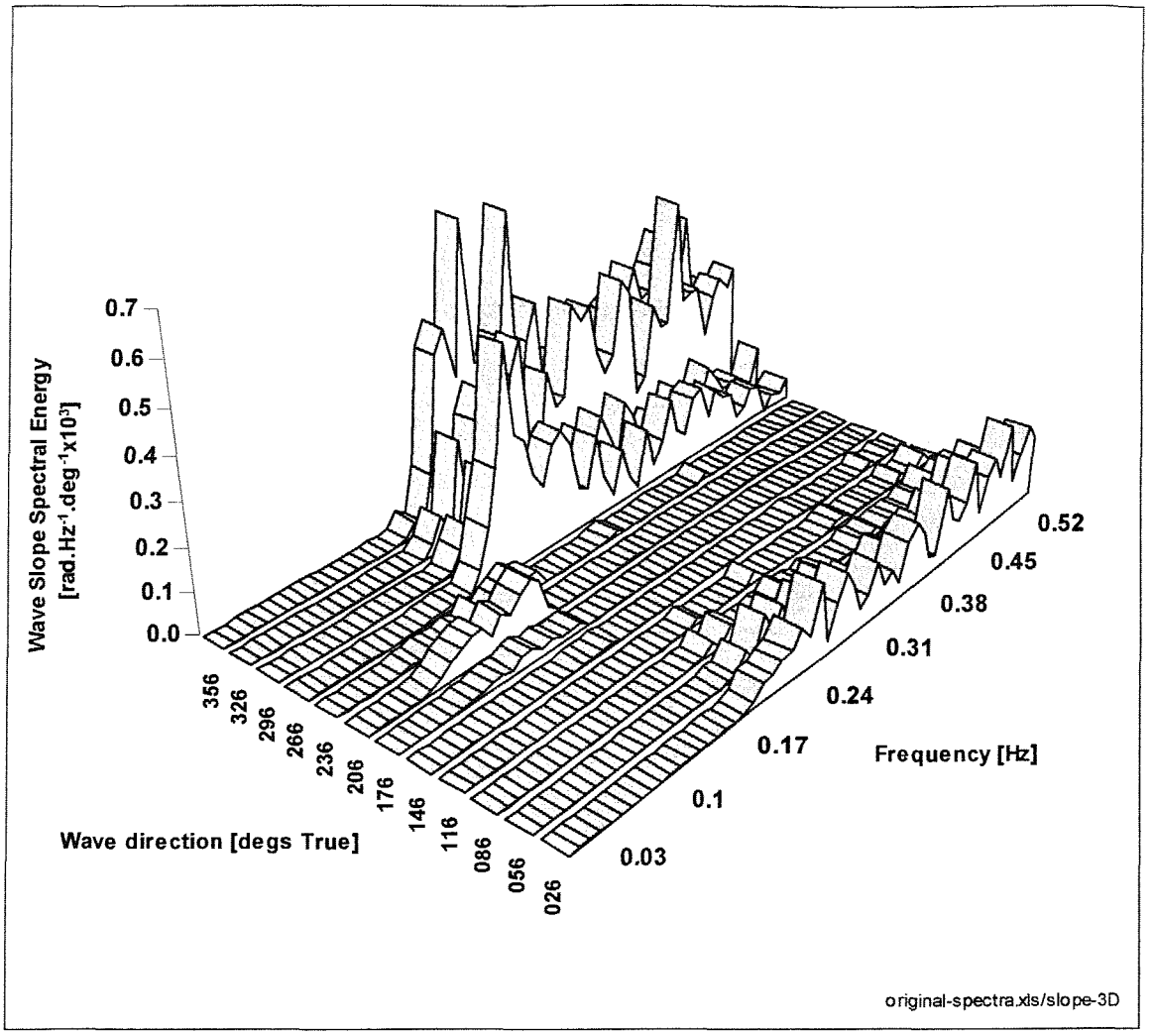

Figure 9.5 Stationary directional wave slope spectrum

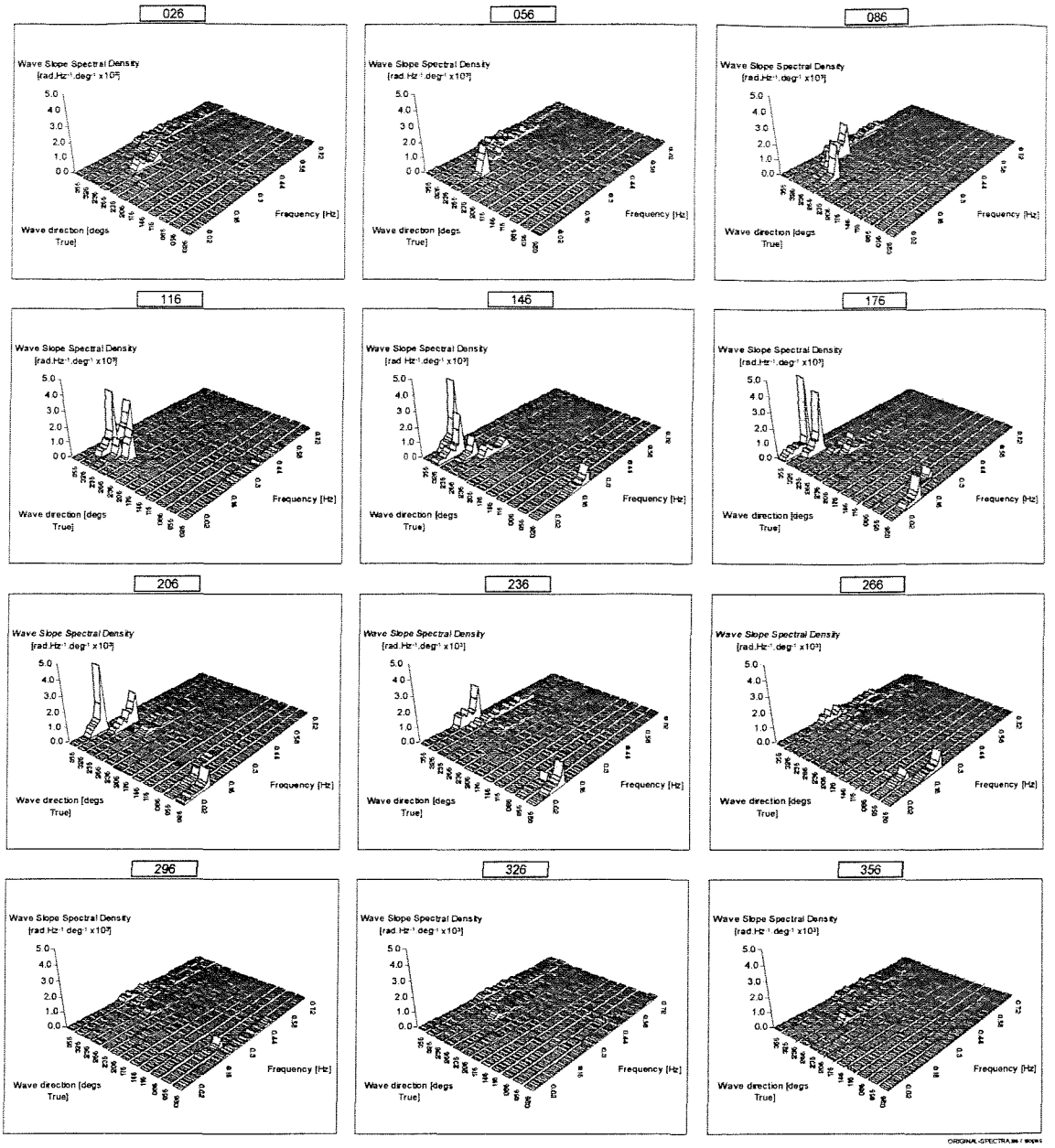

Figure 9.6 Directional wave slope spectra (3-D plot)

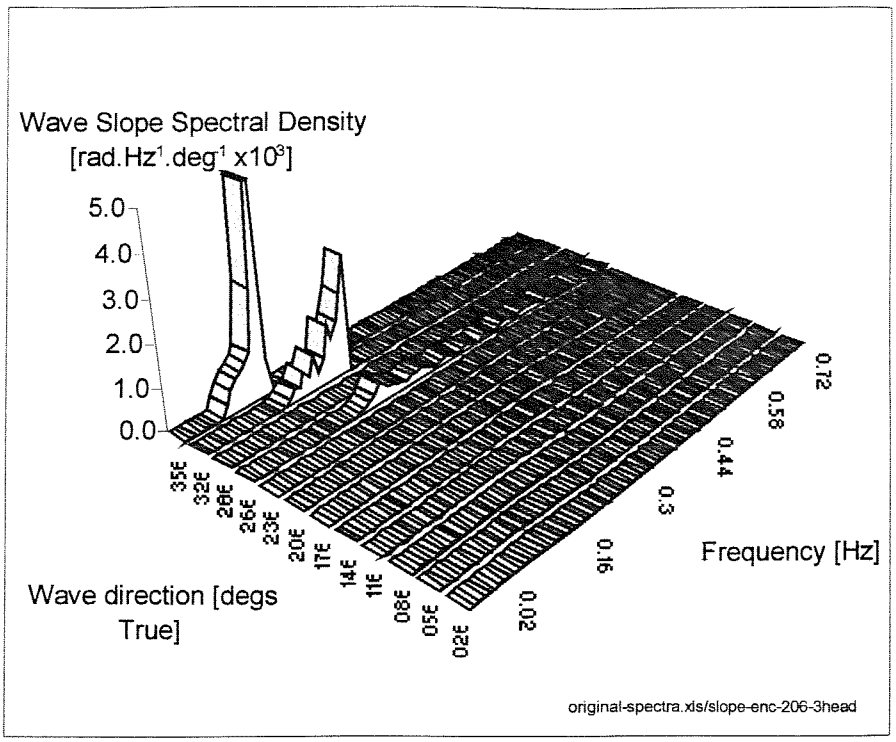

Figure 9.7 Wave slope encounter spectrum with only 3 direction components (compare with Figure 9.6, 206°)

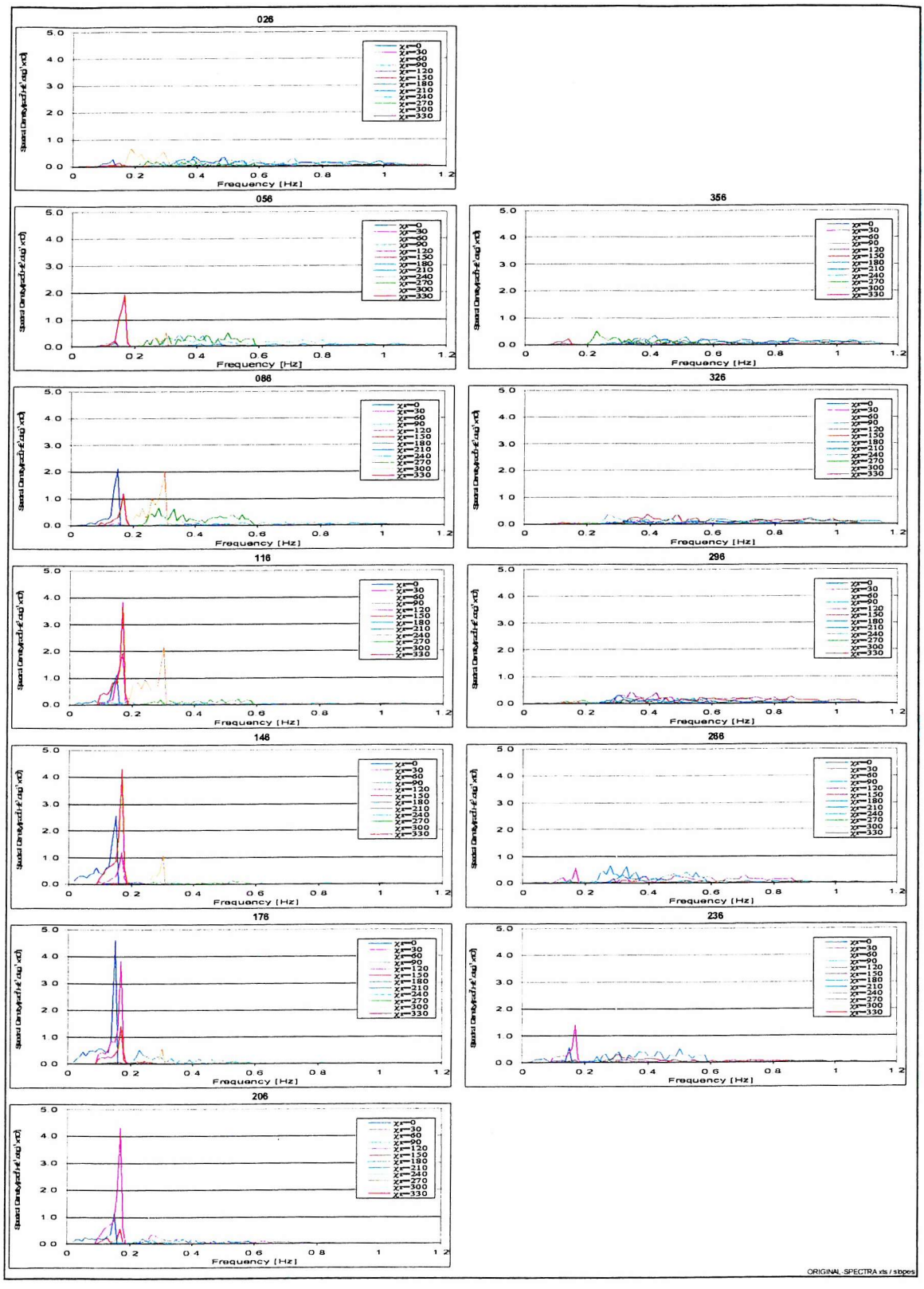

Figure 9.8 Directional wave slope spectra

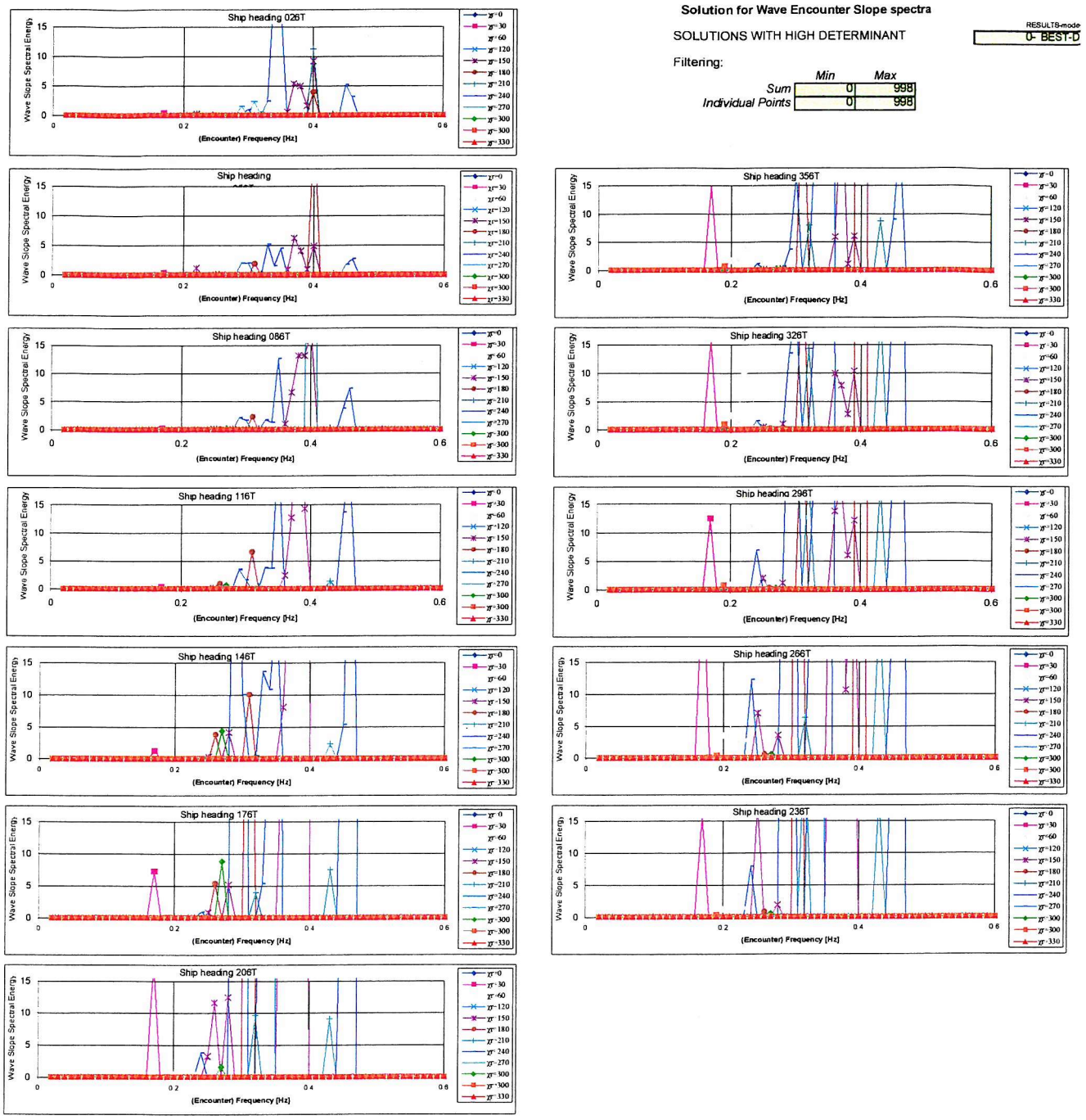

Figure 9.9 Solution for encounter wave slope spectrum - selection by high determinant, 'mode 0'

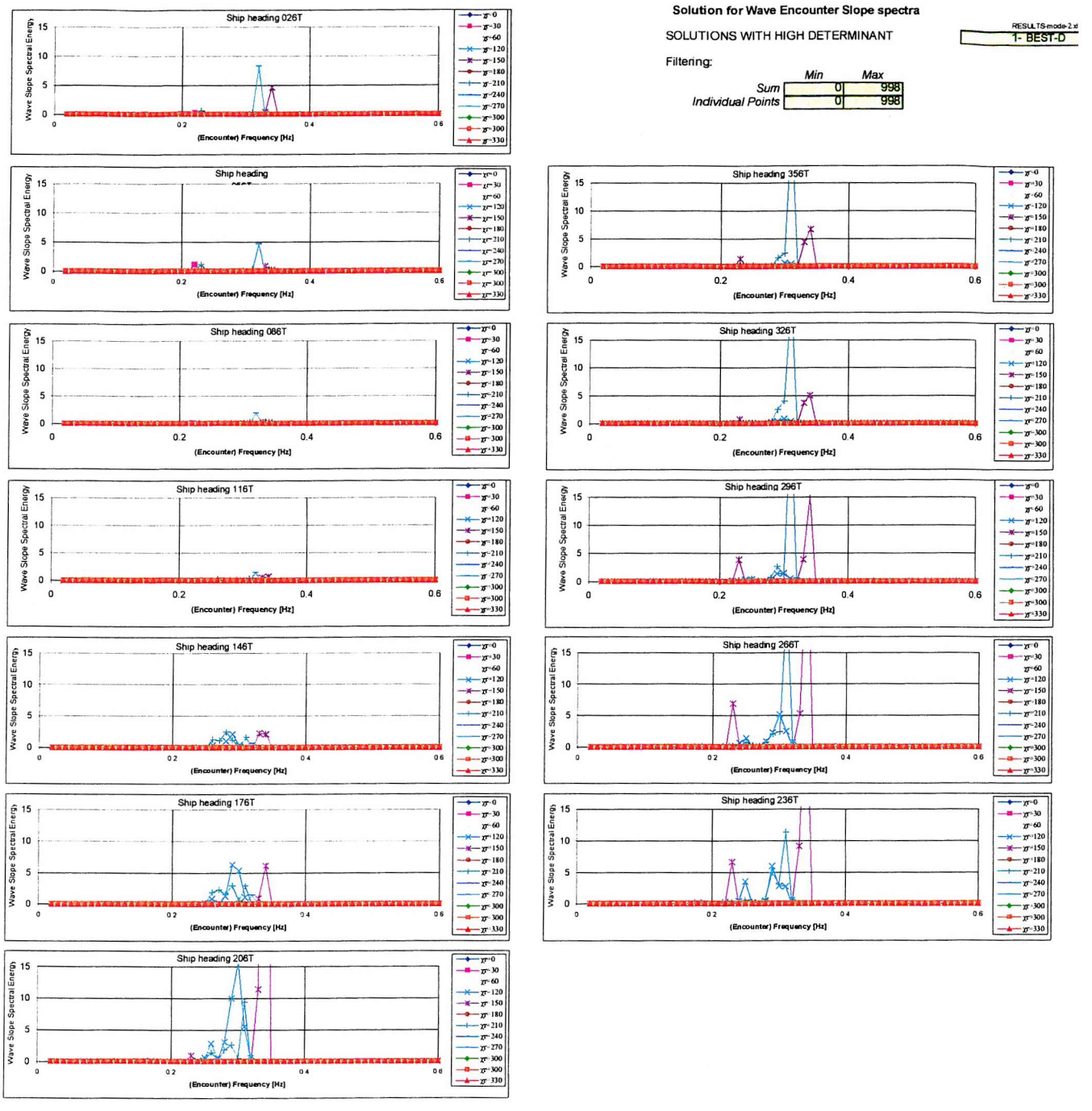

Figure 9.10 Solution for encounter wave slope spectrum
- selection by high determinant, 'mode 1'

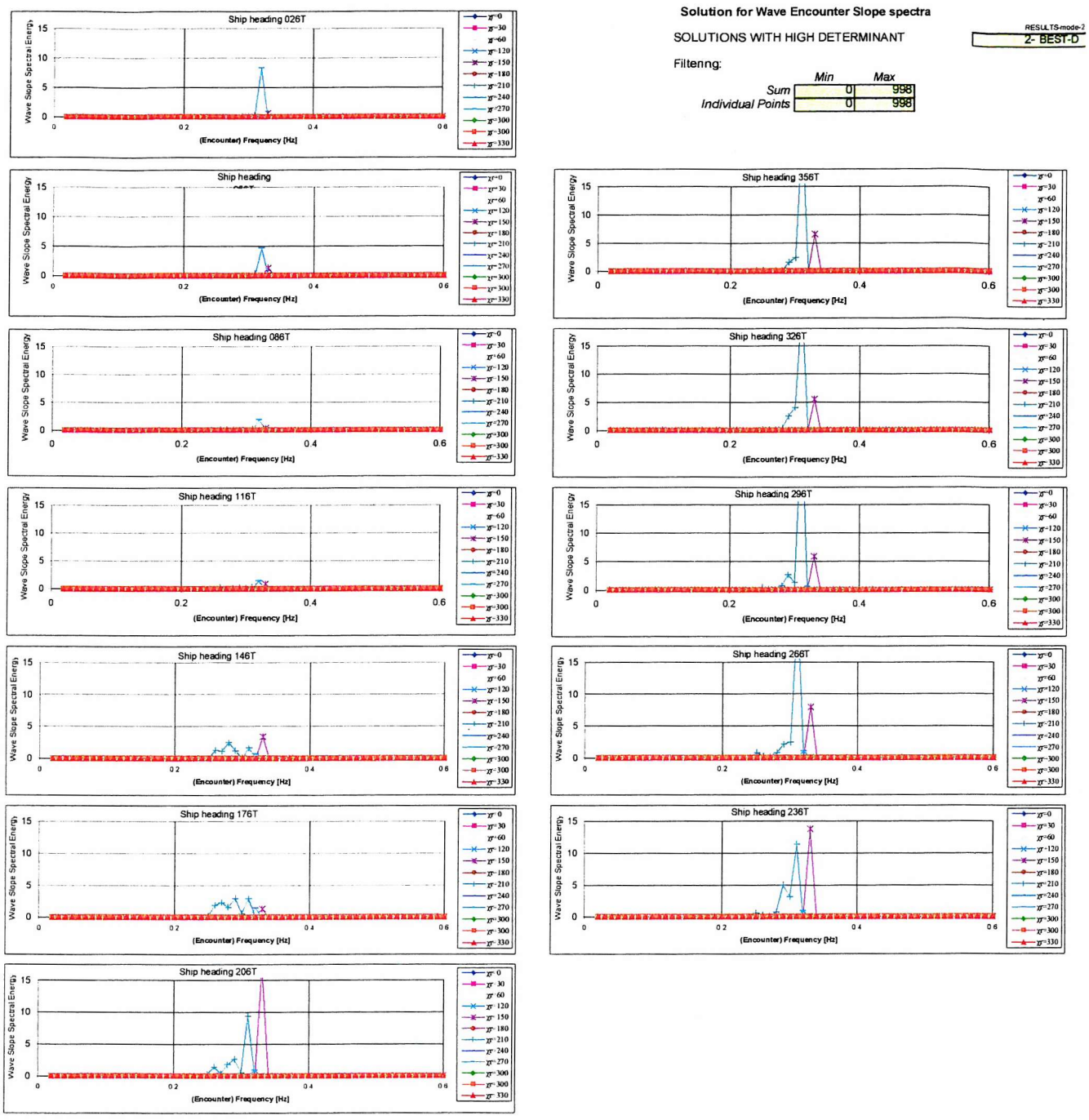

Figure 9.11 Solution for encounter wave slope spectrum
- selection by high determinant, 'mode 2'

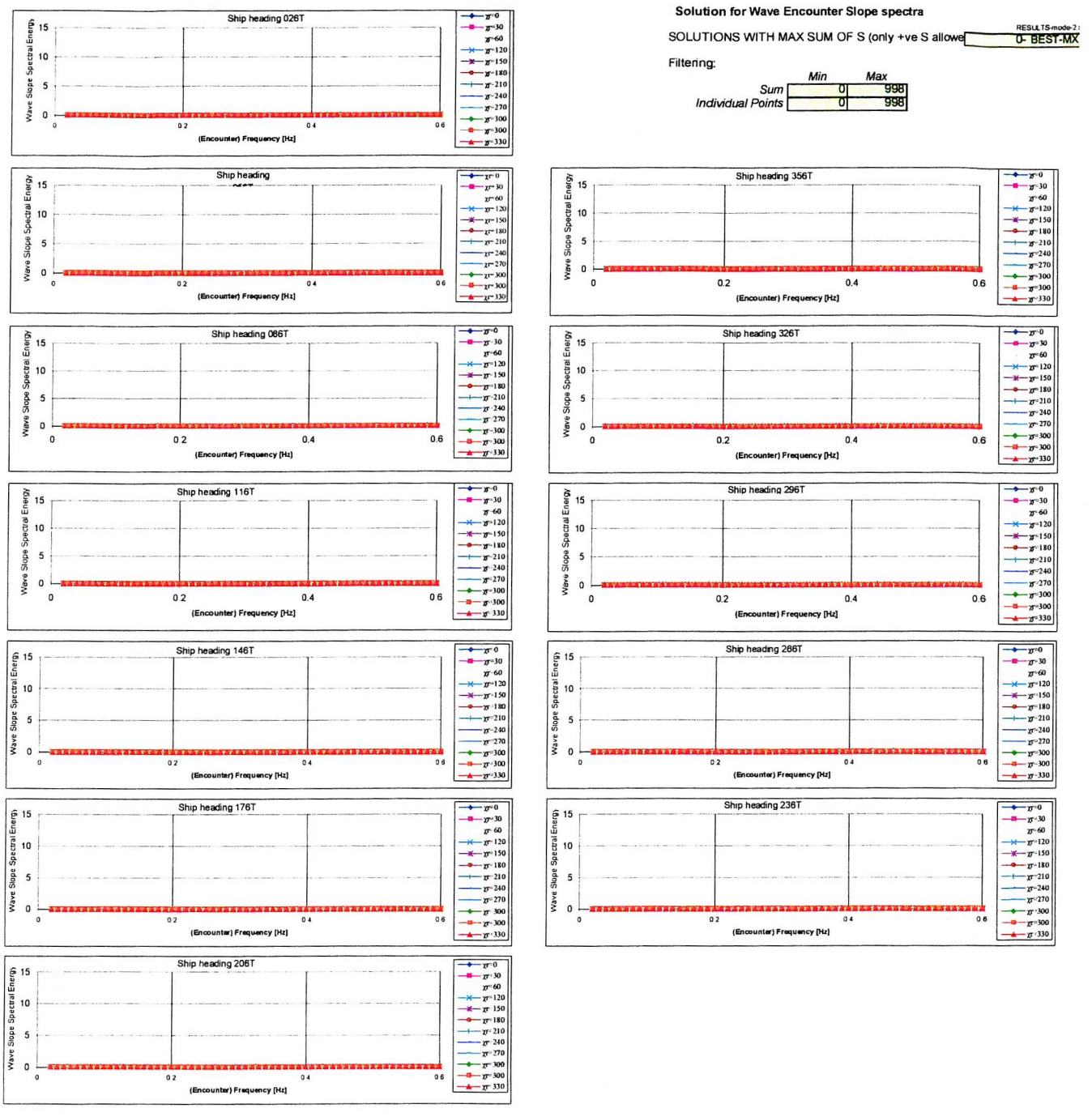

Figure 9.12 Solution for encounter wave slope spectrum - selection by high energy sum (negative points allowed), 'mode 0'

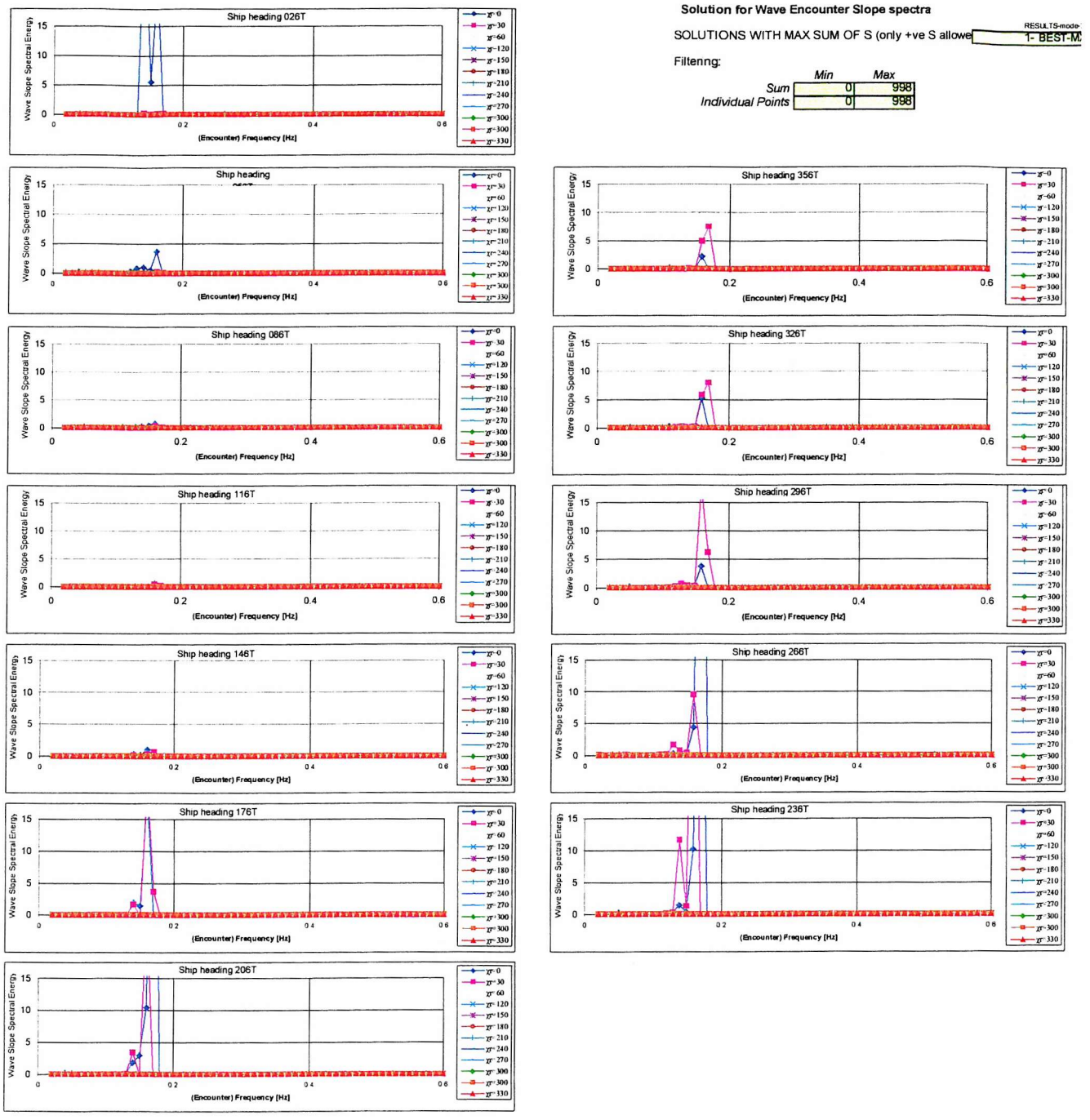

Figure 9.13 Solution for encounter wave slope spectrum - selection by high energy sum (negative points allowed), 'mode 1'

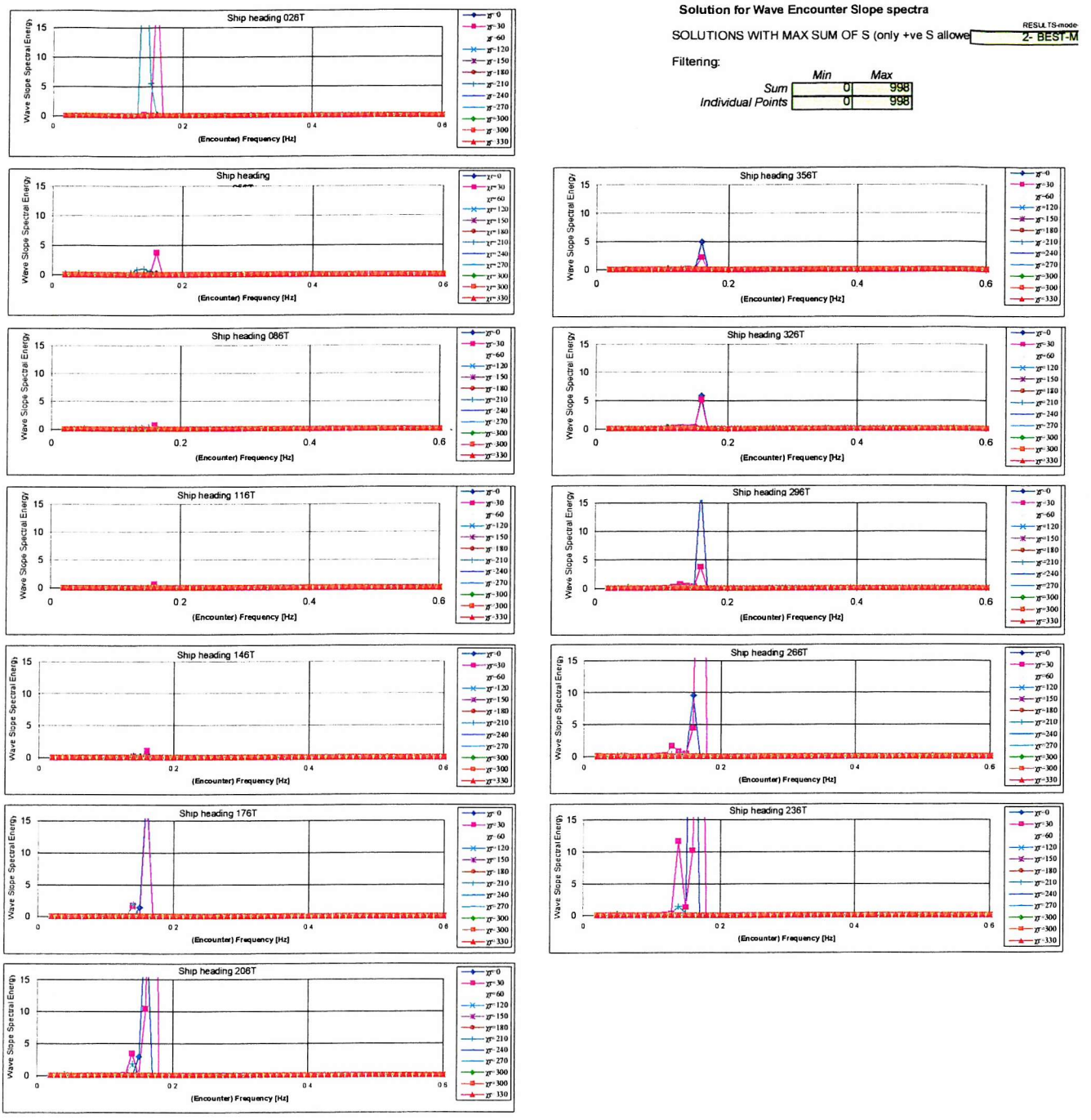

Figure 9.14 Solution for encounter wave slope spectrum - selection by high energy sum (negative points allowed), 'mode 2'

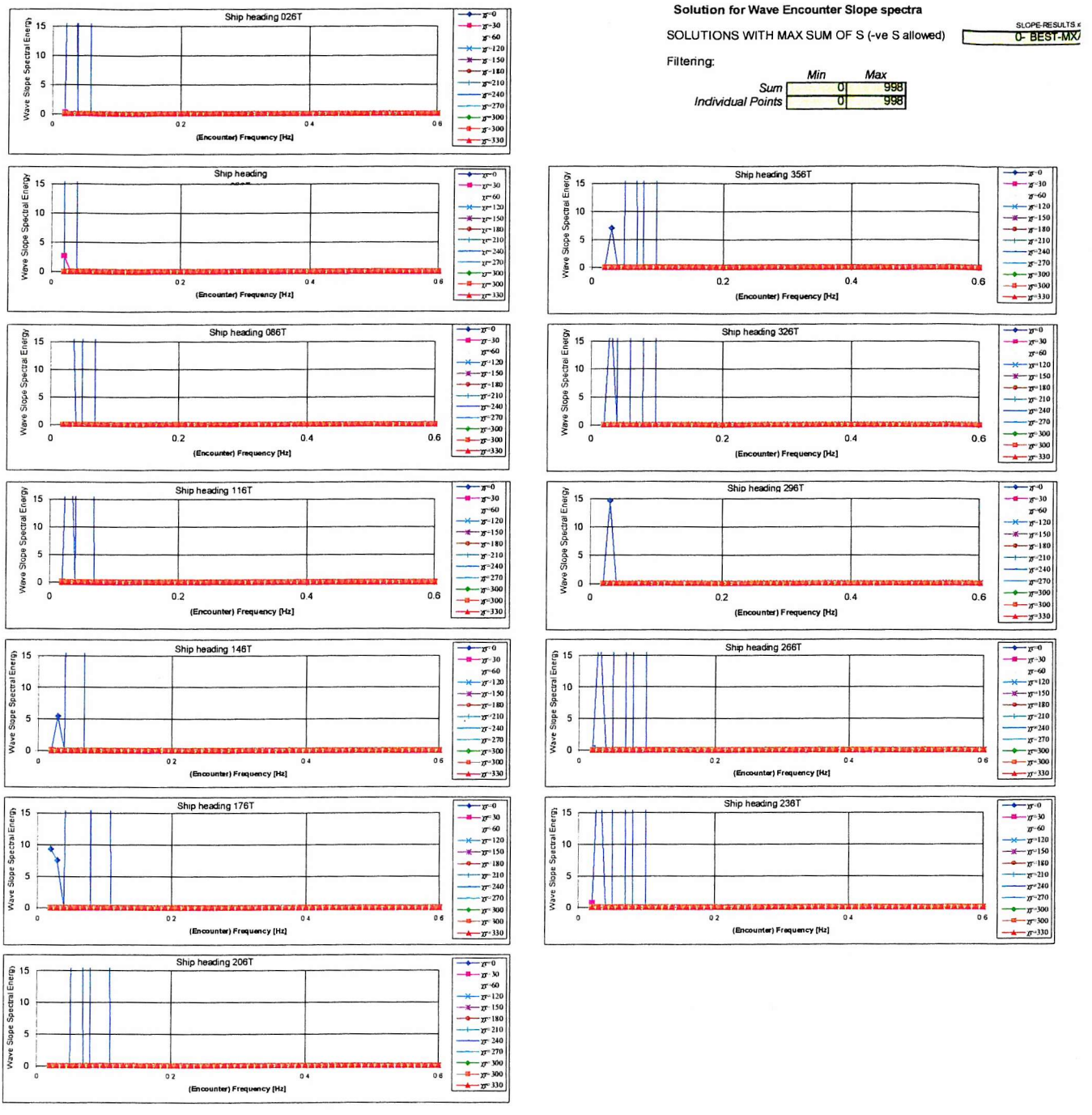

Figure 9.15 Solution for encounter wave slope spectrum
- selection by high energy sum (only positive points allowed), 'mode 0'

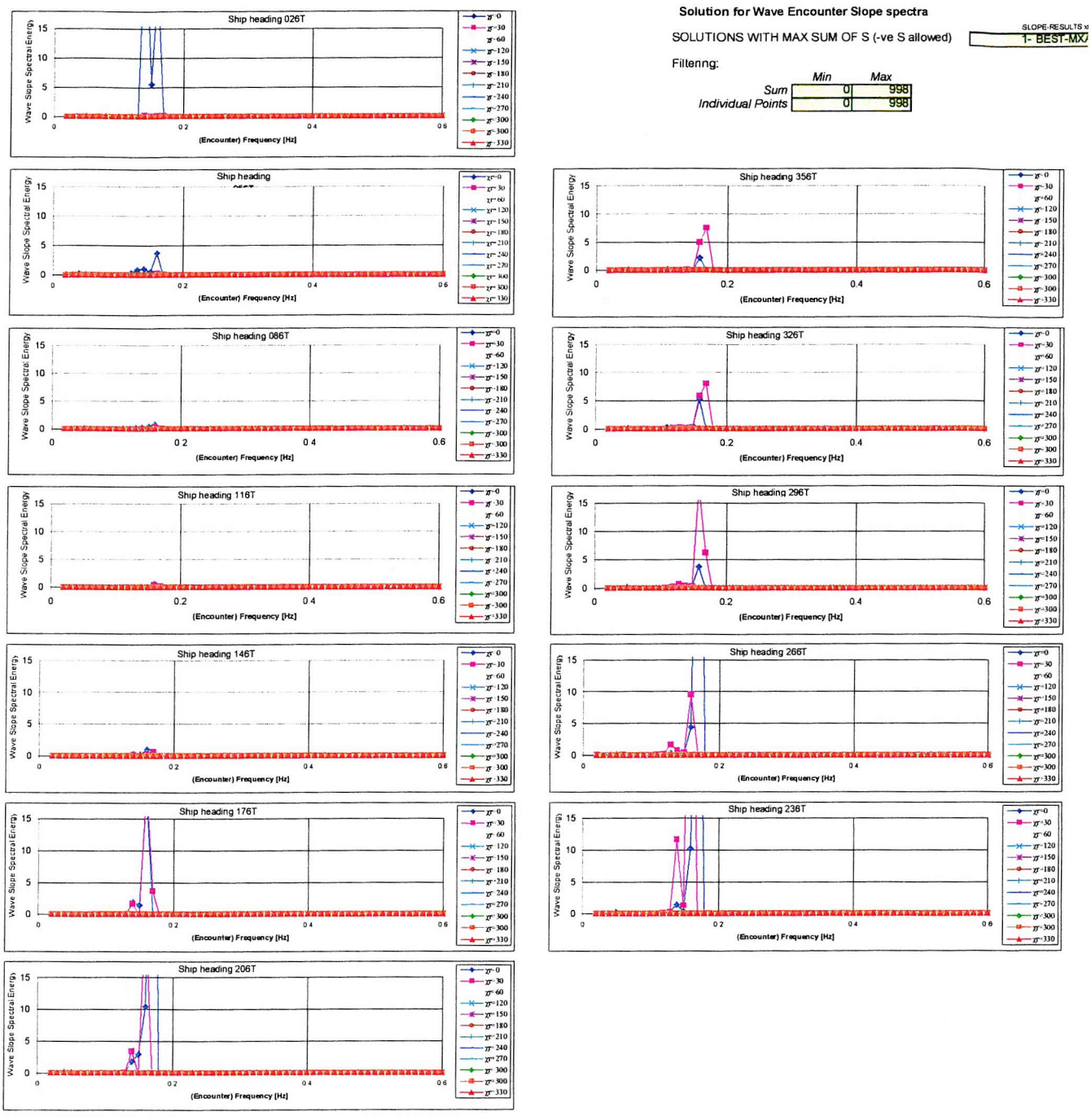

Figure 9.16 Solution for encounter wave slope spectrum - selection by high energy sum (only positive points allowed), 'mode 1'

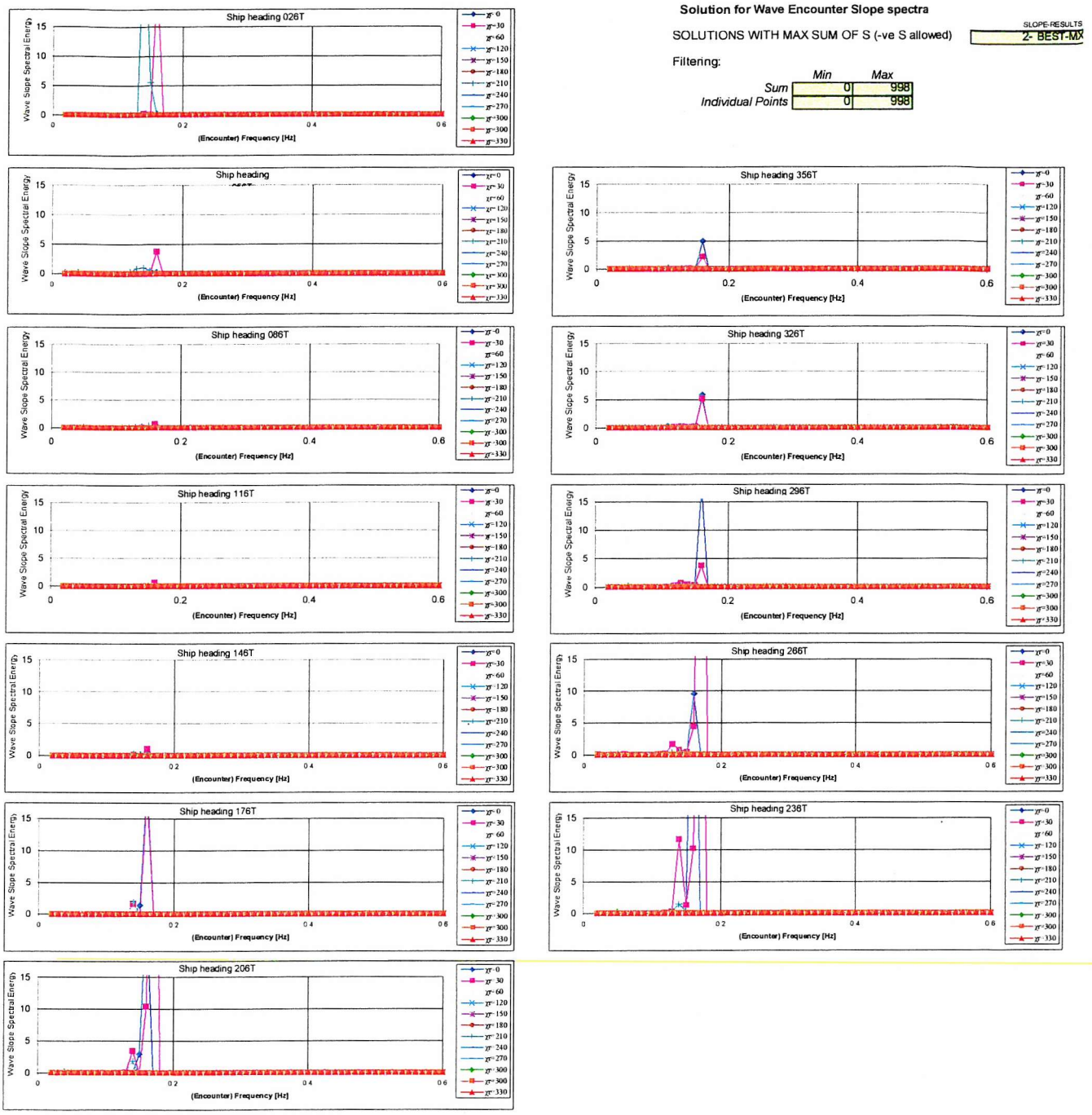

Figure 9.17 Solution for encounter wave slope spectrum - selection by high energy sum (only positive points allowed), 'mode 2'

10. CONCLUSIONS AND RECOMMENDATIONS

"They are ill discoverers that think there is no land, when they can see nothing but sea."
Sir Francis Bacon

10.1 Summary discussion

Seakeeping trials are usually conducted and analysed as part of the acceptance process for ships. Whilst several characteristics are often of interest, such as deck wetness frequency or slamming loads and frequency, it is usually the ship motions that are of principal interest. The results are used to validate that the measured ship motion magnitudes agree well with the predictions made or model test results for the ship during its design process. More advanced analysis might be performed to derive the frequency response of the ship, the Response Amplitude Operators or RAOs. Trials results might also be used for the purposes of validating the predictions of seakeeping theories and software, at the motion or RAO level. In any case, conducting successful seakeeping trials is difficult since reliable measurements must be made of the ship motions, the wave environment and the ship speed and heading, as well as detailed knowledge of the ship hydrostatic properties; none of these quantities are easy to measure. If a seakeeping trial is fortunate enough to encounter rough weather in its allotted programme time, the wave environment and the therefore the ship motions offer a complex and random set of data to understand.

Seakeeping theories and the resulting computer models are, however, mostly validated against scale model tests. Model tests are seen as an essential part of the hydromechanics design cycle since ship prototypes are extremely rare. They offer a cost effective way to identify problems with the design, as sea conditions can be modelled in the laboratory on demand, and have been trusted source of information for many years. Nevertheless, there are several disadvantages with the model testing approach – fundamentally, the balance of forces on the model may not be correct when Froude scaling (of speed and wave height) is applied. Model testing also tends to simplify reality somewhat, for example, test tank models are usually towed at constant speed,

whereas ships at sea are free to surge. This must modify the ship motions measured in the tank. Waves in the tank are also highly simplified compared with ocean conditions – regular or irregular waves generated in most test tanks in the world propagate in just one direction.

It is thus argued that despite the difficulty in conducting successful seakeeping trials, this is the only situation where the ship is unequivocally behaving in its true way, and not subject to some simplification or modelling process. The three-way relationship between the waves, the ship motion, and the motion response functions is explored. In particular, the thesis has argued that it is the multidirectional nature of natural sea waves that offers the biggest challenge. This thesis has offered ways to both mitigate the effects of these waves on the ship motions if a simple approach is taken, and to fully account for this complexity if a more detailed approach is made.

The literature review established the state of the art in the relevant topics, the fields of wave modelling, wave measurement for trials, and the reporting of seakeeping trials themselves. It was established that trials are not being conducted and reported in a way which expresses the underlying uncertainties in the ship and the seaway, and in particular the measurement and treatment of the effects of wave directionality are sparingly addressed.

The aims of the thesis were thus firstly to establish a rationale for seakeeping trials that has provision for the effects of these complex natural seas, and to illustrate the effect of short crested and bimodal wave spectra on the ship motions with several full scale trials examples. Having established this technique, the aim was the to show that Response Amplitude Operators can be calculated for ships in these wave conditions. A further aim was to show how uncertainty in the properties of the ship and the wave environment can taken account of in the analysis, something rarely seen in the literature.

The final aim was to approach the nature of wave behaviour, ship response function and ship motion from a reversed perspective and show that the characteristics of the seaway can be calculated from the ship motions even in complex wave systems. The literature

review suggested that robust, practical and sufficiently detailed approaches have not previously been successful.

In summary, the highlights of the thesis are indicated below:

- The 'star' trajectory of seakeeping runs at a wide range of headings of the compass is proposed as the standard way to conduct seakeeping trials so that the effect of wave directionality can be detected and represented meaningfully.
- Given that the long crested seas assumption is likely to be made for the majority of seakeeping trials where RAO evaluation is required, the example of a frigate is used to demonstrate methods that may be used to calculate sea state acceptance criteria for ship trials.
- Full scale seakeeping trials results are presented in a variety of seaways. With the aid of a 'star' trajectory evolution, they clearly show how the ship motions vary in character in long crested, short crested unimodal, and bimodal seas.
- Naval architects are encouraged to use error bars or equivalent with computed data. It is proposed that seakeeping calculations may essentially be treated as experiments where some variation in the quantities 'measured' can be expected. The 'random uncertainty' method described is an efficient way to incorporate uncertainty in the ship and environmental conditions into the computed results.
- The calculation of ship transfer functions in an arbitrary directional wave field is demonstrated. The example was a frigate trial made at slow speed in bimodal seas. A matrix solution of simultaneous equations of encounter wave spectra and motion spectra, at discrete frequencies was used.
- The calculation of significant wave height based only on ship motion statistics by multiple linear regression was demonstrated. An accuracy of the order of 10-20% compared with wave buoy data was found for a range of sea states. In blind tests, the calculation performed more consistently and more accurately than some commercially available systems.
- Equation 9.12 showed that computation of wave slope entirely in the encounter frequency domain is still subject to the 'following seas' problem. This has important

consequences for attempts to combine (encounter) ship motions and RAOs in a 'reverse calculation' of the sea spectral characteristics.

- A calculation of directional wave spectrum of transfer functions and motion spectra was demonstrated, but judged unsuccessful. This was by matrix solution of simultaneous equations at discrete encounter frequency steps. The problems were mathematical, the matrix equations easily become ill-conditioned when using real data. However, the use of discrete frequency steps is seen as a fundamental difficulty with this approach

10.2 Conclusions

The literature review in Chapter 2 gave a background to the issues that must be addressed when considering the behaviour of ships at sea and concluded that the reporting of trials, and process of comparing with computer predictions, is not often carried out with proper consideration of all the variables that have a bearing on the results. In particular it is the reporting and use of the directional content of the wave environment where the weakness lies.

One objective was to demonstrate the effect of multidirectional seas on ship motions - gathering ship trials data with good quality measurement of the simultaneous directional wave field was recommended as a worthwhile exercise in its own right. That objective has been achieved in this thesis - Chapter 3 argued for a 'star' trajectory as a standard for ship trials, and furthermore Chapter 5 presented results for five different vessels of a range of sizes and types.

Another recommendation was to research areas where uncertainty and the sensitivity of measured and predicted results might be accounted for. This objective in partly dealt with in Chapter 4 which goes some way in addressing the issue in terms of the identification of suitable wave conditions to minimise the uncertainty due to the effect of waves. Chapter 6 goes on to address the objective more directly and illustrates a practical method whereby uncertainty in the ship condition can be used to give error bands for computed results.

This principal theme of this thesis has been that wave spreading and directionality (particularly 'confused' bimodal sea with swell and wind sea components) have a great effect on the character of ship motions. This means that correlation with software predictions or calculation of RAOs by simple methods based on long crested waves are virtually impossible unless the waves are indeed perfectly long crested - a rare occurrence. Chapter 4 illustrated the point with strip theory calculations in directionally spread waves, and Chapter 5 demonstrated the effect on the motions of ships at sea. Chapter 7 included work showing that the RAO could be calculated by the technique proposed by Fryer (1991), from seas with an arbitrary directional content, with some success.

Additionally the literature review suggested that robust and practical methods did not exist to make a 'reverse calculation' of the sea characteristics given the ship motion. The attempt to extend the techniques of Chapter 7 to make this calculation, allowing fully for directionality of the seaway, must be judged a failure, attributed primarily to the use of narrow and discrete frequency steps. However in Chapter 8, a much simpler method to estimate the significant wave height, based on the ship motion statistics alone, performed well against test data.

The thesis has considered the inter-relationship between ship motions, their response functions, and the sea state, with particular consideration of multidirectional seaways. A bank of methodologies and techniques has been presented which accounts for the effect of these spread and bimodal seas. A successful prediction of wave height based on the ship motions is a worthy development in its own right. For ship motions and RAOs, adoption of the techniques for analysis and presentation of the results will allow the quality and confidence in full-scale seakeeping assessments to be improved. Furthermore, the rational approach makes validation of ship motion theory against trials results a more realistic possibility. In turn this could lead to improvements in the software, with less reliance placed on model tests and more on the true, complex motions ships at sea.

10.3 Recommendations

In the quest for answers scientific research inevitably raises more questions, and this work is no exception. Accordingly it is possible to identify the specific areas of this thesis where further effort would be fruitful, and to recommend in general directions that research in the field might take. These ideas are given in this section.

The work of Chapter 3 should be continued to identify a practical sea state requirement for sea trials. Programming the methodology would allow results to be rapidly attained for several different size ships. Using 'noise' waves somewhat smaller than the 0.5m used here, and relaxing the limit of 5% acceptable error somewhat, to, say, 10%, would give a less strict limit on the corresponding acceptable spreading. This might also assist in the determination of a general minimum sea state for seakeeping trials to be defined.

Linear superposition has not been proved adequately with full-scale trials data in bimodal seas. The computation required is very similar to that required for motion prediction in short crested, unimodal seas. Ship motion data like that of Chapter 5 is suitable for the purpose of validation. The main step is deciding how to deal with the directional wave spectrum – perhaps as two or more separate, unimodal spectra, or alternatively to use the Juszko and Graham (1993) representation of the full wave field.

It is recommended that work continues to further confirm that the techniques of Chapter 7 work for a wide range of ships and sea conditions e.g. using the research vessel, patrol vessel and trimaran trials results.

The work of Chapter 8 can easily be extended as described, to include wind speed as a parameter, and use different functions of roll and pitch. Considering the ship motions periods in ensemble would better define the ship relative heading, the frequency content, and possibly deduce something of its directional character.

Chapter 9 used discrete frequencies without success to calculate the directional wave spectrum. Its is recommended that further progress this field requires the development alternative methods using the full spectra, perhaps involving iteration with an estimate

stationary directional spectrum, to avoid this pitfall and the complication of the 'following seas' problem.

Programmes for the long-term collection of wave information, directional wave spectra in particular, should be encouraged and supported. This includes networks of wave measurement buoys and the publication of quantitative data from satellite altimeters. Satellite data from SAR should also be further developed to make the availability of period and direction information more routine.

REFERENCES

Aertssen G, van Sluys M F. SERVICE PERFORMANCE TRIALS ON A LARGE CONTAINERSHIP. Trans RINA 1972 pp.429-447

Aertssen G. SERVICE PERFORMANCE TRIALS ON A LARGE CONTAINERSHIP. Trans RINA 1966 pp.305-343

Aken H M, Bouws E. FREQUENCY RESPONSE OF A SHIPBORNE WAVE RECORDER.

Andrew R N, Lloyd A R J M. FULL-SCALE COMPARATIVE MEASUREMENTS OF THE BEHAVIOUR OF TWO FRIGATES IN SEVERE HEAD SEAS. Trans RINA Vol. 123 1981

Bales S L, Lee W T, Voelker J M. STANDARDISED WAVE AND WIND ENVIRONMENTS FOR NATO OPERATIONAL AREAS. DTNSRDC/SPD-0919-01. July 1981

Barber N F. A DIFFRACTION ANALYSIS OF A PHOTOGRAPH OF THE SEA. Nature Vol. 164, p485, 1949.

Barber N F. FINDING THE DIRECTION OF TRAVEL OF SEA WAVES. Nature Vol. 174 No.4440 pp1049-1050. 1954

Beal R C (ed.) DIRECTIONAL OCEAN WAVE SPECTRA - LABRADOR SEA EXTREME WAVES EXPERIMENT (LEWEX). John Hopkins University Press, 1991.

Bretschneider C L. WAVE VARIABILITY AND WAVE SPECTRA FOR WIND GENERATED GRAVITY WAVES. Beach Erosion Board Tech. Memo. No.113, US Army Corps of Engineers, 192p. 1959.

Canham H J S, Cartwright D E, Goodrich G J, Hogben N. SEAKEEPING TRIALS ON O.W.S. WEATHER REPORTER. Trans RINA 1962 pp.447-492

Carter D J T, Challenor P G, Cotton PD. SURFACE WAVE STATISTICS FROM SATELLITE ALTIMETERS. RINA Intl Conf on Seakeeping and Weather. London 1995.

Cartwright D E, Longuet-Higgins M S. THE STATISTICAL DISTRIBUTION OF THE MAXIMA OF A RANDOM FUNCTION. Proceedings of the Royal Society A 237 pp212-232. 1956.

Cartwright D E. THE SCIENCE OF SEA WAVES AFTER 25 YEARS. International symposium on dynamics of marine vehicles and structures in waves. Office of Naval Research/RINA, University College London, 1-5 April 1974.

Chryssostomidis C, Oakes M C. SELECTION OF WAVE SPECTRA FOR USE IN SHIP DESIGN. International Symposium on Ocean Wave Measurement and Analysis, New Orleans USA 9-11 September 1974

Clarke J D, Price W G, Temarel P. THE INFLUENCE OF SEAWAY DESCRIPTION ON SHIP RESPONSES CALCULATED FROM COMPUTER TIME SIMULATIONS. Symposium on Description and Modelling of Directional Seas. Technical University, Denmark. June 18-20 1984

Crossland P, Johnson M C. SPECIFYING AND VERIFYING GOOD STANDARDS OF SEAKEEPING FOR NAVAL VESSELS. Proc. International Marine Design Conference, Kyongju, South Korea, 1999.

Darbyshire J. THE GENERATION OF WAVES BY WIND. Proc. Royal Society A 215(1122) pp299-328. 1952.

Dipper M J. SHIP-BORNE WAVE HEIGHT MEASUREMENTS. Marine Technology Vol. 34 No 4, October 1997.

Donelan M A , Hamilton J, Hui W H. DIRECTIONAL SPECTRA OF WIND GENERATED WAVES. Phil. Trans. Royal Society of London A315, pp509-562. 1985.

Earle M D, Steele K E, Wang D W C. COMMENTS AND DISCUSSION ON 'WAVE DIRECTION ANALYSIS FROM DATA BUOYS' BY MIN-CHIH HUANG AND JIA-YUAN CHEN. Ocean Engineering 27(2000) pp1265-1272

Ewing J A. SOME RESULTS FROM THE JOINT NORTH SEA WAVE PROJECT OF INTEREST TO ENGINEERS. International Symposium on Dynamics of Marine Vehicles and Structures in Waves. Office of Naval Research/RINA, University College London, 1-5 April 1974.

Fernanades A A, Sarma Y V B, Menon H B. DIRECTIONAL SPECTRUM OF OCEAN WAVES FROM ARRAY MEASUREMENTS USING PHASE/TIME/PATH DIFFERENCE METHODS. Ocean Engineering 27(2000) pp345-363

Fryer D K. THE APPLICATION OF RANDOM SIGNALS TO MODELS FOR EVALUATING THE PERFORMANCE OF SHIPS. PhD Thesis, Portsmouth Polytechnic, 1991.

Fryer D K, Johnson M, Hawkes P J. MODEL TESTING IN NATURAL SEAS. International Shipbuilding Progress 41 No.425 pp5-23. 1994

Gerritsma J, Beukelman W. ANALYSIS OF MODIFIED STRIP THEORY FOR THE CALCULATION OF SHIP MOTION AND WAVE BENDING MOMENTS. Netherlands Ship Research Centre (now TNO) Report 96S. 1967

Goda Y. A COMPARISON OF SEVERAL FUNCTIONAL FORMS OF DIRECTIONAL WAVE SPECTRUM. Proc. RealSea '98 3-4 February 1998 Taejon Korea pp1-21. 1998

Graham R, Juszko B-A. PARAMETERIZATION OF DIRECTIONAL SPECTRA AND ITS INFLUENCE ON SHIP MOTION PREDITOINS. Journal of Ship Research. Vol.37 No.2 pp.138-147, June 1993.

Guedes Soares C, Trovão M F S. SENSITIVITY OF SHIP MOTION PREDICTIONS TO WAVE CLIMATE DESCRIPTIONS. Int.Shipbuild.Prog.39 No.418 (1992)

Hasselmann K, Barnett T P, Bouws E, Carlson H, Cartwright D E, Enke K, Ewing J A, Gienapp H, Hasselmann D E, Kruseman P, Meerburg A, Müller P, Olbers D J, Richter K, Sell W, Walden H. MEASUREMENTS OF WIND-WAVE GROWTH AND SWELL DECAY DURING THE JOINT NORTH SEA WAVE PROJECT (JONSWAP). Deutschen Hydrographischen. Zeitschrift. A8 No.12. 1973

Hasselmann K, Alpers W. THE RESPONSE OF SYNTHETIC APERTURE RADAR TO OCEAN SURFACE WAVES. Proc. Wave Dynamics and Radio Probing of the Ocean Surface, Miami, Florida, May 13-20 1981.

Hirayama T, Minami K, Hiramatsu M. DIRECTIONAL OCEAN WAVE MEASUREMENT UTILIZING RUNNING SHIP MOTIONS AND RADAR IMAGES. Proc. 16th OMAE Yokohama Japan. - Vol. II Safety and Reliability. ASME 1997.

Hirayama T. ADVANCED EXPERIMENTAL TECHNIQUES. ITTC Seakeeping Committee Meeting, Osaka 1992.

Hisaki Y. ESTIMATION OF WAVE SPECTRA USING HIGH-FREQUENCY OCEAN RADAR. Okinawa Radio Observatory. Journal of The Communications Research Laboratory. Vol.43 No 3. Nov 1996.

Hope K J. MEASURED SEAKEEPING ON AN AUSTRALIAN OFFSHORE PATROL BOAT. RINA Symposium 'Warship95 - Offshore Protection Vessels' London June 14-15 1995

Hosking R J, Joyce D C, Turner J C. FIRST STEPS IN NUMERICAL ANALYSIS. Hodder & Stoughton 1981. ISBN 0-340-19008-6

Hua J, Palmquist M WAVE ESTIMATION THROUGH SHIP MOTION MEASUREMENTS. RINA International Conference on Seakeeping and Weather. London 1995.

Iseki T. BAYESIAN ESTIMATION OF WAVE SPECTRA IN FOLLOWING SEAS. University of Glasgow Department of Naval Architecture and Ocean Engineering. Report NAOE-96-35, Feb 1996.

Iseki T, Ohtsu K. BAYESIAN ESTIMATION OF DIRECTIONAL WAVE SPECTRA BASED ON SHIP MOTIONS. Proc. NAV'94 Rome.

Juszko B, Graham R. DEVELOPMENT OF A STATISTICAL WAVE CLIMATE DESCRIPTION BASED ON 10 PARAMETER SPECTRA. 1993.

Kinsman B. WIND WAVES THEIR GENERATION AND PROPAGATION ON THE OCEAN SURFACE. Prentice-Hall. 1965

Komen G J, Cavaleri L, Donelan M, Hasselmann K, Hasselman S, Janssen P A E M. DYNAMICS AND MODELLING OF OCEAN WAVES. Cambridge University Press. 1996

Lloyd A R J M. SEAKEEPING SHIP BEHAVIOUR IN ROUGH WEATHER. First Edition - Ellis Horwood, Chichester. 1989.

Lloyd A R J M SEAKEEPING SHIP BEHAVIOUR IN ROUGH WEATHER. Revised Edition Published by the author 26 Spithead Avenue, Gosport, Hants UK. 1998.

Longuet-Higgins M S, Cartwright D E, Smith N D. OBSERVATIONS OF THE DIRECTIONAL SPECTRUM OF SEA WAVES USING THE MOTIONS OF A FLOATING BUOY. Proc. Conference 'Ocean Wave Spectra', Easton, Maryland, May 1-4 1961.

Longuet-Higgins M S. THE STATISTICAL ANALYSIS OF A RANDOM, MOVING SURFACE. Philosophical Transactions of the Royal Society A(966), 249 pp321-387. 1956.

Maggi A. SEAKEEPING: A COMPARISON OF NUMERICAL AND TOWING TANK PREDICTIONS WITH FULL SCALE MEASUREMENT. RINA International Conference on Ship Motions and Manoeuvrability, London, 1998.

Maximadji A. DETERMINATION OF MEAN SEA WAVE SPECTRUM PERIOD ON THE BASIS OF MEASURED MEAN PITCHING PERIOD. Proc. 8th International Congress on Marine Technology, Istanbul Turkey. 1997.

McCreight K. A NOTE ON THE SELECTION OF WAVE SPECTRA FOR DESIGN EVALUATION. US Naval Surface Warfare Center, Carderock Division, report CRDKNSWC-HD-974-02. January 1998.

Mitsuyasu H et al. OBSERVATION OF THE POWER SPECTRUM OF OCEAN WAVES USING A CLOVERLEAF BUOY. Journal of Physical Oceanography Vol. 10 1980.

Mitsuyasu H et al. OBSERVATIONS OF DIRECTIONAL SPECTRUM OF OCEAN WAVES USING A CLOVERLEAF BUOY. J.Phys.Oceanography Vol.5 1975

Montgomery P, Crossland P. USER GUIDE FOR THE PAT-95 SUITE OF SHIP MOTION COMPUTER PROGRAMS. DRA/SS/SSSHE/CR95030. July 1995

Neumann G. ON OCEAN WAVE SPECTRA AND A NEW METHOD OF FORECASTING WIND GENERATED SEA. Beach Erosion Board Tech. Memo. No.43, US Army Corps of Engineers, 42p. 1953.

Ochi M K, Hubble E N. SIX PARAMETER WAVE SPECTRA. Proc. 15th Coastal Engineering Conference, Honolulu Hawaii. pp301-328. 1976

Panicker N. REVIEW OF TECHNIQUES FOR DIRECTIONAL WAVE SPECTRA. Waves74. Vol.1 pp.669-688.

Phillips O M. THE EQUILIBRIUM RANGE IN THE SPECTRUM OF WIND GENERATED WATER WAVES. J.Fluid Mech. 4 pp426-434. 1958

Pierson W J, Moskowitz L. A PROPOSED SPECTRAL FORM FOR FULLY DEVELOPED WIND SEAS BASED ON THE SIMILARITY THEORY OF S.A. KITAIGORODSKII. Journal of Geophysical Research Vol. 69 pp5181-5190,5202. 1964

Reed A M, Dipper M J Jr, Brady T F, Turner C R, Dinsenbacher A L. SEAKEEPING AND STRUCTURAL PERFORMANCE OF THA A-FRAME SWATH VESSEL SEA SHADOW. Trans SNAME Vol. 105 1997 pp491-519.

Saito K, Maeda K. AN ESTIMATION OF OCEAN WAVE CHARACTERISTICS BASED ON MEASURED SHIP MOTIONS. 7th International Conference on Stability of Ships and Ocean Vehicles 1999.

Sandison S, Woolaver D, Dipper M, Rice M. SEA TRIALS OF THE SWATH SHIP USNS VICOTIROUS (T-AGOS 19) Marine Technology Vol.31 No4 Oct. 1994.

Schendel U. SPARSE MATRICES: NUMERICAL ASPECTS WITH APPLICATIONS FOR SCIENTISTS AND ENGINEERS. Ellis Horwood 1989. ISBN 0-7458-0635-X

Stilwell D, Pilon R O. DIRECTIONAL SPECTRA OF SURFACE WAVES FROM PHOTOGRAPHS. J.Geophys.Res. Vol.79 No.9. 1974 pp1277-1284

Takezawa S, Hirayama t. NEW EXPERIMENTAL TECHNIQUES IN DIRECTIONAL SPECTRUM WAVES. 19th Symposium on Naval Hydrodynamics. Seoul Korea. 1992.

Teague C C, Tyler G L, Joy J W, Stewart R H. SYNTHETIC APERTURE OBSERVATIONS OF DIRECTIONAL WAVE HEIGHT SPECTRA FOR 7s OCEAN WAVES. Nature Physical Science Vol.244 August 1973.

Tedeschi R. SEA STATE MEASUREMENTS IN THE ROSS SEA BASED ON SHIP MOTIONS. Proc. 9th ISOPE, Best, France, May 30-June 4 1999.

Tucker M J. A SHIPBORNE WAVE RECORDER. Trans RINA 98(3) pp236-246. 1956

Tucker M J. A WAVE-RECORDER FOR USE IN SHIPS. Nature October 1952.

Tucker M J. WAVES IN OCEAN ENGINEERING. Ellis Horwood. 1991.

Wachnik Z G, Zarnick E E. SHIP MOTIONS PREDICTION IN REALISTIC SHORT CRESTED SEAS. Trans SNAME Vol73 1965.

Watkins D S. FUNDAMENTALS OF MATRIX COMPUTATIONS. Wiley 1991.

Webster W C, Dillingham J T. DETERMINATION OF DIRECTIONAL SEAS FROM SHIP MOTIONS. Proc Directional Wave Spectra Application Berkeley USA 1981.

Webster W C, Trudell R W. STATISTICS OF LOCAL MOTIONS ON A SHIP. Proc Directional Wave Spectra Application Berkeley USA 1981.

Williams A J. AN INVESTIGATION INTO THE MOTIONS OF SHIPS AT SEA. Trans INA 1953 pp.70-91

Young I R, Verhagen L A, Banner M L. A NOTE ON THE BIMODAL DIRECTIONAL SPREADING OF FETCH-LIMITED WIND WAVES. J.Geophys.Res. Vol.100 No.C1 pp773-778 1995.